

# **SOVIET ATOMIC ENERGY**

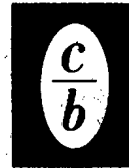
**АТОМНАЯ ЭНЕРГИЯ  
(АТОМНАЯ ЭНЕРГИЯ)**

**TRANSLATED FROM RUSSIAN**



**CONSULTANTS BUREAU**

## NEW BOOKS IN SERIES FROM



### REVIEWS OF PLASMA PHYSICS

**M. A. Leontovich, Editor.** A systematic, 5-volume review of the present status of plasma theory, serving both as an introduction for students and for researchers entering the field, and as an authoritative, up-to-date presentation of current knowledge for physicists prepared by Soviet experts. Each volume contains a number of integrated tutorial reviews. **Volume 1**, a comprehensive introduction to "classical" plasma physics, has just been published. Volumes 2-5 are in preparation. Each volume, \$12.50.

### LEBEDEV PHYSICS SERIES

**D. V. Skobel'tsyn, Editor.** Complete English translations of the Proceedings ("Trudy") of the Lebedev Physics Institute of the USSR Academy of Sciences. The first three volumes in this distinguished series of Special Research Reports have just been published: **Optical Methods of Investigating Solid Bodies** (Volume 25), 194 pages, \$22.50. **Cosmic Rays** (Volume 26), 262 pages, \$27.50. **Research in Molecular Spectroscopy** (Volume 27), 214 pages, \$22.50.

### STRUCTURE OF GLASS

**Volume 4: Electrical Properties of and Structure of Glass.** **O. V. Mazurin, Editor.** These 29 papers report original research on the relationship between electrical properties and the structure of glass, prefaced by a section on Glass in a Direct Electric Field by Mazurin. Approx. 150 pages, 1965, \$17.50.

### THE GROWTH OF CRYSTALS

**Volume 4.** **A. V. Shubnikov and N. N. Sheftal', Editors.** Forty-two papers presented at the All-Union Conference on Crystal Growth held at the Institute of Crystallography in Moscow. Approx. 200 pages, 1965, \$20.00.

### SOVIET PROGRESS IN APPLIED ULTRASONICS

**Volume 2: Ultrasonics in the Chemical Industry.** By **V. A. Nosov.** Designed to furnish Western scientists and engineers with updated coverage of Soviet advances in applications of ultrasonics. This Special Research Report is divided into three parts: the general concepts of elastic, sonic, and ultrasonic waves; the applications of ultrasonics in chemical technology; and ultrasonic devices for inspection and analysis. 172 pages, \$25.00.

All Consultants Bureau books are translated from Russian.

**Standing orders are welcomed:** Orders placed for all titles in a series, will be filled at a 10% discount on a 14-day approval basis.

## CONSULTANTS BUREAU

227 West 17th Street, New York, New York 10011

ATOMNAYA ÉNERGIYA  
EDITORIAL BOARD

A. I. Alikhanov	A. I. Leipunskii
A. A. Bochvar	M. G. Meshcheryakov
N. A. Dollezhal'	M. D. Millionshchikov
K. E. Erglis	( <i>Editor-in-Chief</i> )
V. S. Fursov	I. I. Novikov
I. N. Golovin	V. B. Shevchenko
V. F. Kalinin	A. P. Vinogradov
N. A. Kolokol'tsov	N. A. Vlasov
( <i>Assistant Editor</i> )	( <i>Assistant Editor</i> )
A. K. Krasin	M. V. Yakutovich
I. F. Kvartskhava	A. P. Zefirov
A. V. Lebedinskii	

# SOVIET ATOMIC ENERGY

A translation of **ATOMNAYA ÉNERGIYA**  
A publication of the Academy of Sciences of the USSR

© 1966

CONSULTANTS BUREAU ENTERPRISES, INC.  
227 West 17th Street, New York, N. Y. 10011

Volume 18, Number 3

March, 1965

## CONTENTS

	P A G E	
	ENG.	RUSS.
Report on the Award of the I. V. Kurchatov Gold Medal and Prize . . . . .	253	201
The Microtron and Areas of its Application—S. P. Kapitsa . . . . .	255	203
Accelerator with Nonlinear Helical Focusing—V. V. Vecheslavov and Yu. F. Orlov . . . . .	262	209
Introduction of an Ion Beam into the Cyclotron—V. A. Gladyshev, L. N. Katsaurov, A. N. Kuznetsov, L. P. Martynova, and E. M. Moroz . . . . .	268	213
Quasiclassical Model of Ternary Fission—B. T. Geilikman and G. I. Khlebnikov . . . . .	274	218
Concerning the Emission Times of $\gamma$ -Quanta as a Result of Fission—G. V. Val'skii, D. M. Kaminker, G. A. Petrov, and L. A. Popeko . . . . .	279	223
Application of the Yvon—Mertens Method for Solving Albedo Problems in the Neutron Diffusion Theory—Yu. N. Kazachenkov and V. V. Orlov . . . . .	283	226
Use of the Method of Moments for Solving Equations of Neutron Thermalization in Infinite Media—M. V. Fedulov . . . . .	290	232
Electromagnetic Pumps for Alkali Metals—N. I. Marin, V. A. Povsten', T. V. Doktorova, and E. M. Avilova . . . . .	298	239
A Stainless Steel with High Capture Cross Section for Thermal Neutrons—I. S. Lupakov and N. A. Vasil'ev . . . . .	302	242
Distribution of Sr <sup>90</sup> in the Surface Level of Soils in the Soviet Union in 1959-1960 —V. I. Baranov, F. I. Pavlotskaya, G. A. Fedoceyev, É. B. Tyuryukanova, L. M. Rodionova, E. V. Babicheva, L. N. Zatsepina, and T. A. Vostokova . . . . .	305	246
ABSTRACTS OF DEPOSITED ARTICLES		
Spatial and Energy Distribution of Scattered $\gamma$ -Radiation from a Unidirectional Source in an Infinite Air Medium—S. M. Ermakov, V. G. Zolotukhin, V. I. Kukhtevich, E. S. Matusevich, and B. A. Efimenko . . . . .	311	251
Angular and Energy Distribution of Scattered $\gamma$ -Radiation Near an Isotropic Source in an Infinite Air Medium—Yu. I. Kolevatov, V. I. Kukhtevich, E. S. Matusevich, and O. A. Trykov . . . . .	313	252
Spatial Distribution of the Dose Rate of Air-Scattered Neutrons from a Unidirectional Point Source—S. F. Degtyarev and V. I. Kukhtevich . . . . .	315	253
Certain Nonlinear Problems in Nuclear Reactor Theory—O. B. Moskalev and V. A. Chuyanov . . . . .	317	254
Effect of a Conducting Diaphragm on Plasma Equilibrium in Tokamak Devices —V. D. Shafranov . . . . .	318	255
Adiabatic Pinching of Hot-Ion Plasma (Description of the Device and the First Experiments) —A. V. Bortnikov, N. N. Brevnov, V. G. Zhukovskii, and M. K. Romanovskii . . . . .	320	256

Annual Subscription: \$95

Single Issue: \$30

Single Article: \$15

All rights reserved. No article contained herein may be reproduced for any purpose whatsoever without permission of the publisher. Permission may be obtained from Consultants Bureau Enterprises, Inc., 227 West 17th Street, New York City, United States of America.

**CONTENTS** (continued)

	<b>P A G E</b>	
	<b>ENG.</b>	<b>RUSS.</b>
Rules for Depositing (Storing) Articles . . . . .	322	257
<b>REVIEW OF THE GENEVA CONFERENCE</b>		
Investigations into the Problem of Controlled Thermonuclear Fusion—S. D. Fanchenko . . . . .	323	258
Isotopes and Radiation—A. S. Shtan' . . . . .	327	260
The Use of Isotopes and Radiation Sources in Hydrology and Hydrogeology—N. V. Churaev, A. I. Yakovlev, M. P. Volorovich, N. Ya. Flekser, and S. Ya. Vartazarov. . . . .	332	264
The Problem of Radioactive Waste Removal—A. N. Marei . . . . .	337	268
<b>LETTERS TO THE EDITOR</b>		
Determination of the Total Energy Lost by a Beam of Electrons as a Result of its Interaction with a Plasma—A. K. Berezin, Ya. B. Fainberg, L. I. Bolotin, and G. P. Berezina . . . . .	341	271
The Operation of the Cylinderizer in the Stellarator—B. I. Gavrilov, F. V. Karmanov, and G. P. Maksimov. . . . .	345	273
Experimental Verification of the Possibility of Using Stub Retarding Systems in Accelerator Technology—P. I. Gos'kov . . . . .	348	275
Total Interaction Cross Section of Neutrons with Benzene, Toluene and Sodium Acetate in the Energy Range 0.03–0.5 eV—I. S. Anisomov, V. I. Nikitin, A. I. Saukov, and A. A. Ugodenko . . . . .	350	277
Resonance Structure of the Cross Sections and its Influence on the Scattering Anisotropy for Fast Neutrons and their Transmission in Iron—A. P. Suvorov, A. G. Guseinov, and M. N. Nikolaev. . . . .	352	278
Measuring the Moderation Length of Neutrons from a Po-Be Source in Graphite-Water Lattices—Yu. M. Shalashov . . . . .	358	282
Method of Investigating $\gamma$ -Radiation from the (n, $\gamma$ ) Reaction on Separated Isotopes —É. A. Rudak and E. I. Firsov . . . . .	361	285
Dependence of the Counting Efficiency in Recording Fast Neutrons on the Geometry of Plastic Scintillators—V. G. Zolotukhin and G. G. Doroshenko. . . . .	365	287
Calculation of the Effective Resonance Integral for a Lump Consisting of a Mixture of Nuclei of a Resonance Absorber and Continuous Cross-Section Absorber —Yu. G. Pashkin and V. V. Chekunov. . . . .	369	290
Presentation of the Reactor Dynamics Equations in Terms of the Reciprocal Period —N. G. Chelintsev . . . . .	373	292
Effect of Pressure on the Heat Transfer in Nucleate Boiling of Liquid Metals —V. M. Borishanskii and K. A. Zhokhov . . . . .	377	294
Measurement of Radioactivity at the Surface of Aqueous Solutions—M. A. Belokurova, N. E. Tsvetaeva, M. N. Kulichenko, and L. A. Ivanova . . . . .	380	296
Investigation of Sorption of Radioiodine on Activated Charcoal, and Study of Forms of Gaseous Iodine in Air—T. I. Smolkina and A. A. Chubakov . . . . .	383	298
Radioactive Fallout on the Far-Eastern Shoreline of the Pacific Ocean in 1962-1963 —E. I. Markichev, A. D. Shramchenko, A. S. Lapardina, V. V. Peretti, E. I. Vasil'kov, and V. V. Skornyakov. . . . .	386	300
<b>NEWS OF SCIENCE AND ENGINEERING</b>		
Physical Startup of the VK-50 Boiling Water Reactor at the Ul'yanovsk Nuclear Power Station—A. Kubrochenko and V. Parfir'ev . . . . .	389	302
Nuclear Instrumentation Discussed at Comecon—N. A. Shekhovtsov . . . . .	390	302
Symposium on the Radiation Chemistry of Polymers—M. Kaplunov . . . . .	392	304
Plasma Physics Seminar at Trieste . . . . .	395	305
French Research Reactors and Power Reactors—V. A. Tsykanov . . . . .	396	306



# CONTENTS (continued)

	P A G E	
	ENG.	RUSS.
American Water Desalinization Specialists View Soviet Work . . . . .	400	309
British Scientists Visit the USSR . . . . .	401	309
Radioisotope Advances in the Lithuanian SSR—S. Geciauskas and K. Valacka . . . . .	402	310

The Russian date "Podpisano k pechati" of this issue was 3/3/1965 . This is equivalent to "approved for printing." Publication did not occur prior to this date, but must be assumed to have taken place reasonably soon thereafter.

Publisher

REPORT ON THE AWARD OF THE  
I. V. KURCHATOV GOLD MEDAL AND PRIZE

Translated from *Atomnaya Énergiya*, Vol. 18, No. 3,  
pp. 201-202, March, 1965



By decision of the Praesidium of the Academy of Sciences of the USSR, the Igor' Vasil'evich Kurchatov gold medal for 1965 was conferred upon Yu. D. Prokoshkin, Doctor of Phys. Math. Sci., and the I. V. Kurchatov Prize was awarded to A. F. Dunaitsev, V. I. Petrukhin, Yu. D. Prokoshkin, V. I. Rykalin, for their observation and investigation of the beta-decay of the  $\pi$ -meson ( $\pi^+ \rightarrow \pi^0 + e^+ + \nu$ ). This research was conducted with the aid of the 680-MeV synchrocyclotron of the Joint Institute for Nuclear Research.



Anatolii Fedorovich  
Dunaitsev



Valentin Ivanovich  
Petrukhin



Yurii Dmitrievich  
Prokoshkin



Vladimir Ivanovich  
Rykalin

The special interest displayed by physicists in research on the beta-decay process of the pion is due to the possibility of directly verifying, by such a course of study, the validity of one of the main and general principles of the universal theory of weak interactions: the hypothesis of the conservation of vector current in transitions with no change in strangeness. This theoretical assertion put forth for the first time by the Soviet physicists Ya. B. Zel'dovich and S. S. Gershtein, and independently by the American physicists M. Gell-Mann and R. Feynman, extends to the field of weak interactions, a fact quite familiar in electrodynamics, viz., that electrical charges on all the elementary particles are identical regardless of what interactions a particle participates in. The charges on the positron and proton are identical in the strict sense, despite the fact that the proton takes part in strong interactions in addition to electromagnetic interactions, while the positron does not.

This difference in behavior with respect to strong interactions means a difference in the magnetic moments of these particles, but not in their charges.

The beta-decay process of the pion is singled out as a transition within the isotopic multiplet at zero spin, from a large number of other weak interaction processes. Despite the fundamental nature of the pionic beta-decay, this process had not been detected experimentally until very recently, because of the extremely low expected probability (about  $10^{-8}$ ) and the consequent experimental difficulties.

Scientific staff members of the Nuclear Problems Laboratory of the Joint Institute for Nuclear Research, viz. A. F. Dunaitsev, V. I. Petrukhin, Yu. D. Prokoshkin, and V. I. Rykalin, were the first in the world to find a solution to this tricky problem — they detected the beta-decay of the pion and carried out an experimental investigation of the phenomenon.

In their preparation of the experiments, the authors designed a very elegant sophisticated high-speed electronic system capable of recording rare cases of beta-decay of pions and separating them out from the thousand times more frequent events of appearance of neutral pions via charge transfer between charged pions.

The basic components of this electronic system are a five-beam oscillograph with a resolution of  $10^{-10}$  sec and a multichannel coincidence circuit with  $10^{-9}$  sec resolution. High-resolution total-absorption Cherenkov spectrometers of high effectiveness and background insensitivity were designed to record the gammas emitted in the decay of neutral pions. These instruments are the most highly advanced presently existing with such operating parameters.

The investigations were carried out since late 1961 on the synchrocyclotron of the Nuclear Problems Laboratory. The beta-decay of the pion was discovered as a result of protracted measurements: 43 cases of this mode of decay were recorded. All the characteristics of the observed phenomenon added to the evidence of the reliable identification made of this mode of decay alone. The total decay probability was  $\frac{W(\pi \rightarrow \pi^0 + e^+ + \nu)}{W(\pi \rightarrow \mu^+ + \nu)} = (1.1 \pm 0.2) \cdot 10^{-8}$ . Both this value and the energy spectrum of pion-decay positrons are in excellent agreement with theoretical prediction. The experimentally determined constant  $G$  characterizing the beta-decay intensity of the pion was found to be  $G = (1.03 \pm 0.11)G_\beta$ , where  $G_\beta$  is the vector constant of the neutron beta-decay process.

The experimental results obtained by researchers at CERN, Berkeley, and Columbia University, where studies on the beta-decay of the pion were initiated somewhat later, are in accord with these findings.

## THE MICROTRON AND AREAS OF ITS APPLICATION

(UDC 621.384.611.3)

S. P. Kapitsa

Translated from *Atomnaya Énergiya*, Vol. 18, No. 3,  
pp. 203-209, March, 1965  
Original article submitted June 15, 1964

The present article is a survey of the basic results obtained in investigating and developing a microtron with a high-current beam. This new type of electron accelerator is compared with other medium-energy electron accelerators. The areas of application of the microtron in various branches of science and technology are briefly considered.

The development of modern accelerator technology follows two trends. On the one hand, accelerators with ever higher energies, which make it possible to solve new problems in elementary particle physics, are being constructed while, on the other hand, an ever increasing importance is attached to lower-energy accelerators, which are necessary for investigations in nuclear physics as well as for experiments connected with the use of high-energy particles in other areas of physics and technology. It is possible that accelerators have found the widest application in those areas of science where the equipment and investigation methods developed in nuclear physics have been employed most widely. In particular, radiation chemistry has developed in this manner.

Electron accelerators which serve as sources of fast electrons and gamma bremsstrahlung gained the most widespread use in these fields. Therefore, it would be of interest to consider the possibilities offered by the high-current microtron, which constitutes a new efficient medium-energy electron accelerator.

The principle of the electron cyclotron was set forth in 1944 by Veksler in the first of his papers devoted to the principle of phase stability [1]. Acceleration based on this method was first achieved in Canada [2]. However, this and other similar experiments did not result in the construction of an efficient accelerator, so that, until lately, the inherent possibilities of the microtron were not recognized and realized. The question of widespread application of this type of accelerator arose only after completion of the work performed at the S. I. Vavilov Institute of Physical Problems, Academy of Sciences of the USSR, which led to the construction of an efficient high-current microtron.

Before considering the application of microtrons, we shall recall the main physical principles on which they are based, and we shall briefly survey the results obtained in recent years at the Institute of Physical Problems and other laboratories in the Soviet Union.

#### Operating Principle and Parameters of the Microtron

Electrons are accelerated in a microtron by a constant-frequency alternating electric field in a uniform and steady magnetic field. In the vacuum chamber, the electrons move along circles which have a common tangent point (Fig. 1). The accelerating resonator is mounted at this place. With each passage through the accelerating gap, the electrons acquire a certain energy increment  $\Delta E$  and pass to the next circle (orbit). The synchronism of electron motion and the variation of the superhigh-frequency field are a consequence of the fact that the duration of every subsequent revolution is longer than the duration of the preceding revolution by the period  $T$  of the superhigh-frequency field. The revolution time  $t$  of a relativistic particle in the magnetic field  $H$  is proportional to its total energy  $E$ ,

$$t = \frac{2\pi E}{eHc}, \quad (1)$$

while the condition of synchronism in the microtron corresponds to the following relationship between  $\Delta E$  and  $H$  and the increment  $\Delta t$  of the revolution time:

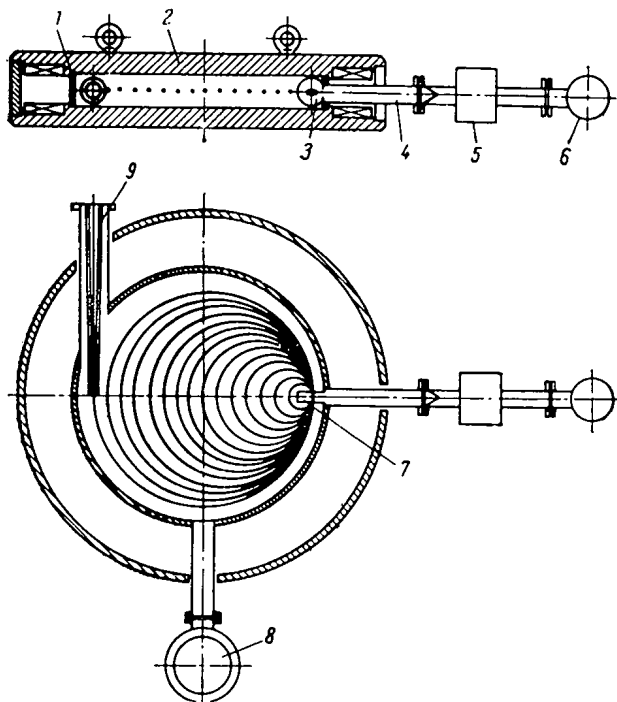


Fig. 1. Schematic diagram of the microtron. 1) Chamber; 2) magnet; 3) resonator; 4) waveguide; 5) ferrite; 6) magnetron; 7) electron emitter; 8) high-vacuum pump; 9) extraction.



Fig. 2. Small microtron of the Institute of Physical Problems.

adequate, and the accelerator current and efficiency were low. Because of this, the microtron was not considered as an efficient accelerator.

The improvements which resulted in the construction of a high-current microtron are based on new methods of inducing particle into the acceleration process and the use of an efficient thermionic cathode for electron emission.

$$\Delta t = \frac{2\pi\Delta E}{eHc} = T. \quad (2)$$

This relationship can be conveniently transformed into the relationship

$$\frac{\Delta E}{E_0} = \frac{H}{H_0} = \Omega, \quad (3)$$

where  $E_0 = mc^2$  is the electron rest energy and  $H_0 = (2\pi E_0 / ecT) = (2\pi E_0 / e\lambda)$  is the cyclotron value of the magnetic field for the wavelength  $\lambda$  of the accelerating voltage. Microtrons, as well as linear accelerators, usually operate in the 10-cm superhigh-frequency range. At a frequency of 3000 Mc ( $\lambda = 10$  cm), the cyclotron field is equal to 1070 Oe. The  $\Omega$  parameter constitutes the basic characteristic of the accelerating conditions, and all the accelerator properties and its limiting parameters are connected with this quantity. Since  $\Omega \approx 1$ , the particles are accelerated to an energy of the order of the rest energy with each passage through the resonator. Essentially, this constitutes the basic difference between a microtron and other accelerators of relativistic particles with automatic phase control (synchrotrons and phasotrons), where the energy increment with each passage through the accelerating gap can be small.

A consequence of the above property of microtrons is the fact that the strength of the electric accelerating field is comparable to the strength of the magnetic field. For electrons,  $E_0 = 511$  keV, and the increase in their energy by such a value with each passage through the resonator constitutes the basic difficulty in microtron design. This difficulty was solved by using high-power generators of waves in the centimeter range, which were initially developed for radar. It is obvious that, in its existing form, the microtron is unsuitable for the acceleration of heavy particles, since their rest energy is very high.

After  $N$  revolutions, the energy of the electrons moving in the equilibrium phase will be equal to

$$E = N\Omega E_0 + E_i. \quad (4)$$

where  $E_i$  is the injection energy. Toroidal resonators were used earlier in microtrons. The injection of electrons was achieved as a result of their emission directly from the walls of the flight gap, so that  $E_i = 0$ . The imposition of the accelerating conditions on the particles was not controllable, the beam focusing was in-

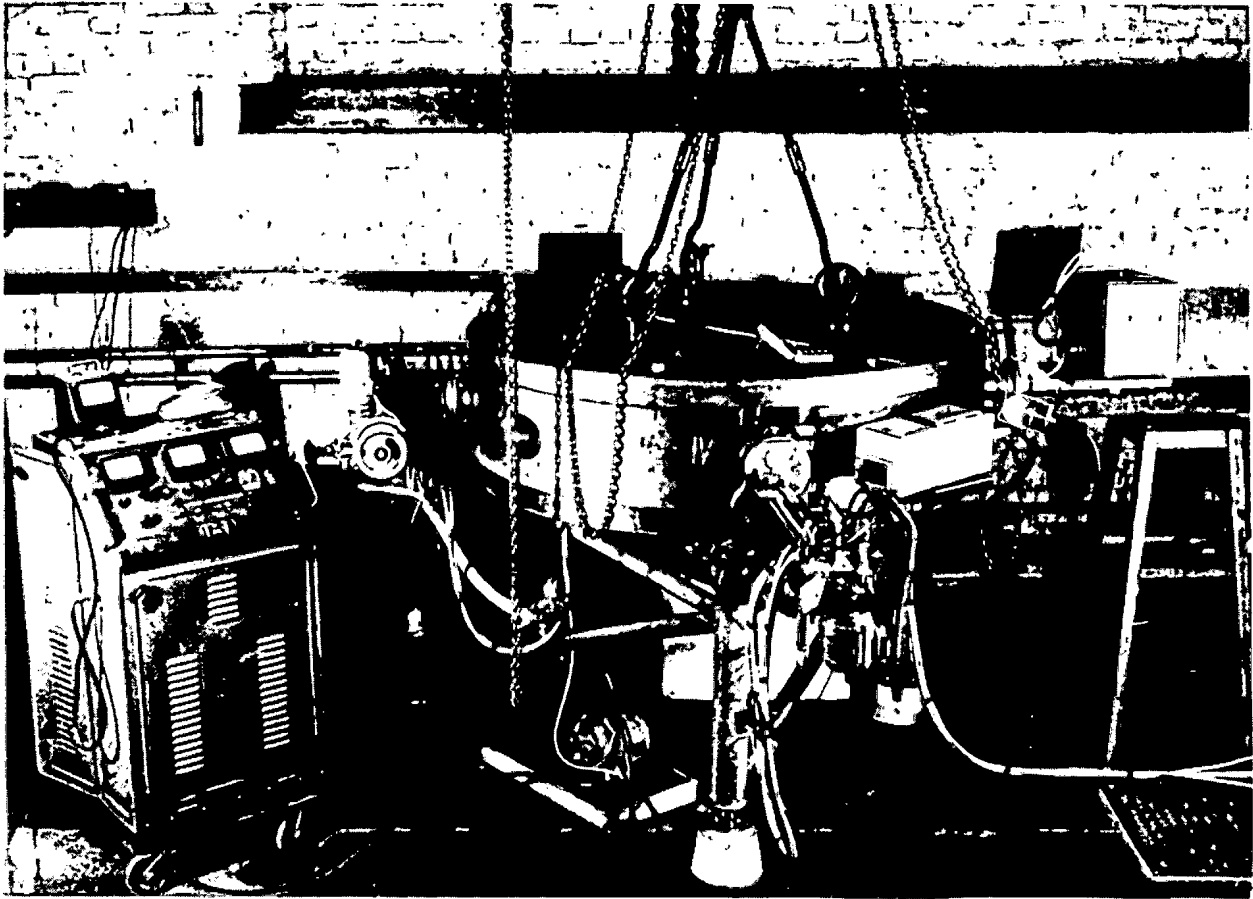


Fig. 3. Large microtron of the Institute of Physical Problems.

Resonators consisting of square and round cavities, similar to one of the linear-accelerator resonators, are used. The electron emitter is mounted on the outside flat wall of the resonator [3]. Electron emission occurs under the direct action of the high-frequency electric field and is controlled by varying the cathode temperature. Thus, in contrast to linear accelerators or betatrons, the microtron does not have an electron gun.

Several methods can be used for inducing electrons into the acceleration process. Under the so-called first conditions of injection, the cathode is mounted at one half of the resonator radius. For the assigned geometry, the injection conditions are satisfied in a wide range of  $\Omega$  values, from 0.8 to 1.6, which allows smooth variation by a factor of up to 2 for a fixed position and a constant number of orbits. This constitutes a new microtron characteristic, which is of great practical importance, since it facilitates flexible control of the beam energy. Under the second set of conditions, the cathode is located near the resonator axis, and the electrons pass through an additional opening in the resonator wall. Under these conditions, electrons can be accelerated for  $\Omega$  values ranging from 1.8 to 3 or higher.

The resonator constitutes the most important unit of the accelerator. The resonators are usually demountable and are made of oxygen-free copper, annealed and brazed in vacuum. The resonator's Q-factor is usually equal to 6000-10,000. By deforming one of its walls, the resonator frequency can be mechanically tuned to the frequency of the superhigh-frequency oscillator. It is interesting to note that the operating strength of the magnetic field in the resonator is close to the strength of the steady magnetic field; it attains 500-800 kV/cm. Experience shows that such fields can be produced even in relatively poor vacuum ( $10^{-6}$ - $10^{-5}$  mm Hg), which is sufficient for the microtron's operation. Lanthanum hexaboride ( $\text{LaB}_6$ ), which is characterized by high emission density, and great resistance and stability, serves as the electron emitter. The shape and the position of the cathode, the resonator dimensions, and also the efficiency of capture and the dynamics of electrons, are calculated by means of an electronic computer by numerically integrating the equations of electron motion in the accelerator [4].

The spacing between the orbits (the orbit step) is virtually constant and is equal to about 3 cm for  $\lambda = 10$  cm. Therefore, the extraction of particles from the accelerator does not involve difficulties; the electrons are extracted

through an iron channel, which screens the field near the last orbit. The extraction efficiency is close to 90-100%.

As a result of phase stability, the electrons in the beam are bunched into blobs with a length of  $\frac{1}{15} - \frac{1}{20} \lambda$ , which follow each other at a distance equal to the wavelength  $\lambda$  [5]. The energy spread is proportional to  $\Omega$  and does not depend on the number of orbits. For  $\Omega = 1$ ,  $\delta E = \pm 20$  keV.

The magnetic field in the microtron is usually rendered uniform. The field strength in the chamber is equal to 1000-2000 Oe and is maintained by the electromagnet, where the pole shape determines the required field uniformity. The magnetic field sends the particles back to the resonator, thereby accomplishing a peculiar 360° focusing. Essentially, the requirements for the field uniformity are similar to the requirement for the rectilinearity of the beam in linear accelerators. Nonuniformity of the field, especially in the direction perpendicular to the common diameter of the orbits, leads to their drift and a loss of particles. The basic focusing of the beam is effected only by the electromagnetic field of the resonators which, in contrast to the field in a linear accelerator, exerts a focusing action on the electrons. The focusing strength depends on the shape of the through-flight openings. Thus, for instance, in the case of oval openings and  $N = 10$ , the vertical dimension of the beam (along the magnetic field) is equal to about 2 mm for a divergence of  $1.5 \cdot 10^{-3}$  rad, while the horizontal dimension is 3-4 mm for a divergence of  $1.5 \cdot 10^{-2}$  [6-8].

The high-frequency system of the microtron usually consists of a magnetron oscillator and a decoupling and matching element (a ferrite or a load), which is located in the waveguide channel between the magnetron and the resonator. The power necessary for the resonator's excitation is proportional to  $\Omega^2/\lambda$  and is equal to 250 kW for  $\lambda = 10$  cm and  $\Omega = 1$ . The microtron efficiency, defined as the ratio of the power supplied to the resonator to the beam power is presently equal to 30-35%.

The first 12-orbit high-current microtron [3] that was constructed in 1958 at the Institute of Physical Problems has now been reconstructed. The new small microtron is shown in Fig. 2. The diameter of the poles is 750 mm, while the magnet weighs 900 kg. At the 17th orbit, the electron energy attains 10 MeV for  $\Omega = 1.2$  and 18 MeV for  $\Omega = 2$ . The mean beam power is 0.5 kW for a current of up to 50 mA in pulses with a duration of 2.5  $\mu$ sec and a repetition frequency of 400 cps. The accelerator's power consumption is equal to 15 kW. Figure 3 shows the general view of the large microtron at the Institute of Physical Problems. The pole diameter is 110 mm; the microtron is calculated for 30-45 MeV [9]. At the present time, an energy of 25 MeV for a current of up to 20 mA in pulses was obtained in this accelerator at the 28th orbit. A similar accelerator is presently being prepared for operation at OIYaI for work in combination with a fast pulse reactor.

What are the maximum expected energies and currents in the microtron?

The maximum energy that can be secured in the microtron depends on the number of orbits and the parameter  $\Omega$  in correspondence with expression (4). The maximum number of orbits is determined by the maximum allowable nonuniformity of the magnetic field, which is inversely proportional to the square of the number of orbits [10]. According to the present state of magnetic technology, the maximum number of orbits is apparently equal to 50-100. An obvious way to increase the energy is to use large  $\Omega$  values. At this moment, resonators with  $\Omega = 2$  have been calculated and constructed, and resonators with  $\Omega = 3$  or higher values have been calculated. Considering the switch to large  $N$  and  $\Omega$  values, a reasonable estimate of the maximum microtron energy would be 50-100 MeV.

The beam current is naturally connected with the power of the superhigh-frequency source. The current is physically limited by the interaction between the beam and the resonator and by the coherent radiation of bunches during their motion in the chamber [11]. Theoretical estimates of the maximum current yield values of 1-10 A (for  $\Omega = 1$ ); the maximum current value increases with an increase in  $\Omega$ . The above current values have not yet been achieved experimentally; the maximum microtron current that has been obtained is equal to about 100 mA.

It should be mentioned that, at the present level of the technology of continuous generation of superhigh-frequency oscillations, it is possible to produce continuous-operation microtrons with an energy of about 30 MeV and a beam power measured in tens of kilowatts or more. The scale of such an accelerator would be comparable with that of a standard cyclotron.

#### Comparison of the Microtron with Other Accelerators

It would be most interesting to compare the microtron with a linear electron accelerator, to which it bears the greatest resemblance with respect to its essential properties. The basic difference between them is that a linear

accelerator constitutes a machine consisting of many resonators connected in series and having a single common beam, while the microtron can be considered as a device with parallel acceleration of many beams in a single resonator and a correspondingly lower value of the characteristic impedance. However, in the case of a microtron, there exists in practice a threshold power value (about 100 kW) beyond which electrons can be accelerated independently of their final energy, which is determined only by the number of orbits and the magnet dimensions. In the case of linear accelerators, regardless of the absence of such a lower limit, the power necessary for exciting a linear accelerator of reasonable length at comparable energies is much higher than the power required for exciting the single resonator in a microtron. This results in the fact that a linear accelerator, in its present form, will always constitute a pulse-action accelerator, barring an excessive increase in length or the use of cooled resonators, in particular, superconducting resonators.

Linear accelerators provide the possibility of high-current acceleration of very short duration as a result of the electromagnetic energy stored in them. In a microtron, due to the necessity of accelerating particles to strictly defined values, such a possibility of operation under unsteady-state conditions does not exist.

In comparison with linear accelerators, the simplicity of the microtron constitutes its overwhelming advantage. The microtron does not have an electron gun, which would require additional supply sources. The high-frequency circuit and the resonator design are much simpler in the microtron. A microtron uses self-exciting nontunable magnetrons, which are characterized by great simplicity and efficiency in comparison with the high-power amplifying klystrons used in linear accelerators.

Comparing the microtron to direct-action accelerators — electrostatic and high-voltage rectifying devices — we see that virtually the same high monochromaticity of the beam can be achieved in the microtron. However, the maximum microtron energy is much higher than the energy of direct-action accelerators. In the region of high energies (up to 5 MeV), modern high-voltage rectifying devices have a considerable continuous power (up to 100 kW) and high efficiency (50-80%). At the present time, they probably constitute the best high-power sources of fast particles in this energy range. However, the above advantages will be decisive only if the power of the device is considerable. In the case of low power values, where energy losses play a secondary role, it is more convenient to use microtrons or single-section linear accelerators, since the accelerator efficiency under these conditions is not so important, while the dimensions of the devices are smaller.

Betatrions and microtrons cover approximately the same energy range. However, the basic advantage of a microtron in comparison with a betatron consists in its much higher intensity. Thus, at 12 MeV, the intensity of the bremsstrahlung beam in the small microtron of the Institute of Physical Problems is equal to 3000 R/min. In contrast to the betatron, the electron beam can be extracted from the microtron without difficulties. The design of the accelerator is very compact, while the energy efficiency of the microtron is much higher than that of a betatron.

Thus, in the range of medium energies (from 5 to 30-50 MeV), the microtron has presently many advantages and new properties in comparison with other types of accelerators.

The physical principles of the operation of high-current microtrons have been thoroughly investigated, and the basic technical problems connected with their design have been solved on the basis of the machines already constructed. In the next few years, this accelerator will undoubtedly be further developed, while the power of the machines and the energy will be raised. However, the possibilities of high-current microtrons can be clearly visualized even now. Therefore, it would be of interest to discuss the new developments and fields of application that this accelerator offers in science and technology [12].

#### Areas of Microtron Application

The high qualities of the microtron beam make it a promising injector for high-energy accelerators, such as synchrotrons [13]. We should mention here the interesting experiments performed at the P. N. Lebedev Institute of Physics, Academy of Sciences of the USSR, on the acceleration of positrons in a microtron [14]. As a result of introducing an ingenious conversion circuit and the subsequent acceleration of positrons, a record ratio  $n_{e^+}/n_{e^-} = 1$  to  $2 \cdot 10^{-6}$  was obtained in this accelerator. It should be noted that the energy of accelerated positrons is equal to the energy of initial electrons in this accelerator.

The progress in the field of experimental nuclear physics is connected with the development of the appropriate investigation equipment. In the medium-energy range, the basic criterion for accelerators is the power. The



precisely defined energy and the high intensity in a microtron offer new possibilities in nuclear physics, in particular in studies of photonuclear reactions. The use of continuous-action microtrons is especially promising for the solution of such problems. Progress in the field of these classical branches of nuclear physics is possible only if new experimental equipment is provided and high-power accelerators are used.

The microtron can be an efficient source of fast neutrons as a result of the  $(\gamma, n)$ -reaction. For the  $(\gamma, n)$ -reaction on heavy elements (U, Pb, W), the most advantageous energy is 25-30 MeV, while, for light elements (Be, D), the energy should be  $\leq 10$  MeV. However, high-power linear electron accelerators are more suitable for these purposes, since there are no stringent requirements for a monoenergetic beam in such cases. Due to the above-mentioned possibility of operation under conditions of large currents with energy storage and pulse shortening, very large instantaneous values of fast-neutron fluxes can be obtained by means of linear accelerators. On the other hand, the use of small microtrons as neutron generators is very promising for purposes of radioactivation analysis. Thus, for instance, the theoretical mean neutron flux produced by the small microtron of the Institute of Physical Problems is not less than  $10^{12}$  neutrons/sec. The use of microtrons for analysis based on the determination of elements with respect to their photonuclear reaction threshold is also promising. The accelerator's simplicity and the controllability of the beam energy are the decisive factors in this case.

The efficient focusing in microtrons results in a small focusing point on the target, which offers great possibilities for using the microtron in industrial flaw detection.

The production of electron and bremsstrahlung beams at energies of up to 20-40 MeV provides a basis for the widespread application of microtrons in medical radiology for gamma-therapy and irradiation by fast electrons. The accelerator's simplicity and reliability and the accurately defined beam energy are also of special importance in this case. Therefore, the microtron now constitutes perhaps the best accelerator for medical purposes, since it has advantages in comparison with betatrons, where the production of extracted electron beams is difficult, and with linear accelerators, where the above energies cannot be achieved without using multisection accelerators, which are characterized by complex and cumbersome superhigh-frequency supply. The use of efficient electron accelerators — microtrons — is also advisable for beam disinfection and decontamination of materials, food products, seeds, etc.

The wide field of application of electron accelerators is related to problems of radiation chemistry and new radiation methods for the treatment and modification of materials (metals, semiconductors, and polymers). In a brief survey, it is impossible to give even a cursory outline of this field of accelerator application. We shall mention only that, on the one hand, this field requires accelerators for laboratory and semi-industrial investigations; such accelerators must have great flexibility and diversity of the parameters. On the other hand, many new production methods, for instance the radiation vulcanization of tires, already urgently require high-power sources of fast electrons and bremsstrahlung and gamma radiation. In research as well as in industry, the high-current microtron offers new possibilities in high-energy radiation techniques.

In this article we did not touch upon other fields of microtron application, in particular the fields of megavolt electronics, relativistic plasma, and injection in accelerators. These fields form a part of modern physics and electronics, while the microtron essentially represents one of the results of developments in these fields. Our purpose was to discuss the possibilities offered by the development of a new type of accelerator in other fields of science and technology. The realization of these possibilities will depend to a large extent on how well the properties of the microtron will be understood and the trends of its application in science and the national economy visualized.

#### LITERATURE CITED

1. V. I. Veksler, DAN SSSR, 43, 346 (1944).
2. W. Henderson, H. LeCaine, and R. Montalbetti, Nature, 162, 699 (1948).
3. S. P. Kapitsa, V. P. Bykov, and V. N. Melekhin, ZhÉTF, 39, 997 (1960); 41, 376 (1961).
4. S. P. Kapitsa et al., ZhÉTF, 41 (1961).
5. V. P. Bykov, ZhÉTF, 44, 576 (1963).
6. V. N. Melekhin, ZhÉTF, 42, 622 (1962).
7. K. A. Belovintsev et al., Atomnaya énergiya, 15, 62 (1963).
8. V. M. Melekhin, in: Transactions of the International Conference on Accelerators, Dubna, August 21-27, 1963 (edited by A. A. Kolomenskii et al.) [in Russian] (Atomizdat, Moscow, 1964).

9. S. P. Kapitsa et al., in: Transactions of the International Conference on Accelerators, Dubna, August 21-27, 1963 (edited by A. A. Kolomenskii et al.) [in Russian] (Atomizdat, Moscow, 1964), p. 1053.
10. V. P. Bykov, ZhTF, 33, 337 (1963).
11. S. P. Kapitsa and L. A. Vainshtein, ZhÉTF, 42, 821 (1962).
12. S. P. Kapitsa, Vestnik AN SSSR, No. 10, 65 (1961).
13. K. A. Belovintsev et al., Atomnaya énergiya, 14, 359 (1963).
14. K. A. Belovintsev and F. P. Denisov, Atomnaya énergiya, 16, 253 (1964).

## ACCELERATOR WITH NONLINEAR HELICAL FOCUSING

(UDC 621.384.60)

V. V. Vecheslavov and Yu. F. Orlov

Translated from *Atomnaya Énergiya*, Vol. 18, No. 3,  
pp. 209-213, March, 1965

Original article submitted March 19, 1964

The theory of an accelerator with nonlinear helical focusing is developed. The fundamental formulas are obtained for the example of cubic focusing. An approximate calculation of the region of stability, adiabatic attenuation, mechanism of transverse automatic phase stabilization, and effect of perturbations is given. In quantitative characteristics, the accelerator is close to the strong-focusing type.

A solution to the equations of motion of a charged particle in a nonlinear helical field (for the example of a cubic field) was obtained in [1] without taking account of the many perturbing effects. The motion has the nature of a superposition of comparatively large, nonlinear, coupled  $r$ - $z$  oscillations, similar to a helical motion around a circular orbit, and small nonlinear oscillations. The frequencies of the various oscillations are determined by the amplitude of the nonlinear oscillations. In this sense there is no essential difference between spiral and sign-constant [2] nonlinear focusings.

The effect of harmonic perturbations in nonlinear focusing essentially differs from the linear case by the development of phase stability of the nonlinear oscillations [3,4].

In this paper we propose to use transverse phase stabilization in order to avoid passing through resonances during acceleration. In contrast to sign-constant nonlinear focusing, conditions with a time-constant magnetic field are here impossible; hence, passage through resonance is in no way justified. In the case considered, the ordinary synchrotron condition, in which the field grows proportionally to the particle momentum, is possible. It is precisely this condition (the only reasonable one in helical focusing) which is considered below.

A helical-focusing synchrotron may be set up, for example, in the form of deflecting magnets with a homogeneous field, alternating along the orbit, and short, nonlinear (six- or eight-pole) lenses set around the orbit with rotational pitch  $l$ . It is assumed that the length  $l$  is much larger than the length of the magnets and lenses. The fine structure of the field within the period (length of period equals  $l/3$  and  $l/4$  for quadratic and cubic fields, respectively) is a source of additional phase stabilization of the transverse oscillations, which is not considered here. Below we shall operate with the mean quantities  $\langle H \rangle$  and  $(\partial^k H / \partial r^k)$ , omitting the averaging sign. Regarding the focusing as strong, we shall neglect the terms  $r/R$ .

Although the character of motion in nonlinear helical focusing differs substantially from the case of ordinary linear focusing, the quantitative characteristics (phase volume, tolerances) are quite close for comparable parameters of these two cases. In this respect, the accelerator with helical nonlinear focusing has no advantage over ordinary accelerators, but is of interest because of its characteristics for obtaining an accelerated beam.

Estimate of the Region of Stability

Without accounting for perturbations, the particle motion obeys the equation

$$\varphi'' + 2i\alpha\varphi' - \alpha^2\varphi + \gamma\varphi^3 = 0. \quad (1)$$

Here,

$$\gamma = \frac{1}{6} \cdot \frac{\partial^3 H}{\partial u^3} \cdot \frac{1}{HR},$$

$$\varphi = (r + iz) \exp(-i\alpha x) = u + iv, \quad \alpha = \frac{2\pi}{l},$$

where  $u, v$  are the axes of a coordinate system rotating in a helix, and  $x$  is the coordinate along the orbit.

The nonlinear helical part of the oscillations, according to [1], is presented in the form of a Fourier series

$$\varphi(x) = \sum_k a_{2k+1}(\nu) \exp[(-i)^{2k+1}(2k+1)(1+\nu)\alpha x] \quad (2)$$

with fundamental frequency  $\nu$ , which has the sense of the number of  $r$ - $z$  oscillations in length  $l$ .

The coefficients  $a_{2k+1}(\nu)$  are found from the relations

$$\left. \begin{aligned} |a_1|^4 &= \frac{\alpha^4 \nu^2 (4+3\nu)^2}{3\nu^2} \left( 1 - \frac{7\nu^4}{3(4+3\nu)^2(4+5\nu)^2} + \dots \right), \\ a_3 &= \frac{\nu a_1^3}{\alpha^2 (4+3\nu)^2} \left( 1 + \frac{2\nu^4}{(4+3\nu)^2(4+5\nu)^2} + \dots \right), \\ a_5 &= \frac{3\nu^3 |a_1|^2 a_1^5}{\alpha^6 (4+3\nu)^4 (4+5\nu)^2} \dots \end{aligned} \right\} \quad (3)$$

For  $\nu > 0$  (particle motion in the direction of rotation of the lenses), series (2) converges for any values of  $\nu$  (and not only for  $\nu \ll 1$ , as assumed in [1]). In cases  $\nu < 0$  and  $|\nu| \approx 1$ , series (2) and (3) diverge. From the requirement of stability for series (2), it follows that there are no solutions, at least in the range  $0.6 < |\nu| < 1.7$  (in a quadratic field in the range  $0.5 < |\nu| < 2.0$ ).

Further limitations on the quantity  $|\nu|$  arise from analysis of small linear oscillations  $\Delta\varphi$  around the helix orbit. These are represented in the form of a superposition of harmonics with frequencies  $\mu; 2 - \mu; 4(1 + \nu)K + \mu; 4(1 + \nu)K + 2 - \mu$ ; where  $K$  is a whole number, and the quantity  $\mu$  is explained below. The following four are the main harmonics:

$$\Delta\varphi = b_{11}e^{-i(1+\mu)\alpha x} + c_{11}e^{-i(1+2\nu-\mu)\alpha x} + b_{31}e^{i(3+2\nu+\mu)\alpha x} + c_{31}e^{i(3+4\nu-\mu)\alpha x} + \dots \quad (4)$$

The values of  $\mu, b_{ik},$  and  $c_{ik}$  are found from the system:

$$\left. \begin{aligned} \alpha^2 \mu^2 b_{11} &= 3\nu (a_1^{*2} b_{31}^* + 2a_1^* a_3^* c_{11}^* + a_3^{*2} c_{51}^* + \dots), \\ \alpha^2 (2\nu - \mu)^2 c_{11} &= 3\nu (a_1^{*2} c_{31}^* + 2a_1^* a_3^* b_{11}^* + a_3^{*2} b_{51}^* + \dots), \\ \alpha^2 (4 + 2\nu + \mu)^2 b_{31} &= 3\nu (a_1^{*2} b_{11}^* + 2a_1^* a_3^* b_{51}^* + a_3^{*2} c_{71}^* + \dots), \\ \alpha^2 (4 + 4\nu - \mu)^2 c_{31} &= 3\nu (a_1^{*2} c_{11}^* + 2a_1^* a_3^* c_{51}^* \dots); \\ \alpha^2 (4 + 4\nu + \mu)^2 b_{51} &= 3\nu (a_3^{*2} c_{11}^* + 2a_1^* a_3^* b_{31}^* + a_1^{*2} b_{71}^* \dots), \\ \alpha^2 (4 + 6\nu - \mu)^2 c_{51} &= 3\nu (a_3^{*2} b_{11}^* + 2a_1^* a_3^* b_{31}^* + a_1^{*2} c_{71}^* + \dots), \\ \alpha^2 (8 + 6\nu + \mu)^2 b_{71} &= 3\nu (a_1^{*2} b_{51}^* + 2a_1^* a_3^* b_{91}^* + \dots), \\ \alpha^2 (8 + 8\nu - \mu)^2 c_{71} &= 3\nu a_1^{*2} c_{51}^* + \dots \end{aligned} \right\} \quad (5')$$

For  $\nu \ll 1$  solutions differing from the trivial  $\mu = \nu$  may be obtained from the theory of perturbations, taking as the zeroth approximation expression (4) and not allowing for Eq. (5'') and subsequent equations:

$$\mu = \nu \left[ 1 \pm 2\sqrt{2} \left( 1 + \frac{3\nu}{2(4+3\nu)} - \frac{\nu^2}{(4+3\nu)^2} + \dots \right) \right]. \quad (6)$$

By itself, series (6) converges well even for  $\nu \gg 1$ . However, for  $\nu \rightarrow \infty$ , we obtain  $\mu$  of the order  $5\nu; -3\nu$ . Putting these values of  $\mu$  in (5') and (5''), we observe that for  $\nu \rightarrow \infty$  the coefficients on the left-hand side of Eq. (5'') are an order smaller than those in front of  $b_{11}, c_{11}, b_{31}, c_{31}$  in (5'). Hence, for  $\nu \gg 1$ , we must take account of Eq. (5''), taking as the zeroth approximation  $b_{51}, c_{51}, b_{71}, c_{71}$  instead of  $b_{11}, c_{11}, b_{31}, c_{31}$ . However, carrying out the calculation in this approximation, we obtain new values of  $\mu$  for  $\nu \rightarrow \infty$ ;  $\mu$  of the order of  $9\nu; -7\nu$ . This forces us to consider the four equations following (5''), etc.

Thus, for  $\nu \rightarrow \infty$  all the terms of the series (4) are of the same order and series (4) diverges, starting from the value of  $\nu$  for which the coefficients in front of  $b_{ik}$  and  $c_{ik}$  on the left-hand side of (5'') become equal to the coefficients in Eq. (5').

These considerations lead to the following rough estimate of the region of stability in the cubic field:

$$\left. \begin{aligned} 0 \leq \nu \leq 1, \frac{\gamma |a|^2}{\alpha^2} \leq 4, |a|^2 \approx r_0^2 + z_0^2, \\ 0 > \nu \geq -0.5, \frac{\gamma |a|^2}{\alpha^2} \leq 0.7. \end{aligned} \right\} \quad (7)$$

### Transverse Phase Stabilization

Before considering transverse phase oscillations, we must elucidate the adiabatic damping of free nonlinear oscillations during acceleration. Equation (1) has the Hamiltonian

$$\begin{aligned} \mathcal{H}_\varphi &= \mathcal{P}_\varphi \mathcal{P}_\varphi^* + i\alpha (\varphi^* \mathcal{P}_\varphi - \varphi \mathcal{P}_\varphi^*) \\ &+ \frac{\gamma}{4} (\varphi^4 + \varphi^{*4}) = |\varphi'|^2 - \alpha^2 |\varphi|^2 + \frac{\gamma}{4} (\varphi^4 + \varphi^{*4}), \end{aligned}$$

in which the generalized momentum  $\mathcal{P}_\varphi = \varphi' + i\alpha\varphi$  is canonically conjugate to the variable  $\varphi^*$ . The adiabatic invariant

$$I = P \oint \mathcal{P}_\varphi d\varphi^* = P \int_0^{2\pi/(1-\nu)\alpha} (\varphi' + i\alpha\varphi) \frac{d\varphi^*}{dx} dx, \quad (8)$$

where P is the particle momentum. This gives

$$\begin{aligned} I &= 2\pi P \alpha \sum_0^\infty |a_{2k+1}|^2 (2k+1) [(2k+1)(1+\nu) + (-1)^{k+1}] \\ &= 2\pi P \alpha \nu |a_1|^2 \left( 1 + \frac{\nu}{4+3\nu} + \dots \right) \approx P \frac{2\pi \alpha^3 \nu^2 (4+3\nu)}{\sqrt{3}\gamma} \left( 1 + \frac{\nu}{4+3\nu} + \dots \right). \end{aligned} \quad (9)$$

In order that the accelerated particle should not pass through resonance, it is necessary to preserve the value of  $\nu$ , together with which  $a_1$  and  $\mu$  remain constant.

Without phase stabilization this is possible for  $\gamma/P \propto \partial^3 H / \partial r^3 \cdot 1/H^2 = \text{const}$ . This condition is technically inconvenient and unsuitable, since the quadratic law  $\partial^3 H / \partial r^3 \propto H^2$  leads to a very small value of the focusing field  $\partial^3 H / \partial r^3$  at the onset of acceleration, and hence to a very small capture of particles.

It is easy to maintain constancy of the quantities  $\nu$ ,  $\mu$ , and  $|a|^2$  by means of harmonic azimuthal perturbations of the field  $\Delta H_z = h_q \cos(qx/R)$ ,  $h_q/H = \text{const}$ ,  $(\partial^3 H / \partial r^3)(1/H) = \text{const}$ . In this case there exists a helical periodic orbit with frequency  $\nu_0 = q/R\alpha$ , having basically the form (2) with  $\nu = \nu_0$ . Small oscillations around this orbit are divided into betatron oscillations with frequencies  $\mu$  from formula (6) with  $\nu = \nu_0$ , and transverse-phase oscillations with relatively low frequency  $\Omega \ll \nu$ , proportional to  $(h_q/H)^{1/2}$ , the synchrotron condition with transverse phase stabilization.

We shall consider that  $h_q$  does not depend on r and z, though this condition is not obligatory. The equation of motion, allowing for only the resonance harmonic, may be written in the form

$$\varphi'' + 2i\alpha\varphi' - \alpha^2\varphi + \gamma\varphi^*3 = \frac{h_q}{2HR} e^{-i\left[\left(\alpha + \frac{q}{R}\right)x + \beta\right]} \quad (10)$$

with forced periodic solution

$$\varphi_q = A_1 e^{-i\left[\left(\alpha + \frac{q}{R}\right)x + \beta\right]} + A_3 e^{3i\left[\left(\alpha + \frac{q}{R}\right)x + \beta\right]} + \dots \quad (11)$$

Here

$$\left. \begin{aligned} A_3 &= \frac{\gamma A_1^3}{\alpha^2 \left(4 + \frac{3q}{R\alpha}\right)^2}, \\ A_1 &\approx -\frac{h_q}{2HR} \cdot \frac{1}{\frac{q^2}{R^2} - \frac{3\gamma^2 |A_1|^4}{\alpha^2 \left(4 + \frac{3q}{R\alpha}\right)^2}}. \end{aligned} \right\} \quad (12)$$

The periodic solution with very small amplitude  $A_{11} = (-R/2q^2)(h_q/H)$  does not relate to automatic phase stabilization. The solution of interest to us, expanded into a series in  $h_q/H$ , is

$$A_{10} = \pm \left[ \frac{\alpha q (4 + 3\nu_0)}{\sqrt{3R\gamma}} \right]^{1/2} + \frac{R}{8q^2} \cdot \frac{h_q}{H}. \quad (13)$$

It is assumed that  $(R/A_{10})(h_q/H)(1/q^2) \ll 1$ .

Small deviations from the helical orbit (11), (13) will be sought as before in the form (4) with  $\nu = \nu_0 = q/R\alpha$ , lying in the region (7). This leads to an equation for  $\mu$ :

$$\left[ \mu^2 - \frac{9\gamma^2 A_{10}^4}{\alpha^2 (4 + 2\nu_0 + \mu)^2} \right] \left[ (2\nu_0 - \mu)^2 - \frac{9\gamma^2 A_{10}^4}{\alpha^2 (4 + 4\nu_0 - \mu)^2} \right] - \frac{36\gamma^4 A_{10}^8}{\alpha^8 (4 + 3\nu_0)^4} = 0. \quad (14)$$

Apart from the root of formula (6), we find two more roots,  $\mu = \nu_0 \pm \Omega$ ,  $\Omega \ll 1$  (these roots now replace the trivial multiple root  $\mu = \nu$  in the absence of phase stabilization). Expanding (14) into a series in  $\Omega$  and retaining terms of order  $\Omega^2$  and  $h_q/H$ , we obtain (without allowing for a change in the energy of the particles):

$$\Omega^2 = \frac{4 + 3\nu_0}{16 + 24\nu_0} \cdot \frac{\nu_0^2}{q^2} \cdot \frac{R}{A_{10}} \cdot \frac{h_q}{H} = \frac{4}{M^2} \cdot \frac{R}{A_{10}} \cdot \frac{h_q}{H} \cdot \frac{4 + 3\nu_0}{4 + 6\nu_0}, \quad (15)$$

where  $M = 4L/l = 8\pi R/l$  is the number of periods of the magnetic structure. The frequency  $\Omega$  must be kept between integral and semiintegral resonances. Putting  $\Omega \approx (k + \epsilon) R\alpha$  ( $k \ll q = \text{whole number}$ ,  $|\epsilon| \leq \frac{1}{2}$ ), we obtain the tolerance for the maintenance of constancy in the ratio  $h_q/H$ :

$$\frac{\Delta h_q}{H} \approx 2 \frac{\Delta \Omega}{\Omega} \approx \frac{1}{4k} \quad \text{for} \quad \Delta \epsilon \approx \pm \frac{1}{8}, \quad (16)$$

this tolerance being comparatively easy. In order to estimate the phase volume of the transverse oscillations which can be included in the accelerating condition without loss of stability, let us carry out another derivation of the transverse-phase oscillations, taken in principle from [4].

Multiplying (10) by  $\varphi^{*}$  and adding to the complex conjugate (CC) equation, we obtain

$$\frac{d\mathcal{H}_\varphi}{dx} = \left( \frac{d\mathcal{H}_\varphi}{dx} \right)_{\text{ad}} + \frac{h_q}{2HR} (\varphi^{*'} e^{-i \left[ \left( \alpha + \frac{q}{R} \right) x + \beta \right]} + \text{CC}). \quad (17)$$

Here the term  $\left( \frac{d\mathcal{H}_\varphi}{dx} \right)_{\text{ad}}$  takes account of the adiabatic damping of nonlinear oscillations with growth of particle energy. For  $\nu \ll 1$   $\mathcal{H}_\varphi \approx 2\nu\alpha^2 |a_1|^2$  and, according to (9),  $\left( \frac{d\mathcal{H}_\varphi}{dx} \right)_{\text{ad}} \frac{1}{\mathcal{H}_\varphi} = -\frac{d\nu}{dx} \cdot \frac{1}{\nu}$ . The second term on the right in (17) describes the resonance setting up of transverse oscillations, if the frequency  $\nu$  is close to the resonance frequency  $\nu_0$ . The two terms on the right on average compensate one another, i.e.,  $\langle \mathcal{H}_\varphi \rangle = \mathcal{H}_0 = \text{const}$ , which corresponds to the constancy  $\langle \nu \rangle = \nu_0$ . Let us put  $\varphi' = i\alpha(1 + \nu) e^{-i\alpha(1 + \nu)x} a_1$  into (17) and introduce phase  $\varphi = (\nu - \nu_0) \alpha x - (\pi/2) - \beta - \xi_0$ , where  $\xi_0$  is the phase of  $a_1$ ,  $f = \Phi - \Phi_0$  and  $\Delta\mathcal{H} = \mathcal{H} - \mathcal{H}_0$ ; then we shall obtain (without accounting for damping of transverse-phase oscillations):

$$\frac{d\Delta\mathcal{H}}{dx} = \frac{h_q}{2HR} A_{10} \alpha (1 + \nu_0) (\cos \Phi - \cos \Phi_0) \approx -\frac{h_q A_{10} \alpha (1 + \nu_0) \sin \Phi_0}{HR} f, \quad (18')$$

$$\frac{df}{dx} = \alpha (v - v_0), \quad (18'')$$

$$\frac{h_q A_{10} \alpha (1 + v_0) \cos \Phi_0}{HR} = - \left( \frac{d\mathcal{E}}{dx} \right)_{ad} \approx \frac{\mathcal{E}_0}{P} \cdot \frac{dP}{dx}. \quad (18''')$$

After second differentiation of (18'') we obtain

$$\frac{d^2 f}{d(ax)^2} + \Omega^2 f = 0, \quad (19)$$

$$\Omega^2 = \left( \frac{\partial v}{\partial \mathcal{E}} \right)_0 \frac{h_q}{H} \cdot \frac{A_{10}}{R} (1 + v_0) \sin \Phi_0.$$

Here the factor  $\sin \Phi_0$ , absent in (15), allows for the acceleration of the particles. If the value of  $h_q/H$  is high enough, then  $\sin \Phi_0 \approx 1$ .

Equations (18') and (18'') have the integral of motion

$$\frac{1}{2} \left( \frac{d\Phi}{dax} \right)^2 - \frac{\Omega^2}{\sin \Phi_0} (\sin \Phi - \Phi \cos \Phi) = \text{const.} \quad (20)$$

For  $\cos \Phi_0 \approx 0$  the tolerable scatter in phase  $\Delta \Phi_{\max} \approx 2$ , and the tolerable scatter in the derivative

$$\Delta v_{\max} \approx \Omega. \quad (21)$$

The small oscillations around the orbit (11), (13) may be approximately represented in the form

$$r + iz = A_{10} e^{-iav_0 x} \left( 1 + \frac{b}{A_{10}} e^{-i\alpha x} - \frac{b^*}{A_{10}} e^{i\alpha x} + \frac{c}{A_{10}} e^{-i\alpha \Omega x} - \frac{c^*}{A_{10}} e^{i\alpha \Omega x} + \dots \right), \quad (22)$$

where  $b$  and  $c$  are arbitrary constants;  $\kappa = \mu - \mu_1 \approx 2\sqrt{2} v_0$ , in which  $|b|/A_{10} \leq \frac{1}{2}$ ,  $|c|/A_{10} \leq \frac{1}{2}$  are permissible. The last estimate follows both from the convergence of (22) and from (21). In fact, expanding in series,

$$e^{-i(av_0 x + \Delta \sin \alpha \Omega x)} \approx e^{-iav_0 x} (1 - \Delta \sin \alpha \Omega x + \dots) \quad (23)$$

and comparing with (22), we find  $\Delta = 2|c|/A_{10}$ ; on the other hand, the maximum derivative of the phase in (23) equals  $\alpha v_0 + \alpha \Omega \Delta = \alpha(v_0 + \Delta v_{\max})$ , i.e.,  $\Delta v_{\max} \approx \Omega \Delta$ , and, according to (21),  $\Delta \approx 1$ . These considerations lead to the following estimate of the phase volume  $\omega$  of the free oscillations around the spiral orbit:

$$\omega \leq A_{10}^2 \left( \frac{A_{10}}{R} \right)^2 M^2 v_0^2 \text{ cm}^2 \cdot \text{sr}. \quad (24)$$

#### Tolerances on Perturbation of the Field

Let there be a random azimuthal perturbation of the field with harmonic  $q + q'$  ( $v_0 = q/R\alpha$ ). In the presence of automatic phase stabilization we must consider this perturbation in the linearized equation for small oscillations around the helical orbit

$$\Delta \varphi'' + 2i\Delta \varphi' \alpha - \alpha^2 \Delta \varphi + \{3\gamma A_1^* e^{2i[(\alpha + \frac{q}{R})x + \beta]} + 6\gamma A_1^* A_3^* e^{-2i[(\alpha + \frac{q}{R})x + \beta]} + \dots\} \Delta \varphi^* = -\frac{\Delta h}{2HR} e^{-i[(\alpha + \frac{q+q'}{R})x + \delta]}. \quad (25)$$

This gives forced oscillations of the form

$$\Delta \varphi = b_1 e^{-i[(\alpha + \frac{q+q'}{R})x + \delta]} + c_1 e^{-i[(\alpha + \frac{q-q'}{R})x + 2\beta - \delta]} + b_3 e^{i[(3\alpha + \frac{3q+q'}{R})x + 2\beta + \delta]} + c_3 e^{i[(3\alpha + \frac{3q-q'}{R})x + 4\beta - \delta]} + \dots \quad (26)$$

If the frequency of the perturbation is close to one of the frequencies  $\mu_i$  of the linear oscillations  $(q + q')/R\alpha = \mu_i + \varepsilon$ , then

$$|b_1| \approx |c_1| \approx \frac{\Delta h}{HR\alpha^2} \cdot \frac{3}{8(\kappa + \varepsilon)^2} \cdot \frac{(4 + 3\nu_0)^2}{48 + 108\nu_0 + 54\nu_0^2}. \quad (27)$$

In the worst case, when  $\kappa = \Omega \approx \frac{k+1/2}{R\alpha}$ ,  $\varepsilon \sim 1/8R\alpha$ ,  $\nu_0 \approx \frac{1}{2}$ , we have the tolerance

$$\frac{|b_1|}{A_{10}} \ll 1, \quad \frac{\Delta h}{H} \cdot \frac{R}{A_{10}} \cdot \frac{1}{(k+1)^2} \ll 1. \quad (28)$$

### Coefficient of Expansion of the Orbit

Let us calculate the coefficient of expansion of the orbit  $\alpha_p = d \ln L / d \ln p$ . The changes in the synchrotron oscillations with respect to the ordinary accelerator reduce to a change in  $\alpha_p$ . For the synchrotron oscillation of momentum we must make the substitution

$$\frac{\Delta h}{H} \rightarrow -\frac{\Delta p}{p}, \quad q + q' = 0.$$

in (25) and (26). Then

$$b_1 = \frac{\Delta p}{p} \cdot \frac{1}{R\alpha^2\nu_0^2} \left[ \frac{(4 + 2\nu_0)^2 (16 + 56\nu_0 + 37\nu_0^2)}{3(4 + 3\nu_0)^2 (16 + 56\nu_0 + 37\nu_0^2) + 4(4 + 2\nu_0)^2 (4 + 4\nu_0^2)} \right]. \quad (29)$$

Here the expression in square brackets depends very weakly on  $\nu_0$ , varying from 0.14 to 0.18 for  $0 < \nu_0 < 1$ , and may be taken as one-sixth for  $\nu_0 \approx \frac{1}{2}$ .

The general solution of the equations of motion takes the form

$$\varphi = e^{-i\alpha x} (r + iz) = A_1 e^{-i(1+\nu_0)\alpha x} + A_3 e^{3i(1+\nu_0)\alpha x} + \dots + b_1 e^{-i\alpha x} + c_1 e^{-i(1+2\nu_0)\alpha x} + b_3 e^{i(3+2\nu_0)\alpha x} + \dots \quad (30)$$

Using (30) and averaging over  $x$ , we find

$$\langle r \rangle \approx b_1. \quad (31)$$

Whence

$$\alpha_p = \frac{\langle r \rangle}{R} \approx \frac{1}{6} \cdot \frac{1}{\alpha^2 R^2 \nu_0^2} = \frac{1}{6} q^{-2}. \quad (32)$$

### LITERATURE CITED

1. Yu. F. Orlov, ZhÉTF, 45, 932 (1963).
2. Yu. F. Orlov, ZhÉTF, 43, 1308 (1962).
3. B. V. Chirikov, DAN SSSR, 125, 1015 (1959).
4. Yu. F. Orlov, in: Proceedings of the International Conference on Accelerators, Dubna, 1963 [in Russian] (Atomizdat, Moscow, 1964), p. 90.



## INTRODUCTION OF AN ION BEAM INTO THE CYCLOTRON

(UDC 621.384.11)

V. A. Gladyshev, L. N. Katsaurov, A. N. Kuznetsov,  
L. P. Martynova, and E. M. Moroz

Translated from *Atomnaya Énergiya*, Vol. 18, No. 3,

pp. 213-218, March, 1965

Original article submitted March 19, 1964

The external injection of ions into the sectoral cyclotron is described. The ion beam is injected into the magnetic field in the median plane, and is conveyed without loss to the accelerating gap of the D's.

The external injection of ions into the cyclotron is of special present interest in connection with the problem of accelerating polarized ions, since sources of polarized particles, just as certain other complex ion sources, cannot be placed in the center of the cyclotron. Since, for external injection, acceleration begins from some initial energy, it is possible thereby to avoid the difficulties associated with the first turns in the central part of the cyclotron.

One means of solving this problem is to introduce the beam along the vertical axis of the cyclotron and rotate it by an electrostatic deflecting system through  $90^\circ$  in the median plane [1]. The most serious failings of axial beam input would appear to be the considerable particle loss and the complexity of the deflecting system.

In this paper we show that external injection of the beam can be achieved in the median plane of the magnet. This may be done especially simply in sectoral cyclotrons. The beam may here be taken right up to the accelerating gap between the D's almost without loss, which is particularly important for polarized particles. As we know, in an inhomogeneous magnetic field, charged particles experience drift across the gradient of the magnetic field. This may conveniently be used in a sectoral cyclotron, the particle beam being so directed as to drift up to the central region of the cyclotron along the boundary of one of its sectors.

In effecting external injection in the median plane of the sectoral cyclotron, the following conditions must be satisfied: 1) the initial injection conditions must be so chosen that the beam will not become defocused on entry into the magnetic field of the cyclotron; 2) the drift of particles toward the central region of the cyclotron should preserve the focusing of the beam; 3) in the central region, the particles being injected should be passed on to the calculated trajectory from which acceleration is subsequently to begin. Let us consider these problems in order.

In order to determine the conditions of motion of the charged particles in the inhomogeneous magnetic field for which focusing forces appear, let us consider the solution of the general motion of charged particles in a magnetic field

$$\mathbf{F} = \frac{e}{c} [\bar{v} \cdot \bar{H}]. \quad (1)$$

In a rectangular system of coordinates, let the y axis lie along the edge of the magnet, the x axis perpendicular to the edge in the direction of the field gradient, and the z axis perpendicular to the median plane of the magnetic field. Then the equation of motion of the particles in the vertical plane will take the form

$$m\ddot{z} = \frac{e}{c} (\dot{x}H_y - \dot{y}H_x). \quad (2)$$

Since the gradient of the field is directed along the x axis,  $H_y = 0$ . Expanding  $H_x$  in series and retaining only the first term for small z, and also using the condition  $\text{rot } H = 0$ , we obtain from expression (2)

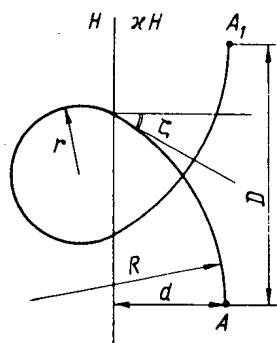


Fig. 1. Scheme of charged particle drift along the boundary of magnetic fields  $H$  and  $xH$ .

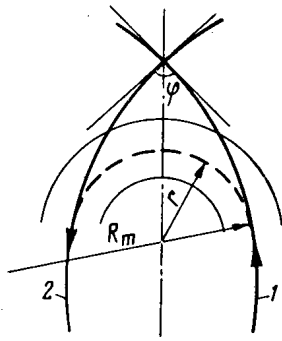


Fig. 2. Transfer of charged particles in the magnetic field from one trajectory to another by means of a cylindrical electrostatic field.

$$m\ddot{z} = -y \frac{\partial H_x}{\partial x} z. \quad (3)$$

It follows from this equation that, if the trajectory deviates from the median plane at a particular point in the inhomogeneous field, there is a focusing force when the center of curvature of the trajectory passing through that point and the magnetic field gradient vector proceeding from the point lie on the same side of the trajectory [2]. Thus, on introducing a beam into the magnetic field, in one half of the region between the sectors in the sector cyclotron (see region 1 in Fig. 4) there is a focusing force, while for the second region (see region 2 in Fig. 4) the force is defocusing, i.e., the beam must be introduced into the magnetic field in region 1.

Some general conclusions regarding focusing during the drift of particles along the edge of the magnetic sector may be drawn in the following way. Let us suppose that the field intensity in the sector is  $H$  and in the gaps  $\kappa H$ , where  $\kappa = \text{const} < 1$ . Using the notation of Fig. 1, we may write

$$\zeta = \arctan \tau,$$

where

$$\tau = \frac{1 - \xi}{\sqrt{1 - (1 - \xi)^2}}, \quad \xi = \frac{d}{R}, \quad (4)$$

the loop periodicity being

$$D = 2r \frac{1 - \kappa}{\kappa} \sqrt{1 - (1 - \xi)^2}. \quad (5)$$

Here  $r$  is the radius of curvature in the field  $H$ , and  $R$  is that in the field  $\kappa H$  ( $R = r/\kappa$ ). On the way to the central region of the cyclotron, the beam may describe a series of loops. The length of each loop is

$$L = \pi r \frac{1 + \kappa}{\kappa} \left( 1 - \frac{2\zeta}{\pi} \cdot \frac{1 - \kappa}{1 + \kappa} \right), \quad (6)$$

and the frequency of "revolution" of the particles (or, more precisely the frequency of describing loops), equals

$$\omega = \frac{2\pi\beta c}{L} = \frac{z_e H}{m_0 c \gamma} \cdot \frac{1}{\frac{1 + \kappa}{2\kappa} - \frac{\zeta}{\pi} \cdot \frac{1 - \kappa}{\kappa}}, \quad \gamma = \frac{1}{\sqrt{1 - \beta^2}}. \quad (7)$$

The quality of the magnetic focusing of the particles is characterized by the ratio of frequencies  $\omega_r$  and  $\omega_z$  (horizontal and vertical particle oscillations) to frequency  $\omega$

$$\frac{\omega_{r,z}}{\omega} = \frac{\mu_{r,z}}{2\pi}, \quad \cos \mu_{r,z} = \frac{A_{11}^{r,z} + A_{22}^{r,z}}{2}. \quad (8)$$

Here,  $A_{j,k}^{r,z}$  are the matrix elements of matrix  $A^{r,z}$  of the horizontal and vertical betatron oscillations, characterizing the change in coordinates on negotiating the loop:

$$\begin{pmatrix} y \\ y' \end{pmatrix}_{\text{at point A}} = A^r \begin{pmatrix} y \\ y' \end{pmatrix}_{\text{at point A}_1},$$

$$\begin{pmatrix} z \\ z' \end{pmatrix}_{\text{at point A}} = A^z \begin{pmatrix} z \\ z' \end{pmatrix}_{\text{at point A}_1}, \quad (9)$$

where  $y$  and  $z$  are, respectively, the horizontal and vertical deviations of the particle,  $y' = dy/dl$ ,  $z' = dz/dl$  (here,  $dl$  is the element of trajectory length).

The matrix  $A^r$  is not difficult to find, on calculating the product of six matrices:

$$A^r = \begin{pmatrix} s & \frac{r}{\kappa} c \\ -\frac{\kappa c}{r} & s \end{pmatrix} \begin{pmatrix} 1 & 0 \\ \frac{\tau(1-\kappa)}{r} & 1 \end{pmatrix} \begin{pmatrix} -s & rc \\ -\frac{c}{r} & -s \end{pmatrix} \begin{pmatrix} -s & rc \\ -\frac{c}{r} & -s \end{pmatrix} \begin{pmatrix} 1 & 0 \\ \frac{\tau(1-\kappa)}{r} & 1 \end{pmatrix} \begin{pmatrix} s & \frac{r}{\kappa} c \\ -\frac{\kappa c}{r} & s \end{pmatrix} \\ = \begin{pmatrix} 1 & 0 \\ \frac{r\kappa(1-\kappa)\tau}{r} & 1 \end{pmatrix} \quad (10)$$

Here we have used the following notation:

$$s = \sin \zeta = 1 - \xi, \quad c = \cos \xi = \sqrt{1 - (1 - \xi)^2}, \quad \tau = \tan \zeta = \frac{s}{c}. \quad (11)$$

The radial focusing of ions in the magnetic system considered differs little from focusing in a homogeneous magnetic field, since

$$\cos \mu_r = A_{11}^r = A_{22}^r = 1, \quad \mu_r = 2\pi, \quad \frac{\omega_r}{\omega} = 1. \quad (12)$$

Carrying through the corresponding calculations for the vertical focusing of the ions, we obtain

$$A^z = \begin{pmatrix} 1 & \frac{r}{\kappa} \left( \frac{\pi}{2} - \zeta \right) \\ 0 & 1 \end{pmatrix} \begin{pmatrix} 1 & 0 \\ -\frac{\tau}{2} (1-\kappa) & 1 \end{pmatrix} \begin{pmatrix} 1 & r \left( \frac{\pi}{2} + \zeta \right) \\ 0 & 1 \end{pmatrix} \begin{pmatrix} 1 & r \left( \frac{\pi}{2} + \zeta \right) \\ 0 & 1 \end{pmatrix} \begin{pmatrix} 1 & 0 \\ -\frac{\tau}{2} (1-\kappa) & 1 \end{pmatrix} \\ \times \begin{pmatrix} 1 & \frac{r}{\kappa} \left( \frac{\pi}{2} - \zeta \right) \\ 0 & 1 \end{pmatrix} = \begin{pmatrix} a_{11} & a_{12} \\ a_{21} & a_{22} \end{pmatrix} \begin{pmatrix} a_{22} & a_{12} \\ a_{21} & a_{11} \end{pmatrix} = \begin{pmatrix} A_{11}^z & A_{12}^z \\ A_{21}^z & A_{22}^z \end{pmatrix}, \quad (13)$$

and, hence,

$$\cos \mu_z = A_{11}^z = A_{22}^z = 2a_{11}a_{22} - 1. \quad (14)$$

Here,

$$a_{11} = 1 - \frac{1-\kappa}{\kappa} \tau \left( \frac{\pi}{2} - \zeta \right), \quad (15)$$

$$a_{22} = 1 - (1-\kappa) \tau \left( \frac{\pi}{2} + \zeta \right). \quad (16)$$

Putting (15) and (16) into (14), we find

$$\cos \mu_z = 1 - \frac{1-\kappa^2}{\kappa} \tau \left[ \pi - 2\zeta \frac{1-\kappa}{1+\kappa} - \frac{1-\kappa}{1+\kappa} \frac{\tau}{2} (\pi^2 - 4\zeta^2) \right]. \quad (17)$$

The conditions for the stability of vertical motion of the ions  $|\cos \mu_z| \leq 1$  take the form

$$0 \leq \tau \left( \pi \frac{1+\kappa}{1-\kappa} - 2\zeta \right) - \frac{\tau^2}{2} (\pi^2 - 4\zeta^2) \leq \frac{2\kappa}{(1-\kappa)^2}. \quad (18)$$

This inequality was evaluated numerically for an actual field, and the calculations showed that the region of stability was approximately characterized by the inequalities

$$1 - \kappa < \xi \leq 1, \quad (19)$$

somewhat more severe than (18). It follows from analysis of the inequalities that there always exists a wide interval of initial conditions for which the ions being injected may be brought up to the central region without experiencing defocusing.

It is always possible to transfer the particles to the calculated trajectory in the central region of the cyclotron by means of the electric field of a cylindrical condenser. For simplicity, let us consider motion in a homogeneous

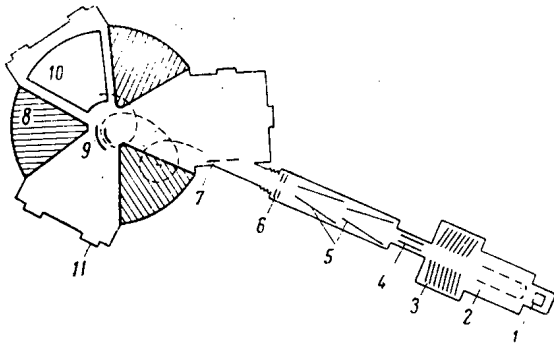


Fig. 3. Arrangement of sector cyclotron. 1) Source; 2) system of electrostatic focusing lenses; 3) accelerating tube; 4,5) control electrodes; 6,7) movable diaphragms; 8) magnet sectors; 9) cylindrical condenser for deviating the beam; 10) D; 11) windows for observation and photography.

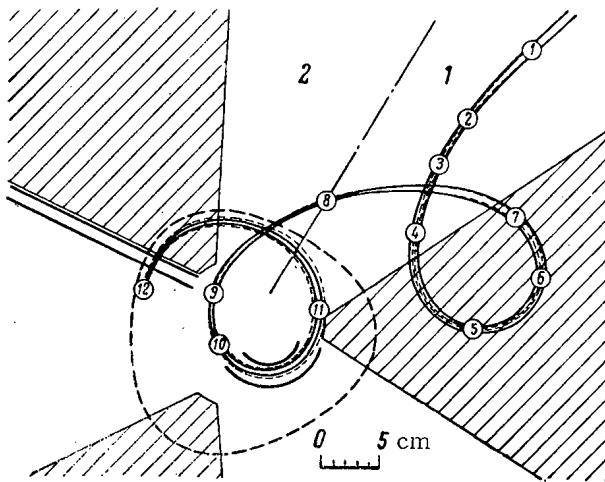


Fig. 4. Trajectory of the beam for external injection. Continuous lines correspond to dimensions of beam in median plane, dashed lines to dimensions in the vertical; the closed dashed line shows the equilibrium orbit for 40-keV deuterons; the numbers on the trajectory show the points at which the beam was photographed.

At the same time, the focusing of the beam in the median plane and along the vertical was examined, the calculations showing that focusing was completely satisfactory. The experimental trajectory was in good agreement with the calculations.

Experiments were made with  $H_2^+$  ions from a Penning-type source, focused by a system of electrostatic lenses to an energy of 30 keV by a small accelerating tube. The energy scatter was  $\pm 0.1\%$ . The beam was guided on its way to the accelerating chamber by a system of deflecting plates and movable diaphragms.

For separating the beam with respect to mass, the fringe field of the cyclotron itself was used. The siting of the diaphragm separating out a beam of the desired mass was calculated from the formula

$$h_m = \frac{l^2}{2} \sum_{k=1}^m \frac{2(m-k)+1}{R_k}, \quad (22)$$

giving the total beam deviation  $h_m$  in the fringe magnetic field from the rectilinear trajectory. This formula is derived on the assumption that the whole trajectory in the fringing field is divided into  $m$  parts, such that the length  $l$

magnetic field, such as almost always exists in the central region. Let us suppose that we require to move the particles from trajectory 1 to trajectory 2 (Fig. 2). The radius of curvature of these trajectories is  $R_m$ . Thus, the problem reduces to finding the circles with radius  $r$  inscribed in this trajectory, and this is always possible. The geometric locus of the centers of these circles is on the bisectrix of the angle  $\varphi$  at the point of intersection of trajectories 1 and 2. The radius of curvature of a charged particle moving in mutually perpendicular electric and magnetic fields may be expressed as

$$r = \frac{R_m R_e}{R_m + R_e}, \quad (20)$$

where  $R_m = 4.57 \cdot 10^3 (WM)^{1/2} / H$  (in the nonrelativistic case),  $R_e =$  radius of curvature in the electric field ( $R_e = 2W / \epsilon$ ). Here  $W$  is the kinetic energy in keV,  $\epsilon$  is the electric field strength in kV/cm,  $M$  is the mass of the ion in nucleon mass units.

The minimum voltage on the cylindrical condenser required to take the particles from trajectory 1 to trajectory 2 may be calculated from the formula

$$\epsilon_{\min} = \frac{2W}{R_m} \cdot \frac{\cos \varphi/2}{1 - \cos \varphi/2}. \quad (21)$$

In this case,  $r$  has a maximum value. If, for constructional or other reasons, the condenser cannot be sited in the place where  $\epsilon = \epsilon_{\min}$ , it may be put in some other suitable place, but this will require a greater electrical field strength. In our experiments,  $\epsilon = 6.5$  kV/cm.

An experimental check of the possibility of external injection by the means indicated was made on a three-sector cyclotron with straight sector edges. The diameter of the magnet was 720 mm. It is proposed to accelerate deuterons to an energy of 350 keV in the cyclotron. The general scheme of the apparatus appears in Fig. 3. Numerical calculations on an electronic computer enabled us to determine the range of initial conditions of insertion for which the particles moving in the actual field of the cyclotron would reach the required region. At the same

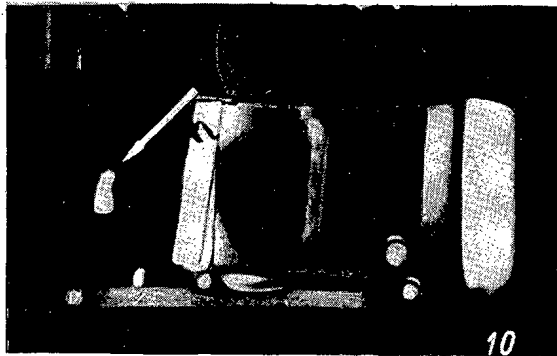
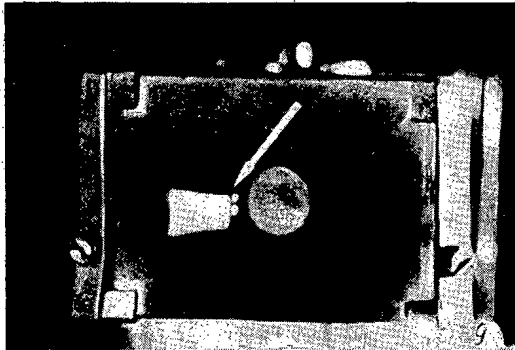
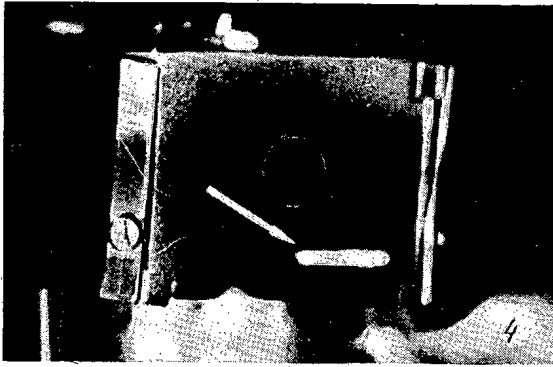


Fig. 5. Photographs of the trace of the beam on the quartz at points 4, 9, and 10 (see Fig. 4).

Figure 5 shows photographs in which the shape of the beam cross section can be seen at certain characteristic points. The numbers on the photographs correspond to those on the trajectory of Fig. 4, and indicate the place in which the photograph was taken. The Faraday cylinder with aperture can be seen in the photographs. This was 18 mm long in the vertical direction and 29 mm in the horizontal. The aperture diameter was 5 mm. The arrows indicate the points at which the quartz luminesced under the action of the beam. The best luminescence of the quartz was selected each time, and for this reason the photographs show the beam at different points of the Faraday cylinder.

The beam was 5 x 5 mm in size on entering the accelerating chamber, and its vertical extent fell to 1.2 (dashed line in Fig. 4) on entering the gap between the sectors (point 4). Before emerging from the sector it broadened to 4 mm and then, coming out of the sector, it again contracted to 3 mm at point 8. On the second turn, the trajectory passed through a short section in a defocusing field, and this broadened the beam in the vertical sense to 12 mm on emerging from the cylindrical condenser. Then it again contracted to 5 mm in the region of the accelerating gap of the D's. In the median plane (continuous lines in Fig. 4), the beam was again quite well focused. On the first turn, the beam width did not exceed 9 mm, and on emerging from the sector the beam contracted to 0.8 mm (at point 8). Then it broadened to 4.5 mm at point 9 and again contracted to 2 mm at the entrance into the cylindrical condenser. From the condenser, the beam emerged broadened to 4 mm, and at the accelerating gap again contracted to 1.5 mm. It is interesting to note that the beam is focused to minimum dimensions in both the vertical and horizontal direction at point 8.

of each is  $l \ll R_m$  (mean radius of curvature of the trajectory in that section). Experiment showed that this formula could be satisfactorily applied to calculate the site and size of the separating diaphragms.

The position of the beam in the chamber and its parameters were determined by means of a Faraday cylinder with inlet diameter 50 mm. The cylinder could be placed in any part of the accelerating chamber at the necessary angle to the beam. This was achieved by means of a ball-and-socket joint in a Teflon seal and a movable rod in a Teflon seal of the Wilson type. The Faraday cylinder could also be rotated through 360° around its vertical axis. This arrangement made it possible to determine the direction of the beam, its dimensions, and the value of the current along the whole trajectory. The outer walls of the Faraday cylinder were covered with quartz plates. The luminescence of the quartz facilitated visual observation and photography of the beam and the determination of its cross section.

Figure 4 shows a beam trajectory traced by the means described. Here, the distance between the continuous lines reflects the beam cross section in the median plane, and the distance between the dashed lines indicates the vertical beam cross section.

By varying the voltage on the focusing system of the source over a slight range (in our experiments the voltage was about 2 kV), the beam can be focused in various parts of the camera, beginning from the entrance diaphragm and ending with the accelerating gap of the D's. At the entrance into the accelerating chamber the beam is defined by the entrance diaphragm. In our experiments, the diaphragm was 5 x 5 mm in size. The cross section of the beam was such as to permit 90% to pass through the diaphragm.

In the present experiment,  $\xi = 0.5$ ,  $\kappa = 0.6$ , and condition (19) was hence satisfied right up to the central region of the magnet. The beam indeed proved to be well-focused, as shown by Figs. 4 and 5.

The current at the entrance into the accelerating chamber was  $1.5 \mu\text{A}$ , and this passed right up to the accelerating gap between the D's without loss. Afterwards the beam was accelerated. One  $60^\circ$ -sector D was employed. The accelerating voltage was 15 kV at a frequency of 3 Mc/sec. The voltage from the generator was fed to a quarter-wave helical line at the end of which lay the D. After the first two turns, the current in the accelerated beam was  $0.3 \mu\text{A}$ , i.e., 20% of the current fed to the D. This coincided with the estimate for the capture efficiency in the accelerating condition. Subsequently, acceleration proceeded almost without loss, and the beam current observed at radius 28 cm was also  $0.3 \mu\text{A}$ .

The authors are grateful to A. A. Kolomenskii for useful discussions.

#### LITERATURE CITED

1. A. Fox et al., Nucl. Instrum. and Methods, No. 18, 19; 25 (1962).
2. J. Livingood, Principles of the Operation of Cyclical Accelerators [Russian translation] (IL, Moscow, 1963).

## QUASICLASSICAL MODEL OF TERNARY FISSION

(UDC 539.173)

B. T. Geilikman and G. I. Khlebnikov

Translated from *Atomnaya Énergiya*, Vol. 18, No. 3,  
pp. 218-223, March, 1965

Original article submitted February 24, 1964

In this paper, the classical model of ternary fission with the emission of an  $\alpha$ -particle, taking account of the  $\alpha$ -particle energy distribution in the fissioned nucleus is investigated. The energy and angular distributions of the emitted  $\alpha$ -particles are calculated. The theoretical distributions agree satisfactorily with the experimental data.

Ternary fission with the emission of  $\alpha$ -particles was discussed theoretically in [1], in which the classical model of three osculating spheres (two fission fragments and an  $\alpha$ -particle) was used. For this, it was assumed that the center of the  $\alpha$ -particle was not located on the straight line joining the centers of the fission fragments, and that the initial velocity of the  $\alpha$ -particle was equal to zero.

In the present paper, the classical model is considered also for ternary fission with the emission of an  $\alpha$ -particle, since the parameters  $2Z_1e^2/\hbar v_\alpha$ ,  $2Z_2e^2/\hbar v_\alpha$ , and  $Z_1Z_2e^2/\hbar v_\alpha$  are large in comparison with unity ( $v_\alpha$  is the velocity of the  $\alpha$ -particle;  $v$  is the velocity of the relative motion of the fission fragments). In accordance with modern concepts of the nucleus, it can be assumed that the  $\alpha$ -particle, which exists in a state of oscillation in the nucleus, has a certain probability as an individual complex in the neck of the fissioning nucleus, where the diameter of the neck becomes of the order of the  $\alpha$ -particle dimensions. As a result of this, in contrast to Tsien's model [1], the  $\alpha$ -particle obviously will be found on the straight line joining the centers of the fission fragments. Because of deformation of the fissioning nucleus, the Coulomb barrier for the  $\alpha$ -particle in the neck region is reduced and simultaneously the depth of the nuclear potential well is decreased. This decrease is particularly significant in the later stages when the thickness of the neck coincides with the diameter of the  $\alpha$ -particle, since, as a result of this, the  $\alpha$ -particle is not surrounded by nucleons from the peripheral side. According to an estimate based on a calculation of the shape of the fissioning nucleus by the water droplet method (see [2]), the Coulomb barrier in the center of the neck prior to scission is 20-25% less than in the nondeformed nucleus. Since the triggering time from the saddle point to the point of scission of the neck is considerably greater than the nuclear time and, consequently, the process of deformation of the nucleus is adiabatic [2], the increase of the floor of the potential well is also adiabatic and, therefore, the energy of the  $\alpha$ -particle measured from the floor of the potential well, i.e., its kinetic energy, remains unchanged. Thus, by lowering the Coulomb barrier and increasing the floor of the potential well in the region of values of the neck thickness close to the diameter of the  $\alpha$ -particle, the energy of the  $\alpha$ -particle may prove to be higher than the barrier and, consequently, the particle is ejected from the nucleus.

It should be noted that for the  $\alpha$ -active nuclei being considered, even in the case of nondeformation of the nucleus, the energy of the  $\alpha$ -particle is positive and is equal to the decay energy. Emission of an  $\alpha$ -particle obviously leads automatically to scission of the neck and to the formation of fission fragments. Thus, in the model being considered, a significant role in the emission of the  $\alpha$ -particle is played by its initial kinetic energy and not by the potential energy as in the model in [1].

In order to calculate the energy and angular distribution of the  $\alpha$ -particles, it is necessary to integrate the equations of motion of the fission fragments and of the  $\alpha$ -particle:

$$M_1 \frac{d^2 \bar{r}_1}{dt^2} = -\text{grad}_{\bar{r}_1} U, \quad M_2 \frac{d^2 \bar{r}_2}{dt^2} = -\text{grad}_{\bar{r}_2} U, \quad m_\alpha \frac{d^2 \bar{r}_\alpha}{dt^2} = -\text{grad}_{\bar{r}_\alpha} U. \quad (1)$$

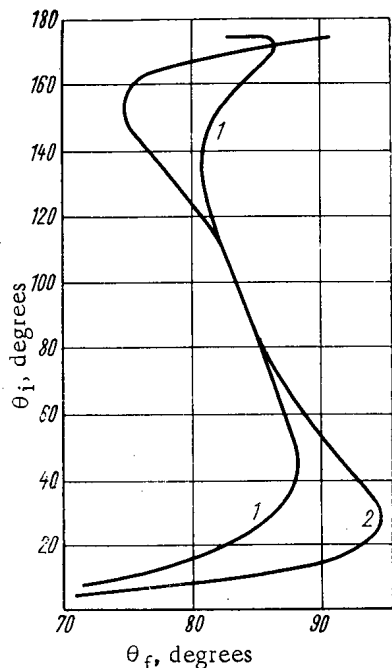


Fig. 1. Relationship between  $\theta_i / (\theta_f)$  for thermal neutron fission of  $U^{235}$ : 1)  $E_\alpha^0 = 0.5$  MeV; 2)  $E_\alpha^0 = 2.0$  MeV.

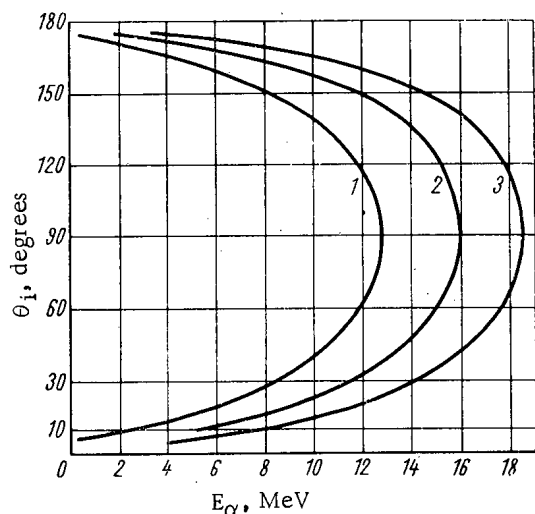


Fig. 2. Relationship between  $\theta_i(E_\alpha^f)$  for the case of thermal neutron fission at different values of  $E_\alpha^0$ : 1) 0.2 MeV; 2) 0.5 MeV; 3) 1.0 MeV.

taken from [2]:  $\alpha_2^{(i)} = 0.26$ ;  $\alpha_3^{(i)}$  varies as a function of the magnitude of the ratio  $A_1/A_2$  (0.079-0.086).

The equations of motion in dimensionless variables were twice independently programmed by the Runge-Kutta method for integrating a system of ordinary differential equations, after which numerical calculations were carried out on the computer.

For the initial conditions, the values were used of the  $\alpha$ -particle energy above the barrier value  $E_\alpha^0 = 0-2$  MeV and the equilibrium distribution of the initial velocities of the  $\alpha$ -particles with respect to direction. The initial velocity of the fission fragments was calculated in accordance with the experimental value for the kinetic energy of the fission fragments for ternary fission and for a mass ratio selected in accordance with [3]. Since the  $\alpha$ -particle

The expression for U was taken from [2]:

$$\begin{aligned}
 U = & \frac{Z_1 Z_2}{a} \cdot \frac{e^2}{r_0} \left\{ 1 + \frac{3}{5a^2} \sum_{i=1}^2 \alpha_2^{(i)} A_i^{2/3} + \frac{3}{7a^3} \sum_{i=1}^2 \alpha_3^{(i)} A_i \right. \\
 & + \frac{3}{35a^2} \sum_{i=1}^2 [\alpha_2^{(i)}]^2 \left( 4A_i^{2/3} + \frac{3A_i^{4/3}}{a^2} \right) \\
 & + \frac{3}{7a^2} \sum_{i=1}^2 [\alpha_3^{(i)}]^2 \left( \frac{8}{15} A_i^{2/3} + \frac{3}{11} \cdot \frac{A_i^{4/3}}{a^2} + \frac{200}{429} \cdot \frac{A_i^2}{a^4} \right) \\
 & + \sum_{i=1}^2 \alpha_2^{(i)} \alpha_3^{(i)} \left( \frac{4}{7} \cdot \frac{A_i}{a_3} + \frac{5}{11} \cdot \frac{A_i^{5/3}}{a^5} \right) + \frac{18}{7a^5} \\
 & \times (\alpha_2^{(1)} \alpha_3^{(2)} A_1^{2/3} A_2 + \alpha_2^{(2)} \alpha_3^{(1)} A_1 A_2^{2/3}) + \frac{54}{25} \cdot \frac{\alpha_2^{(1)} \alpha_2^{(2)} (A_1 A_2)^{2/3}}{a^4} \\
 & + \frac{180}{49} \cdot \frac{\alpha_3^{(1)} \alpha_3^{(2)} A_1 A_2}{a^6} \left. \right\} + \frac{Z_1 Z_\alpha}{a_1} \cdot \frac{e^2}{r_0} \\
 & \left\{ 1 + \frac{3}{5a_1^2} \alpha_2^{(1)} A_1^{2/3} + \frac{3}{7a_1^3} \alpha_3^{(1)} A_1 + \frac{3}{35a_1^2} [\alpha_2^{(1)}]^2 \right. \\
 & \times \left( 4A_1^{2/3} + \frac{3A_1^{4/3}}{a_1^2} \right) + \frac{3}{7a_1^2} [\alpha_3^{(1)}]^2 \left( \frac{8}{15} A_1^{2/3} \right. \\
 & + \frac{3}{11} \cdot \frac{A_1^{4/3}}{a_1^2} + \frac{200}{429} \cdot \frac{A_1^2}{a_1^4} \left. \right) \left. \right\} + \frac{Z_2 Z_\alpha}{a_2} \cdot \frac{e^2}{r_0} \\
 & \times \left\{ 1 + \frac{3}{5a_2^2} \alpha_2^{(2)} A_2^{2/3} + \frac{3}{7a_2^3} \alpha_3^{(2)} A_2 + \frac{3}{35a_2^2} \right. \\
 & \times [\alpha_2^{(2)}]^2 \left( 4A_2^{2/3} + \frac{3A_2^{4/3}}{a_2^2} \right) + \frac{3}{7a_2^2} [\alpha_3^{(2)}]^2 \\
 & \times \left( \frac{8}{15} A_2^{2/3} + \frac{3}{11} \cdot \frac{A_2^{4/3}}{a_2^2} + \frac{200}{429} \cdot \frac{A_2^2}{a_2^4} \right) \left. \right\}
 \end{aligned}$$

Here,  $Z_i, \alpha$  and  $A_i = M_i/m$  are the atomic numbers and atomic weights of the fission fragments, respectively, where  $i = 1, 2$  and  $m$  is the mass of the nucleon;  $\alpha_2^{(i)}$  and  $\alpha_3^{(i)}$  are the quadrupolar and octupolar deformation parameters of the fission fragments, respectively;  $r_0 = 1.2 \cdot 10^{-13}$  cm;  $a_1 r_0 = d$  is the distance between the centers of gravity of the heavy fragments;  $a_1 r_0 = d_1$  is the distance between the centers of gravity of the first fission fragment and the  $\alpha$ -particle;  $a_2 r_0 = d_2$  is the distance between the centers of gravity of the second fission fragment and the  $\alpha$ -particle.

We shall neglect the change of  $\alpha_2^{(i)}$  and  $\alpha_3^{(i)}$  as a result of motion of the fission fragments and the  $\alpha$ -particle, since, by increasing  $d, d_1,$  and  $d_2,$  the effect of the quadrupole and octupole potentials become insignificant. The shape of the fissioning nucleus at the instant of scission of the neck, i.e., the values of  $\alpha_2^{(i)}$  and  $\alpha_3^{(i)}$  for the fission fragments, are also



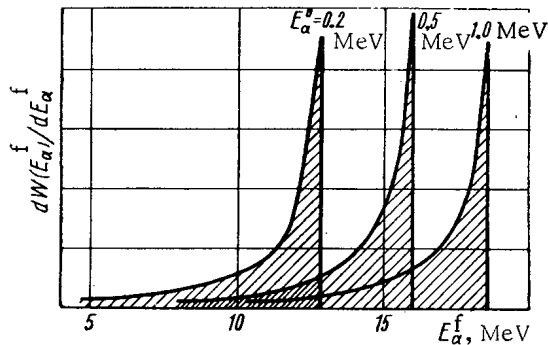


Fig. 3. Energy distribution of  $\alpha$ -particles from ternary fission of  $U^{235}$  for different values of  $E_{\alpha}^0$ .

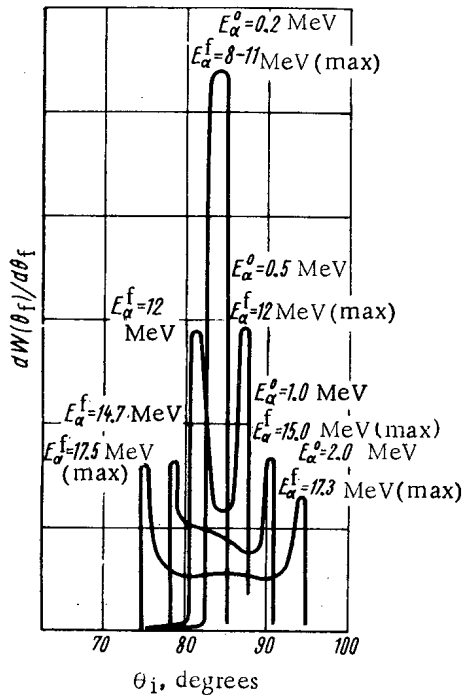


Fig. 4. Angular distribution of  $\alpha$ -particles from ternary fission of  $U^{235}$  for different values of  $E_{\alpha}^0$ .

1.47. The results of the energy and angular distribution calculations for these same cases are presented in Figs. 3 and 4. The spread of the angular distribution at the maximum due to quantum effects is computed in Fig. 4. Figure 5 shows for comparison the energy distribution of the  $\alpha$ -particle from ternary fission for  $E_{\alpha}^0 = 0.5$  MeV for three nuclei:  $U^{235}$  for thermal neutron fission and  $Cm^{242}$  and  $Cf^{252}$  as a result of spontaneous fission. Moreover, calculations were carried out for the purpose of explaining the effects of fluctuations of the site of emission of the  $\alpha$ -particle from the neck of the fissioning nucleus.

It can be seen from Fig. 3 that  $E_{\alpha}^f$  increases sharply for a small increase of  $E_{\alpha}^0$ . This result is easily explained. It is obvious that the energy  $E_{\alpha}^f$  should be a maximum if the fission fragments were stationary and it should be close to zero if, at the initial instant,  $v_{\alpha}/v_{ff} \ll 1$  ( $v_{ff}$  is the velocity of the fission fragments, and  $v_{\alpha}$  is the velocity of the  $\alpha$ -particle). Actually,  $v_{\alpha} \approx (2E_{\alpha}^f/m_{\alpha})^{1/2}$  and  $v_{ff} \approx (2E_{ff}/m_{ff})^{1/2}$  are values of a single order ( $E_{\alpha} \approx 15-20$  MeV;  $E_{ff} \approx 150$  MeV). Consequently,  $E_{\alpha}^f$  is increased sharply even for a small increase of  $E_{\alpha}^0$ , i.e., as a result of increasing  $v_{\alpha}^0/v_{ff}^0$ . The broadening of the angular distribution of the  $\alpha$ -particles observed in Fig. 4 as a result of increasing  $E_{\alpha}^0$  is also easily explained:  $\alpha$ -particles, emitted at angles close to zero and  $\pi$ , at a large initial energy  $E_{\alpha}^0$ , overcome more easily the repulsion of the fission fragments, which returns the  $\alpha$ -particle to an angle close to  $\pi/2$ ; in view of this, the angular distribution is found to be wider than at small values of  $E_{\alpha}^0$ .

distribution with respect to energy is not sufficiently well known, even in the undeformed nucleus, and the decrease of depth of the nuclear potential well in the region of the neck is also unknown, the calculations were carried out on the assumption that the distribution with respect to the energy of the  $\alpha$ -particle above the barrier is constant up to a certain maximum energy  $E_{\alpha}^0 \max$ . The best agreement of the calculated with the experimental results is observed at an energy  $E_{\alpha}^0 \max = 1.0$  MeV. This is explained as follows: when, because of deformation of the nucleus, the barrier  $V_k$  is reduced to the value of the maximum kinetic energy  $T_{\max}$  of the  $\alpha$ -particle in the nucleus, the probability of emission of an  $\alpha$ -particle for  $V_k = T_{\max}$  is still very small because of the small volume of the phase space of the  $\alpha$ -particles. Only for a considerable excess of  $T_{\max}$  over  $V_k$  is this probability found to be sufficiently large.

For an  $\alpha$ -particle, whose velocity at the initial instant of motion forms an angle  $\theta_i$  with the direction of motion of the light fission fragment, the probability of finding this same fission fragment at the end of a path at an angle  $\theta_f$  to the direction of motion is determined, obviously, by the formula:

$$dW(\theta_f) = \frac{1}{2} \sin \theta_i (\theta_f) \frac{d\theta_i}{d\theta_f} d\theta_f.$$

Hence it is easy to understand that the distribution with respect to energy will have the form

$$dW(E_{\alpha}^f) = \frac{1}{2} \sin \theta_i (E_{\alpha}^f) \frac{d\theta_i}{dE_{\alpha}^f} dE_{\alpha}^f,$$

where  $E_{\alpha}^f$  is the final energy of the  $\alpha$ -particle.

Calculations were carried out for the compound nuclei  $U^{235}$ ,  $Pu^{240}$ ,  $Cm^{242}$ , and  $Cf^{252}$  for the most probable mass ratio of the heavy fragments as well as for mass ratios  $A_1/A_2$  equal to 1.1, 1.25, and 1.9.

Figures 1 and 2 show the results of numerical calculations for  $\theta_i(\theta_f)$  and  $\theta_i(E_{\alpha}^f)$  in the case of thermal neutron fission of  $U^{235}$  for the most probable value of the ratio  $A_1/A_2$  equal to

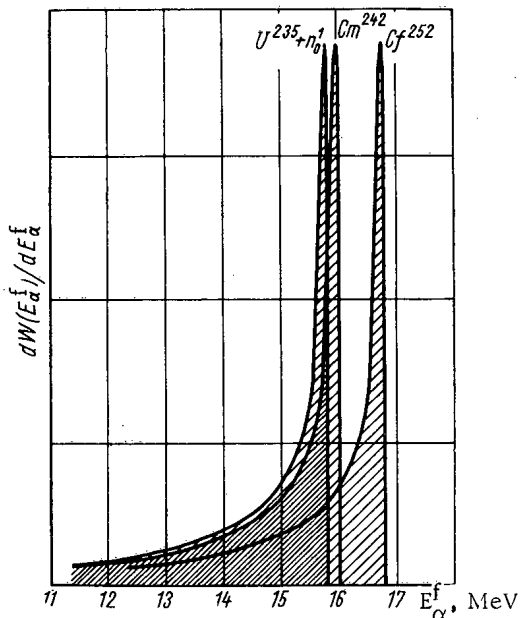


Fig. 5. Energy distribution of  $\alpha$ -particles from ternary fission for  $U^{235} + n_0^1$   $\frac{A_1}{A_2} = \frac{129}{103}$  ;  
 $Cm_{spont}^{242} \frac{A_1}{A_2} = \frac{132}{106}$  ;  $Cf_{spont}^{252} \frac{A_1}{A_2} = \frac{138}{110}$

distribution according to initial energy was assumed to be in the form of a "step" for which the existence of an  $\alpha$ -particle "tail" with high energies was not taken into account.

Averaging of the fission fragments with respect to mass ratios, point of emission, thickness, and, consequently also, with respect to the length of the neck, should also lead to broadening of the distribution curve. The calculated angular distribution, as well as the experimental distribution, is observed to be broader with increase of  $\alpha$ -particle energy (see Fig. 4).

In the thermal neutron fission of  $U^{235}$  within the range  $E_{\alpha}^0 = 0-1.0$  MeV, the calculated energy distribution of the  $\alpha$ -particles (see Fig. 7) agrees well with the experimental data of [4]. However, for this the maximum energy of

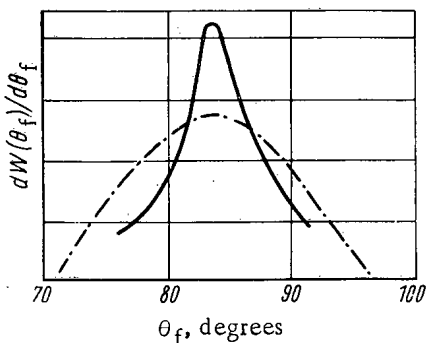


Fig. 6. Calculated spectrum of the angular distribution of  $\alpha$ -particles from ternary fission of  $U^{235}$ . - - - - spectrum constructed according to experimental data from [4].

The calculations showed that significant changes of mass (and charge) ratios of the heavy fragments (from 1.1 to 1.9) change the energy distribution of the  $\alpha$ -particles only insignificantly (maximum difference about 0.5 MeV). Deviations from the most probable point of emission of the  $\alpha$ -particle displace the energy distribution of the  $\alpha$ -particles to the side of larger energies. For example, a change of the emission point by 12% of the distance between centers of the fission fragments to the side of the lighter as well as to the side of the heavier fragment displaces the spectrum to the higher-energy side by 3.5 MeV. The distribution with respect to angle, as a result of these fluctuations, becomes broader.

On the basis of the calculations carried out, averaging with respect to the initial energy of the  $\alpha$ -particles was undertaken, reckoned from the barrier (see above) for the thermal neutron fission of  $U^{235}$  and for the most probable mass ratio, and for the case of  $\alpha$ -particle emission from the thinnest point of the neck. The distribution with respect to angle and the energy spectrum of the  $\alpha$ -particles obtained as a result of such averaging are shown in Figs. 6 and 7. It can be seen from the figures that the calculated angular distribution of the  $\alpha$ -particles agrees satisfactorily with the experimental data of [4].

The somewhat greater sharpness of the calculated distribution is associated, obviously, with the fact that the  $\alpha$ -particle

is associated, obviously, with the fact that the  $\alpha$ -particle

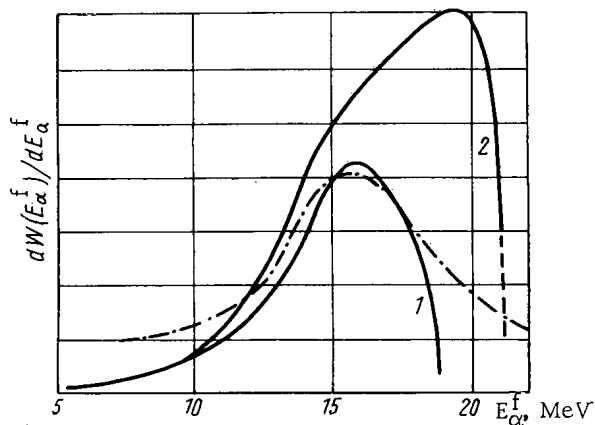


Fig. 7. Energy spectrum of  $\alpha$ -particles from ternary fission of  $U^{235}$ . Averaging is carried out for two energy intervals of  $E_{\alpha}^0$ . 1) 0-1.0 MeV; 2) 0-2.0 MeV; - - - - experimental energy distribution from [4, 5].

the calculated spectrum is somewhat lower than the observed limit (28 MeV). By carrying out the additional averagings mentioned above, the upper limit of the calculated spectrum is displaced to the side of higher energies.

It should be noted that for the assumptions made the given scheme of calculations describes well the observed triton spectrum: thus, for the spontaneous fission of  $\text{Cf}^{252}$ , the maximum calculated energy distribution is located at 8.1 MeV, and for the experimental spectrum it is at 8.5 MeV [6].

This paper was presented at the International Conference on Nuclear Physics in Budapest in September 1963. After completion of the project we learned of a preprint of an unpublished paper by Halpern which was also devoted to the calculation of the angular and energy distribution of  $\alpha$ -particles in ternary fission [7]. The model used in [7] differs considerably from the one considered above.

In conclusion, we feel it our duty to express thanks to D. F. Davidenko and L. A. Kurnosov for assistance in carrying out the numerical calculations.

#### LITERATURE CITED

1. S. Tsien, *J. Phys. et radium*, 9, 6 (1948).
2. B. T. Geilikman, *Atomnaya énergiya*, 6, 290 (1959).
3. U. Schmitt and I. Nelar, *Phys. Rev. Lett.*, 9, 427 (1962).
4. I. A. Perfilov, Yu. F. Romanov, and Z. I. Solov'eva, *Usp. fiz. nauk*, 21, 471 (1960).
5. I. A. Perfilov et al., *ZhÉTF*, 44, 1833 (1963).
6. R. Nobles, *Phys. Rev.*, 126, 1508 (1962).
7. I. Halpern, Preprint, CERN, Geneva, 1963.

CONCERNING THE EMISSION TIMES OF  $\gamma$ -QUANTA  
AS A RESULT OF FISSION<sup>1</sup>

(UDC 539.173.4)

G. V. Val'skii, D. M. Kaminker, G. A. Petrov,  
and L. A. Popeko

Translated from *Atomnaya Énergiya*, Vol. 18, No. 3,  
pp. 223-226, March, 1965

Original article submitted February 26, 1964; revision submitted April 20, 1964

The emission times of  $\gamma$ -quanta in the thermal neutron fission of  $U^{235}$  were measured by the method of geometrical discrimination of individual sections of the path of the fission fragments. Collisions between fission fragments and  $\gamma$ -quanta were recorded as a function of the distance of the collimator axis from the target. In contrast to the data of certain earlier reports, the conclusion is drawn that the main bulk of fission  $\gamma$ -radiation is emitted after a time of less than  $5 \cdot 10^{-11}$  sec. It was found that within the interval  $3 \cdot 10^{-10}$ - $2 \cdot 10^{-8}$  sec, not more than 5-10% of the  $\gamma$ -radiation accompanying fission is emitted.

An investigation of the lifetime of the excited states of the fission products formed by the fission of heavy nuclei is of considerable interest for the theory of fission. This problem has been elucidated in a number of papers, but their results are not always in good agreement. In [1], by using a gas scintillator for recording the fission fragments and a plastic scintillator for recording the  $\gamma$ -quanta, it was found, by the method of delayed coincidences, that in the spontaneous fission of  $Cf^{252}$  not more than 15% of all the photons accompanying fission are emitted within the interval of 1-3 nsec, not more than 3% over the interval 3-5 nsec, not more than 3% over the interval 5-10 nsec, and not more than 10% over the interval 10-50 nsec. For the fraction of photons emitted after intervals longer than  $5 \cdot 10^{-8}$  sec, the authors of [1] found an upper limit of 50%. The authors of other papers have investigated the time distribution of the  $\gamma$ -radiation in the thermal neutron fission of  $U^{235}$ .

In [2], the  $\gamma$ -ray spectra were investigated in delayed coincidences from fission fragments over the time interval  $5 \cdot 10^{-8}$  to  $10^{-5}$  sec. It was found that within the stated interval 5.7% of the  $\gamma$ -quanta are emitted with energies up to 2 MeV; the main fraction of this radiation is emitted more rapidly. In [3], the  $\gamma$ -ray fission spectra were investigated in pulse coincidences from a fission chamber. Lead absorbers with a thickness of 15 mm could be installed inside the chamber so that the  $\gamma$ -detector could be screened from the active layer. In this case only  $\gamma$ -quanta were recorded which were emitted by fragments traversing a definite distance from the target. From comparison of the coincidence intensity with and without absorber, the author of [3] found that over the photon energy range of 30-250 keV the lifetime lies within the limits 0.5-2.5 nsec. In [4], a fission chamber was used with an adjustable collecting electrode. A layer of  $U^{235}$  was coated onto the fixed wall of the chamber, directly behind which was located the  $\gamma$ -detector. For sufficiently long lifetimes ( $\tau$ ), the coincidence intensity should depend on the position of the collecting electrode. As a result, it was found that  $\tau = (0.5-2.0) \cdot 10^{-9}$  sec. Finally, in [5], it was found from measurements by the delayed coincidence method that for fission  $\gamma$ -quanta over the energy range of 25-100 keV, the value of  $\tau$  was bounded by the limits  $10^{-9}$  to  $10^{-10}$  sec and a tendency was noted for  $\tau$  to increase with decrease of the  $\gamma$ -ray energy.

An attempt is made in this paper to estimate the emission of  $\gamma$ -quanta directly from light fission fragments by a geometrical-discrimination method similar to the method which has been used repeatedly for determining the lifetime of excited states of the products of nuclear reactions.

<sup>1</sup>Report obtained from the editor of ZhÉTF, where it was presented on July 26, 1963.

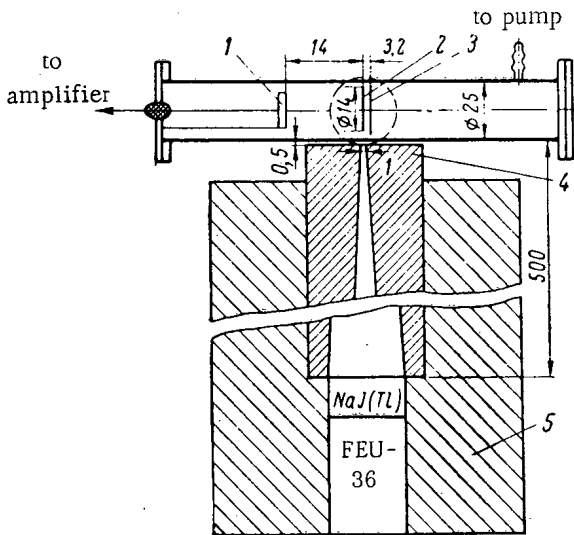


Fig. 1. Layout of experimental assembly: 1) semiconductor detector; 2)  $U^{235}$  target; 3) fission fragment collector; 4) lead collimator; 5) shielding of  $\gamma$ -detector.

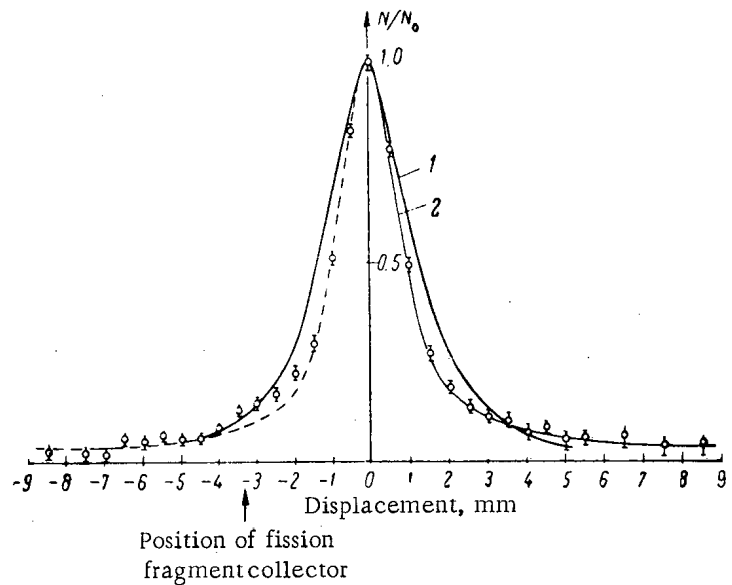


Fig. 2. Relationship between coincidence count rate and collimator displacement: 1) calculated curve for  $\tau = 5 \cdot 10^{-11}$  sec; 2) experimental curve.

The problem did not arise here of investigating the time dependence of the  $\gamma$ -quanta on their energy. The layout of the experiment is shown in Fig. 1. The layer of  $U^{235}$  oxide, with a density of  $100 \mu\text{g}/\text{cm}^2$ , was carried on a metallized film of PVC acetate with a thickness of about  $30 \mu\text{g}/\text{cm}^2$ . The diameter of the spot was about 14 mm. The fission fragments were recorded by a silicon detector with an operating area of  $10 \times 10$  mm located at a distance of 14 mm from the plane of the target. The target and the fission fragment detector were arranged along the axis of an evacuated thin-walled (0.5 mm thick) aluminum tube with a diameter of 25 mm. The chamber axis was located horizontally and perpendicular to the axis of incidence of a beam of neutrons with a diameter of about 25 mm issuing from the horizontal channel of a reactor.

Gamma-quanta were recorded with a scintillation counter located below the chamber on a special carriage. An NaI(Tl) crystal was used, of height and diameter 60 mm, with a photomultiplier FEU-36. The distance from the chamber axis to the center of the crystal was approximately 55 cm. In order to reduce background, the gamma-counter was surrounded by a lead shield. The fission  $\gamma$ -rays fell onto the crystal through a lead collimator with an entrance slit 1 mm wide and 20 mm long located almost up against the chamber and perpendicular to its axis, and the exit hole was a circle of diameter 60 mm. The chamber remained fixed for the measurements and the  $\gamma$ -detector, together with the shielding, could be moved along the chamber axis. Only those  $\gamma$ -quanta could participate in the pulse coincidences from the fission fragments which were emitted by the light fragment within the limits of a small portion of its path,  $x/v$  seconds after fission, where  $x$  is the distance from the screen to the collimator axis and  $v$  is the velocity of the fragment. By measuring the relationship between the coincidence intensity and  $x$ , data can be obtained concerning the lifetime of the  $\gamma$ -radiation emitted by the light fragment.

The electronic equipment was a fast-slow coincidence circuit with time delay conversion into pulse amplitude. This method of coincidence recording permitted reliable discrimination between true coincidences and random coincidences, which was important under conditions of a large and varying load on the  $\gamma$ -counter, especially in the presence of geometrical factors which strongly attenuated the intensity of the fission  $\gamma$ -rays. By means of a discriminator in the fission fragment recording channel, pulses from  $\alpha$ -particles were excluded, so that there was no reduction in intensity of the fission fragment count, which was verified by plotting the pulse spectra from the fission fragment detector by means of an analyzer with and without control by the discriminator pulses. By a similar method the recording level was established of the  $\gamma$ -radiation at which the  $\gamma$ -spectrum of an  $\text{Hf}^{181}$  ( $E_{\text{min}} = 56$  keV) was almost undistorted, while the photomultiplier noises were reliably suppressed. It was established by special experiments, in which the  $\gamma$ -autocoincidence curves for the  $\text{Au}^{198}$  line were recorded when a known attenuation was introduced into one of the channels, that almost 100% efficiency of coincidence recording was achieved with  $\gamma$ -quanta energy of

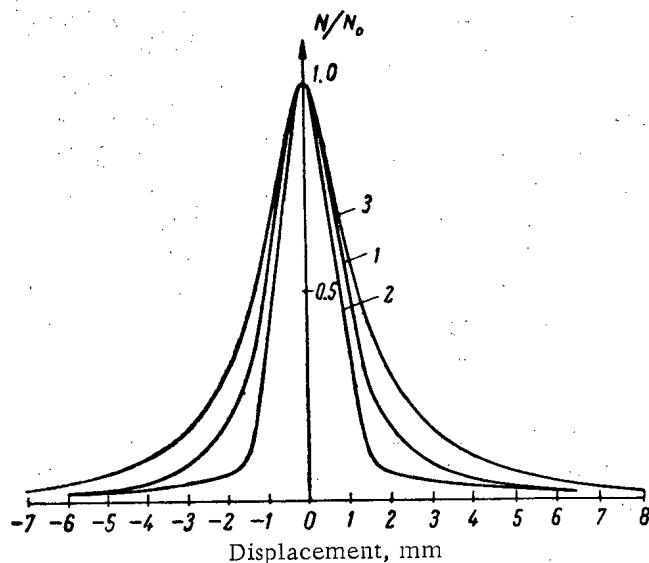


Fig. 3. Transmission curves of the collimator. 1) For fission  $\gamma$ -spectrum; 2) for  $\text{Hf}^{181}$  source; 3) for  $\text{Co}^{60}$  source.

$\gamma$ -quanta which were emitted by the fission fragments but delayed by more than 20 nsec were not taken into account.

The coincidence intensities obtained, reduced to an identical number of recorded fission fragments, were plotted on graphs as a function of the distance  $x$  from the collimator axis to the plane of the target. This relationship, averaged with respect to six series of measurements, is shown in Fig. 2 (curve 2).

The transmission characteristics for  $\text{Hf}^{181}$  and  $\text{Co}^{60}$  sources were obtained by measuring the count rates of the  $\gamma$ -quanta from the appropriate sources positioned at the site of the target, for various collimator positions. In order to plot the characteristics with the fission spectrum, the working target was superimposed on an auxiliary fission fragment detector with a diameter of the functional surface of 15 mm and from the other side it was covered with an aluminum foil of thickness  $7.5 \text{ mg/cm}^2$ , so that the fission fragments only just emerged out of the target limits. The transmission characteristics with the fission spectrum were plotted by the same procedure as the operating curves and were used in our calculations. The value assumed in the calculations for the velocity component along the chamber axis of the fission fragments was  $10^9 \text{ cm/sec}$ . The actual  $\gamma$ -radiation source (the light fragments) was represented in the form of the sum of plane stationary sources distance  $0.25 \text{ mm}$  from each other with intensities proportional to the areas of the appropriate sections of the exponent  $\exp(-x/v\tau)$ . Assuming that for all these sources the collimator characteristics are described by one and the same curve (curve 1 in Fig. 3), the curve shapes were calculated by numerical integration with different values of  $\tau$  for all photons ( $2 \cdot 10^{-11}$ ,  $5 \cdot 10^{-11}$ ,  $10^{-10} \text{ sec}$ , etc.).

The calculated curves were compared with the experimental curve. Figure 2 shows the calculated curve (1) for  $\tau = 5 \cdot 10^{-11} \text{ sec}$ . From comparison with the experimental points it can be seen that the bulk of the radiation recorded corresponds to  $\tau < 5 \cdot 10^{-11} \text{ sec}$ .

In order to determine the fraction of admixed "slower" radiation, a fission fragment collector located at a distance of about 3.2 mm from the target (see Fig. 1) was used. It can be seen in Fig. 2 that in the region of 3-3.5 mm there is some increase of the experimental points above the dashed curve, which represents the mirror reflection of the opposite slope of the experimental curve. The magnitude of this increase permits the conclusion to be drawn that within the time interval  $3 \cdot 10^{-10} - 2 \cdot 10^{-8} \text{ sec}$ , where the collector method is used successfully, 5-10% of the total recorded radiation is emitted. Assuming an over-all efficiency for our  $\gamma$ -counter relative to the total fission spectrum of about 80%, and taking into account that the greater part of the delayed radiation probably lies in the soft spectral region, where the efficiency is even higher, it can be shown that the data obtained correspond to 10-20% of the radiation with lifetimes in the range  $5 \cdot 10^{-11} - 5 \cdot 10^{-10} \text{ sec}$ . Calculation shows that an admixture  $\geq 20\%$  of transitions with  $5 \cdot 10^{-11} < \tau < 5 \cdot 10^{-10} \text{ sec}$  should lead to a marked change of shape of the experimental curve. The upper limit of  $5 \cdot 10^{-11} \text{ sec}$  for the main fraction of photons emitted as a result of fission is reliably established also from other measurement series carried out with the target. One side of the target was covered so that the delayed

about 60 keV. The same result was obtained by comparing the pulse spectra of  $\gamma$ -quanta from a  $\text{Co}^{60}$  source, obtained in the analyzer with and without pulse control of the coincidence circuit. In this experiment, the fission fragment detector with preamplifier was replaced by an auxiliary  $\gamma$ -counter and  $\gamma$ - $\gamma$  coincidences were recorded. The resolving time of the electronic circuit was 6-8 nsec. The intensity of the coincidence count for various positions of the collimator relative to the target was determined by the areas of the coincidence curves after deducting the background of random coincidences which was computed according to the analyzer channel corresponding to the time "prior to fission." The analyzer channel width corresponded to 1.25 nsec.

All coincidences recorded over the time interval  $t \geq 20 \text{ nsec}$  after the instant of fission were not taken into consideration in the calculation. As a result of this, counts caused by coincidences from pulses from the capture of fission neutrons in the  $\text{NaI(Tl)}$  crystal were almost completely eliminated. At the same time

radiation from the emitted fission fragments should cause asymmetry of the experimental curve or, at least, broadening of it. Neither the one nor the other could be observed, within the limits of experimental error. In one of the variants of the calculation for a double-sided target a narrower collimator characteristic, plotted with  $Hf^{181}$  (curve 2 in Fig. 3), was taken as the basis. The calculated curve obtained for  $\tau = 5 \cdot 10^{-11}$  sec proved to be somewhat broader than the experimental curve. All this, obviously, confirms the accurate establishment of the upper limit for the lifetime of the main fraction of transitions. Thus, the experiments carried out indicate that the main fraction of transitions with energies in excess of 60 keV occur with times of  $\tau \leq 5 \cdot 10^{-11}$  sec, which is contrary to the data from [4]. The upper admixture limit of transitions with times  $5 \cdot 10^{-11} \leq \tau \leq 5 \cdot 10^{-10}$  amounts to approximately 20%. The lifetime (10-20%) of the transitions lies within the limits  $5 \cdot 10^{-10} \leq \tau \leq 3 \cdot 10^{-8}$ . The data obtained do not contradict the concept that the  $\gamma$ -quanta in fission are emitted by the fission fragments after the emission of the prompt neutrons. The multipolarity of the radiation, obviously, is primarily E1 and, in any case for the admixed part of the radiation, does not exceed E2.

The project was carried out on the reactor at the A. F. Ioffe Physicotechnical Institute of the Academy of Sciences of the USSR. The authors take the opportunity of expressing their thanks to the reactor operating personnel for smooth operation of the equipment during the measurements.

#### LITERATURE CITED

1. A. Smith, P. Fields, and A. Friedman, *Phys. Rev.*, 104, 699 (1956).
2. F. Maienshtein et al., In: *Proceedings of the Second International Conference on the Peaceful Uses of Atomic Energy. Collection of reports by foreign scientists [in Russian] (Atomizdat, Moscow, 1959), Vol. 2, p. 297.*
3. V. V. Sklyarevskii, D. E. Fomenko, and E. P. Stepanov, *ZhÉTF*, 32, 256 (1957).
4. B. M. Shiryaev, *Bulletin AN SSSR, Ser. Fiz.*, 25, 143 (1961).
5. S. De'si, A. Lajtai, and L. Nagy, *Acta phys. Acad. scient. hung.*, 15, 185 (1962).

APPLICATION OF THE YVON-MERTENS METHOD  
FOR SOLVING ALBEDO PROBLEMS  
IN THE NEUTRON DIFFUSION THEORY

(UDC 621.039.512.4)

Yu. N. Kazachenkov and V. V. Orlov

Translated from *Atomnaya Énergiya*, Vol. 18, No. 3,  
pp. 226-232, March, 1965  
Original article submitted March 19, 1964

We have derived approximate albedo equations where, in contrast to the ordinarily used diffusion approximation, we used the Yvon-Mertens method, which involves the expansion of the angular dependence of the neutron flux at the interface between two media for neutrons entering and emerging from the medium. The results of calculation indicate that this method is considerably more accurate than the method involving the diffusion approximation. Albedo equations were derived for the spectrum of slow neutrons reflected from media containing heavy atoms, and expressions for the albedo and the "temperature" of reflected neutrons were obtained.

Albedo equations are widely used in solving astrophysical problems [1,2], and they are also used to a certain extent in many problems of neutron physics [3,4]. It would be of interest to write the approximate albedo equations by using the method proposed by Yvon and developed by Mertens [5]. This method consists in expanding the angular distribution of the neutron flux by using a system of orthogonal polynomials, not throughout the entire solid angle  $4\pi$ , but separately in two hemispheres (forward and back). The point is that, precisely at the interface between the media, the angular distributions of the flux in these two hemispheres are usually sharply different, which leads to errors in using the method of spherical harmonics. However, in determining the albedo, we are interested in the angular distribution of the radiation emerging from the medium for a certain given flux of radiation incident to the medium.

Calculations show that even the zeroth approximation of the Yvon-Mertens method yields results which are in good agreement with exact calculations for media characterized by any degree of absorption. This confirms the advisability of using the Yvon-Mertens method. In the present article we shall derive the albedo equations for flat, spherical, and cylindrical layers, and we shall also solve the problem of the reflection of thermal neutrons from a heavy-atom medium by taking into account the thermalization effects.

#### Derivation of the Albedo Equations

As was mentioned earlier, near the interface between media, the neutron flux is defined by means of different analytical expressions for  $\mu > 0$  and  $\mu < 0$  ( $\mu$  is the cosine of the angle between the direction of neutron motion and the internal normal to the surface of the medium). It can be expected that the convergence of the series will be better if the flux is expanded separately for  $\mu > 0$  and  $\mu < 0$  than if the ordinary method of spherical harmonics is used. Legendre polynomials of the argument  $2\mu - 1$  and  $2\mu + 1$  can be used as complete orthogonal systems of functions for  $\mu > 0$  and  $\mu < 0$ , respectively.

Assume that a neutron flux  $P_i(2\mu - 1)$  is incident to the medium, that the reflected flux is equal to  $F^- = \sum_k \beta_{ik} P_k(2\mu + 1)$ , and that the flux transmitted through the medium is  $F^+ = \sum_k t_{ik} P_k(2\mu - 1)$ . We shall

write the equations for the albedo  $\beta_{ik}$  by using the method of separating the processes occurring in a thin surface layer of the medium [3].



We shall assume that the medium consists of two adjacent layers ( $R_1R$ ) and ( $RR_2$ ). We shall denote the albedo and the transmission function for both layers by  $\beta_{ik}^n(R_1R)$ ,  $t_{ik}^n(R_1R)$ ;  $\beta_{ik}^n(RR_2)$ ,  $t_{ik}^n(RR_2)$ , where  $n = \pm 1$  ( $n = 1$  at the boundary  $R_1$ , and  $n = -1$  at the boundary  $R_2$ ). In this notation,  $R_2 \equiv R_{-1}$ .

Assume that the following flux is incident to the boundary with the radius  $R_n$  (see Fig. 1):

$$F_n(R_n, \mu) = P_i(2\mu - n) F_n(R_n).$$

The flux  $F_{-n}(R_n)$  reflected from the ( $R_1R_2$ ) layer will consist of

a) neutrons reflected from the ( $R_nR$ ) layer:

$$F_{-n}^{(1)} = F_n(R_n) \beta_{ih}^n(R_nR) P_h(2\mu + n)$$

(the summation is performed with respect to all recurring indices except  $n$ );

b) neutrons transmitted through the ( $R_nR$ ) layer, reflected from the ( $R_{-n}R$ ) layer, and again transmitted through the ( $R_nR$ ) layer:

$$F_{-n}^{(2)} = F_n(R_n) t_{il}^n(R_nR) \beta_{ih}^n(R_{-n}R) t_{hp}^{-n}(R_nR) P_p(2\mu + n),$$

c) neutrons transmitted through the ( $R_nR$ ) layer, reflected from the layers ( $R_{-n}R$ ), ( $R_nR$ ), and again from ( $R_{-n}R$ ), and transmitted through the ( $R_nR$ ) layer:

$$F_{-n}^{(3)} = F_n(R_n) t_{il}^n(R_nR) \beta_{im}^n(R_{-n}R) \beta_{mp}^{-n}(R_nR) \beta_{py}^n(R_{-n}R) t_{yh}^{-n}(R_nR) P_h(2\mu + n)$$

The total reflected neutron flux will be equal to

$$F_{-n}(R_n) = F_{-n}^{(1)} + F_{-n}^{(2)} + F_{-n}^{(3)} + \dots = F_n(R_n) \left\{ \beta_{ih}^n(R_nR) + t_{il}^n(R_nR) \beta_{im}^n(R_{-n}R) \right. \\ \left. \times \frac{1}{1 - \beta_{mp}^{-n}(R_nR) \beta_{py}^n(R_nR)} t_{yh}^{-n}(R_nR) P_h(2\mu + n) \right\}$$

or

$$F_{-n}(R_n) = F_n(R_n) \beta_{ih}^n(R_1R_2) P_h(2\mu + n),$$

where

$$\beta_{ih}^n(R_1R_2) = \beta_{ih}^n(R_nR) + t_{il}^n(R_nR) \beta_{im}^n(R_{-n}R) \frac{1}{1 - \beta_{mp}^{-n}(R_nR) \beta_{py}^n(R_{-n}R)} t_{yh}^{-n}(R_nR). \quad (1)$$

We shall assume that the ( $R_nR$ ) layer is thin; then  $R = R_n + n\Delta R$ . Considering that

$$\beta_{ih}^n(R_{-n}R_n + n\Delta R) \approx \beta_{ih}^n(R_{-n}R_n) + n\Delta R \frac{\partial \beta_{ih}^n}{\partial R_n},$$

we shall write (1) with an accuracy to terms of the order of  $\Delta R$ . We shall then obtain a system of differential equations for  $\beta_{ik}^n$ :

$$\beta_{ih}^n(R_1R_2) = \Delta \beta_{ih}^n + \Delta t_{il}^n \left[ \beta_{im}^n(R_1R_2) + n\Delta R \frac{\partial \beta_{im}^n}{\partial R_n} \right] \Delta t_{mn}^{-n} + \beta_{il}^n(R_1R_2) \Delta \beta_{lp}^{-n} \beta_{ph}^n(R_1R_2), \quad (2)$$

where  $\Delta \beta_{ik}^n$  and  $\Delta t_{ik}^n$  are the albedo and the transmission function for a thin layer, respectively, which can be derived from the kinetic equation.

#### Solution of the Albedo Equations for a Flat Layer

If the medium to which the neutrons are incident is flat,  $\Delta \beta_{ik}^n$  and  $\Delta t_{ik}^n$  (in this case  $\Delta \beta_{ik}^n = \Delta \beta_{ik}^{-n}$  and  $\Delta t_{ik}^n = \Delta t_{ik}^{-n}$ ) can be found from the kinetic equation

$$\mu \frac{\partial F}{\partial x} + F(x, \mu) = \frac{h}{2} \int_{-1}^1 F(x, \mu') d\mu', \quad (3)$$

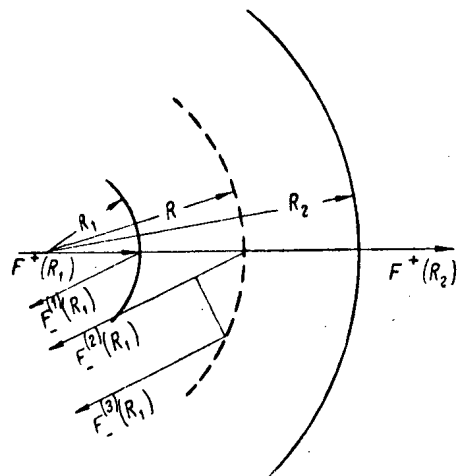


Fig. 1. Diagram for the derivation of the expression for reflected neutron fluxes.

where  $h = \Sigma_s / \Sigma$ . Henceforth, it will be assumed that the neutrons are isotropically scattered in the laboratory coordinate system.

If we write (3) in terms of finite differences, we can find  $\Delta\beta_{ik}$  and  $\Delta t_{ik}$ . Assume that a neutron flux  $P_i(2\mu - 1)$  is incident to a thin flat layer whose thickness is  $\Delta x$ . Then, the flux transmitted through the layer is equal to  $P_i(2\mu - 1) + \Delta x \sum_k c_{ik} P_k(2\mu - 1)$ , while the reflected flux is equal to  $\Delta x \sum_k b_{ik} P_k(2\mu + 1)$ . The coefficients  $b_{ik}$

and  $c_{ik}$  are related to  $\Delta\beta_{ik}$  and  $\Delta t_{ik}$  by the following expressions:  $\Delta\beta_{ik} = \Delta x b_{ik}$ ,  $\Delta t_{ik} = \Delta x c_{ik}$  for  $i \neq k$ ,  $\Delta t_{ii} = 1 + \Delta x c_{ii}$ . If only zero-degree polynomials are retained in the expansion of the expression for the flux (zeroth approximation), the values of the coefficients can be obtained from Eq. (3):

$$C_{00} = -(2-h), \quad b_{00} = h.$$

In this case, the system of equations (2) for a semiinfinite medium is reduced to the single equation

$$h\beta_{00}^2 - 2(2-h)\beta_{00} + h = 0. \quad (4)$$

For the two-dimensional problem, the term  $\partial\beta_{ik}^n / \partial R_n$  of system (2) changes to  $d\beta_{ik}/dx$ , where  $x$  is the thickness of the medium, and it vanishes for  $x \rightarrow \infty$ , since the reflected flux does not change with the addition of a finite thickness to the half-space.

By solving Eq. (4), we obtain

$$\beta_{00} = \frac{2-h}{h} - \sqrt{\left(\frac{2-h}{h}\right)^2 - 1}. \quad (5)$$

The minus sign is used in front of the radical, since the albedo must be equal to unity for  $h = 1$ . It is of interest to compare  $\beta_{00}$  with the exact albedo value  $\beta$ , which can be expressed by using the tabulated Ambartsumyan function  $H(\mu)$  [1]:

$$\beta = \frac{h}{2} \int_0^1 d\mu \int_0^1 d\mu_0 \frac{\mu H(\mu) H(\mu_0)}{\mu + \mu_0} = \frac{h}{4} \left[ \int_0^1 d\mu H(\mu) \right]^2. \quad (6)$$

For the sake of comparison, the table provides the exact albedo values calculated by means of Eq. (6), the albedo obtained by means of (5), and, finally, the albedo determined by using the diffusion approximation. It is obvious from the table that even the zeroth approximation of the Yvon-Mertens method yields an albedo value which is very close to the exact value. For still smaller  $h$  values, the albedo obtained by means of the zeroth approximation of the Yvon-Mertens method coincides with the exact albedo value.

The Yvon-Mertens method is also applicable to finite-thickness layers. In this case, in the zeroth approximation, system (2) is reduced to the differential equation

$$\frac{d\beta_{00}(x)}{dx} = h\beta_{00}^2 - 2(2-h)\beta_{00} + h = 0, \quad (7)$$

where  $x$  is the layer thickness, and  $\beta_{00}(0) = 0$ . By solving this equation, we obtain

$$\beta_{00}(x) = \frac{2-h}{h} - \sqrt{\left(\frac{2-h}{h}\right)^2 - 1} - \left\{ h \left[ \frac{1}{(2-h) - \sqrt{(2-h)^2 - h^2}} + \frac{1}{2\sqrt{(2-h)^2 - h^2}} \right] \times e^{4\sqrt{1-h}x} - \frac{h}{2\sqrt{(2-h)^2 - h^2}} \right\}^{-1}. \quad (8)$$

The good results obtained by using the Yvon-Mertens method in the case of a two-dimensional geometry indicate that this method can probably be successfully used in the case of spherical or cylindrical geometry.

Solution of the Albedo Equations for the Spherical and Cylindrical Geometries

For a spherical geometry, the  $\Delta\beta_{ik}^h$  and  $\Delta t_{ik}^h$  values can be obtained from the kinetic equation

$$\mu \frac{\partial F}{\partial r} + \frac{1-\mu^2}{r} \frac{\partial F}{\partial \mu} + F = \frac{h}{2} \int_{-1}^1 F(r, \mu') d\mu'. \tag{3'}$$

In the zeroth approximation, considering (3'), systems (2) will be reduced to the equations

$$\frac{\partial \beta_{\pm}}{\partial r_{\pm}} + 2(2-h)\beta_{\pm} + \left(h \pm \frac{\alpha}{r_{\pm}}\right)\beta_{\pm}^2 + \left(h \mp \frac{\alpha}{r_{\pm}}\right) = 0, \tag{7'}$$

where the upper sign pertains to the incidence of neutrons to the inside surface of the spherical layer;  $r_+$  and  $r_-$  are the inside and outside radii of the spherical layer, respectively;  $\beta_+(r_+)$  and  $\beta_-(r_-)$  are the albedo values for neutrons incident to the inside and the outside surfaces of the spherical layer, respectively;  $\beta_{\pm}(r_{\pm} = r) = 0$ ;  $\alpha = \frac{1}{2}$ .

Assume that the outside radius is infinite and that neutrons are incident to the inside surface of the layer; then, Eq. (7') must be solved for the following boundary condition:

$$\beta_+(\infty) = \frac{2-h}{h} - \sqrt{\left(\frac{2-h}{h}\right)^2 - 1}. \tag{5'}$$

In this case, the solution for  $\beta_+$  can be written in the form of a series,

$$\beta_+(r_+) = \sum_{k=0}^{\infty} \frac{\beta_k^+}{r_+^k}, \tag{8'}$$

where the  $\beta_k^+$  values do not depend on  $r_+$ . The following recurrent relationships are obtained for the coefficients of series (8'):

$$\left. \begin{aligned} \beta_0^+ &= \frac{2-h}{h} - \sqrt{\left(\frac{2-h}{h}\right)^2 - 1}, \\ \beta_1^+ &= -\frac{\alpha(\beta_0^{+2} - 1)}{2h\beta_0 - 2(2-h)}, \\ \beta_k^+ &= \\ &= \frac{(k-1)\beta_{k-1}^+ - h \sum_{l=1}^{k-1} \beta_{k-l}^+ \beta_l^+ - \alpha \sum_{l=0}^{k-1} \beta_{k-l-1}^+ \beta_l^+}{2h\beta_0^+ - 2(2-h)}, \end{aligned} \right\} \tag{9}$$

where  $k > 1$ . For  $r_+ \rightarrow \infty$ , series (8'), as was to be expected, is transformed into the corresponding expression for the half-space. The problem can be solved in the zeroth approximation also for a finite-thickness layer. In this case, the solution can be found in the form of the series

$$\beta^{\pm}(r_+, r_-) = \sum_{k=0}^{\infty} \frac{\beta_k^{\pm}(r_- - r_+)}{r_{\pm}^k}. \tag{8''}$$

For  $\beta_k^+(r_- - r_+)$ , the following recurrent relationships hold:  $\beta_0^+(r_- - r_+)$  is equal to series (8), i.e., to the albedo of a flat layer with the thickness  $r_- - r_+$ , obtained in the zeroth approximation:

TABLE 1. Albedo Values Obtained by Means of Different Methods

h	Exact $\beta$ value	Yvon - Mertens method, $\beta_{00}$	Diffusion approximation, $\beta_{dif}$
1	1	1	1
0.9	0.520	0.520	0.460
0.8	0.381	0.372	0.311
0.7	0.290	0.286	0.221
0.6	0.226	0.230	0.150
0.5	0.172	0.179	0.098
0.4	0.127	0.126	0.059

$$\beta_1^+(r_- - r_+) = -\alpha \int_0^{r_- - r_+} |\beta_0^+(z') - 1| \exp \left\{ 2 \int_0^{z'} [(2-h) - h\beta_0^+(z)] dz \right\} dz' \exp \left\{ -2 \int_0^{r_- - r_+} [(2-h) - h\beta_0^+(z'')] dz'' \right\},$$

$$\beta_k^+(r_- - r_+) = - \int_0^{r_- - r_+} a_k(z') \exp \left[ \int_0^{z'} C(z) dz \right] dz' \exp \left[ - \int_0^{r_- - r_+} C(z'') dz'' \right], \quad (10)$$

where  $k > 1$ .

The following notation is used in the above relationships:

$$C(z) = 2(2-h) - 2h\beta_0^+(z), \quad (11)$$

$$a_k(z) = (k-1)\beta_{k-1}^+(z) - h \sum_{l=1}^{k-1} \beta_{k-l}^+ \beta_l^+(z) - \alpha \sum_{l=0}^{k-1} \beta_{k-l-1}^+(z) \beta_l^+(z).$$

If  $-\alpha$  is everywhere substituted for  $\alpha$  in (10) and (11), (8<sup>n</sup>) will describe  $\beta^-(r_+, r_-)$ , while  $\beta_0^+(r_- - r_+) = \beta_0^-(r_- - r_+)$ . The albedo of a cylindrical layer can be determined in a similar manner. In the zeroth approximation, all expressions for a spherical layer hold if  $\alpha/2$  ( $\alpha = \frac{1}{2}$ ) is substituted for  $\alpha$  in them.

#### Thermalization of Neutrons

The Yvon-Mertens method can be successfully used not only for solving single-velocity problems, but it can also be applied to the problem of the reflection of thermal neutrons from media with an allowance for the change in neutron energy (thermalization of neutrons).

Assume that neutrons fall on a half-space which does not absorb neutrons. We shall also assume that the moderator nuclei are heavier, i.e., that their mass is much larger than the neutron mass. In each collision between a neutron and a moderator nucleus, its energy (or the absolute velocity value) changes slightly. Davydov [6] showed that this makes it possible to use the Fokker-Planck method, i.e., one can switch from the integral to a differential expression in the kinetic equation. The velocity direction changes to a great extent in every collision; one cannot switch to the differential expression in this case.

Since we are neglecting nonelastic collisions with nuclei of the medium, the expressions obtained hold only if the mean neutron energy is lower than the first excitation levels of nuclei in the medium. Moreover, we shall consider that the moderator nuclei are distributed as a free gas. Brockhouse and Hurst [7] have shown that this assumption applies to the scattering of neutrons on the nuclei of a medium whose atomic weight is larger than the atomic weight of aluminum. On the basis of all that has been said above, one can use the results obtained in [8]. The neutron density is described by the equation

$$v \nabla N - \frac{1}{v^2} \cdot \frac{\partial}{\partial v} \left[ v^2 A_1 N + \frac{\partial}{\partial v} (v^2 A_2 N) \right] + v \Sigma N = \frac{\Sigma}{2} \int_{-1}^1 N(\mu') d\mu', \quad (12)$$

where  $A_1 = (1/lM)(mv^2 - 3kT)$ , where  $m$  is the neutron mass,  $M$  is the mass of the moderator nucleus,  $l = 1/\Sigma$  is the mean free path in the moderator, which is assumed to be constant,  $k$  is the Boltzmann constant, and  $T$  is the temperature of the medium ( $^{\circ}\text{K}$ ).

We shall now switch to the new function  $N_0 = N/v^2$ . Instead of  $v$ , let us introduce the dimensionless velocity  $v' = v(m/kT)^{1/2}$ , express  $E$  in  $kT$  units, and express the masses of the moderator nuclei in neutron mass units. Then, expression (12) will assume the following form:

$$v' \nabla N_0 - \frac{1}{2Ml} \left[ v' \frac{\partial^2 N_0}{\partial v'^2} + (2v'^2 - 1) \frac{\partial N_0}{\partial v'} + 4v' N_0 \right] + \frac{v'}{l} \left[ N_0 - \frac{1}{2} \int_{-1}^1 d\mu' N_0(\mu') \right] = 0. \quad (13)$$

If  $E$  is substituted for the variable  $v'^2$  in (13), and  $x$  is expressed in  $l$  units, we obtain

$$\mu \frac{\partial N_0}{\partial x} - \frac{2}{M} \left[ E \frac{\partial^2 N_0}{\partial E^2} + E \frac{\partial N_0}{\partial E} + N_0 \right] + N_0 - \frac{1}{2} \int_{-1}^1 d\mu' N_0(\mu') = 0. \quad (13)$$

It was indicated in [9] that this equation holds for neutron energies satisfying the inequalities  $M \gg 4kT/E$  and  $E \ll MkT/4$ . Thus, Eq. (13) holds for the entire region of  $v'$  values for sufficiently large  $M$  values. We shall seek  $N_0$  in the form of a series in terms of Legendre polynomials of the argument  $2\mu \pm 1$  and in terms of first-degree Laguerre polynomials. We shall consider that  $v'^2 = E$  in our notation; then,

$$N_0(E) = Ee^{-E} \left\{ \begin{array}{l} \sum_{n,l} a_n^l(x) L_n^{(l)}(E) P_l(2\mu - 1), \mu > 0, \\ \sum_{n,l} b_n^l(x) L_n^{(l)}(E) P_l(2\mu + 1), \mu < 0. \end{array} \right\} \quad (14)$$

If we retain only zeroth power terms in the expansion with respect to Legendre polynomials, we obtain very simple expressions. If the density of incident neutrons is

$$N_0^+ = Ee^{-E} \sum_n a_n^0 L_n^{(0)}(E),$$

the density of reflected neutrons will be

$$N_0^- = Ee^{-E} \sum_n \frac{a_n^0 L_n^{(0)}(E)}{\left[ \frac{4n}{M} + 1 + \sqrt{\left( \frac{4n}{M} + 1 \right)^2 - 1} \right]}. \quad (15)$$

For large  $n$  values, the coefficient in front of  $L_n^{(0)}(E)$  in the expansion of the density of reflected neutrons will be equal to  $1/n$  of the corresponding coefficient in the expression for incident neutrons. In the case of incident neutrons with the energy  $E_0$ , the neutron density will be equal to

$$\left. \begin{array}{l} N_0^+(E) = \delta(E - E_0) = Ee^{-E} \sum_n \frac{L_n^{(0)}(E_0) L_n^{(0)}(E)}{n! (n+1)!}, \\ N_0^-(E) = Ee^{-E} \sum_n \frac{L_n^{(0)}(E_0) L_n^{(0)}(E)}{n! (n+1)! \left( \frac{4n}{M} + 1 + \sqrt{\left( \frac{4n}{M} + 1 \right)^2 - 1} \right)} \end{array} \right\} \quad (16)$$

We can calculate the albedo of the medium and the energy albedo:

$$\beta_n = \int \beta_0(E_0, E) dE,$$

$$\beta_E = \frac{1}{E_0} \int \beta(E_0, E) E dE.$$

As was to be expected,  $\beta_n = 1$ , which corresponds to the absence of absorption. For  $\beta_E$ , the following zeroth approximation expression is obtained:

$$\beta_E = \frac{1}{E_0} \left[ 2 + \frac{E_0 - 2}{\frac{4}{M} + 1 + \sqrt{\left( \frac{4}{M} + 1 \right)^2 - 1}} \right], \quad (17)$$

where  $E$  is expressed in  $kT$  units. The second term in (16) characterizes the deviation of the mean energy of reflected neutrons from the Maxwellian energy, which is equal to 2. If  $E_0 = 2$ , we have  $\beta_E = 1$ , i.e., in the case of incidence of neutrons with an energy equal to the mean energy of the Maxwellian spectrum, the neutrons are reflected with the same mean energy. For  $M \rightarrow \infty$ ,  $\beta_E \rightarrow 1$ , i.e., the thermalization of neutrons does not occur. The absorption given by the  $1/v$  law can be taken into account in a rather simple manner, since absorption occurs only for slow neutrons. This means that, for  $\mu < 0$ , the coefficients in front of  $L_n^{(0)}(E)$  in (14) change considerably for not very large  $n$  values. However, the actual calculations lead to rather cumbersome expressions.

It is of interest to compare the results based on neutron thermalization that were obtained by using the Yvon-Mertens method in the zeroth approximation with the exact calculations performed by T. Kh. Sedel'nikov [4]. Assume that neutrons having a Maxwellian distribution with a temperature  $T$ , different from the temperature  $T_0$  of the medium, are incident to the medium. Then,

$$N_0^+(E) = \lambda^2 E e^{-\lambda E}, \quad \lambda = \frac{T}{T_0}.$$

Let us calculate the mean energy of reflected neutrons:

$$\bar{E} = \lambda^2 E_0 \int_0^\infty E e^{-\lambda E} \beta_E dE = 2 \left[ 1 - \left( 1 - \frac{1}{\lambda} \right) \left( \frac{4}{M} + 1 - \sqrt{\left( \frac{4}{M} + 1 \right)^2 - 1} \right) \right]$$

and introduce  $\bar{T}_{\text{isotr}}$  by using the expression

$$\bar{T}_{\text{isotr}} = \frac{1}{2} \bar{E} T. \quad (19)$$

Then, we obtain the following from (18):

$$\bar{T}_{\text{isotr}} = T \left[ 1 - \left( 1 - \frac{T_0}{T} \right) \left( 1 + \frac{4}{M} - \sqrt{\left( 1 + \frac{4}{M} \right)^2 - 1} \right) \right]. \quad (20)$$

The analogous value in [4] is given by

$$\bar{T}_{\text{isotr}}^{\text{sed}} = T \left[ 1 - \left( 1 - \frac{T_0}{T} \right) \frac{1 - \sqrt{\frac{2}{M}}}{1 + \sqrt{\frac{2}{M}}} \right] = T \left[ 1 - \left( 1 - \frac{T_0}{T} \right) \frac{1 + \frac{2}{M} - 2 \sqrt{\frac{2}{M}}}{1 - \frac{2}{M}} \right]. \quad (21)$$

It should be mentioned that expressions (20) and (21) hold for  $1/(M)^{\frac{1}{2}} \ll 1$  and, therefore, after expanding these expressions with respect to  $1/(M)^{\frac{1}{2}}$ , we obtain

$$\bar{T}_{\text{isotr}} = T \left[ 1 - \left( 1 - \frac{T_0}{T} \right) \left( 1 - \frac{2\sqrt{2}}{\sqrt{M}} + \frac{4}{M} - \frac{2\sqrt{2}}{M^{3/2}} + \dots \right) \right], \quad (20')$$

$$\bar{T}_{\text{isotr}}^{\text{sed}} = T \left[ 1 - \left( 1 - \frac{T_0}{T} \right) \left( 1 - \frac{2\sqrt{2}}{\sqrt{M}} + \frac{4}{M} - \frac{4\sqrt{2}}{M^{3/2}} + \dots \right) \right]. \quad (21')$$

#### LITERATURE CITED

1. V. A. Ambartsumyan et al., *Theoretical Astrophysics* [in Russian] (Gosteorizdat, Moscow, 1953).
2. Sh. Chandrasekhar, *Transfer of Radiant Energy* [Russian translation] (IL, Moscow, 1953).
3. T. Kh. Sedel'nikov, *Albedo Equations in the Theory of Neutron Diffusion and Moderation* [in Russian] (Atomizdat, Moscow, 1960).
4. T. Kh. Sedel'nikov, *Atomnaya Énergiya*, **12**, 522 (1962).
5. R. Mertens, *Compt. rend.*, **236**, 1753 (1953).
6. B. Davydov, *DAN SSSR*, **2**, 212 (1934).
7. B. Brochouse and D. Hurst, *Phys. Rev.*, **88**, 542 (1952).
8. B. I. Davydov, *ZhÉTF*, **6**, 463 (1936).
9. E. Cohen, Report submitted by the USA at the First International Conference on the Peaceful Uses of Atomic Energy (Geneva, 1955).

USE OF THE METHOD OF MOMENTS FOR SOLVING EQUATIONS  
OF NEUTRON THERMALIZATION IN INFINITE MEDIA

(UDC 621.039.51.12:539.125.52)

M. V. Fedulov

Translated from *Atomnaya Énergiya*, Vol. 18, No. 3,

pp. 232-238, March, 1965

Original article submitted March 7, 1964

The possibility of using the method of moments for solving the integral equation of neutron thermalization in an infinite homogeneous medium is investigated. Comparisons are made with the exact solution for certain cases of moderation in monatomic gases.

We shall consider the problem of determining the spectrum of neutrons which are moderated in an infinite homogeneous medium. The neutron sources are uniformly distributed in space; the velocity of emitted neutrons is infinitely high. The neutron density  $N(x)$  satisfies the equation [1]

$$[w(x) + V(x)] N(x) - \int_0^{\infty} G(x, x') N(x') dx' = 0. \quad (1)$$

Here,  $x$  is the neutron velocity in  $(2kT/m)^{1/2}$  units, where  $T$  is the temperature of the medium ( $^{\circ}K$ ),  $m$  is the neutron mass,  $k$  is the Boltzmann constant,  $G(x, x')dx$  is the probability that scattering will be experienced in unit time, as a result of which a neutron whose velocity is  $x'$  will acquire a velocity in the  $x, x + dx$  interval,  $V(x) = \int_0^{\infty} G(x', x) dx'$  is the probability of scattering, and  $w(x)$  is the probability of capture.

In view of the fact that, in collision with a moderator atom, the probability that the neutron velocity will increase by a value considerably exceeding the thermal velocity, i.e., by a value of the order of unity, is low, the kernel  $G(x, x')$  in the region bounded by the axis  $x'_0 = 0$  and the diagonal  $x' = x$  differs considerably from zero only near the diagonal in a band with a width of the order of unity. This property of the kernel makes it possible to find in a relatively simple manner, a solution in the region of high velocities. After choosing a sufficiently large limiting velocity value  $x_0$  in order to ensure the required accuracy, and considering that the collisions of neutrons whose velocities exceed  $x_0$  occur as if the moderator atoms were at rest, the approximate solution is found for velocities exceeding  $x_0$ . Then, by substituting this solution in Eq. (1), we obtain a nonhomogeneous equation with a finite upper limit.

This equation can be solved by using several methods. One of them consists in seeking the solution as a sum of a series of linearly independent functions, whose coefficients are determined by means of the method of moments (see, for instance, [2]). It is known that the method of moments is equivalent to the method of replacing the kernel of the integral equation by a degenerate kernel. On the other hand, if the kernel of the equation can be reduced to the symmetric form, the method of moments is equivalent to Ritz' variational method if the functional is in bilinear form and the trial function is given as the sum of a series of linearly independent functions. The possibility of reducing the scattering kernel to the symmetric form in solving Eq. (1) follows directly from the principle of detailed balance:

$$G(x, x') M(x') = G(x', x) M(x),$$

where  $M(x) = \text{const } x^2 \exp(-x^2)$  is the Maxwellian distribution.

In the thermalization theory, the method of moments was used in solving space-energy problems. In this, it was assumed that the energies of neutrons emitted by the sources were close to the thermal energies (see, for instance, [3,4]). Much closer to our work are the investigations performed by Zaretskii and Sedel'nikov [5], who used the variational method for determining the effective temperature of the neutron gas in the case of sources with infinitely high energy. Below, we shall consider the possibility of using the variational method for solving Eq. (1) with an arbitrarily high degree of accuracy.

After choosing a certain velocity value  $x_0$ , we introduce a new kernel  $\tilde{G}(x, x')$ , which coincides with  $G(x, x')$  everywhere except in the region defined by the inequalities  $x' < x$  and  $x > x_0$ , in which  $\tilde{G}(x, x') = 0$ . We shall also introduce  $\tilde{V}(x) = \int_0^{\infty} \tilde{G}(x', x) dx'$ . The solution of the equation

$$[w(x) + \tilde{V}(x)] \tilde{N}(x) - \int_0^{\infty} G(x, x') \tilde{N}(x') dx' = 0 \quad (1')$$

must tend rapidly to the solution of Eq. (1) with an increase in  $x_0$  due to the above-mentioned property of  $G(x, x')$ .

In the  $x > x_0$  region, which will be referred to as the first region, the solution of Eq. (1') coincides with the solution of the Volterra equation

$$[w(x) + \tilde{V}(x)] \tilde{N}^{(1)}(x) - \int_x^{\infty} \tilde{G}(x, x') \tilde{N}^{(1)}(x') dx' = 0. \quad (2)$$

Assume that the solution of Eq. (2) is known. The solution of Eq. (1') in the second region ( $0, x_0$ ) satisfies the equation

$$[w(x) + \tilde{V}(x)] \tilde{N}^{(2)}(x) - \int_0^{x_0} G(x, x') \tilde{N}^{(2)}(x') dx' = Q(x),$$

where

$$Q(x) = \int_0^{x_0} G(x, x') \tilde{N}^{(1)}(x') dx'. \quad (3)$$

By using the principle of detailed balance, it can readily be shown that the bilinear functional

$$I(v) = \int_0^{x_0} [w(x) + \tilde{V}(x)] M^{-1}(x) v^2(x) dx - \int_0^{x_0} \int_0^{x_0} G(x, x') M^{-1}(x) v(x') v(x) dx' dx - 2 \int_0^{x_0} Q(x) M^{-1}(x) v(x) dx \quad (4)$$

attains its extremal value when  $v$  coincides with the solution of Eq. (3). If the degree of absorption is low, the solution of Eq. (3) only slightly differs from the Maxwellian distribution  $M(x)$ . Therefore, it is advisable to use a trial function in the following form:

$$\tilde{N}_n^{(2)} = M(x) \sum_{k=0}^n A_k \varphi_k(x), \quad (5)$$

where  $\varphi_k(x)$  are linearly independent functions,  $\varphi_0(x) = 1$ , and  $A_k$  are constant coefficients, which can be determined by using Ritz' method.

By setting the derivatives of  $I(\tilde{N}_n^{(2)})$  with respect to  $A_k$  equal to zero, we obtain a system of linear algebraic equations in terms of  $A_k$ :

$$\sum_{k=0}^n (\alpha_{ik} + \beta_{ik}) A_k = q_i, \quad (6)$$



where

$$\left. \begin{aligned} \alpha_{ik} &= \int_0^{x_0} w(x) M(x) \varphi_i(x) \varphi_k(x) dx, \\ \beta_{ik} &= \int_0^{x_0} \left[ \tilde{V}(x) M(x) \varphi_k(x) - \int_0^{x_0} G(x, x') M(x') \varphi_k(x') dx' \right] \varphi_i(x) dx, \\ q_i &= \int_0^{x_0} Q(x) \varphi_i(x) dx = \int_0^{x_0} \int_{x_0}^{\infty} G(x, x') \tilde{N}^{(1)}(x') \varphi(x) dx' dx. \end{aligned} \right\} \quad (6')$$

From the symmetry of the product  $G(x, x')M(x')$  follows the symmetry of the  $\beta_{ik}$  coefficients, while, from  $\varphi_0 = 1$ , it follows that  $\beta_{0k} = 0$ .

The  $N_n^{(2)}(x)$  function with the coefficients  $A_k$ , determined from system (6), constitutes an approximate solution of Eq. (3). It should be mentioned that this solution will not change if, instead of  $\varphi_k$ , their independent linear combinations are introduced. This statement is based on the elementary principles of the theory of linear spaces. The solution  $N_n^{(2)}$  possesses the following remarkable property. Since the total number of neutrons entering the second region from the first region is equal to the number of neutrons absorbed in the second region, the following relationship holds for the exact solution of Eq. (3):

$$\int_0^{x_0} \tilde{N}^{(2)}(x) w(x) dx = \int_0^{x_0} Q(x) dx. \quad (7)$$

However, from the first equation of system (6) and from  $\beta_{0k} = 0$ , it follows that relationship (7) is satisfied for the approximate solution  $N_n^{(2)}$  for any  $n$ .

It was mentioned above that the variational method based on the use of a bilinear functional and a trial function in the form of a series sum is equivalent to the replacement of the kernel in the integral equation by a degenerate kernel. It is only necessary to determine correctly the weight in the orthogonalization of the expansion functions and to replace the kernel and the right-hand side of the equation by sections of their Fourier series. Actually, we shall normalize  $\varphi_k$ ,

$$\int_0^{x_0} \varrho(x) \varphi_i(x) \varphi_k(x) dx = \delta_{ik}, \quad (8)$$

where

$$\beta(x) = M(x) [w(x) + \tilde{V}(x)],$$

and we shall consider that these functions constitute the first  $n + 1$  functions of a certain complete system. Let us replace  $G(x, x')$  and  $Q(x)$  by sections of their Fourier series:

$$\left. \begin{aligned} G_n(x, x') &= \varrho(x) \sum_{k=0}^n g_k(x') \varphi_k(x), \\ Q_n(x) &= \varrho(x) \sum_{k=0}^n q_k \varphi_k(x), \end{aligned} \right\} \quad (9)$$

where

$$g_k(x') = \int_0^{x_0} G(x, x') \varphi_k(x) dx, \quad (9')$$

while the  $q_k$  values were determined earlier. It is readily seen that series (5) with the coefficients  $A_k$ , determined from (6) and (6'), constitutes the solution of the equation

$$[w(x) + \tilde{V}(x)] \tilde{N}_n^{(2)}(x) - \int_0^{x_0} G_n(x, x') \tilde{N}_n^{(2)}(x') dx' = Q_n(x)$$

so that, as  $n$  increases unboundedly,  $\tilde{N}_n^{(2)}(x)$  tends to  $\tilde{N}^{(2)}(x)$ .

Let us now consider the question of the uniformity of the approximation of  $N^{(2)}(x)$  by means of series (5).

The coefficients  $g_k(x')$  and  $q_k$  are determined so that the integrals  $\int_0^{x_0} [\Delta_n^G(x, x')]^2 \rho^{-1}(x) dx$  and  $\int_0^{x_0} [\Delta_n^Q(x)]^2 \rho^{-1}(x) dx$  have the minimum values (here,  $\Delta_n$  is the deviation of the approximate function from the exact function). Due to the exponential rise of the weighting function  $\rho^{-1}(x)$  for large argument values, the functions  $g(x, x')$  and  $Q(x)$  are approximated by series (9) in a highly nonuniform fashion, i.e.,  $\Delta_n^G(x, x')$  and  $\Delta_n^Q(x)$  are much smaller for  $x$  values than for  $x \approx 1$ . This, in turn, leads to nonuniformity in the approximation of the  $N^{(2)}(x)$  function by means of series (5), which can be estimated by considering that, in the first place, the function  $\psi(x) = \lambda(x) \tilde{N}^{(2)}(x)$ , where  $\lambda^2(x) = M^{-1}(x)[w(x) + \tilde{V}(x)]$ , constitutes the solution of the equation

$$\psi(x) - \int_0^{x_0} K(x, x') \psi(x') dx' = f(x),$$

in which the kernel  $K(x, x') = \lambda(x') \rho^{-\frac{1}{2}}(x) G(x, x')$  is symmetric, while  $f(x) = \rho^{-\frac{1}{2}}(x) Q(x)$  and, in the second place,  $\psi_n = \lambda(x) \tilde{N}_n^{(2)}(x)$  constitutes the solution of the equation

$$\psi_n(x) - \int_0^{x_0} K_n(x, x') \psi_n(x') dx' = f_n(x),$$

where  $K_n(x, x') = \lambda(x') \rho^{-\frac{1}{2}}(x) G_n(x, x')$  and  $f_n(x) = \rho^{-\frac{1}{2}}(x) Q(x)$ , while  $g_k(x')$  and  $q_k$ , determined by Eqs. (6') and (9'), yield the minimum values for the integrals

$$\int_0^{x_0} [\Delta_n^K(x, x')]^2 dx, \quad \int_0^{x_0} [\Delta_n^f(x)]^2 dx.$$

Thus, the nonuniformity of the approximation of  $\tilde{N}^{(2)}(x)$  by means of series (5) is characterized by the factor  $\lambda(x)$ , i.e., near  $x_0$ , the deviation of  $\tilde{N}_n^{(2)}(x)$  from  $\tilde{N}^{(2)}(x)$  is much smaller than at  $x \approx 1$ . This fact, which generally reduces the approximation accuracy, can still be useful if the capture cross section has resonance near  $x_0$ .

It should also be mentioned that, due to the high accuracy of approximation of the solution in the second region near  $x_0$ , the approximate solution  $\tilde{N}_n(x)$ , which is equal to  $\tilde{N}_n^{(1)}(x)$  in the first region and  $\tilde{N}_n^{(2)}(x)$  in the second, experiences a discontinuity whose magnitude is of the order of the deviation of  $\tilde{N}_n^{(1)}(x)$  from the exact solution of Eq. (3). Naturally, for a fixed number of terms in series (5), there is always a sufficiently large  $x_0$  value for which the solution  $\tilde{N}_n(x)$  is continuous. In this case, for  $x \approx 1$ , the deviation of the approximate solution from the exact solution may be exceedingly large.

The choice of the limiting velocity  $x_0$  depends on the absorber concentration and the required calculation accuracy. One can use a constant limiting velocity in a wide range of the medium's absorption ability values, which would make it possible to use the same  $\beta_{ik}$  coefficients characterizing the moderating power of the medium for a large number of problems with different absorption values. Generally speaking, the  $\beta_{ik}$  coefficients depend on the moderator temperature. However, this dependence can be neglected if a very high accuracy is not required. In the case of an ideal gas where the scattering cross section does not depend on the relative neutron velocity, the function  $G(x, x')$  and, consequently, the  $\beta_{ik}$  coefficients, are perfectly independent of temperature.

The calculation of the  $\alpha_{ik}$  coefficients, which characterize the absorption ability of the medium, is trivial if the capture cross sections of all the absorbers contained in the medium obey the  $1/v$  law, i.e., if the capture probability does not depend on the velocity. If the  $1/v$  law does not hold for all absorbers, the coefficients characterizing a certain given absorber can be calculated beforehand. In solving a specific problem, using the linear dependence

of the  $\alpha_{ik}$  coefficients on the absorption probability, these coefficients could be calculated in the form of a sum with respect to all the absorbers contained in the medium by taking into account the concentration of these absorbers.

In determining  $\tilde{G}(x, x')$ , we did not take into account the possibility of a neutron acquiring energy if its velocity exceeds  $x_0$ . We shall now neglect altogether the motion of the moderator atoms, the interference of neutron waves, and the interatomic bonds if the neutron velocity exceeds the limiting velocity. Then in the region defined by the inequalities  $x < x'$  and  $x' > x_0$ , we have the following (the scattering in a center-of-mass system is assumed to be spherically symmetric):

$$\tilde{G}(x, x') = \sum_j \frac{(\mu_j + 1)^2}{2\mu_j x'} [\eta(x - \omega_j x') - \eta(x - x')] \Sigma_{sj}(x'), \tag{10}$$

where  $\Sigma_{sj}$  and  $\mu_j$  are the partial scattering cross section and the mass (expressed in neutron mass units) of the  $j$ -th isotope, respectively;

$$\omega_j = \frac{\mu_j - 1}{\mu_j + 1},$$

$\eta(t)$  is a step function:

$$\eta(t) = \begin{cases} 0 & \text{for } t < 0, \\ 1 & \text{for } t > 0. \end{cases}$$

If  $x > x_0$ , the following expression holds for  $\tilde{V}(x)$ :

$$\tilde{V}(x) = 2 \sum_j x \Sigma_{sj}(x'). \tag{10'}$$

However, even with this simplification of the expression for the scattering probability, an analytical solution of Eq. (2) can be obtained only in the case of hydrogen. If, for the calculation of the  $q_i$  values, which characterize

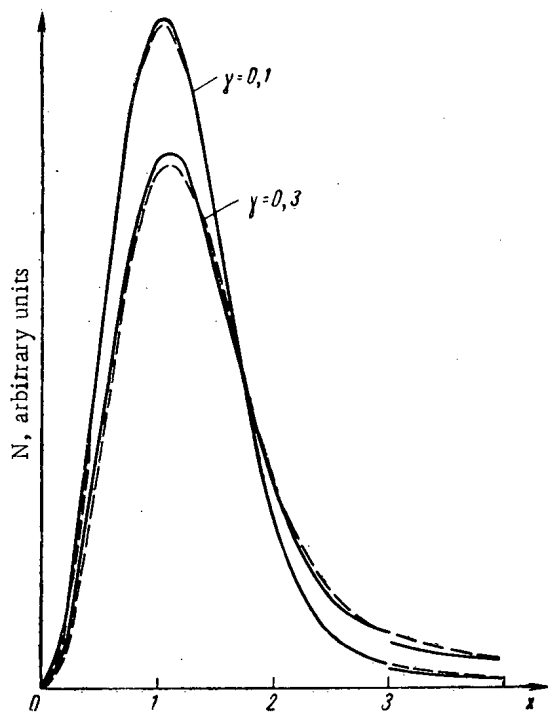


Fig. 1. Spectrum of neutrons in a monatomic gas with  $\mu = 1$ . The capture cross section obeys the  $1/v$  law. Solid line, calculation according to method of moments; broken line, exact calculation.

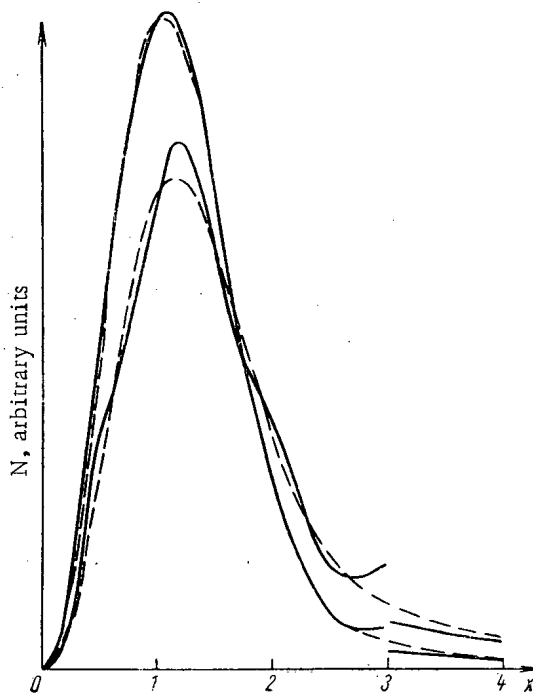


Fig. 2. Spectrum of neutrons in a monatomic gas with  $\mu = 20$ . The capture cross section obeys the  $1/v$  law. Solid line, calculation according to method of moments; broken line, exact calculation for  $\mu = \infty$ .

the flux of neutrons moving from the first to the second region, we use the approximate solution of Eq. (2), the  $q_i$  values will generally not correspond to the absorption of neutrons in the first region. Therefore, it is advisable first to calculate  $q_0$  by using the expression for the probability of absorption in the first region:

$$q_0 = 1 - \int_{x_0}^{\infty} w(x) \tilde{N}^{(1)}(x) dx,$$

and then to use Eqs. (6') for finding the  $q_i/q_0$  ratios. For the calculation of these ratios, one can apparently use the coarsest approximation for  $N^{(1)}$  - its asymptotic form at infinity:  $\tilde{N}^{(1)} \approx 1/x_2$ .

In order to estimate the applicability of the approximate solutions, we shall consider a medium consisting of a monatomic gas with a scattering cross section independent of the relative velocity and with moderator atomic mass values equal to 1 and 20. For  $\mu = 1$ , the approximate solution can be compared with the exact solution of the Wigner-Wilkins equation while, for  $\mu = 20$ , it can be compared with the solution of the equation for a heavy gaseous moderator [1]. The choice of a mass value equal to 20 is more or less arbitrary and is related to the fact that the calculation of the  $\beta_{ik}$  coefficients for large  $\mu$  values is very cumbersome. On the other hand,  $\mu = 20$  is sufficiently large to use the solution of the equation for a heavy moderator for purposes of comparison.

In all calculations,  $N^{(1)}(x)$  was used in the following form:

$$\tilde{N}^{(1)}(x) = \frac{\text{const}}{x[x + \gamma(x)]} \exp \left\{ -\frac{2}{\xi} \int_x^{\infty} \frac{\gamma(t) dt}{t[t + \gamma(t)]} \right\}, \quad (11)$$

where  $\gamma(x) = w(x)/\Sigma_s$ , and  $\xi$  is the logarithmic energy decrement for a zero-temperature moderator. We used  $k$ -degree polynomials as the expansion functions  $\varphi_k(x)$ ; the  $q_i$  values for  $\mu = 1$  were calculated exactly, while, for  $\mu = 20$ , the asymptotic form  $q_i/q_0$  was used in calculating  $N^{(1)}$  ( $N^{(1)} \approx 1/x_2$ ). The error due to this is obviously negligibly small; for  $\mu = 1$  and  $\mu = \infty$  it is equal to zero. Actually, for  $\mu = 1$ , the  $q_i$  values depend only on the total neutron flux moving from the first to the second region and, therefore,

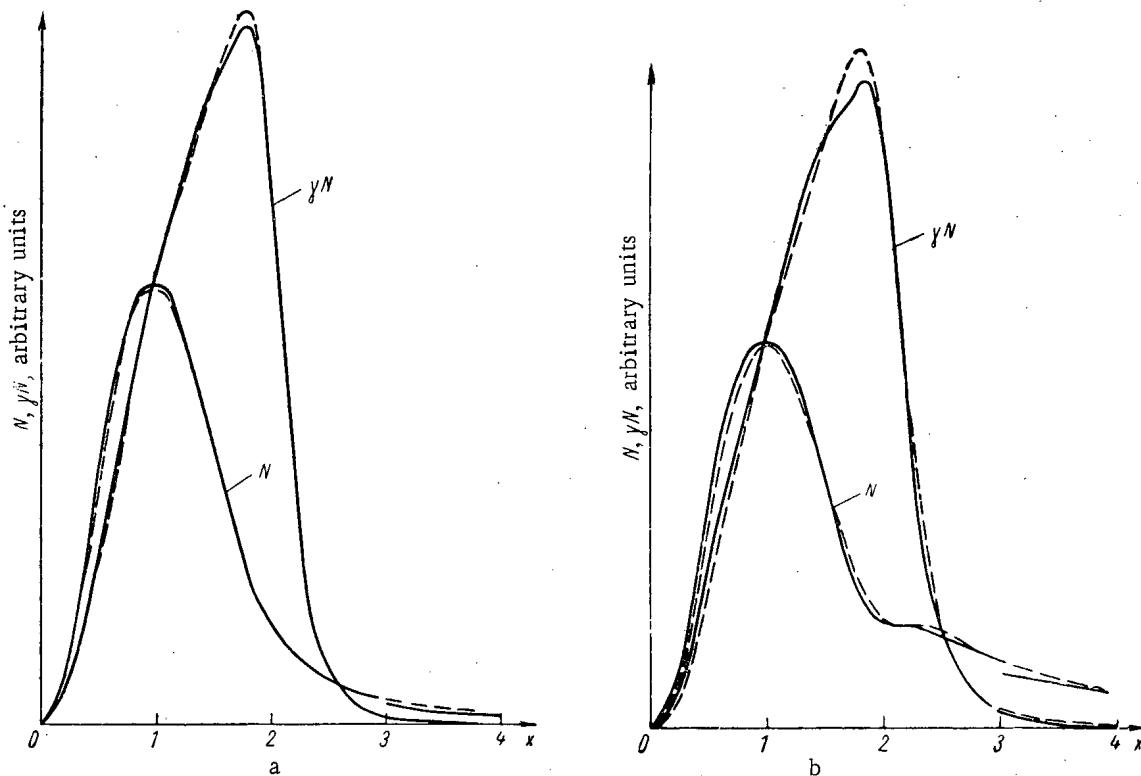


Fig. 3. Neutron spectrum and absorption density in a monatomic gas with  $\mu = 1$ . a)  $\gamma(1) = 0.1$ ; b)  $\gamma(1) = 0.3$ . Solid line, calculation based on the method of moments; broken line, exact calculation.

TABLE 1. Values of the Mean Capture Probability

$\gamma(1)$	$\gamma_{av}$		
	exact calc.	method of moments	Maxwell spectrum
0.1	0.1603	0.1596	0.1661
0.3	0.462	0.458	0.507

$$\frac{q_i}{q_0} = \frac{\int_0^{x_0} \varphi_i(x) x dx}{\int_0^{x_0} \varphi_0(x) x dx}$$

For  $\mu = \infty$ , due to the  $\delta$ -like character of the  $G(x, x')$  function, the  $q_i$  values depend only on the  $\tilde{N}^{(1)}$  value for  $x = x_0$ ; consequently,

$$\frac{q_i}{q_0} = \frac{\varphi_i(x_0)}{\varphi_0(x_0)}$$

Figures 1 and 2 show the  $N(x)$  curves, calculated by means of the exact and the approximate methods for two values of the capture probability, which was assumed to be independent of the velocity ( $\gamma/\xi$  was equal to 0.1 and 0.3, respectively). Eleven terms of series (5) were used ( $n = 10$ ), while  $x_0$  was equal to 3. For convenience of graphic representation, the neutron flux was assumed to be proportional to the capture probability at infinity. Approximate calculation of the spectrum for  $\mu = 20$  yields a much worse result than for  $\mu = 1$ . This is entirely understandable, since, in the first place, with an increase in the mass, the thermalization effect increases in the high-velocity region and, in the second place, the functions  $G(x, x')$  and  $Q(x)$  assume a peaklike form and series (9) converge very slowly. However, for large  $\mu$  values, the maximum deviation from the exact solution of Eq. (1) is connected not with the fact that the solution of Eq. (1') is approximate, but with the substitution of  $G(x, x')$  for  $\tilde{G}(x, x')$  which, in view of the local character of the scattering kernel, leads to a considerable increase in density in the second region near  $x = x_0$ .

We shall now consider the case of moderation where the capture probability depends on the energy. We shall use a monatomic gas with  $\mu = 1$  as the moderator while, for the absorber, we shall use  $\text{Sm}^{149}$  which, for  $E_0 = 0.0976$  eV, has resonance with  $\Gamma_\gamma = 0.064$  eV [6]. We shall assume that the temperature of the medium is equal to 0.025 eV, and we shall use a ratio of the absorber concentration to the moderator concentration for which  $\gamma(1)$  is equal to 0.1 and 0.3. We shall exclude from consideration the  $E > 0.4$  eV region (the region where  $x > x_1 = 4$ ), thereby neglecting the effect of thermalization on the spectrum for  $x > x_1$  in the  $x < x_1$  region. It should be mentioned that the thermalization effect is also neglected in the  $x_0 < x < x_1$  region (as in the first example,  $x_0 = 3$ ). However, the result of disregarding this is actually investigated in this article, while the  $x > x_1$  region is not considered at all.

Figure 3 shows the  $N(x)$  curves and the absorption densities  $\gamma(x)N(x)$ , calculated by means of the exact and the approximate methods (for  $n = 10$ );  $\text{Sm}^{149}$  was used as the absorber. It is difficult to estimate the importance of discrepancies between the curves calculated by means of the approximate and the exact methods. This problem must be solved separately in each individual case. In practical applications, averaging of any function with respect to the assigned spectrum is usually of the greatest interest. As an example, the table provides the values of the mean capture probability, reduced to the scattering cross section:

$$\gamma_{av} = \frac{\int_0^{x_1} \gamma(x) N(x) dx}{\int_0^{x_1} N(x) dx}$$

The third column of the table provides the results obtained by averaging  $\gamma(x)$  with respect to the spectrum:

$$N(x) = \begin{cases} Ax^2 \exp\left(-\frac{x^2}{\beta}\right) & \text{for } x \leq x^*, \\ \frac{B}{x[\gamma(x) + x]} \exp\left\{-2 \int_x^{x_1} \frac{\gamma(t) dt}{t[\gamma(t) + t]}\right\} & \text{for } x \geq x^*. \end{cases}$$

The limiting velocity  $x^*$  and the  $A/B$  ratio were determined from the condition of the continuity of  $N(x)$  for  $x = x^*$  and the balance relationship, while  $\beta$ , which is the ratio of the effective temperature of the neutron gas to the moderator temperature, was obtained by using the Coveillot expression [7], which has the following form for  $\mu = 1$ :

$$\beta = 1 + 0.92\gamma(1). \quad (12)$$

The 0.92 coefficient was determined by analyzing the exact calculations for the case where the absorption cross section obeys the  $1/v$  law, i.e., for a constant capture probability. It is seen from the table that the mean probability of  $\text{Sm}^{149}$  capture is much higher than the capture probability for  $x = 1$ ; therefore, a lower value of the effective temperature is obtained by using Eq. (12). However, it is clear that an increase in  $\beta$  will result in an even larger deviation from the exact  $\gamma_{av}$  value, since the maximum of the spectrum will be shifted toward resonance. Thus, in comparison with the method of moments, less accurate results are obtained when the Maxwell spectrum is used for averaging the capture probability.

In conclusion, the author hereby acknowledges his indebtedness to Yu. P. Pushkareva, who composed the program for the electronic computer and performed the calculations.

#### LITERATURE CITED

1. E. Cohen, In: Transactions of the International Conference on the Peaceful Uses of Atomic Energy, Geneva, 1955 [in Russian] (Izd. AN SSSR, Moscow, 1958), Vol. 5, p. 487.
2. L. V. Kontorovich and V. I. Krylov, Approximate Methods of Higher Analysis [in Russian] (Fizmatgiz, Moscow-Leningrad, 1962).
3. M. V. Kazarnovskii, A. V. Stepanov, and F. L. Shapiro, In: Transactions of the Second International Conference on the Peaceful Uses of Atomic Energy. Reports by Soviet Scientists [in Russian] (Gosatomizdat, Moscow, 1959), Vol. 1, p. 469.
4. M. V. Kazarnovskii and F. L. Shapiro, Neutron Physics [in Russian] (Gosatomizdat, Moscow, 1961), p. 169.
5. S. I. Drozdov et al., In: Transactions of the Second International Conference on the Peaceful Uses of Atomic Energy. Reports by Soviet Scientists [in Russian] (Gosatomizdat, Moscow, 1959), Vol. 1, p. 486.
6. J. Hughes and R. Schwartz, Atlas of Neutron Cross Sections. Second Edition [Russian translation] (Atomizdat, Moscow, 1959), p. 316.
7. A. Weinberg and E. Wigner, Physical Theory of Nuclear Reactors [Russian translation] (IL, Moscow, 1961).

## ELECTROMAGNETIC PUMPS FOR ALKALI METALS

(UDC 621.039.534.9)

N. I. Marin, V. A. Povsten', T. V. Doktorova, and E. M. Avilova

Translated from *Atomnaya Énergiya*, Vol. 18, No. 3,

pp. 239-242, March, 1965

Original article submitted March 6, 1964

The development of a series of electromagnetic helical pumps rated at 0.1 to 150 m<sup>3</sup>/h for laboratory purposes is described together with their characteristics and constructional features.

The development of scientific investigations into molten-metal heat carriers requires the creation of reliable and convenient pumps for carrying out experimental work on laboratory test systems. The following demands are made of such pumps: prolonged operation at heat-carrier temperatures 675-1075°K and higher, hermetic sealing (especially important in pumping radioactive heat carriers), easy and smooth control of the delivery of liquid, minimum over-all size.

At the present time, both mechanical and electromagnetic pumps are used for these purposes. The latter have a number of positive qualities. They contain no moving parts, gaskets, or glands. They operate noiselessly and require little servicing. The relatively low efficiency of electromagnetic pumps is not of great significance for laboratory use.

Electromagnetic pumps, like electrical machines, are divided into dc and ac types.

The dc pumps are most promising for work at high temperatures and are distinguished by higher efficiency. They are fed, however, from special dc sources at high currents and low output voltage (3000 to 20,000 A at 0.5 to 2 V), the creation of which presents great difficulty.

Single-phase ac pumps are very simple, and have therefore enjoyed wide popularity. A serious failing of this type of pump is the comparatively short life of the working parts (500 to 1000 h), which limits their use.

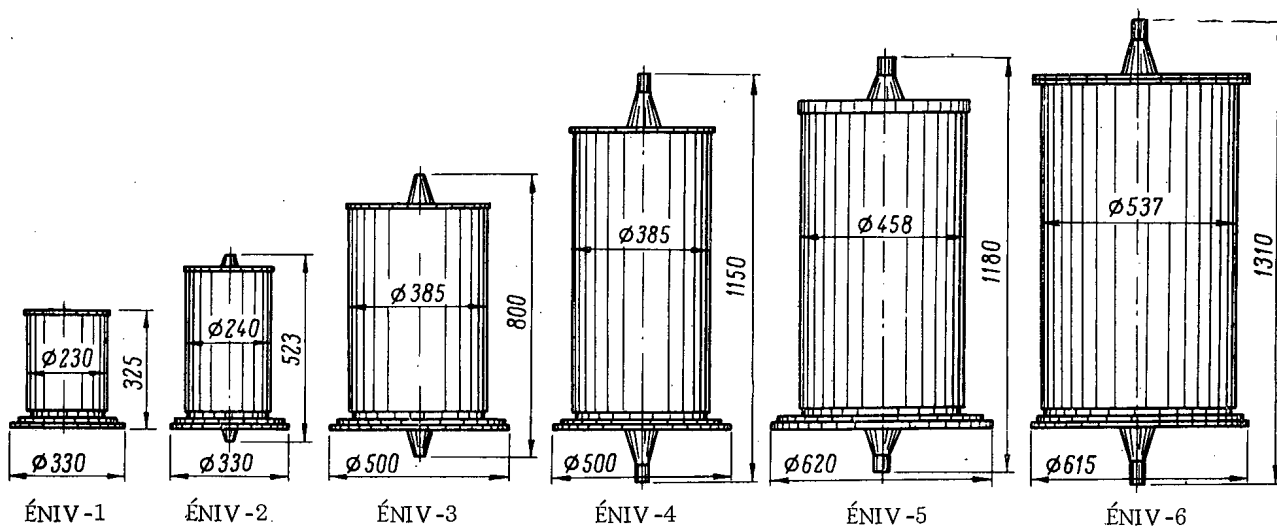
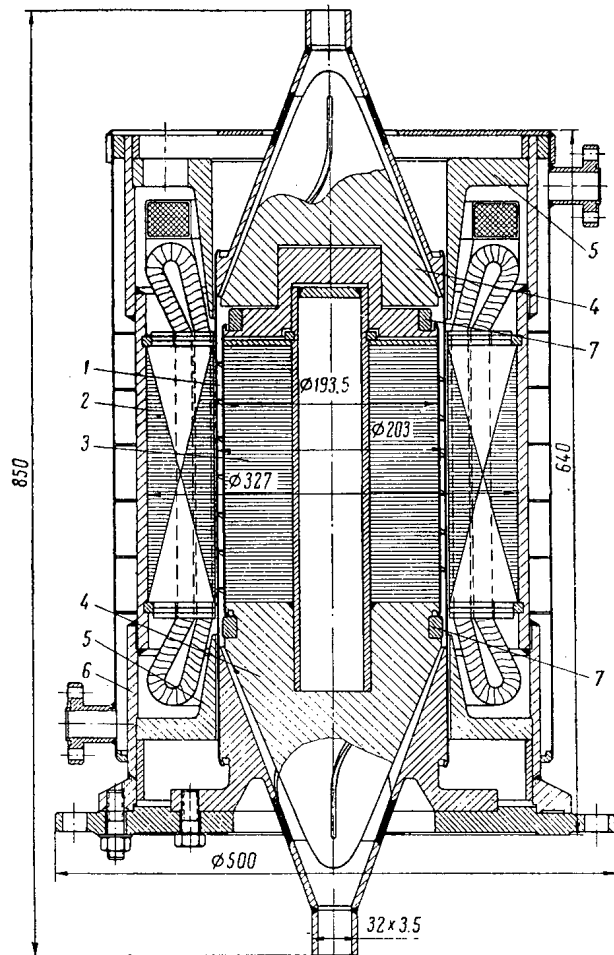


Fig. 1. Dimensions of helical electromagnetic pumps.

TABLE 1. Main Characteristics of the Series of Helical Electromagnetic Pumps

Characteristics	Type of pump					
	ENIV-1	ENIV-2	ENIV-3	ENIV-4	ENIV-5	ENIV-6
Delivery, m <sup>3</sup> /h	0.4	2	10	50	85	150
Pressure · 10 <sup>-5</sup> N/m <sup>2</sup>	4.7	2.5	6	5	4.5	6
Heat carrier	K	NaK	NaK	NaK	NaK	NaK
Operating temp., °K	725	875	675	675	675	775
Power kVA	3.7	7	33	59	140	170
Weight, kg	100	120	400	550	650	1200

Fig. 2. Schematic arrangement of a 10 m<sup>3</sup>/h helical electromagnetic pump.

packet. A three-phase winding is set in channels in the stator. The whole electrical insulation of the stator is made on a silicon-organic basis.

In order to reduce heat losses and ensure normal working conditions of the winding, a heat-insulating air gap lies between the working part and the stator. In addition, heat is carried away from the winding by water-cooling. Since the outflow of heat from the end part of the windings is harder than from the central region, between the working part and the end windings are placed wedge-shaped copper sleeves 5 capable of being cooled.

Suitable three-phase ac pumps for laboratory use include those of the helical type, distinguished by compactness and giving high pressures. These pumps are fed directly from a three-phase ac network, and make it possible to change the direction of pressure of the molten metal by reversing the phases of the stator winding. Moreover, they permit a supply of one of the main parts of the pump (the stator) to be made available by electrical machinery factories in conjunction with serially produced electric motors. For this reason, from the very beginning, preference was given to pumps of the helical type in the Physical Power Institute of the State Committee for the Use of Atomic Energy, USSR.

It was necessary to develop a pump for transporting NaK alloy at 10 m<sup>3</sup>/h at a pressure of  $6 \cdot 10^{-5}$  N/m<sup>2</sup>. This pump may be used for a large number of test systems. The temperature of the heat carrier at the first stage did not exceed 675°K.

Subsequently, a series of helical electromagnetic pumps with nominal deliveries of 0.5, 2, 10, 50, 85, and 150 m<sup>3</sup>/h and nominal pressures 2.5 to  $6 \cdot 10^{-5}$  N/m<sup>2</sup> was developed on the basis of tests made in the manufacture, improvement, and service of this pump. Depending on the rating and physical properties of the metal being pumped, the efficiencies of these pumps varied from 5 to 25%. The table and Fig. 1 indicate the main characteristics of the series of pumps developed.

The same constructional arrangement was taken for the whole series of helical electromagnetic pumps, the pump being disposed vertically, ensuring convenient discharge of the molten metal. From considerations of compactness, axial in- and outflow of the metal was chosen.

The construction of the 10 m<sup>3</sup>/h electromagnetic pump is shown in Fig. 2, and its general view in Fig. 3. The pump consists of the body 6, the stator 2 (the three-phase winding of which creates the rotating magnetic field), the internal core 3 (serving to complete the circuit of the magnetic flux), the working part 1, and the input and output guiding cones 4.

The stator core is composed of electrotechnical steel sheet. The sheets are pressed into the body, and the whole packet held by spring rings placed in grooves in the body on both sides of the packet. To ensure precise assembly and prevent slipping of the packet, a longitudinal key is arranged in a groove of the body and



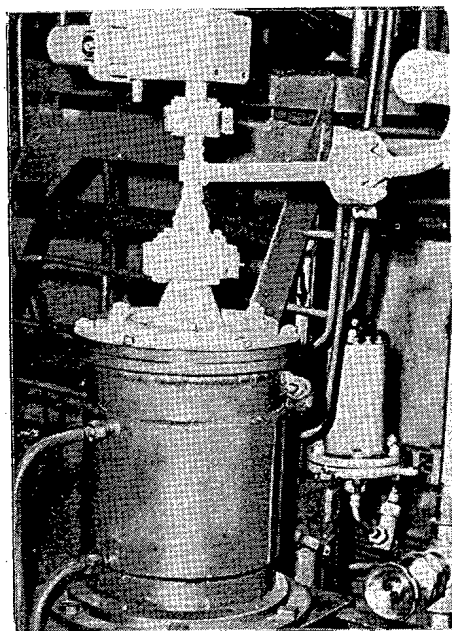


Fig. 3. General view of a 10 m<sup>3</sup>/h electromagnetic pump.

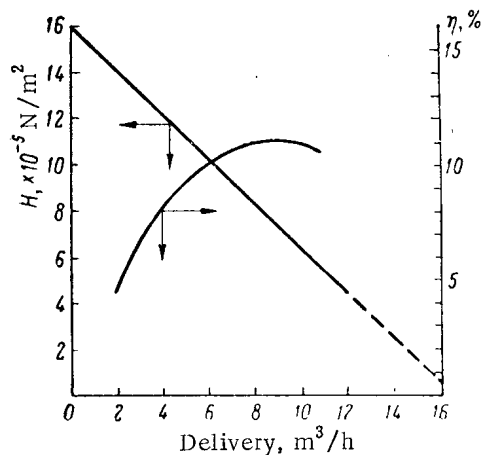


Fig. 4. Experimental characteristics of a 10 m<sup>3</sup>/h helical electromagnetic pump.

continued to work successfully. For some tens of hours it worked at an alloy temperature of 670°K with brief rises to 700 or 750°K. During service there was no case of the system ceasing to work on account of the pump going out of order. The pump worked stably, noiselessly, and with a minimum demand for servicing. At the present time two such pumps are operating satisfactorily in the radioactive loop circuit of the BR-5 reactor with NaK alloy. The duration of service of the pumps in this circuit is more than 10,000 h at a mean temperature of 625°K in the alloy. For some tens of hours the pumps operated at alloy temperatures 725-775°K. Figure 4 shows the experimental characteristics of these pumps.

A pump rate at 0.4 m<sup>3</sup>/h has so far operated for more than 500 h, pumping molten potassium at 525 to 575°K. For 10 h it operated at metal temperature 815°K and for 1 h at 900°K. Meanwhile, the temperature of the winding did not rise above 365°K, which indicates the possibility of using such pumps to pump molten potassium at temperatures above 875°K. The end sections of this pump were preliminarily heated by auxiliary nichrome heaters in ceramic beads, and the central part of the pump tract was heated by the thermal power losses in the walls of the working part.

The inner core is made of electrotechnical steel plates laid on the tube of the lower guiding cone.

A shaped flange is slid on to the free end of the tube, and on this freely sits the upper guiding cone. The upper and lower guiding cones are of similar construction, with "blades" welded onto them along a helical line. The slope of the helical line varies between 9 and 90°. The guiding cones are intended to produce a smooth change in the velocity and direction of motion of the heat carrier on entering and leaving the pump. Rings 7, set on the internal core, play the same part as the short-circuiting rings in the asynchronous electric motor. The working part is made in the form of a stainless steel tube, on the inside of which is cut a helical spiral, transforming the rotational movement of the liquid into forward motion. Apart from this, the spiral strengthens the working part. A stainless steel shell serves as inner wall of the working part; this houses the packet of plates of the inner core. The thermal expansion of the working part is compensated by means of the external tubing, for which a suitable compensation system must be provided.

The stator and internal core are set up on a thrust flange which ensures coaxial alignment.

Up to the present, pumps with 0.4 to 85 m<sup>3</sup>/h deliveries have been made and tested. During the testing, certain difficulties associated with the electrical insulation of the plates in the internal core were overcome. The electrical insulation of the plates must operate at a temperature of 675 to 775°K. Initially the plates were insulated with liquid glass with an admixture of alundum or a high-temperature silicon-organic protective coating. In these cases, however, the evolution of gases and vapor from the insulation on heating led to an increase in pressure in the internal space of the core, as a result of which the walls of the working part deformed and the internal hydraulic resistance of the pump increased considerably. For this reason the insulation in question was replaced by the oxide type. The pumps had stable characteristics, in satisfactory agreement with calculated values.

Pumps with a nominal delivery of 10 m<sup>3</sup>/h have been used for longer periods. On the whole they have been operated on the test bed for more than 50,000 h. One such pump operated more than 20,000 h with NaK alloy at a mean temperature of 530°K and

The 50 m<sup>3</sup>/h pump has so far worked more than 2000 h at a metal temperature of 525 to 625°K and is ready for tests.

In using a 150 m<sup>3</sup>/h pump one must bear in mind the fact that the height of the channel in the working parts of the electromagnetic pumps in the series developed is relatively small (2 to 10.5 mm). Hence, in some cases where the liquid metal is insufficiently pure, there may be blocking of the channel.

The individual pumps of the series were calculated for pumping a definite heat carrier. They may, however, also be used for pumping other alkali metals, but in so doing one must take account of the electrical conductivity of the molten metal and the stability of the material in the working part. For a higher electrical conductivity of the metal, the supply voltage must be correspondingly lowered, since otherwise the pump may develop an impermissibly high pressure for a low delivery.

Thus, in the course of development, we have been able to design a convenient and reliable construction of electromagnetic helical pumps for pumping liquid alkali metals at a temperature of 675 to 725°K. The pumps have small over-all size, are easily and smoothly regulated by adjusting the supply voltage, and may be coupled directly to the electrical network.

At the present time work is continuing on perfecting the construction of the pumps and measures are being taken to raise the maximum temperature of the metal pumped (to 825 or 875°K and higher).

In conclusion, the authors thank N. M. Turchin for help in testing the pumps. They also thank Chief Engineer of the "Dynamo" Works, I. L. Litvak, and the factory staff who took part in preparing the stators.

A STAINLESS STEEL WITH HIGH CAPTURE CROSS SECTION  
FOR THERMAL NEUTRONS

(UDC 621.039.546/669.15)

I. S. Lupakov and N. A. Vasil'ev

Translated from *Atomnaya Énergiya*, Vol. 18, No. 3,  
pp. 242-245, March, 1965  
Original article submitted March 11, 1964

Data are given on the technological and mechanical characteristics of a new stainless steel of the austenite class, mark ÉP-229 (Kh17G21N15T), with a relatively high capture cross section for thermal neutrons. The authors describe its stability to general and intercrystallite corrosion in water plus steam and its structural stability under prolonged exposure to high temperatures. This steel can be used instead of nickel or Kh18N10T steel in certain parts of nuclear reactors.

Steel ÉP-229 (Kh17G21N15T), which has relatively high capture cross section for thermal neutrons, was developed for use in certain parts of nuclear reactors instead of nickel and steel Kh18N10T, which are not altogether satisfactory. Nickel has a relatively high capture cross section ( $0.42 \text{ cm}^{-1}$ ), but it is scarce and hard to work. Steel Kh18N10T fails on account of its inadequate capture cross section ( $0.25 \text{ cm}^{-1}$ ). Steel ÉP-229 is relatively cheap and workable, and has a macroscopic capture cross section for thermal neutrons of  $0.46 \text{ cm}^{-1}$  — higher than for stainless steel, Nimonic or nickel. The high cross section is achieved by adding a large amount of manganese, which has a capture cross section 2.5 times higher than nickel. Manganese also has a short half-life of induced radioactivity [1]. The neutron-physics and other properties of ÉP-229 thus make it suitable in certain cases for replacing pure nickel or Kh18N10T.

An important property of any material is its workability, i.e., the ease with which it can be rough-fabricated and processed by hot and cold deformation, welded, machined, etc. The workability of ÉP-229 under hot and cold plastic deformation was confirmed during the preparation of high-grade electropolished tubes of  $17.0 \times 1.5 \text{ mm}$  diameter. The tubes were prepared both from centrifugally cast and from forged blanks with the following certified composition (wt. %): C  $\leq 0.1$ ; Si  $\leq 0.8$ ; Mn = 20.0-22.0; Cr = 16.0-18.0; Ni = 14.0-16.0; Ti = 0.35-0.70; S  $\leq 0.03$ ; P  $\leq 0.045$ .

In investigating the steel's structure with the aim of choosing the optimum composition, it was found that adding 0.5% or more Ti causes the formation of a new phase, whose quantity increases with the Ti content. In its appearance and in its distribution among the austenite which forms the main structural constituent, this new phase somewhat resembles the  $\alpha$ -phase. However, x-ray analysis showed that it is really a  $\chi$ -phase, with microhardness twice as great as that of the austenite.

As the steel was intended for welded structures, it was necessary to test its weldability. The difficulty here was the presence of the manganese. The effect of manganese on the weldability of austenitic steel is known to depend on the composition of the welded seam [2]. In two-phase austenite-ferrite seams of steel 18-8, increase in the manganese content (which causes the appearance of a wholly austenitic structure in the seam metal) can lead to the appearance of heat cracks. However, if the introduction of 5-7% Mn in the seam structure does not eliminate the ferrite component, the deleterious effect of manganese does not appear. Welded seams of steel 25-20 (of purely austenitic structure) become more resistant to heat cracks on additional alloying with manganese [2]. Favorable effects of manganese on weldability are also noted in [3].

TABLE 1. Weldability of Steel ÉP-229

Mark of welded steel	Mark of welding rod	Cracks present
ÉP-229 + ÉP-229	ÉP-229	None
ÉP-229 + ÉP-229	Sv-04Kh19N11M3	None
ÉP-229 + Kh18G10T	ÉP-229	None
ÉP-229 + Kh18N10T	Sv-04Kh19N11M3	None

TABLE 2. Tension Testing of Initial Welded Specimens

Mark of welded steel	Mark of welding rod	Strength, kg/mm <sup>2</sup>	Point of failure
ÉP-229 + ÉP-229	ÉA-400/10	55.3	Main metal, seam
ÉP-229 + ÉP-229	ÉP-229	54.8	Main metal
ÉP-229 + ÉP-229 (tubes)	Sv-04Kh19N11M3	54.7	Same
ÉP-229 + ÉP-229 (tubes)	ÉP-229	52.5	Same
ÉP-229 + ÉP-229	No welding rod	49.7	Seam

TABLE 3. Tension Testing of Welded Specimens after Annealing at 350°C

Mark of welding rod	Annealing time, h	Strength, kg/mm <sup>2</sup>	Point of failure
ÉP-229	500	54.9	Seam
ÉP-229	1500	56.6	Seam
ÉA-400/10	500	56.8	Main metal
ÉA-400 10	1500	58.0	Main metal

TABLE 4. Impact Bending Tests of Welded Specimens

Mark of welding rod	Aging time, h	Impact strength, kg/cm <sup>2</sup>	Notch location
ÉP-229	Initial state	11.0	Seam
ÉP-229	500	8.0	Seam
ÉP-229	1500	8.6	Seam
ÉP-229	Initial state	8.3	Fusion zone
ÉP-229	500	7.6	Same
ÉP-229	1500	11.2	Same
ÉA-400/10	Initial state	8.5	Same
ÉA-400/10	500	7.2	Same
ÉA-400/10	1500	7.8	Same

6032-58, without heating. It was found that 17 × 1.5-mm tubes of fourth-melt ÉP-229, welded with rods of ÉP-229, ÉA-400/10, and Sv04Kh19N11N3 or without rods, did not undergo intercrystallite corrosion.

ÉP-229 can be satisfactorily arc-welded, argon-arc welded, and contact seam welded. Welded joints between this steel and 0Kh18N10T did not tend to form heat cracks. The seam was of high strength for all types of welding. For arc welding, we recommend ÉA-400/10 electrodes, and for argon-arc welding we recommend the use of welding rods of the main metal and Sv-04Kh19N11M3 wire.

The strength and ductility of the steel were determined by tension testing of fivefold specimens of 6-mm diameter at 20, 350, and 500°C. The impact strength was measured at room temperature on austenitized Menage specimens at 1050°C. The results (Table 5) show that ÉP-229 has fairly good mechanical characteristics both at room temperature and at 350 and 500°C, i.e., its strength properties are comparable with those of 0Kh18N10T.

Steel ÉP-229 contains 20-22% manganese; there is no information on the effect of such a quantity on the weldability of this type of steel. T-shaped specimens were used to investigate the tendency of welded seams to form heat cracks during welding. The specimens were welded with a "noodle" of the base metal, wires of Sv-04Kh19N11M3 and ÉA-400/10 electrodes. They were then examined for cracks. The welds were broken on the press and again examined; the results are shown in Table 1.

It was found that steel ÉP-229 does not tend to form heat cracks on welding.

To estimate the strength and adhesiveness of the welded joints, we made butt joints of 6- to 10-mm thick strips and tubes 17 × 1.5 mm in diameter. Specimens were then prepared for testing by tension, flexing, and impact bending. Those for impact bending were 5 × 10 × 55 mm, while the cross sections of the working part of the specimens for tension and flexing were 5 × 15 mm and 4 × 10 mm, respectively. The tests were made in accordance with GOST 6996-54. The specimens were tested either directly after welding (Table 2) or after retention at 350°C for 500 or 1500 h (Table 3). It is seen that rod welding gives fairly strong seams initially. For rodless welding, the strength of the seams on the 17 × 1.5 mm tubes was somewhat reduced.

Increasing the retention time at 350°C is found to cause some strength increase in the welded specimens, evidently due to aging.

Table 4 shows test results for welded specimens under impact bending, either immediately after welding or after annealing for 500 or 1500 h at 350°C. It is found that the weld seams and fusion zones have fairly high impact strength, which is not much affected by the annealing.

Specimens welded with ÉP-229 or ÉA-400/10 welding rods withstood bending through 180°C.

The welded specimens were tested for intercrystallite corrosion resistance by the AM method of GOST

TABLE 5. Mechanical Properties of Steel at Room and High Temperatures

Test temp., °C	$\sigma_B$ ,	$\sigma_{0.2}$ ,	$\delta$ , %	$\psi$ , %	$\alpha_R$ ,
	kg/mm <sup>2</sup>	kg/mm <sup>2</sup>			kg · m/cm <sup>2</sup>
20	58.7	25.0	36.3	53.7	10.2
350	47.0	19.2	29.5	47.3	—
500	44.9	17.3	26.4	46.7	—

TABLE 6. Corrosion Tests at 350°C and 170 atm

Oxygen content of water, mg/liter	Test duration, h	Corrosion rate, g (m <sup>2</sup> · day)	GOST 5272-50 scale mark
0.025	50	0.22	2
	300	0.026	1
	500	0.004	0
	1000	0.003	0
1	50	0.29	3

From Table 6 it is seen that the corrosion rate in de-aerated water ( $\leq 0.025$  mg/liter O<sub>2</sub>) decreases with increase of test duration; increasing the O<sub>2</sub> content to 1 mg/liter does not appreciably increase the corrosion rate. ÉP-229 is thus a very corrosion-resistant steel.

We have thus developed a steel, ÉP-229 (Kh17G21N15T) with macroscopic capture cross section for thermal neutrons of 0.46 cm<sup>-1</sup>, possessing adequate mechanical and corrosion properties. It has high structural stability under prolonged heating at 350°C and is scarcely embrittled. It can be satisfactorily arc-welded, argon-arc welded, or contact seam welded. Its workability is adequate for the production of tubes, plates, and moldings. It can be used as a material for absorbing thermal neutrons, replacing steel Kh18N10T, nimonic, or technically pure nickel.

## LITERATURE CITED

1. B. Price, K. Horton, and K. Spinney, International series of monographs on nuclear energy: Radiation shielding. Pergamon Press (1957).
2. B. I. Medovar, Welding of Chrome-Nickel Austenitic Steels (Mashgiz, Moscow, 1958).
3. H. Weigand, Schweissen und Schneiden, 10, 2 (1958).

To test the degree of embrittlement caused by high working temperatures, we studied the effect on the mechanical properties and structure caused by prolonged heating. For this purpose, the austenitized impact specimens were heated at 350° for 500, 1000, and 4000 h. During this time, the impact toughness and hardness were determined and the microstructure examined. The impact toughness and hardness did not change appreciably after 4000 h, i.e., the steel was not embrittled and retained its toughness. Metallographic investigations of these specimens showed that after austenitization from 1050°C the steel acquires the austenite structure with a small amount of the  $\chi$ -phase. No appreciable change was found after keeping at 350°C for 4000 h, which showed the structure to be adequately stable.

To test the corrosion resistance and suitability for use in wet steam at high temperatures, we investigated the general corrosion in water at 350°C and 170 atm. Austenitized specimens were tested in water containing 0.06 mg/liter chloride ion and 0.025 mg/liter oxygen, and also in water containing up to 1 mg/liter oxygen. The test durations were 50, 300, 500, and 1000 h.

DISTRIBUTION OF  $\text{Sr}^{90}$  IN THE SURFACE LEVEL OF SOILS  
IN THE SOVIET UNION IN 1959-1960

(UDC 551.577.7)

V. I. Baranov, F. I. Pavlotskaya, G. A. Fedoceyev,  
É. B. Tyuryukanova, L. M. Rodionova, E. V. Babicheva,  
L. N. Zatsepina, and T. A. Vostokova<sup>1</sup>

Translated from *Atomnaya Énergiya*, Vol. 18, No. 3,  
pp. 246-250, March, 1965

Original article submitted February 6, 1964; after revision May 13, 1964

Data are presented on the distribution of  $\text{Sr}^{90}$  throughout the territories of the Soviet Union in 1959-1960. The distribution is observed to be of a latitudinal nature with maximum values within the limits 50-30°N. On the average, the  $\text{Sr}^{90}$  content in the surface level of soil coverage with a thickness of up to 5 and 15 cm amounted to 14.1 and 17.8 mCi/km<sup>2</sup>, respectively. The absence of any increase in content of this isotope in 1960 as compared with 1959 indicates that during the period investigated the quantity of  $\text{Sr}^{90}$  deposited from the atmosphere onto the earth's surface corresponded to the quantity which, because of various processes, was removed from the upper layer with a thickness up to 5 cm.

In studying the ways of assimilating radioactive products from nuclear explosions into the human organism, it is essential to know the content of the various radioactive isotopes in all links of the food chain, commencing with the soil and the vegetation covering. This is due to the fact that as a result of deposition from the atmosphere the radioactive isotopes are retained directly in the above-ground part of the plant or are concentrated in the upper layer of the soil, whence they enter the plant through the root system.

There is available, at present, a great deal of information concerning the determination of the  $\text{Sr}^{90}$  content — one of the most dangerous radioactive isotopes to the health of mankind — in the upper layer of the soil coverage of a number of countries [1-3]. The aim of the present paper is to produce similar data for the Soviet Union.

Samples were collected in June-July 1959 and July-September 1960 on level, open virgin land sections by means of special frames with an area of 25 × 20 cm and depths of 0-5 cm (at certain points with layers up to 5, 5-10, and 10-15 cm). The sampling points were selected on the basis of a preliminary radiometric survey with the usual  $\beta$ - $\gamma$ -radiometers over a grid 5 × 10 m; the necessity for this arose because the  $\text{Sr}^{90}$  content of samples of the soil — vegetation coverage collected at relatively small distances from one another may differ by more than a factor of two. This can be seen from the data of Table 1 (here, and henceforth, the mean arithmetical values of two parallel determinations are given).

The  $\text{Sr}^{90}$  contents were determined by a radiochemical method after leaching with 6 N HCl [4].<sup>2</sup>

A correction for the contribution to the chemical yield of the carrier by stable strontium, contained to a concentration of more than 30 mg/kg in the samples was introduced. The analytical error ( $\sigma/\bar{x} \cdot 100\%$ , where  $\sigma$  is the mean-square error;  $\bar{x}$  is the arithmetic mean value) for samples with a radioactivity  $\geq 50$  dpm was  $\leq 10\%$  and with a radioactivity of  $< 50$  dpm it was  $\leq 15\%$ .

<sup>1</sup>V. V. Emel'yanov, L. I. Belyaeva, N. I. Levkina, and I. V. Molchanova participated in carrying out the radiochemical analyses.

<sup>2</sup>All fractions of the soil coverage were analyzed; soil paper, lithoidal and vegetation, since they may contain a significant part of the  $\text{Sr}^{90}$ .

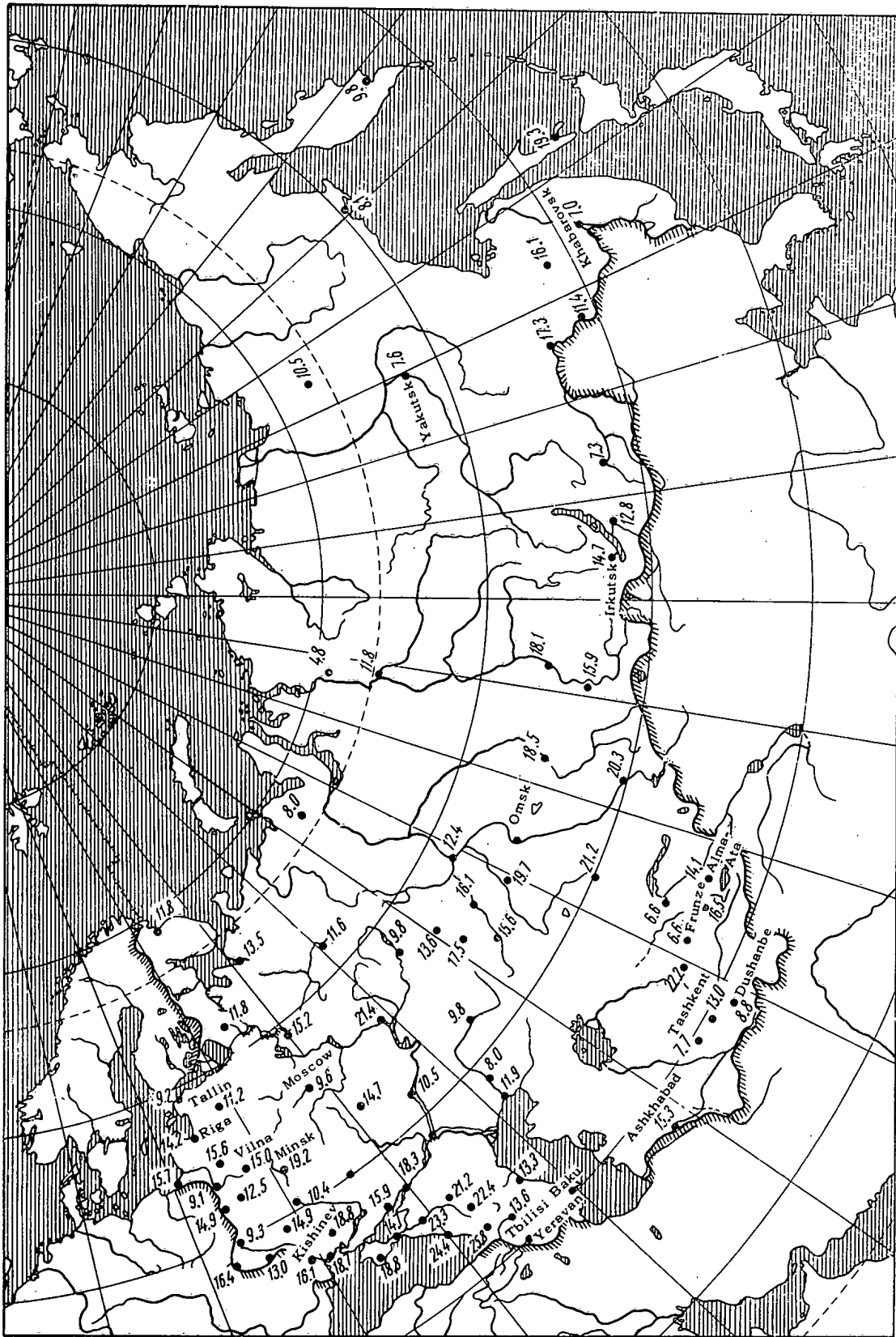


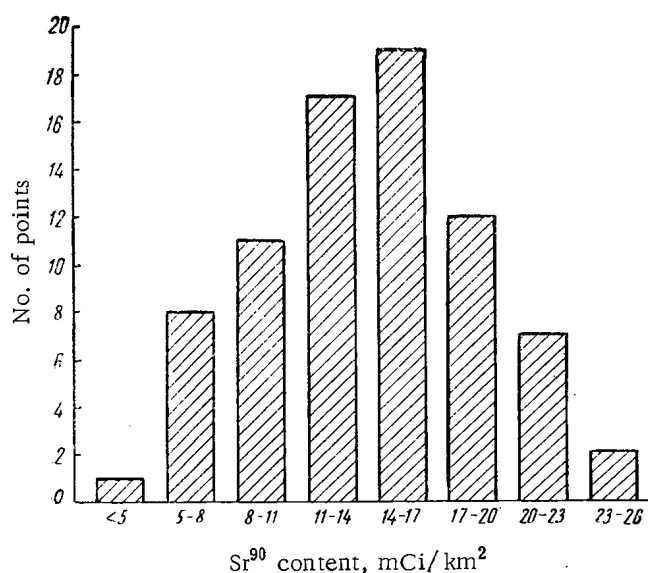
Fig. 1. Distribution of  $Sr^{90}$  ( $mCi/km^2$ ) in the surface (5 cm) level of the soil covering of the USSR in 1959-1960.

TABLE 1. Fluctuation of the Sr<sup>90</sup> Content at Different Sample Collection Points

Country	Time of collection	Distance between collection points 1 and 2, km	Sr <sup>90</sup> content, mCi per km <sup>2</sup>		
			pt.1	pt.2	diff.
USSR	1960	5-8	13.5	17.2	3.7
Japan [5]	1958	4-8	11.9	9.6	2.3
USA [5]	1958	3.2	6.5	15.4	8.9
Norway [6]	1960	2.0	27.7	13.0	14.7

TABLE 2. Sr<sup>90</sup> Content of Soil Coverage of Certain Regions of the USSR

Region	Sr <sup>90</sup> content, mCi/km <sup>2</sup>		Av. annual rainfall, mm
	June-July 1959	July-Sept. 1960	
Forest zone	13.6	13.6	459
Forest zone	17.0	15.7	761
Forest zone	10.6	12.5	518
Forest-steppe zone	12.1	9.3	691
Forest-steppe zone	22.7	17.3	463
Forest-steppe zone	17.2	14.7	379
Meadowland-steppe	23.4	23.3	618
Meadowland-steppe	20.6	21.2	585
Dry steppe zone	24.4	21.2	321
Dry steppe zone	16.5	16.5	398
Dry steppe zone	23.5	22.2	546
Dry steppe zone	6.8	7.7	147
Dry steppe zone	15.3	11.5	228
Wet subtropical zone	21.8	24.4	1400
	17.5	16.5	

Fig. 2. Histogram of Sr<sup>90</sup> content in the surface level of soil covering.

Data concerning the Sr<sup>90</sup> content in the upper (5 cm) level of soil coverage are presented in Fig. 1, from which it can be seen that the radioactive strontium is distributed nonuniformly throughout the earth's surface. This is due mainly to the geographical position of the point of observation, as well as to atmospheric circulation laws and the volume of the air masses between the troposphere and stratosphere. The most frequent content of this isotope in the upper 5 cm of the soil is 10-20 mCi/km<sup>2</sup> (Fig. 2).

A comparison of the Sr<sup>90</sup> content in the soil covering of different regions (Table 2) with the average data throughout the country shows that it was almost unchanged from the second half of 1959 through September 1960. This is explained by the fact that the samples were collected in June-July 1959 after the main rainfall during the time of the spring maximum [7]. Rainfall in the second half of 1959 was several times less than at the beginning of the year [8, 9]. It was calculated in [8] that from April through July 1959, Sr<sup>90</sup> deposition was five times greater than for the remaining 8 months. Its contribution, owing to the rainfall in 1960, was also insignificant [1]; as a result of this the content of radioactive products in air in the Spring of 1960 was three to five times less than in these same months of 1959 [8]. The almost constant Sr<sup>90</sup> content in the soils of the USA in 1959 and 1960 are noted in [2] (46.3 and 49.3 mCi/km<sup>2</sup>, respectively).

Thus, the conclusion can be drawn that during the period under investigation, the quantity of Sr<sup>90</sup> deposited from the atmosphere onto the earth's surface corresponded with the quantity which, because of various processes, was being removed from the upper layer with a thickness of 5 cm.

In order to determine the extent of Sr<sup>90</sup> migration into deeper levels of different types of soils, samples of the soil coverage were analyzed layerwise to a depth of 15-18 cm. The results are shown in Table 3.

It follows from the data in Table 3 that in 1959-1960, 62-88% of the Sr<sup>90</sup> in the upper layer of the soil, with a thickness of 5 cm, was retained in the layer up to 15 cm. The extent of migration into the deeper levels depends, to a considerable degree, on the type of soil. Thus, sandy soils are characterized by a higher content of Sr<sup>90</sup> at a depth of 5-15 cm compared with peat podzolic soils (about 30 and 15%, respectively). On the average, the content of this isotope in the upper 5 cm of the soil amounted to 78.7% in the Soviet Union.

In connection with what has been discussed, for extrapolating the Sr<sup>90</sup> content in the upper 15 cm of



TABLE 3. Sr<sup>90</sup> Distribution with Depth in Different Types of Soil

Type of soil	Time of collection	Depth, cm	Sr <sup>90</sup> content, mCi/km <sup>2</sup>
Pasture, loamy soil of central flood plain (Moscow region)	1960	0- 6	85.0
		6-11	12.6
		11-16	2.4
Podzolic sandy (Moscow region)	1960	0- 6	87.4
		6-11	8.5
		11-18	4.1
Peat-podzolic sandy (Moscow region)	1960	0- 4	87.5
		4-13	8.5
		13-18	4.0
Peat-medium podzolic (Moscow region)	1959	0- 4	82.8
		4- 8	13.3
		8-12	3.9
Peat gleyish, light loamy detrital podzol (Smolensk region)	1960	0- 5	79.7
		5-10	11.9
		10-15	8.9
Peat-subdeveloped sandy soil (Pskovsk region)	1960	0- 5	70.0
		5-15	30.0
Sandy soil (USA) [11]	1958	0- 5	61.8
		5-10	28.5
		10-15	9.7
Sandy soil (USA) [12]	1959	0- 5	72.2
		5-15	23.2
		15-25	4.4
Peat-gleyish ferruginated (Smolensk region)	1960	0- 5	63.0
		5-10	18.7
		10-15	18.3
Peat (Rizhskii region)	1960	0- 5	77.5
		5-15	22.5
Chernozem (Viniitsa region)	1960	0- 5	63.0
		5-10	20.4
		10-15	11.6
Chernozem (Tambovsk region)	1960	0- 5	86.0
		5-15	14.0
Various soils (Federal German Republic) [13]	1958	0- 5	85.0
		5-10	12.0
		10-15	3.0

example, in Norway, the fraction of dry fallout during 1959 fluctuated within the limits of 70-72% [20]. Moreover, the absence of a proportionality relationship may be due to differences in the mobility of Sr<sup>90</sup> in different soils, which in its turn depends on the type of soil, the form of the vegetation coverage, contours and other factors, the study of which is the subject of special investigations.

TABLE 4. Sr<sup>90</sup> Distribution in Soils with Respect to Latitudinal Zone (at mid-1960)

Latitude, North	USSR		Av. world values [1] (up to 15 cm)
	up to 5 cm	up to 15 cm*	
70-60°	10.2	12.8	13.2
60-50°	13.8	17.2	16.9
50-40°	16.2	20.3	24.1
40-30°	—	—	24.0

\* Extrapolated data

the soil coverage of virgin plots covered with herbaceous vegetation, and for comparing the soil contamination level of other countries, it was assumed that (with an error of ±15%) on the average 80% of this isotope is retained in the upper 5 cm.

Data are presented in Tables 4 and 5 concerning the average Sr<sup>90</sup> content in the soil coverage of the Soviet Union and certain countries of the northern hemisphere over several years and over a latitudinal zone. From the data given it can be seen that in 1959-1960 the latitudinal nature of the Sr<sup>90</sup> distribution was maintained over the earth's surface, with maximum values within the limits 30-50°N. The average Sr<sup>90</sup> content in the soil coverage of the Soviet Union is of the same order as in the soils of other countries of the northern hemisphere. By comparison with 1957, the content of this isotope had approximately tripled. It should be noted, however, that the average values give a certain representation of the degree of contamination of the territory of this or other country by radioactive products, but cannot serve as data for estimating the hazard to a specific region, concerning which large differences are indicated between the minimum and maximum values of the Sr<sup>90</sup> content in the soil coverage.

Since it is generally assumed that the main fraction of radioactive products reaches the earth's surface from atmospheric rainfall, a comparison was made with the Sr<sup>90</sup> content in soil subjected to average annual rainfall. As would be expected, there was some correlation but not in all cases, and even where it was observed, the relationship was not proportional. Obviously, this is explained not only by the geographical location of the observation point, but also by the differences in the fractions of "dry" and "wet" fallout and by the rainfall intensity, especially in different seasons of the year. For

TABLE 5. Average Sr<sup>90</sup> Content in the Surface Level of Soils of a Number of Countries, mCi/km<sup>2</sup> (Extreme Values are Given in Brackets)

Country	1957		1958		1959		1960	
	up to 5 cm	5-15 cm	up to 5 cm	5-15 cm	up to 5 cm	5-15 cm	up to 5 cm	5-15 cm
USSR	4.2 [14] (2.1-8.2)	6.0 [14] (3.0-11.7)	—	—	—	—	14.1 (6.6-25.8)	17.8 (8.3-32.8)
England	—	—	9.3* [15] (3.8-38.3)	14.1*[15] (5.8-60.1)	—	—	—	—
Norway	—	—	—	12.4 [6, 16] (4.4-21.3)	—	29.0 [16] (20-50)	—	18.2 [2] (7.5-39.8)
USA	8.5 [17] (2.6-15.5)	10.3 [17] (3.2-16.3)	10.4 [17] (4.5-23.6)	15.6** [6] (6.5-30.4)	—	26.4 [18] (22.0-30.8)	—	24.3 [2] (8.6-53.5)
Japan	—	—	—	—	—	12.8 [19] (3.0-32.0)	—	—
GDR	—	—	—	—	—	—	—	12.0** [3] (4.7-23.1)
Canada	—	—	—	—	—	—	—	18.5 [3] (4.8-29.1)

\*Data obtained for a layer of soil with 4-10 cm thickness.  
\*\*Data obtained for a layer of soil with 20 cm thickness.

Thus, the following conclusions can be drawn:

1. Sr<sup>90</sup> fallout from the atmosphere is distributed nonuniformly throughout the territory of the USSR, and its content in the surface level of soil coverage fluctuates within the range 6.6-25.8 mCi/km<sup>2</sup>; the most frequently observed values are 10-20 mCi/km<sup>2</sup>. On the average, the Sr<sup>90</sup> content in a layer of soil with thickness up to 5 and 15 cm in 1959-1960 amounted to 14.1 and 17.8 mCi/km<sup>2</sup>, respectively.
2. In 1959-1960, the latitudinal nature was maintained for the distribution of Sr<sup>90</sup> in the soil coverage with maximum values within the limits 30-50°N.
3. No significant variations were observed in 1960 of the content of Sr<sup>90</sup> in soil coverage compared with 1959.
4. The extent of Sr<sup>90</sup> migration in the soil coverage depends mainly on landscape-geochemical conditions.

#### LITERATURE CITED

1. Reports of the Scientific Committee on the Effects of Atomic Radiation, of the United Nations Organization Vol. 2 (Appendix E-F), A/5126 (1962) [in Russian].
2. E. Hardy et al., Data from the United Nations Organization. A/AC. 82/G/L, No.822 (1963).
3. H. Reissig, Kernenergie, 5, 191 (1962).
4. F. I. Pavlotskaya et al., Pochvovedenie, No. 2, 105 (1964).
5. Fallout from Nuclear Weapons Test, Vol. 1. United States, Washington, May 5-8, 1959, p. 278.
6. H. Bergh et al., FFiK Intern. Report K-219 (July, 1958).
7. I. L. Karol' and S. G. Malakhov, Global Distribution in the Atmosphere and Fallout on the Earth of Radioactive Products from Nuclear Explosions (Review of the current state of the problem) [in Russian] (Izd. AN SSSR, Moscow, 1960).
8. S. G. Malakhov, Level of Contamination of the Atmospheric Boundary Layer Byproducts from Nuclear Weapon Tests by Measurements in the Podmoskovnye Locality from 1955 to 1959 [in Russian] (Izd. AN SSSR, Moscow, 1960).
9. V. Santgol'zer, Atomnaya énergiya, 9, 56 (1960).

10. P. M. Chulkov, Content of Strontium-90 in Soil and Vegetation Coverage of the Moscow Region [in Russian] (Izd. AN SSSR, Moscow, 1960).
11. Data from United Nations Organization. A/AC. 82/G/L, No. 288 (1960).
12. E. Hardy, HASL-113 (1961).
13. E. Knoop and O. Schoelder, Naturwissenschaften, 45, 436 (1958).
14. B. V. Kurchatov et al., Collection: Soviet Studies Concerning the Danger of Nuclear Weapon Tests [in Russian] (Atomizdat, Moscow, 1959), p. 66.
15. Data from United Nations Organization, A/AC. 82/G/L, No. 354 (1960).
16. Ibid., No. 336 (1960).
17. Ibid., No. 275 (1959).
18. Ibid., No. 335 (1960).
19. Ibid., No. 389 (1960).
20. Ibid., No. 343 (1960).

## ABSTRACTS OF DEPOSITED ARTICLES

SPATIAL AND ENERGY DISTRIBUTION OF SCATTERED  $\gamma$ -RADIATION  
FROM A UNIDIRECTIONAL SOURCE IN AN INFINITE AIR MEDIUM

(UDC 539.171:539.122)

S. M. Ermakov, V. G. Zolotukhin, V. I. Kukhtevich,  
E. S. Matusevich, and B. A. EfimenkoTranslated from *Atomnaya Énergiya*, Vol. 18, No. 3,  
pp. 251-252, March, 1965

Original article submitted March 6, 1964; abstract submitted December 12, 1964

The field of scattered  $\gamma$ -radiation was investigated experimentally and by means of the Monte Carlo method. The energy distributions  $\Phi(E, R, \theta_0)$  were calculated for orientation angles  $\theta_0$  of a unidirectional source in the range from 2 to 180° (ten values). For a distance  $R = 16$  m between the source and the detector, the  $\Phi(E, R, \theta_0)$  value was calculated for initial energies  $E_0$  equal to 0.5, 1.25, 3.0, and 7.0 MeV. For  $E_0 = 1.25$  MeV,  $\Phi(E, R, \theta_0)$  was calculated for  $R$  values equal to 5, 16, and 30 m. For  $R = 16$  m, the  $\Phi(E, R, \theta_0)$  function was measured for  $E_0 = 1.25$  MeV ( $\text{Co}^{60}$  source), using  $\theta_0$  angles equal to 60, 90, 120, and 150°.

The modification of the Monte Carlo method used in our work is known as the method of local calculation of the flux. It was adapted for determining the characteristics of the radiation field in the absence of symmetry with respect to spatial variables [1]. The errors in determining the total flux and the dose rate were estimated to be 7-10%, while the errors in determining the energy distribution within the chosen interval were about 20%. The contribution of annihilation radiation was estimated analytically. For  $R = 16$  m,  $E_0 = 7$  MeV, and  $\theta_0 = 180^\circ$ , the contribution of annihilation quanta was twice as large as the contribution of scattered radiation while, for an isotropic source ( $E_0 = 7$  MeV), the annihilation radiation produced a 12% increase in the dose rate.

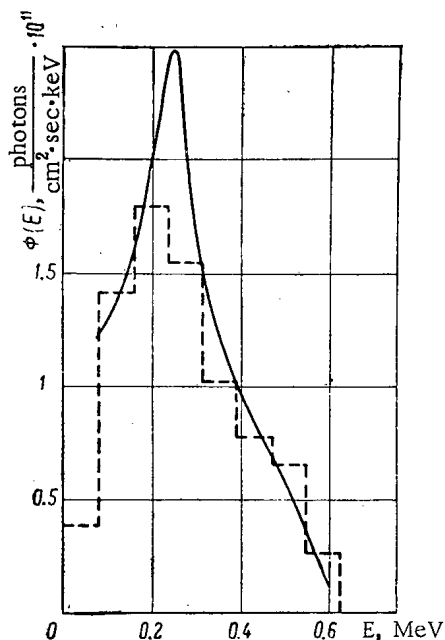


Fig. 1. Value of  $\Phi(E, R, \theta_0)$  for  $R = 16$  m,  $E_0 = 1.25$  MeV, and  $\theta_0 = 60^\circ$  (the histogram represents the result of calculations, while solid curve represents experimental results).

The  $\Phi(E, R, \theta_0)$  values were measured under conditions of an infinitely extended air medium by means of a scintillation

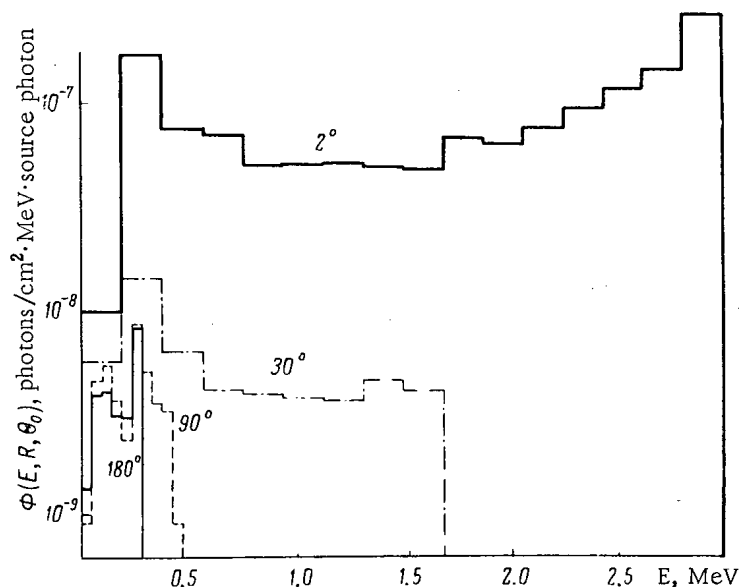


Fig. 2. Calculated  $\Phi(E, R, \theta_0)$  value for  $R = 16$  m,  $E_0 = 3$  MeV, and  $\theta_0$  values equal to 2, 30, 90, and 180°.

spectrometer. The source and the detector were lifted by means of a special suspension device to a height where the influence of the earth was negligibly small. The source's collimation angle was  $7.7^\circ$ . On the average, the measurement errors were equal to 10-15%. The experimental and calculation results are given in Fig. 1. Figure 2 shows the calculated  $\Phi(E, R, \theta_0)$  value. The  $\Phi(E, R, \theta_0)$  function changes only slightly in dependence on R; the relationship  $\Phi(E, R, \theta_0) \approx \Phi(E, \theta_0)/R$  holds approximately for every  $\theta_0$ . The upper limit of the energy distributions is determined by  $\gamma$ -radiation singly scattered at the minimum possible angle for the given geometry.

## LITERATURE CITED

1. V. G. Zolotukhin and S. M. Ermakov, Collection: Problems in the Physics of Reactor Shielding, Edited by D.L. Broder et al. [in Russian] (Gosatomizdat, Moscow, 1963), p. 171.

ANGULAR AND ENERGY DISTRIBUTION OF SCATTERED  $\gamma$ -RADIATION  
NEAR AN ISOTROPIC SOURCE IN AN INFINITE AIR MEDIUM

(UDC 539.171:539.122)

Yu. I. Kolevatov, V. I. Kukhtevich, E. S. Matusevich,  
and O. A. Trykov

Translated from *Atomnaya Énergiya*, Vol. 18, No. 3,  
pp. 252-253, March, 1965

Original article submitted August 3, 1964; abstract submitted December 12, 1964

We performed an experimental investigation of the angular and energy distribution  $\Phi(E, R, \theta)$  of scattered  $\gamma$ -quanta from a  $\text{Co}^{60}$  isotropic point source in an infinite air medium for two values of the distance  $R$  from the source (15 and 30 m) and for different angles  $\theta$  between the source-detector line and the symmetry axis of the unidirectional detector ( $12^\circ \leq \theta \leq 180^\circ$ ).

The energy spectra of  $\gamma$ -quanta were measured by means of a single-crystal scintillation spectrometer with a  $40 \times 40$ -mm NaI(Tl) crystal, which was placed in a lead collimator-container with a total collimation angle  $\Delta\gamma = 10 \pm 0.2\%$ . The matrix method was used in processing the instrumental pulse distributions.

The absolute error of the energy distributions  $\Phi(E, R, \theta)$  was, on the average, equal to 10-15%, while it increased with an increase in the energy of scattered  $\gamma$ -quanta; it attained 100% in the "cutoff" region of energy distributions (the measured effect became weaker than the background). Figure 1 shows a portion of the results obtained

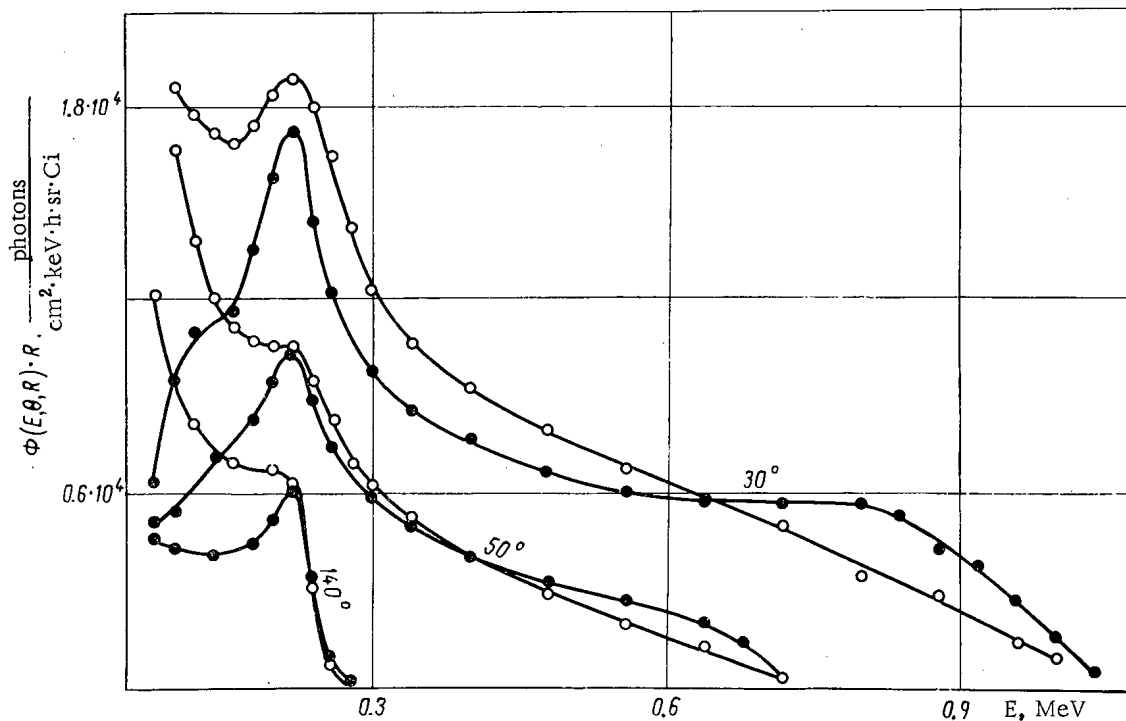


Fig. 1. Angular and energy distribution  $\Phi(E, R, \theta)$  of scattered  $\gamma$ -quanta from a  $\text{Co}^{60}$  isotropic point source in an infinite air medium.  $\circ$ )  $R = 15$  m;  $\bullet$ )  $R = 30$  m.

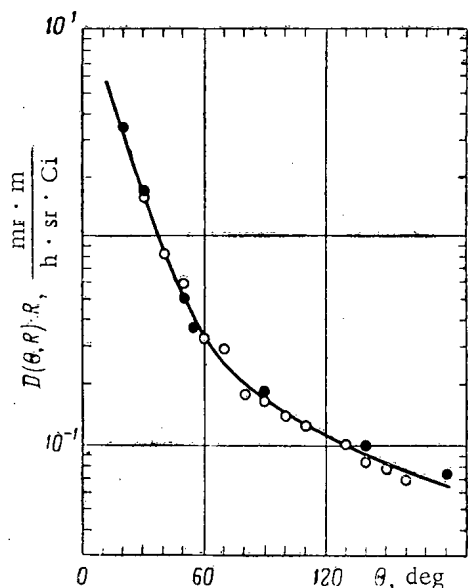


Fig. 2. Angular distribution  $D(R, \theta)$  of the dose rate of scattered  $\gamma$ -radiation from a  $\text{Co}^{60}$  isotropic point source in an infinite air medium.  $\circ$   $R = 15$  m;  $\bullet$   $R = 30$  m.

the angular distribution  $D(R, \theta)$  of the dose rate and the spatial distribution  $D(R, \theta_0)$  of the dose rate [2] of scattered  $\gamma$ -radiation from a  $\text{Co}^{60}$  source indicate that these two geometries can be considered as invertible for the parameter values investigated.

in measuring the  $\Phi(E, R, \theta)$  function for  $R = 15$  m and  $R = 30$  m. All the curves are characterized by the presence of a maximum in the 0.20-0.22 MeV region, which corresponds to  $\gamma$ -quanta singly scattered at angles close to  $180^\circ$ . The angular and energy distributions  $\Phi(E, R, \theta)$  in the region of maximum energies are determined by  $\gamma$ -quanta singly scattered in air at the angle  $\theta$  (with an accuracy to the spectrometer's energy resolution and the experimental errors). The slight reduction in the mean energy of scattered  $\gamma$ -quanta with an increase in the distance  $R$  can be explained by the redistribution of high-energy  $\gamma$ -quanta in the subsequent scattering toward the region of softer energies.

Figure 2 shows the angular distribution of the dose rate of scattered  $\gamma$ -radiation, which was calculated from the angular energy distributions  $\Phi(E, R, \theta)$  for  $R = 15$  m and  $R = 30$  m. It should be mentioned that, for  $R = 15$  m, the relative contribution of multiply (twice or more) scattered  $\gamma$ -radiation to the total dose rate depends linearly on the angle  $\theta$  with a good accuracy ( $\pm 15\%$ ), attaining a maximum of about 50% at  $\theta = 180^\circ$ .

Comparisons between the angular and energy distributions  $\Phi(E, R, \theta)$  (isotropic source - unidirectional detector) and the spatial and energy distributions  $\Phi(E, R, \theta_0)$  of scattered  $\gamma$ -quanta [1] (unidirectional source - isotropic detector) and also between

#### LITERATURE CITED

1. S. M. Ermakov et al., this issue, p. 311.
2. V. I. Kukhtevich et al., *Atomnaya énergiya*, 16, 5 (1964).

SPATIAL DISTRIBUTION OF THE DOSE RATE  
OF AIR-SCATTERED NEUTRONS FROM A UNIDIRECTIONAL POINT SOURCE

(UDC 539.171.4)

S. F. Degtyarev and V. I. Kukhtevich

Translated from *Atomnaya Énergiya*, Vol. 18, No. 3,  
pp. 253-254, March, 1965

Original article submitted June 24, 1964; abstract submitted December 12, 1964

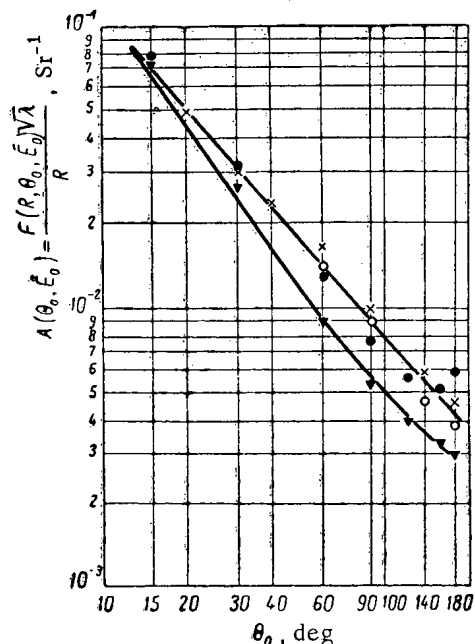


Fig. 1. Dependence of  $A(\theta_0, \bar{E}_0)$  on  $\theta_0$  and  $\bar{E}_0$ .  
Experimental values:  $\times$ )  $E_0 = 1.9$  MeV;  $\circ$ )  $E_0 = 4.2$  MeV.  
Averaged calculated values [2]:  
 $\bullet$ )  $E_0 = 0.33-4$  MeV;  $\nabla$ )  $E_0 = 6-14$  MeV.

We measured the spatial distribution  $F(R, \theta_0, \bar{E}_0)$  of the relative dose rate produced by unidirectional point sources of neutrons with initial energies  $\bar{E}_0$  equal to 4.2 and 1.9 MeV for a distance  $R = 14.8$  m between the source and the detector. The  $F(R, \theta_0, \bar{E}_0)$  value was defined as the ratio of the dose rate of scattered radiation at a given point to the dose rate of direct radiation in vacuum at the same point. The orientation angle  $\theta_0$  of the unidirectional source varied from 20 to 180°. The neutrons were detected by means of a dosimeter for measuring the biological dose [1]. The measurements were performed under conditions where the contribution of the radiation scattered from the earth was negligibly small. For the neutron sources, we used Po-Be ( $E_0 = 4.2$  MeV) and the same source after it was placed in a spherical steel casing ( $\bar{E}_0 = 1.9$  MeV). In determining  $F(R, \theta_0, \bar{E}_0)$  for the two  $\bar{E}_0$  values, we measured  $\bar{\lambda}$ , the mean free path of unscattered radiation in air. The measured  $\bar{\lambda}$  values agreed with an accuracy to about 10% with the values calculated by using the equation

$$\bar{\lambda} = \frac{\int_0^{\infty} s(E) \varepsilon(E) dE}{\int_0^{\infty} s(E) \varepsilon(E) \Sigma_t(E) dE}, \quad (1)$$

where  $s(E)$  is the spectrum of source neutrons,  $\varepsilon(E)$  is the factor for converting the unit flux to the dose rate, and  $\Sigma_t(E)$  is the total macroscopic cross section of interaction between neutrons and air.

The experimental results were compared with calculation data [2]. The Monte Carlo method was used in [2] for calculating the dose rate produced by monoenergetic unidirectional point sources in the range of  $\bar{E}_0$  values from 0.33 to 14 MeV. It follows from an analysis of the calculation and experimental data that, for  $R/\lambda < 1$ ,  $F(R, \theta_0, \bar{E}_0)$  can be approximately expressed in the following manner:

$$F(R, \theta_0, \bar{E}_0) = R\lambda^{-1/2} A(\theta_0, \bar{E}_0). \quad (2)$$

It was found that, with an accuracy to 15-20%,  $A(\theta_0, \bar{E}_0)$  is independent of  $E_0$  within the energy intervals 0.33-4 MeV and 6-14 MeV. The figure shows the averaged calculated  $A(\theta_0, \bar{E}_0)$  values and the experimental data. With an accuracy to  $\pm 20\%$ , the  $F(R, \theta_0, \bar{E}_0)$  quantity can be described by the following expressions (solid curves in the figure):

$$F(R, \theta_0, \bar{E}_0) = 2.1 \frac{R}{\sqrt{\bar{\lambda}} \theta_0^{1.25}}, \quad 0.3 < E_0 < 6.0 \text{ MeV.}$$



$$F(R, \theta_0, \bar{E}_0) = 3.2 \frac{R}{\sqrt{\lambda \theta_0}^{1.45 - 5 \cdot 10^{-4} \theta_0}}, \quad 6.0 < E_0 < 14.0 \text{ MeV}$$

( $\lambda$  and R are expressed in meters, and  $\theta_0$  is given in degrees).

LITERATURE CITED

1. Kh. D. Androsenko and G. M. Smirenkin, PTÉ, No. 5, 64 (1962).
2. Reactor Handbook, Vol. III, Part B, Shielding. Editor E. Blizard, New York, 1962.

## CERTAIN NONLINEAR PROBLEMS IN NUCLEAR REACTOR THEORY

(UDC 621.039.51)

O. B. Moskalev and V. A. Chuyanov

Translated from *Atomnaya Énergiya*, Vol. 18, No. 3,  
pp. 254-255, March, 1965

Original article submitted January 20, 1964; abstract submitted November 19, 1964

Certain problems in nuclear reactor theory lead to a nonlinear steady-state equation of neutron transport where the cross sections of interaction between neutrons and matter depend on an unknown function, the neutron flux, i.e.,  $\Sigma = \Sigma[P, B\Phi(P)]$ , where  $\Sigma$  is the cross section,  $P$  is a point in space,  $\Phi$  is the neutron flux, and  $B$  is a certain operator. The type of operator  $B$  is determined by the actual physical problem at hand. In the present article, we shall consider as such an example the calculation of a nuclear reactor with an assigned spatial distribution of power per unit volume of coolant. The simplest statement of this problem of interaction cross section is given in the form of algebraic functions of the flux  $\Phi$ . Another problem which leads to a nonlinear equation of transport is the calculation of the reactor's steady-state operating conditions where the concentration of the contaminating substance has attained its equilibrium value. In this case, the cross sections can also be expressed in terms of the neutron flux. Finally, as a third example, we can cite a reactor operating at a fairly high energy level where it is necessary to take into account the relationship between the temperature distribution in the reactor and the neutron flux. In this case, the interaction cross sections and also the internal and external geometric characteristics of the reactor depend on the temperature, due to which the neutron transport equation is nonlinear. In the latter example, the temperature in the reactor is determined as a function of the neutron flux by means of the  $B$  operator. Let us consider in greater detail the relationship between the temperature and the neutron flux.

In solving the linear transport equation, it is known that there is only one value of the parameter  $\nu = \nu_0$  for which a steady-state solution of the transport equation can be obtained. The  $\nu_0$  value corresponds to an eigenfunction determined with an accuracy to an arbitrary factor. Thus, the reactor can operate at any power level for a fixed temperature distribution in the reactor. However, it is known that the reactivity depends on the temperature, so that, for instance, a reactor which is supercritical in the cold state will become critical at a sufficiently high power level. This fact cannot be taken into account within the framework of the linear equation of neutron transport. In accordance with the classical results obtained by P. S. Uryson, the positive spectrum of the nonlinear operator of transport from a single point "spreads" to a certain interval. This means that, for any  $\nu > \nu_0$ , there is a specific steady-state solution for a certain given reactor power level (under the assumption that the reactivity decreases with an increase in the power level).

This article is concerned with the existence of a unique positive nontrivial solution of Peierls' nonlinear integral equation:

$$\lambda\Phi(P) = A\Phi,$$

where  $A$  is a nonlinear integral operator, which is assumed to be monotonic. The equation is solved by using the method of successive approximations under natural physical assumptions. The solution is unique if additional limitations are imposed. Thus, if the angular distribution of neutrons is close to an isotropic distribution (if the assumptions on which the diffusion approximation is based are satisfied), the solution is unique if the multiplication constant varies monotonically in dependence on the neutron flux  $\Phi$  that determines the cross sections of interaction between neutrons and the material.

The above investigation was extended to the case of the multivelocity problem with isotropic scattering. However, in this, the operator must satisfy the conditions that are fulfilled in the case of a more limited class of problems.

EFFECT OF A CONDUCTING DIAPHRAGM  
ON PLASMA EQUILIBRIUM IN TOKAMAK DEVICES

(UDC 533.9)

V. D. Shafranov

Translated from *Atomnaya Energiya*, Vol. 18, No. 3,  
pp. 255-256, March, 1965

Original article submitted October 23, 1964; abstract submitted December 29, 1964

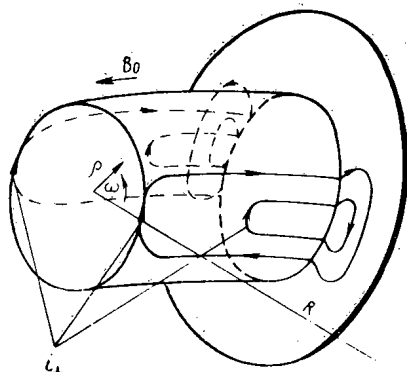


Fig. 1. Current lines closing through the diaphragm.

As is known, the toroidal plasma filament in experimental Tokamak devices [1] is kept in equilibrium as a result of interaction between the longitudinal current  $J$  and the magnetic field's component which is transverse with respect to the toroid plane. In particular, this component is connected with the eddy currents in the conducting sheath. Equilibrium can also be maintained as a result of interaction between the longitudinal magnetic field and the transverse current component  $i_{\perp}$ , which flows through the thin sheath of the plasma filament [2]. Such a current component is possible in a toroidal plasma filament only if the current lines can be closed outside the plasma through external electrodes. The diaphragm shaping the plasma filament can act as such an electrode (see Fig. 1). For a correct interpretation of experimental data on the shift of the plasma filament, it is necessary to have expressions relating the measured values of the azimuthal field  $B_{\omega}$  and of the current  $J_d$  toward the diaphragm to the shift  $\xi_0$  averaged with respect to length. These expressions are given by

$$J_d = J \frac{4a^2}{b^2 - a^2} \cdot \frac{RB_{\omega_0}}{aB_0} \cdot \frac{\xi_0 - \Delta}{a}, \quad (1)$$

$$B_{\omega} = B_{\omega_0} \frac{a}{\rho} - B_{\omega_0} \left\{ \frac{a\Delta}{\rho^2} + \frac{a}{2R} \left[ \ln \frac{\rho}{a} - 1 + \left(1 + \frac{a^2}{\rho^2}\right) \left( \frac{8\pi\rho}{B_{\omega_0}^2} - \frac{1}{2} \right) \right] + \frac{a}{b^2 - a^2} \left(1 + \frac{b^2}{\rho^2}\right) (\xi_0 - \Delta) \right\} \cos \omega. \quad (2)$$

Here,  $B_{\omega_0} = 2J/ca$ ;  $a$  is the radius of the diaphragm opening,  $\rho$  is the present radius,  $\omega$  is the azimuthal range, measured from the equatorial plane from the inside of the torus,  $R$  is the torus radius, and  $\Delta$  is the shift in the absence of the diaphragm [3]:

$$\Delta = \frac{b^2}{2R} \left[ \ln \frac{b}{a} + \left(1 - \frac{a^2}{b^2}\right) \left( \frac{8\pi\rho}{B_{\omega_0}^2} - \frac{1}{2} \right) \right] - \frac{cb^2 B_{\perp}}{2J}, \quad (3)$$

where  $b$  is the radius of the cross section of the conducting sheath, and  $B_{\perp}$  is the transverse component of the external magnetic field.

The dependence of the plasma filament's shift in the equatorial plane on the arc length  $s$ , measured from the diaphragm; is expressed by means of the following approximate relationship, which holds for  $|s| > a$ :

$$\xi(s) = \frac{B_{\omega_0}^2}{2B_0^2 b^2} \Delta s (2\pi R - s). \quad (4)$$

In the limit, when  $B_{\omega_0} \rightarrow 0$ , expressions (3) and (4) can be used for finding an approximate expression for the shift of a plasma filament held in equilibrium in a purely toroidal magnetic field by means of currents flowing off to the diaphragm:

$$\xi(s) = \frac{1}{4} \frac{8\pi p}{B_0^2} \left(1 - \frac{a^2}{b^2}\right) s(2\pi R - s). \quad (5)$$

LITERATURE CITED

1. L. A. Artsimovich, S. V. Mirnov, and S. S. Strelkov, *Atomnaya énergiya*, 17, 170 (1964).
2. S. Yoshikawa, W. Harries, and H. Sinclair, *Phys. Fluids*, 6, 1506 (1963).
3. V. D. Shafranov, *Problems in Plasma Theory* [in Russian] (Gosatomizdat, Moscow, 1963), Vol. 2.

## ADIABATIC PINCHING OF HOT-ION PLASMA

(Description of the Device and the First Experiments)

(UDC 533.9)

A. V. Bortnikov, N. N. Brevnov, V. G. Zhukovskii,  
and M. K. Romanovskii

Translated from *Atomnaya Énergiya*, Vol. 18, No. 3,  
pp. 256-257, March, 1965

Original article submitted August 13, 1964; abstract submitted January 9, 1965

The adiabatic-pinching device is designed for investigating the behavior of hot-ion plasma in a magnetic field that increases in time. The schematic diagram of the device is shown in Fig. 1.

The plasma is produced by injecting atomic hydrogen ions with an energy of 10 keV (or molecular ions with an energy of 7 keV). The ions move in a uniform magnetic field about the axis of the device in a direction almost perpendicular to it. They are reflected by a magnetic mirror, returned to the channel, and trapped by Azotit. The ions are separated from the channel by the rising magnetic field of the separating coil and are squeezed toward the stationary magnetic mirror (longitudinal pinching). The subsequent radial and longitudinal pinching of plasma is effected by means of pinching coils. The steady-state magnetic field is  $H_0 = 2000$  Oe; the maximum magnetic field of the separating coil is  $3 \cdot 10^4$  Oe; the magnetic field of the pinching coils in the mirrors is  $3 \cdot 10^4$  Oe; the mirror ratio is equal to 3.

The ion current, which is equal to 1-5 mA, is injected in pulses whose duration can be varied from 1 to 500 msec. The initial gas pressure before injection of the ion beam is of the order of  $10^{-8}$  mm Hg.

The experimental data given below pertain to the plasma parameters before pinching. The initial density of hot ions before pinching is proportional to the injection current and the duration of the motion of ions in the trap.

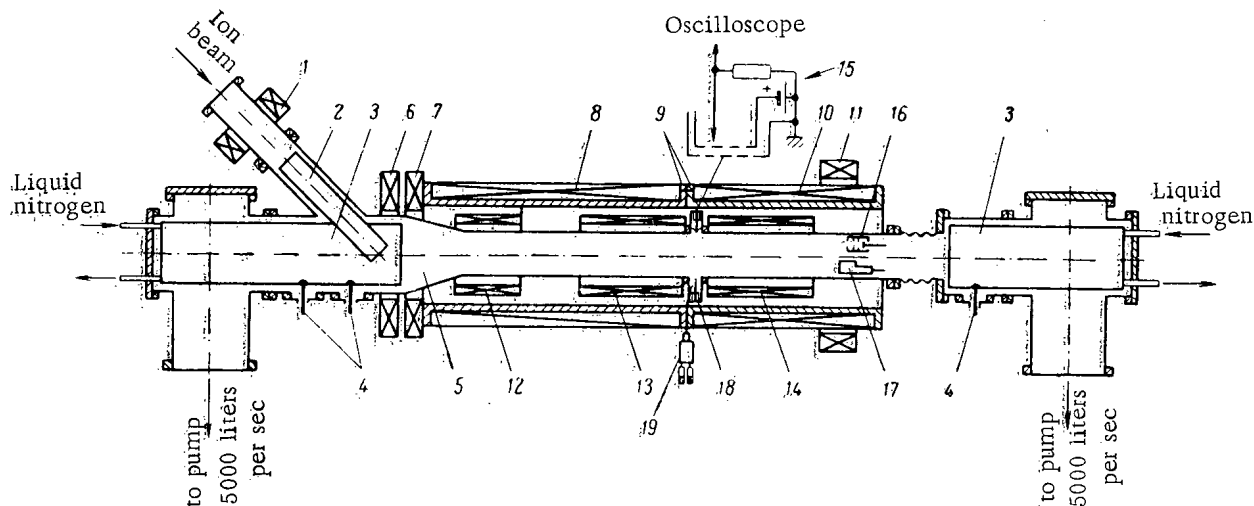


Fig. 1. Diagram of the adiabatic-pinching device. 1) Magnetic lens focusing the ion beam; 2) channel; 3) Azotit; 4) titanium evaporators; 5) chamber; 6,7,8,10,11) steady magnetic field coils; 9) copper screen; 12) separating coil; 13,14) pinching coils; 15) neutral-particle detector; 16) analyzer for energy spectrum of secondary ions; 17) current collector; 18) stub probe; 19) palladium inleakage element.

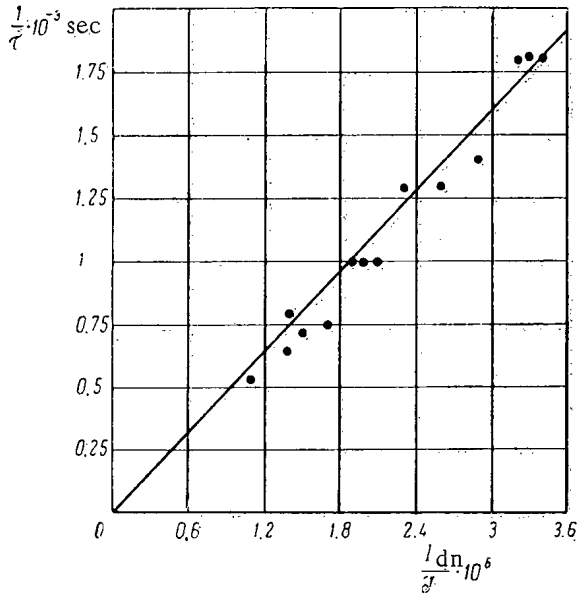


Fig. 2. Dependence of  $1/\tau$  on the flux of fast neutral atoms to the detector.

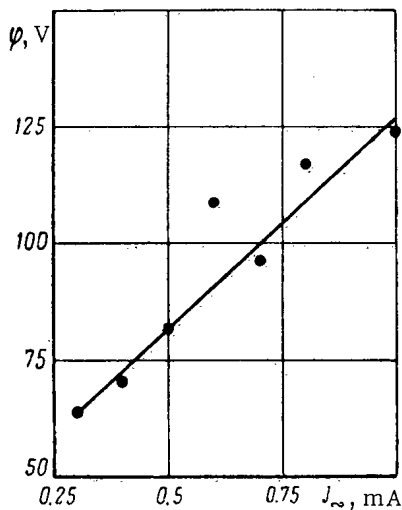


Fig. 3. Dependence of the plasma potential  $\phi$  on the amplitude of the alternating current component.

before they reach Azotit. For the above injection current value and the measured time of ion motion, which was equal to  $30 \mu\text{sec}$ , the maximum density of fast ions was equal to  $10^8 \text{ cm}^{-3}$ .

The neutral gas pressure in the trap during the injection of the ion beam was determined with respect to the flux  $I_{dn}$  of fast atoms to the neutral-particle detector for a known injection current  $I$ . The following dependence was established experimentally:  $I_{dn}/I = 7 r_{eq}$ , where  $r_{eq}$  is the hydrogen pressure (mm Hg) equivalent to the neutral gas pressure in the trap with respect to the flux of neutral particles. If the  $r_{eq}$  value is known, the charge exchange time  $\tau$  for fast ions can be calculated. The thus-calculated  $\tau$  values are in good agreement with the values measured in separating the ion beam from the channel. Figure 2 shows the experimental dependence of  $1/\tau$  on the  $I_{dn}/I$  ratio. The slope of the straight line yields a value  $\sigma_{pv} = 1.4 \cdot 10^{-7}$ , which is close to the theoretical value of  $\sigma_{pv}$  for protons with an energy of 10 keV in hydrogen. Thus, in our case, the basic process leading to the loss of fast ions is the charge exchange.

The plasma potential before the separation of the ion beam from the magnetic channel was determined with respect to the energy of secondary ions that have passed beyond the mirror. It was found that the plasma potential is independent of pressure in a wide range of pressures ( $10^{-5}$ - $10^{-7}$  mm Hg) and that its value is determined by the amplitude of current pulsations in the injected beam. The dependence of the potential on the alternating component of the injection current is given in Fig. 3. The potential value of about 35 V, obtained by extrapolating the straight line to the intersection with the axis of ordinates, apparently corresponds to the plasma potential in the absence of fluctuations of the injected current.

## RULES FOR DEPOSITING (STORING) ARTICLES

Translated from *Atomnaya Énergiya*, Vol. 18, No. 3,  
p. 257, March, 1965

Articles of interest to a limited number of specialists are deposited either on the authors' request or in accordance with the decision of the Editorial Board of the journal.

Detailed abstracts of the deposited articles will be published in the journal, while the complete articles will be kept at the editor's office and sent C.O.D. to readers on request. The volume of the abstracts to be published should not exceed  $\frac{1}{10}$  author's sheet (about two pages of typewritten text), while the maximum volume of the deposited text should not exceed 1 sheet. On the author's request, diagrams, tables, the basic equations, etc., can be included in the abstract within the limits of its over-all volume.

An abstract will be published not later than three to four months after the article has been received at the editor's office (if the article is deposited on the author's request), or after the authors have consented to deposit it (if this decision has been brought by the Editorial Board).

Deposited articles are regarded as scientific publications and are taken into consideration in the defense of dissertations.

The articles submitted for deposition must be suitable for photographic reproduction, and the text, equations, tables, etc., must be clear; the drawings must be made on tracing paper, included in the text, and pasted on the paper, and provided with captions.

The price of a single copy of a deposited article is 40 k. In ordering copies of deposited articles, reference must be made to the registration number of the article given at the end of the abstract.

Orders should be mailed to the editorial office of the journal at the following address: 18 Kirov Street, Center, Moscow.

## REVIEW OF THE GENEVA CONFERENCE

INVESTIGATIONS INTO THE PROBLEM  
OF CONTROLLED THERMONUCLEAR FUSION

S. D. Fanchenko

Translated from *Atomnaya Énergiya*, Vol. 18, No. 3,  
pp. 258-260, March, 1965

In contrast to the Second International Conference on the Peaceful Uses of Atomic Energy in 1958, which for the first time raised the broad scientific discussion of investigating the feasibility of controlled thermonuclear fusion, at the Third Conference only one three-hour Plenary Session was devoted to this problem for a general review of the state of research in various countries of the world. For a more detailed discussion of this problem and of the extensive volume of scientific information, international conferences are now convened regularly by the International Atomic Agency on the physics of high-temperature plasmas. The first of these conferences took place in 1961 in Salzburg (Austria) and the next one is planned to take place in September 1965 at Culham (Great Britain).

At the session on Controlled Thermonuclear Fusion, four review reports were worthy of mention:

1. Report 297 by Academician L. A. Artsimovich, on "Investigations into the problem of controlled nuclear fusion and the physics of high-temperature plasmas in the USSR";
2. Report 195, by A. Snell et al., on "Investigations into controlled thermonuclear reactions in the USA";
3. Report 882 by A. Schlüter (Federal German Republic), on "Investigations into controlled nuclear fusion in Western Europe";
4. Report 881 by K. N. Watson-Munro (Australia), on "Development of research on controlled nuclear fusion and plasma physics in the countries of the world (notably Europe, North America, and the USSR)".

A discussion took place afterward in which the following participated with short reports: M. Trosher (France), T. Consol (France), J. Adams (Great Britain), I. N. Golovin (USSR), K. Fushim (Japan), and K. Watson-Munro (Australia).

Since the complete text of the report by Academician L. A. Artsimovich has been published in the October issue of the journal "Atomnaya Énergiya" for 1964, it will be sufficient to mention here that a detailed review is given in it of the successes of Soviet scientists in the solution of the problem of containment and heating of a plasma, in particular in accomplishing magnetic traps with a combined field, concerning the stability of containment of a plasma pinch in toroidal assemblies with an intense external longitudinal magnetic field, turbulent and cyclotron heating and high-frequency dynamic stabilization of a plasma, etc.

## RESEARCH IN THE USA

The summary report by A. Snell et al. deals principally with the development of those lines of research which were discussed at the previous conference.

Traps with Magnetic Probes. In the "Alice" and "Table Top" assemblies, plasma stabilization by Ioffe's method was successfully tested. In the "Alice" assembly, 12 current-conducting rods were used for this purpose, and the density of the plasma at a temperature of 20 keV was successfully increased to  $3 \cdot 10^9 \text{ cm}^{-3}$  in comparison with the value of  $10^8 \text{ cm}^{-3}$  attained in this trap in the absence of the stabilizing fields. In the "Table Top" assembly fluted instability of the plasma was clearly observed, which was suppressed by transition to the combined magnetic field of the trap because of the use of four or six current-carrying rods according to Ioffe's method. But, also, in the absence of stabilizing fields in the "Table Top" and "Alice" assemblies, it was possible to suppress in specific operating regimes (at high electron temperatures) — magnetohydrodynamic instabilities on account of the finite Larmor radii and due to the presence of a cold conductivity plasma at the electrodes located outside the magnetic probes.



In experiments concerned with the injection of a beam of  $H_2^+$  ions into the DCX-1 assembly with Lorentz ionization in a magnetic field, it was possible to introduce into the trap not more than  $10^{12}$  protons (maximum plasma density at the center was  $10^8 \text{ cm}^{-3}$ ). This limit, obviously, is governed by the appearance of microinstabilities.

As a result of injecting ions of  $H_2^+$  with an energy of 600 keV into the magnetic trap of DCX-2 at a lithium arc with a strong current of 25 A, 40-50% of the ions were dissociated. A plasma density of  $10^{10} \text{ cm}^{-3}$  was achieved in the trap and the energy spectrum of the protons was studied in detail. It is interesting to note that in this assembly, which is represented by the usual magnetic trap with probes, at no time was the appearance of fluted instability observed.

In certain laboratories the investigation of Thetatrons was continued. An attempt was made to stabilize a plasma in a Thetatron by means of a quadripolar magnetic field, but for the time being no positive results have been obtained.

The "Astron" Assembly. On August 1, 1964, injection was commenced of relativistic electrons for forming an E-layer, the magnetic field of which it is proposed to use for stable containment of a plasma. An induction linear electron accelerator is being used at an energy of 4.1 MeV (from 5 to 60 electron bursts per second, with a duration of 0.25  $\mu\text{sec}$  for each burst). The first experiments showed that the lifetime of the relativistic electrons of the E-layer was not 5 sec as expected, but only about 50  $\mu\text{sec}$ . As a possible reason for instability of the E-layer, has been put forward the interaction of the electrons with the intense electromagnetic oscillations developing within the cavity of the assembly.

Investigations of Toroidal Traps. Investigations of current heating, purification, and containment of a plasma were continued in the "Stellarator-C" assembly. The use of a diverter has enabled the concentration to be reduced of the oxygen impurities (which are the most difficult to remove) in a hydrogen plasma by a factor of 80, i.e., down to 0.05%. Almost the entire balance of the buildup and loss of energy by current heating of the plasma has been traced, but losses of plasma from the trap have been observed which are not completely explained, and which increase with increase of current; these losses may be attributed to turbulent diffusion created by the presence of the current. Experiments have been commenced with cyclotron heating of ions in "Stellarator-C." In similar experiments in the magnetic probe trap, an ion temperature of about 1 keV has been achieved.

In the "Levitron" toroidal assembly (with a circular current-conducting core inside the plasma), a plasma instability has been observed which leads to local distortion of the magnetic surfaces and the drift of electrons with energies in excess of 100 eV at a plasma density of  $10^2$ - $10^{13} \text{ cm}^{-3}$ . It is assumed that this is a very small-scaled instability, which originates because of the finite resistance of the plasma as a result of the application of current heating. A new version of the "Levitron" has been constructed with high-frequency plasma heating, where, according to theoretical studies and preliminary experimental results, no such instability should be found.

Other Routes. Of the new experimental lines of investigation, one should mention plasma heating by interaction with electron beams, electron cyclotron heating of the plasma in a continuous cycle, plasma containment and stabilization in axially-symmetrical and toroidal traps with quasi-stationary magnetic field currents which increase toward the periphery and which traverse through the system in one direction from four conductors situated inside the vacuum chamber. The four current-conducting rods used in the linear assembly are parallel to the axis of symmetry, and in the toroidal assembly four current-conducting rings are used, located along the periphery of the torus.

#### PLASMA RESEARCH IN WESTERN EUROPE

As indicated by A. Schlüter's report, the position of the studies of the physics of high-temperature plasmas in Western Europe has undergone a considerable change since the time of the Second Geneva Conference.

While in 1958 the experimental investigations were conducted on a large scale almost entirely by Great Britain, at the present time France, Federal German Republic, and other countries are actively included in them, and the efforts are coordinated by Euratom. Altogether in Western Europe, 43 scientific organizations are engaged in the problem of controlled thermonuclear reactions. The following principal scientific groups are mentioned in Schlüter's report: The Culham Thermonuclear Research Center in Great Britain (110 physicists, with an annual budget of 10 million dollars); the Scientific Society within the structure of the West German Institute of Plasma Physics in Garching (99 physicists, annual budget of 2 million dollars), and the French centers of Fontenay-aux-Roses (75 physicists) and Saclay (17 physicists); the Scientific Society within the structure of the Italian plasma laboratory in Frascati, Dutch

Institutes in Jutphaas and Amsterdam, and the West German center of Jülich (near Aachen); the Institute of Plasma Physics in Stockholm (Sweden); the Danish Scientific Laboratory in Riga; the Plasma Physics Laboratory of Paris University in Orsa, the Plasma Division of the Max Planck Institute (Munich, Federal German Republic). The activities of these West-European scientific organizations is coordinated by a seminar bearing the name European Fusion Research Group. Moreover, each one of the scientific societies listed has its joint council. An extensive program of experiments is to be undertaken. Axially-symmetrical high-current discharges are being studied (self-constricted discharge "Tiber" and the tubular pinched discharge "Faust" in Culham, the tubular pinched discharge in Fontenay-aux-Roses in Garching, an assembly with a self-constricting thin cylindrical layer of plasma "Mirapi" in Frascati) and high-current toroidal discharges ("Zeta" in Culham, a "Levitron" type of assembly in Stockholm and in Aldermaston, and two assemblies in Jutphaas). Investigations are being undertaken into magnetic traps with probes ("MM-II" and "DECA-II" in Fontenay-aux-Roses, "Phoenix" and MTSE in Culham, a trap with a cusped geometry field in Jutphaas), and into toroidal traps of the Stellarator type ("Wendelstein" in Munich). Thetatron are being studied: normal thetatrons in Culham, Jülich, and Garching, the "Karidi" thetatron with sectioned coils for decreasing the inductivity and increasing the bypass emf in Frascati, the "M + S" toroidal thetatron with a crimped field in the "Lupus" and "Quasilimus" versions in Munich. In Culham, an experiment is being undertaken with a plasma pinch in a magnetic field with cusped geometry - Spindle Cusp. In Frascati, dynamic plasma pinch is being studied ("Mafin II" assembly) with commutative explosion of the conducting cylinder, enveloping the magnetic field. In Saclay, assemblies have been constructed for high-frequency plasma containment - PLEIADE, CIRCE, and ICARE, in the last of which the high-frequency field intensity attains 1 MW. In Jutphaas, Fontenay-aux-Roses, and Jülich, experiments are being carried out with plasma injection and plasmoid collision, etc. Among the results obtained, the following may be mentioned.

Magnetic Trap with a Combined Field. The addition of a magnetic field of 6 current-conducting rods by Ioffe's method to the field of the magnetic probe trap MTSE (Culham) has extended the plasma containment time from  $10^{-5}$  to  $5 \cdot 10^{-4}$  sec. In the French probe trap "DECA-II," filled by injection of a plasma bunch, the inclusion of a stabilizing quadrupolar magnetic field has extended the plasma containment time from  $2 \cdot 10^{-5}$  up to 1 to  $2 \cdot 10^{-4}$  sec (over the density range  $10^{10}$ - $10^{13}$   $\text{cm}^{-3}$ ). The use of stabilizing combined fields is being planned also in other assemblies. The successful stabilization of a plasma with a combined field in a thetatron is reported (Culham, Jülich).

Investigation of Plasma Instabilities. In the "Faust" assembly, special experiments have been carried out to compare plasma stability in the normal and in a tubular self-constricting discharge under similar conditions. Although containment in the second case proved to be somewhat better, the level of fluctuation in the plasma was relatively large in both cases. The authors attribute the origination of instability to the finite conductivity of the plasma discharge with the resulting destruction of the field "frozen" into the plasma. This conclusion is substantiated by theoretical calculations and by a model experiment for observing the instability of a column of mercury in a magnetic field with configurations which were characteristic for a tubular self-constricting discharge. In Garching the rapid development was discovered of instabilities due to finite conductivity in the plasma of thetatrons during the trapping in the plasma of the initial magnetic field.

In Munich and Garching, theoretically, and in Saclay experimentally, small-scale plasma instabilities are being studied in traps with magnetic probes, in particular, ionic cyclotron instability.

In Stockholm and Amsterdam, a method of heating a plasma is being studied by imparting to it a macroscopic rotation with subsequent dissipation of this rotational energy into the plasma.

Other Investigations. In some laboratories, different methods are being studied of building up the plasma in the magnetic traps: ion injection, plasma bunch injection, injection of neutral atoms. In the magnetic trap "Phoenix," a beam of neutral atoms is injected with an energy of 20 keV. Lorentz ionization of atoms is used in the magnetic field of the trap. A plasma density of  $10^9$   $\text{cm}^{-3}$  has been attained.

In Munich, the toroidal drift of a plasma has been studied experimentally. In the "M + S" assembly, crimping of the magnetic field enabled the time of existence of the plasma, which is limited by toroidal drift, to be extended by a factor of three.

In the "Mirapi" assembly, a thin cylindrical layer of powdered  $\text{AlLiD}_4$  is blown into the cylindrical vacuum chamber. A powerful ultraviolet flashtube produces the initial ionization. Then, a high potential is applied to the face of the cylinder and rapid collapse of the cylindrical plasma layer occurs. The maximum plasma density attained is  $10^{19}$   $\text{cm}^{-3}$ .

In Garching, an experiment is being prepared for heating a plasma by injecting into it a beam of ions with an energy of 600 keV (beam current 0.5 A).

#### INVESTIGATIONS IN JAPAN AND AUSTRALIA

As mentioned in the report by Watson-Munro, investigations in the controlled nuclear fusion program are being conducted in Sydney University in Australia (the SUPPER assembly — a plasma source with a density of  $10^{13}$  to  $10^{16}$   $\text{cm}^{-3}$  and a temperature of 1 eV, a high-frequency generator with a power of 1 MW at a frequency of 9 Mcs for investigating cyclotron resonance in a plasma; a toroidal assembly for dynamic plasma stabilization with a rotating field; an assembly for investigating plasma waves) and in several research centers in Japan (the universities of Nagoya, Kyoto, Tokyo, Nihon, Osaka, Tokuka, the National Electrotechnical Laboratory, the Tokyo Shibara Electric Company, etc.). Small experiments are being carried out in Africa and in the Latin-American countries. In India, a number of theoretical studies have been undertaken on plasma physics.

In Japan, considerable attention is being paid to the toroidal trap, a toroidal trap with a crimped field — the "Heliotron" (Kyoto) — is being investigated, a toroidal trap with an "undulating" field (Tokyo), a plasma betatron (Tokyo), a Stellarator with high-frequency plasma heating (Osaka). Traps with magnetic probes are also being investigated: the "NX" assembly with molecular ion injection in the Probkotron (Osaka), and assembly with a magnetic field of cusped configuration under the name of "Himera" (Osaka), and an assembly for investigating plasma diffusion across a magnetic field (Tokyo).

In some laboratories, projects are being undertaken on thetatrions, and in Nihon a regime was found of an unstable plasma pinch with a slowly increasing field ( $H_{\text{max}} = 8$  kG, field oscillation half-period 31  $\mu\text{sec}$ ). There are assemblies for investigating tubular pinch discharge (National Electrotechnical Laboratory) and multistage adiabatic plasma pinch (Nagoya, Nihon).

There is a large range of experiments on the transmission of waves and cyclotron resonance in a cold plasma, which are being undertaken on the "QP" assembly (Nagoya) — a Penning source of pure plasma with a density of  $10^{11}$ - $10^{13}$   $\text{cm}^{-3}$  and a temperature of 1 eV — and in the "AWRA-2" assembly (Tokyo) for observing resonance absorption of strong Alfvén waves. Interesting experimental and theoretical results have been obtained.

On the whole, the review of thermonuclear research at the Conference showed that these investigations are being widely developed throughout the whole world and, already, in fact, have been converted into an independent branch of science.

All the participants in the discussions remarked unanimously that in the period between the conferences very considerable progress had been achieved in the fields discussed. One of the most important achievements was undoubtedly the discovery of methods for suppressing large-scale plasma magnetohydrodynamic instabilities and, in particular, the experimental treatment by the Soviet researchers of traps with combined magnetic fields.

However, the thorough experimental and theoretical investigations accomplished over recent years have revealed also new difficulties for achieving controlled thermonuclear reactions, for the surmounting of which even more years of intense research projects will be required. At present, in the words of the Chairman of the British Atomic Energy Authority, Sir William Penney, the annual whole-world expenditure is not less than 100 million dollars. Furthermore, as emphasized by the many problems which emerged on the utilization of the energy from controlled thermonuclear fusion, it is so important for the future of mankind that it justifies completely the enormous means and efforts which have been expended.

## ISOTOPES AND RADIATION

A. S. Shtan'

Translated from Atomnaya Énergiya, Vol. 18, No. 3,  
pp. 260-264, March, 1965

The Third International Conference on the Peaceful Uses of Atomic Energy was devoted mainly to nuclear energy generation and reactor construction. Nevertheless, interesting problems were also discussed in the field of isotope production and utilization.<sup>1</sup>

The USA reports (196, 252)<sup>2</sup> are of interest in the field of isotope production, in which problems for carrying out technological processes are discussed and organizational problems are discussed for the production of large quantities of separated fission product isotopes and isotopes obtained by neutron irradiation in reactors. The prime motives for posing these problems are the fulfillment of a program for constructing small electrical power units (the SNAP program),<sup>3</sup> in which the energy released in the process of radioactive decay is transformed into electrical energy, and also development programs for projects in the field of radiation chemistry and radiation treatment of food products.

For the period from 1961 to 1964, 5 million curies of Sr<sup>90</sup> isotope were produced in the USA; the isotope was converted to the compound SrTiO<sub>3</sub>, which is a ceramic, and which has an excellent thermal stability, radiation resistance, a high strontium content, and a relatively low solubility in water.

In projects concerned with radiation chemistry and radiation treatment of food products, a use is found for Cs<sup>137</sup> radiation sources. In January 1964, a Cs<sup>137</sup> source with an activity of 215,000 Ci was prepared in the Oak Ridge National Laboratory. In the USA, toward the end of 1964, about 1 million curies of Cs<sup>137</sup> had been separated, which was obtained by elution of the cesium fraction from an inorganic solution and subsequent purification using the alum crystallization process.

With the object of increasing the production of isotopes obtained from fission products, a new plant – the Hanford plant – has undertaken the project for the production of isotopes. Comparative data concerning the costs of isotope production in this plant as a function of production outputs are shown in Table 1.

It is assumed that the equipment for separating the fission fragment isotopes from fission fragments will be installed in 1967 and the equipment for purification and packaging toward 1968.

TABLE 1. Comparative Data for the Cost of Certain Radioactive Isotopes as a Function of Production Outputs (252) [1]

Isotope	1964-1966		1967-1968	
	annual output, mCi	cost, \$/Ci	annual output, mCi	cost, \$/Ci
Sr <sup>90</sup>	3-5	1-1.5	10	0.13-0.26
Cs <sup>137</sup>	1-3.5	0.8	10	0.1 -0.23
Pm <sup>147</sup>	0.3	0.75	30	0.03-0.09
Ce <sup>144</sup>	—	—	100	0.01-0.02

Of the isotopes obtained by neutron irradiation, Pu<sup>238</sup> is of considerable interest for "isotope energy production." In order to produce this isotope, three production assemblies and one laboratory are operating in the USA; it is produced in kilogram quantities by irradiating Np<sup>237</sup> which, in its turn, is formed by the irradiation of U<sup>238</sup> (n, 2n reaction) and U<sup>235</sup> (2n, γ reaction).

Isotopes of curium, which are components of the chain leading to the formation of very heavy elements, in particular californium, and which also may serve as heat sources in isotopic current sources, are attracting attention. A program has been completed in the USA for irradiating 10 kg of Pu<sup>239</sup>, as a result of which about 400 g of Cm<sup>244</sup> was obtained; it is proposed to

<sup>1</sup>A list of reports by Soviet scientists was published in Atomnaya Énergiya, 17, No. 3, 235 (1964), and a list of reports by foreign scientists in Atomnoi tekhnike za rubezhom, No. 8, 27 (1964).

<sup>2</sup>The report numbers are shown in curved brackets.

<sup>3</sup>An evaluation of Systems for Nuclear Auxiliary Power. TID-20079, USAEC, 1964.

TABLE 2. Proposed Requirements in Electrical Energy for Space Objectives

Field of application	Name of satellite, station, or project	Approx. power, W	No. of satellites per year			
			1964	1965	1966	1967
Astronomy	Astronomical observatories in satellites	500	—	1	2	1
Solar physics	Solar observatories in satellites	25	2	1	2	1
	Advanced Orbiting Solar Observatory (OSO)	15- 50	—	—	—	2
Geophysics and geodesy	Geophysical observatories in satellites	500	1	3	1	3
	Explorer	15- 50	1	3	1	2
	Monitor — interplanetary research stations	40	1	3	2	2
	International	15- 50	7	5	6	4
	Geodetic satellite "Anna"	50	—	3	2	1
Biophysics	Biological satellites	25	—	1	4	1
Lunar exploration	"Ranger" (impact type)	150-190	4	—	—	—
	"Surveyor" (for lunar landing)	15- 25*	—	5	2	—
	"Surveyor" (for escape into orbit)	125	—	—	4	3
Investigation of planets and interplanetary space	"Mariner" (Mars and Venus)	150-250	2	—	4	2
	"Pioneer"	5-100	—	3	3	1
Meteorology	"Tiros"	25- 50	1	—	—	—
	"Nimbus"	140-250	1	1	1	1
Communications	"Telstar"	60	1	12	10	8
	"Relay"	50	2	—	—	—
	"Syncom"	45-100	1	1	2	—
Military-defense use of satellites	Communication satellites for medium altitudes	25	—	—	—	—
	Communication satellites "Syncom"	100	—	—	—	—
	Sea navigation satellites	25	—	—	—	—

\*Power after lunar landing; power en route, 100 W.

TABLE 3. Possible Terrestrial Use of Isotope Systems

Use	Approx. power of generator, W	Proposed requirements in 1964-1967	
		No. of generators	total power, W
Navigation purposes (Navy)	10	—	—
Antishipping military coastal duties (Navy)	150	—	—
Oceanographic and meteorological instruments (by order of ASN and Navy)	20	—	—
Rocket systems (Air Force)	100	—	—
Meteorological stations	20- 60	50	1000-3000
Coastal beacons in Alaska and the Aleutian Islands	5- 15	70	350-1050
Floating beacons (Alaska)	10	70	700
Oil wells in the Gulf of Mexico	50	100	5000
Radio beacons	5-100	20	100-2000
Automatic seismic stations	60	10-1000	600-6000
Instruments for detecting underwater explosions of rockets and devices for tracking the motion of ships	10	260	2600

TABLE 4. Characteristics of Isotope Current Generators for Space Purposes

Generator	Power of device, end of work life, W	Serv. life, yrs.	Fuel	Parameters at end of service life			Surface area of emitter, m <sup>2</sup>		Dimensions, cm		Entry date into oper.	Object of application
				volt. V	current strength, A	extern. load, ohm	ribbing	body	length	diam.		
SNAP-3	2.7	5	Pu <sup>238</sup>	2.7	1.0	3.0	none	0.055	13.97	12.19	1961	DOD satellite
SNAP-9A	25.0	6	Pu <sup>238</sup>	6.4	4.6	2.0	0.193	0.154	24.13	50.80	1963	DOD satellite
SNAP-11	18.6-25	1/4	Cm <sup>242</sup>	3.0	8.33	0.42	0.093	0.151	27.94	45.72	1965	"Surveyor" satellite
SNAP-17	25.0	5	Sr <sup>90</sup>	6.6	3.8	1.75	0.121	0.140	31.75	16.76	1965	Communication satellite
SNAP-19	22.0	3	Pu <sup>238</sup>	4.75	4.65	1.02	0.095	0.094	24.76	13.56	1965	Interplanetary probe
Undesig.	6 -10	1	Pu <sup>238</sup> or Sr <sup>90</sup>	-	-	-	-	-	-	-	-	Light demonstration instrument

TABLE 5. Characteristics of Terrestrial Isotope Current Generators

Generator	Power of device, W	Service life, years	Fuel		Weight, kg	Length, cm	Diam. cm	Entry date into oper.	Designation or object of application
			form	quant.					
SNAP-3	25	1/4	Po <sup>210</sup>	2	1.8	13.97	12.19	1959	Check of operating principles
Undesignated	4.5	2 min	Sr <sup>90</sup>	18	~760	50.80	45.72	1961	Meteorological station "Axel-Iceberg"
SNAP-7A	10	10	Sr <sup>90</sup>	40	~850	53.34	50.80	1962	Navigation buoy
SNAP-7C								1962	Meteorological station "Antarctica"
SNAP-7B								1963	Beacon
SNAP-7D	60	10	Sr <sup>90</sup>	225	~2100	87.63	55.88	1964	Floating meteorological station
SNAP-7E	6.5	10	Sr <sup>90</sup>	31	~3600**	162.54	80.01	1964	Submarine buoy
SNAP-15A*	0.001	4	Pu <sup>238</sup>	22	0.45	12.70	6.35	1965	Control system
SNAP-15B*	0.001	4	Pu <sup>238</sup>	22	0.45	8.92	7.62	1965	Control system
SNAP-21*	10	5	Sr <sup>90</sup>	-	-	-	-	1965	Deep-water generator

\*Provisional construction.

\*\*Special container for locating in the ocean depths, and withstanding high pressures.

TABLE 6. Processes and Production Capacity

Process	Radiation source	Production output per year
Linkage buildup of polyethylene products (tubes, insulators, etc.)	Accelerator	27 million dollars
Linkage of polyethylene films (or tapes)	Accelerator	1500 T
Irradiation of semiconductor units and circuits	Accelerator	2 · 10 <sup>7</sup> pieces
Production of ethylbromide	Co <sup>60</sup>	400 T
Sterilization	Accelerator and Co <sup>60</sup>	28 million dollars

build a unit for producing  $\text{Cm}^{244}$  in kilogram quantities. This isotope is of special interest because of its extremely suitable characteristics for making thermal blocks for isotopic current sources: its half-life is 18 years and its specific thermal energy release is three times greater than other isotopes with long decay periods. Owing to its high specific energy release,  $\text{Cm}^{244}$  can be used for the thermoelectron conversion method by means of which, as expected, the transformation of heat into electrical energy will be approximately twice as efficient as the thermoelectric method of conversion. It is shown that the cost of producing relatively pure  $\text{Cm}^{244}$  in significant quantities may amount to 1000-2000 dollars/g.

In order to obtain target neutron fluxes in excess of  $10^{15}$  neutrons/cm<sup>2</sup> · sec, the construction of a special reactor will be completed in 1965. The products of irradiation will be gram-quantities of  $\text{Cf}^{252}$ . Projects are under way for producing  $\text{Cm}^{242}$  which is of interest primarily as a source of heat in "isotopic energy generation." This isotope is produced from  $\text{Am}^{241}$  which, in its turn, is formed as a result of the  $\beta$ -decay of  $\text{Pu}^{241}$ . Kilogram quantities of  $\text{Am}^{241}$  have been produced, from which the required quantities of  $\text{Cm}^{242}$  are obtained by neutron irradiation.

Isotopic Current Sources. The production of electrical energy by the direct conversion of the energy from radioactive decay is one of the fundamental lines of utilization of large quantities of radioactive materials obtained from the fission products of nuclear fuels or as the result of neutron irradiation in reactors of the appropriate targets.

Two reports devoted to this problem (217, 318) were presented at the Conference. The working program for isotopic current sources in the USA (the SNAP program) has been going on since 1956 (Tables 2-5). It follows from Table 2 that the probable requirement for electrical sources of energy for space purposes in 1964-1967 will be about 20 kW; the requirement for electrical generators with an output of less than 1 kW after 1967 will be about 5 kW per annum. Large-scale potential regions for the terrestrial use of isotope current sources may demand 20 kW by 1964-1967.

Investigations have been started into the possibilities of using radioactive isotopes as energy sources for small rocket engines (196). Three possibilities are being considered: 1) the heat formed as a result of radioactive decay is used to raise the temperature of a moving gas by direct convection transfer of the heat; 2) the heat is used for thermoactivation of a catalyzer, which accelerates decomposition of a hydrazine fuel; 3) the heat is used for heating up the walls of the operating channels and for raising the temperature of a moving gas. Rocket engines of this type should be distinguished by a high specific impulse and a low thrust and, consequently, they can be used in the upper stages of small unmanned space vehicles for interplanetary flights or for transferring from a low earth orbit to a higher orbit through a trajectory requiring minimum expenditure of energy.

Radiation Processes and Technology. The characteristic feature of the reports presented at the Conference devoted to this problem is the technological-economical approach to the question of industrial realization of radiation processes and the differential choice of radiation sources for achieving these processes.

The technological organization indices of the processes and their economical efficiency are determined by solving the problem of industrial realization of one or other radiation process. Thus, for example, it is reported (198) that the volume of realizable processes in the USA at the present time is estimated at 70 million dollars and is rapidly increasing (Table 6).

In the immediate future the following radiation processes may be used in industry: polymerization of wood-plastic materials; irradiation of feed products (disinfection of wheat and wheat products, sterilization of bacon in tin can containers); irradiation of semiconductor devices with the objective of improving their properties; radiation production of biological oxidizable detergents; polymerization of ethylene and copolymers, and other processes.

Experiments in the field of chemonuclear synthesis are still at the research stage. Chemonuclear processes are being developed for the synthesis of hydrazine,  $\text{NO}_2$ , and ozone, radiation-thermal cracking (RTC) of petroleum products and hydrocarbon gases using fission fragments and reactor radiations (292, 389).

The possible types of reactors for accomplishing radiation-chemical processes are discussed (542).

Activation Analysis. During the last few years, neutron activation analysis has found a wide application in many countries, including Great Britain, USSR, USA, France, Federal German Republic, and Japan. New, up-to-date apparatus have increased considerably the possibilities for activation analysis and have expanded the limits of its applicability. The use of fast and pulsed reactors permits the sensitivity for determining elements to be considerably increased and also to expand the list of element to be determined by the activation method.

The possibility of using  $\text{Am}^{241}$ -Be neutron sources which have advantages over  $\text{Po}^{210}$ -Be and  $\text{Pu}^{239}$ -Be sources for activation analysis is noted. The wide application of small neutron generators in conjunction with modern miniature transistorized electronic equipment will enable this method to be commercialized; at present it can compete effectively with other methods of elementary analysis in the determination of a range of concentrations. Generators supplying a neutron flux of  $10^9$ - $10^{11}$  neutrons/sec with energies of 14 MeV are used effectively for proximate analysis of the elementary composition of samples in cases when chemical methods require a large time expenditure or have a lower sensitivity.

Considerable attention is being paid to such important problems as increasing the service life of a tritium target, which is being accomplished by the use of radiofrequency ion sources and other methods (197).

In some reports (197, 829, 854), new fields of application of radioactivation analysis are discussed: in criminology, investigations of cosmic space, for determining the salt content of lakes, etc.



THE USE OF ISOTOPES AND RADIATION SOURCES  
IN HYDROLOGY AND HYDROGEOLOGY<sup>1</sup>

N. V. Churaev, A. I. Yakovlev, M. P. Volorovich,  
N. Ya. Flekser, and S. Ya. Vartazarov

Translated from Atomnaya Énergiya, Vol. 18, No. 3,  
pp. 264-268, March, 1965

Radioactive isotopes are widely used in hydrology and hydrogeology for the investigation of open water streams, subterranean flow, sediment migration, and the water cycle of soils and earths, and also for the solution of many engineering problems.

In contrast to dyestuffs and salts, appropriately chosen radioactive indicators are little absorbed by soils and are used at lower concentrations, owing to the fact that neither the properties of the filtering liquid nor the properties of the soil are changed. The concentration of radioactive indicator is determined with a high degree of accuracy by means of relatively simple apparatus and coloration and salinity of the water has practically no effect on the measurement accuracy.

1. Investigation of Subterranean Streams

Analysis of the sorption properties of soils shows that the most suitable radioactive indicators are  $I^{131}$  in the compounds NaI and KI, chelate compounds with  $Co^{60}$  and also  $S^{35}$  in the form of a solution of the salt  $Na_2SO_4$ . Labelled water  $T_2O$  and  $D_2O$  find wide application in hydrogeological investigations.

The greater accuracy of measurements of discharge and velocity of subterranean flow as a result of the application of radioactive indicators leads to the necessity for defining more precisely certain standard working formulas used for tracer methods. The first method of application [1] is based on observations of the change of concentration of the indicator introduced into the bore. The standard working equation for discharge of a steady underground stream  $q$  has the following form:

$$q = \frac{W_0}{K\tau} \ln \frac{C_0}{C}, \quad (1)$$

where  $W_0$  is the volume of water in the borehold;  $C_0$  is the initial concentration of indicator;  $C$  is the concentration at time  $\tau$ . The experimental verification of this relationship was carried out by means of radioactive indicators in filtration tubes and underground flumes. Comparison of the measurement results of the discharge by the volume method in a drain and by Eq. (1) showed that for  $K = 1$  the discharge is measured of water passing directly through the borehold. By extending the results of the discharge measurements to an equal cross section of the ground,  $K = 2$  should be introduced, which is associated with disturbance of the ground continuity [2].

The dilution method, as with all tracer methods, is used best of all at quite high filtration rates. In this case, it guarantees the possibility of measuring the underground discharge rate with an error of not more than 3-5%. For filtration rates less than 0.1 cm/day, diffusion of the indicator has a significant effect on the measurement results and the accuracy of the measurement is sharply reduced. It should be noted that the dilution method does not require a preliminary determination of the direction of the underground flow and measurement of the difference of the piezometric levels. Sorption in the ground of the tracer removed from the borehold does not affect the measurement results. A significant advantage also is the use of only one borehold for carrying out the observations. By means of this most promising method, systematic observations can be carried out of the underground flow cycle and also single measurements of the water discharge. The method is used for determining the average values of discharge into the ground as well as for layered measurements [3-5].

<sup>1</sup>Prepared for the Third International Conference on the Peaceful Uses of Atomic Energy, Geneva, 1964.

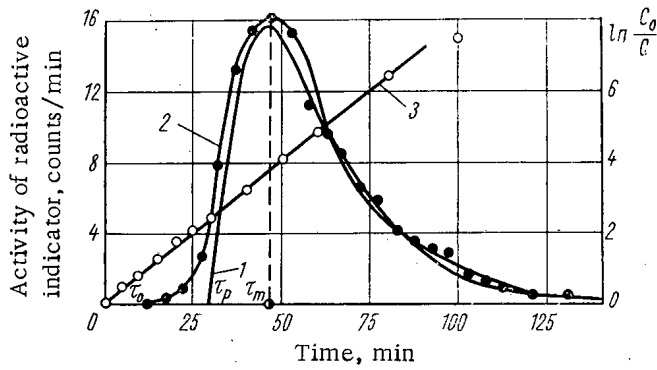


Fig. 1. Graph of the change of concentration of the radioactive tracer  $S^{35}$ : 1) theoretical relationship; 2) controlled well; 3) triggered well.

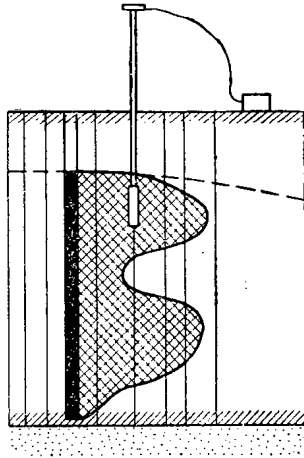


Fig. 2. Results of investigation of water filtration in a peat stratum by the coordinated measurement method (the vertical lines indicate the sites of insertion of the probe).

deviated from it only in the initial portion. This deviation is due to dispersion of the velocity of motion of the water in the ground pores, which is not taken into account in the theory. The latter circumstance, unfortunately, makes it impossible to determine  $\tau_p$  directly by graphs of the transmission of the tracer. However, in order to determine it, values of  $\tau_m$  can be used which agree well for the theoretical and experimental curves (Fig. 1). These quantities are connected by the relationship

$$\tau_m - \tau_p = \frac{W_0 W_H \ln \frac{W_0}{W_H}}{q(W_0 - W_H)}, \quad (3)$$

which can be obtained from Eq. (2), bearing in mind that for  $\tau = \tau_m$ ,  $dM/d\tau = 0$ . Values for the maximum velocity of motion of water into the ground pores can also be found by the time  $\tau_0$ .

Comparison of the water discharges, calculated theoretically and measured in underground flumes by the volume method in a drain, showed that they differ by not more than 3-5%. In the case of large distances between the wells, it is necessary to take into account indicator losses due to scattering-convective diffusion [7].

Radioactive tracers are used for measuring the velocity and direction of motion of water in different soils and hydrotechnological installations. The simultaneous use of the dilution method and of the controlled well method enables the value of the active porosity of soil to be measured in a section between the wells [5].

The second tracer method is the controlled-well method. Theoretical consideration [5] of the dependence of the concentration of radioactive tracer  $M$  on the experiment time  $\tau$  in a controlled well, taking into account the exponential law for measuring the tracer concentration in a "triggered" well, has led to the equation

$$M = \frac{W_0 C_0}{W_0 W_H} \left[ \exp \left( -q \frac{(\tau - \tau_p)}{W_0} \right) - \exp \left( -q \frac{(\tau - \tau_p)}{W_H} \right) \right], \quad (2)$$

where  $W_0$  and  $W_H$  are the volumes of water in the triggered and controlled well, respectively;  $C_0$  is the initial concentration of indicator in the well started from  $\tau = 0$ . The quantity  $\tau_p$  in Eq. (2) corresponds to the theoretical instant of appearance of the tracer in the controlled well which is used also for calculating the velocity of motion of the water. Equation (2) is obtained for the migration of the tracer with a constant average velocity  $v_{av}^*$  without taking account of diffusion of the tracer and its dispersion by the medium. These conditions are well observed in homogeneous soils for quite high filtration rates. The method of calculating the velocity distribution is given in [6].

The equations obtained were verified in experiments with filtration tubes and underground flumes by means of radioactive tracers [5]. The results of one of the experiments are shown in Fig. 1. The linear relationship 3 characterizes the change of the quantity  $\ln C_0/C$  in the triggered well. The function  $M(\tau)$  (curve 1), constructed according to Eq. (2), agrees well with the experimental relationship (curve 2), and

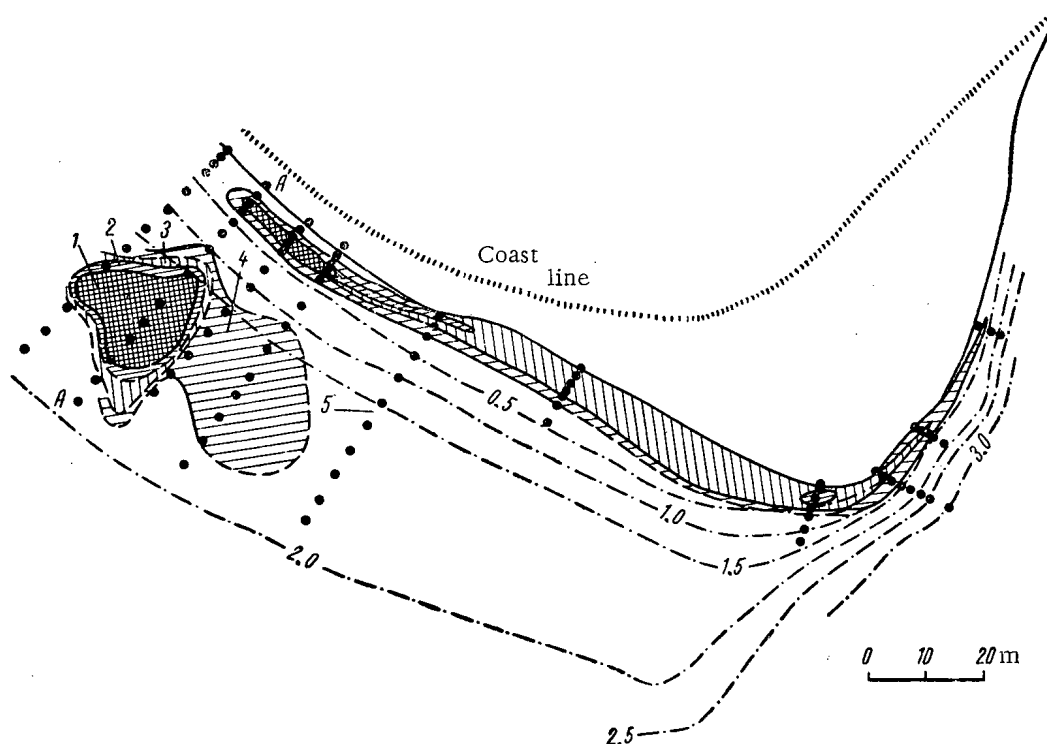


Fig. 3. Distribution of activated sand within the limits of the experimental section during 18 h after introducing the tracer (AA is the injection range). Radiation intensity: 1) more than 400 cpm; 2) from 300 to 400 cpm; 3) from 200 to 300 cpm; 4) from 110 to 200 cpm; 5) radiometric measurement points.

The specific activity of the radioactive tracer is determined by a water sample and the gamma-emitting tracers by lowering probes with radiation detectors into the well, enclosed in a waterproof casing [3]. Special appliances are used for releasing the radioactive tracer, which permit opening of the ampoule containing the solution at a specified depth.

The method of coordinated measurements is based on observations after the radioactive tracer is distributed in the ground, previously introduced into the well. Measurements of the tracer concentration in the ground are conducted along a reference grid by taking samples with soil drills and also by means of probes sunk into the ground. By relating the specific activity values to the ground sections, the path and velocity of motion of the water can be traced through individual layers. Thus, for example, in the experiment whose results are shown in Fig. 2, the movement of water into a peat stratum which had been drained took place principally through two water-conducting layers separated by a relatively watertight layer. The method of coordinated measurements is used for studying drainage of peat tracts [5,8] and mineral soils [9]. Observations can also be carried out by means of this method of the movement of capillary moisture and atmospheric rain water in the upper ground layers.

The radioactive tracer method was used under hydrotechnological conditions for investigating filtration in coffer-dams for protecting the foundation pits of the Volga hydroelectric power station and on the Moscow canal.

Radioactive tracers have also been used for investigating filtration in exploratory coastal and river bed dams of the Gor'kov hydro-network with the object of determining the direction, velocity of motion, and the filtration factors [3]. The special feature for starting was the introduction of the tracer by means of a mechanical device separately into the foundation and body of the dam. It was established that the flow velocity at the foundation of the river bed dam was greater than at its structure. The radioactive tracer method has also found application for investigating the dynamics of salt transfer in soil on models of drainage plots [10]. It has been used also for studying drainage processes of peat beds. On the basis of these projects, the structural classification of peat soils has been compiled and recommendations have been given concerning the most suitable methods for their drainage. It should be mentioned that in the course of drainage, transformation of a stratum from one structural type into another is possible as a result of compaction. An intense migration of moisture is observed in the region of the capillary border to

the side of the open drainage channels with velocities of the same order of magnitude as the filtration velocities. The nature of water movement in undrained peat tracts has also been studied.

Radioactive tracer methods have also been used for investigating the performance of drainage equipment. Observations carried out by this method after changing the effective cross section of the drains and of the water flow rates in them over several years of operation of the drainage channels have permitted a study to be made of the nature of performance of different types of drainage and to make recommendations concerning the suitability of application.

Under laboratory conditions, the radioactive tracer method is used for investigating the porous structure of soil samples, for measuring the content of different categories of combined water, for studying the mechanism of moisture migration in soils as a result of evaporation, by capillary rise and thermal transfer. Processes of the mutual displacement from porous media of two nonmiscible liquids have been investigated by this same method; each liquid was labeled with its own radioactive tracer (for example,  $\text{Rb}^{86}$  and  $\text{I}^{131}$ ) [11].

## 2. Investigation of Erosion Processes and the Dynamics of Sediments

Radioactive tracers have found application also for studying erosion processes. By the introduction of radioactive tracers into eroded or deflated rocks, the intensity can be determined of the destructive processes in these rocks as a result of the effect of different factors, as well as the paths of their transfer and accumulation.

In order to study deflation processes and the transfer of dune or alluvial sands, artificially prepared or natural sands labeled with a radioactive tracer, which are distributed at various sections of the topography, are used as the indicator. By carrying out systematic measurements of the radioactivity in the regions being investigated, deflation and transfer processes can be studied as a result of the effect of various factors (direction and force of the wind, temperature, rainfall, etc.). Radioactive substances which can be used for carrying out these investigations are certain radioactive waste products, low-grade powdered ores of radioactive elements, and radioactive isotopes (for example,  $\text{S}^{35}$ ,  $\text{Cs}^{134}$ ,  $\text{Co}^{60}$ , etc.).

The radioactive tracer method can be used also for studying processes of soil erosion and washing away of friable rocks weathering on slopes and shores of rivers. In order to carry out the investigations, portions of the activated material are distributed in various sections of the topography at the most typical points — over squares with an area of 1-3 m<sup>2</sup>. The study of the migration of the active material in the test squares is carried out by systematic measurements of the intensity of the radiation in their dispersion halo, erosion, and drift along the slope. On the basis of the data concerning the redistribution of activity, source material can be obtained for quantitative calculations of erosion processes and the washing away of friable rocks weathering on the slopes and banks of reservoirs.

Radioactive tracers are used with high efficiency for studying erosion processes in the banks of rivers and for constructing the banks of reservoirs. Depending on local conditions, which determine the intensity of the erosion, the method is selected and the site for positioning the activated material in the rocks forming the banks. If the bank being studied is composed of nonrocky species (clay, sand, etc.), then by means of radioactive tracers inserted in the material being studied the necessary observations can be carried out quite reliably and efficiently. On a coastal slope shallow holes with labeled soil are carefully disposed in a section which is morphologically typical. In rocky types of material the siting of the holes relative to the brow or slope of the bank is selected by also taking account of the height of caving of the eroded slope of the bank and the intensity of the washing out. By carrying out periodic observations on the variation in the radiation intensity at the section of the bank slope being studied, there is a possibility of determining the extent of disintegration of the bank material. By further following the movement of the activated material, it is possible to observe the course of disintegration of the bank and its final stage — migration and deposition of the material from the eroded bank.

Radioactive tracers are used also for observing directly the movement of sediments into the coastal region of the sea [12]. Natural sand labeled with the  $\text{Fe}^{59}$  isotope and taken from the section of shore being investigated has been used as a radioactive tracer for studying the migration of sea sediments. The activated sand was uniformly distributed in the sea at a range oriented with respect to the normal to the shore (Fig. 3). Observations on the migration of the labeled sand were carried out by making systematic radiometric measurements at various depths at reference ranges situated at specified distances from the initial position. The use of radioactive tracers has enabled the direction, velocity, and relative intensity of the longitudinal migration of sandy sediments to be determined, and also to recognize certain qualitative special features of this process. In contrast to other methods, the use of radioactive

tracers enables one to dispense with the collection and laboratory study of sediment samples, and data which characterize the dynamics of the sediments can be obtained directly at the instant of observation.

### 3. Investigation of the Dynamics of Open Streams

The study of the flow and processes of diffusion into the oceans of artificial reservoirs and rivers by means of radioactive tracers is yet another type of application of isotopes in hydrological investigations. Beta- and gamma-emitting isotopes are used for these projects. As in the investigations of subterranean flows, two methods of measurement are used: 1) samples are taken and their activities are subsequently determined; 2) the activities are measured by detectors directly in the medium.

The active substance is introduced into the water by breaking at a specified depth an ampoule containing a solution of a radioactive salt ( $Zn^{65}$ ) in sea water with a concentration of about  $0.01 \mu C/ml$ . In addition, compounds labeled with the isotopes  $Na^{24}$ ,  $P^{32}$ ,  $Br^{82}$ , and  $I^{131}$  are also used.

In the experiments run under tidal ebb conditions, it was established that for weak flow turbulence the tracer cloud is distributed relatively slowly and the concentration of radioactive substance exceeds the background only close to the site of its introduction. In the absence of marked flows, the distribution of concentrations of this substance is approximately uniform in all directions.

The results obtained in winter as a result of measurements with ice are interesting. Direct measurements were made with probes and samples were taken at the same point. The experiments showed a low efficiency for the sampling method. Samples taken at the instant of passage of the maximum tracer concentration do not give reproducible data in view of the flow disturbance as a result of taking samples with bathometers. To obtain the complete picture of the tracer migration process, several detectors must be inserted into the flow. The system of several detectors is effective where one detector is located in the vicinity of the container from which the radioactive substance is released and the rest are located in a circle at some distance, depending on the flow velocity.

#### LITERATURE CITED

1. G. N. Kamenskii, Principles of the Movement of Subterranean Water [in Russian] (Gosgeolizdat, Moscow, 1943).
2. S. A. Kol', Proceedings of the State Hydrogeological Institute, No. 8(62) [in Russian] (Gydrometeoizdat, Moscow, 1948).
3. S. Ya. Vartazarov, V. A. Volokhov, N. Ya. Flekser, and A. I. Yakovlev, Radioactive Isotopes and Nuclear Radiations in the National Economy of the USSR [in Russian] (Gostoptekhizdat, Moscow, 1961), Vol. 2; N. Ya. Flekser and O. P. Shipenko, Prospecting and Conservation of Mineral Resources, No. 6, 42 (1961); N. Ya. Flekser, Gidrotekhn. str-vo, No. 1, 28 (1963).
4. A. A. Abdulaev, Uzb. geol. zh., 1, 57 (1962).
5. M. P. Volarovich, P. I. Il'in, and N. V. Churaev, Torf. prom-ct', No. 7, 9 (1961); Kolloidn. zh., 23, 524 (1961); P. I. Il'in and N. V. Churaev, Torf. prom-st', 5, 18 (1961).
6. O. N. Nosova, Bulletin of the All-Union Scientific Research Institute of Hydrotechnology, 69, 143 (1962).
7. V. P. Nikolayevskii, Prikl. matem. i mekhan., 23, 1042 (1959); Izv. AN SSSR, Mekh. i mash., 5, 189 (1960); Collection: New Methods of Measurements and Instruments for Hydraulic Investigations [in Russian] (Izd. AN SSSR, Moscow, 1961).
8. N. V. Churaev, Torf. prom-st', 8, 20 (1961).
9. V. A. Rozin and V. I. Evdokimova, Drainage of Marshy and Swampy Soils (Izd. ASKhN BSSR, Minsk, 1960).
10. T. A. Abduragimov, S. F. Aver'yanov, and V. V. Rachinskii, Izv. Timiryazevsk. c.-kh. akad., 1, 326 (1963).
11. D. I. Leipunskaya and A. Ya. Pruslin, Proceedings of the All-Union Scientific-Technological Conference on the Use of Isotopes and Nuclear Radiations in the National Economy [in Russian] (Gosenergoizdat, Moscow, 1958), Vol. 4, p. 62.
12. N. V. Glazov, The Use of Radioactive Isotopes in Engineering Surveys [in Russian] (Gosatomizdat, Moscow, 1962); O. K. Leont'yev and B.N. Afanas'yev, Izd. okeanograf. komissii AN SSSR, 3, 73 (1963).

## THE PROBLEM OF RADIOACTIVE WASTE REMOVAL

A. N. Marei

Translated from *Atomnaya Énergiya*, Vol. 18, No. 3,  
pp. 268-270, March, 1965

Several sessions of the Third International Conference on the Uses of Atomic Energy for Peaceful Purposes were devoted to a discussion of problems dealing with radiation safety of the population when exposed to radioactive wastes from atomic industrial installations and atomic power stations. These questions were reflected in the papers,<sup>1</sup> presented at the Conference by India, the United Arab Republic, the Soviet Union, the USA, France, Czechoslovakia, Japan, etc.

The principles of protecting the outlying region from radioactive contamination, used in the USA, Canada, and other countries are essentially identical with those used in the Soviet Union. They are all aimed at reducing the amount of radioactive materials in the removal wastes to levels such that the risk of irradiating the population is below the maximum allowable doses as established by the International Commission on Radiation Protection and other authoritative organizations.

Different means are used to achieve this goal. Most attention is devoted to reducing, as far as possible, the amount of liquid and gaseous waste that have to be removed to the surroundings, principally by rationalizing and improving the engineering processes. These problems were dealt with in the papers by the USSR (379), the USA (278, 282, 869), France (86), and the German Federal Republic (783).<sup>2</sup> One of the methods shown to the participants at the Conference in a short film (USA) is replacement of the chemical method of removal (solution) of the cladding of irradiated fuel elements by a mechanical method, which practically eliminates the liquid radioactive wastes that would normally occur. No less importance attaches to engineering improvement of the production equipment and apparatus in the direction of reducing leakage of radioactive solutions and gases into the surroundings in quantities sufficient to be dangerous (278, 282, 869). In some cases, a solution to the problem is found by making wide use of easily replaceable coverings, which eliminates the need for deactivating the surfaces. In deactivating a large-sized piece of contaminated equipment, successful use has been made of shot-blasting methods, etc. (869). The primary coolant is used over again both in industrial reactors (Oak Ridge) and in reactors intended for scientific research purposes (379, 869). Attention should be given to some of the data presented to acquaint the members of the Soviet delegation with the operation of the research reactor at Grenoble (France). For a volume of distilled water in the first loop of the reactor of about 600 m<sup>3</sup>, return of the water through ion exchange filters occurs at a rate of 1600 m<sup>3</sup> per h.

A large amount of attention is also devoted to reworking and controlled removal of radioactive wastes. These problems were dealt with in a relatively large number of papers from several countries: Belgium (774), Great Britain (188), India (794), the UAR (813), USSR (587), USA (278, 869), France (86, 88), German Federal Republic (783), and Czechoslovakia (775).

It follows from the material presented at the Conference that the highly active liquid wastes produced at the projects concerned are kept in special subterranean containers. This provides conditions which guarantee that they will not get into the surroundings under normal operation, or in case of accident.

This is achieved by having several "barriers" consisting of two metal walls and a concrete wall for the containers (281). Although solidifying the wastes by vitrification (188, 282, 587) or other methods is recognized as being the most advanced procedure, for economical and engineering reasons, these methods have for practical purposes not yet left the experimental stage, and so far are not being used on a production scale.

<sup>1</sup>A list of the papers presented by Soviet scientists was published in *Atomnaya Énergiya*, 17, 3, 235 (1964), and a list of the papers presented by foreign scientists was published in *Atomnaya Tekhnika za Rubezhom*, No. 9, 27 (1964).

<sup>2</sup>The parentheses give the numbers of the papers.

Decontamination of liquid wastes of moderate specific activity ( $10^{-5}$ - $10^{-1}$  curie/liter) is done in different ways. In the majority of countries (USA, Canada, France, et al.), they are deactivated using various methods. In particular, a large amount of attention is given to the use of natural and artificial sorbents, which have a high deactivating effect (86, 88, 278, 282, 775). In addition, in the USA, it is the practice to discard these wastes into the ground by means of adsorbing sumps (Hanford, Oak Ridge). However, it has been shown by experience that this method is far from being always safe. Thus, as reported by W. Belter (869), ten years after starting to discard wastes in adsorbing sumps, a considerable amount of  $Ru^{106}$  had started to get through into the river. Discarding the old adsorbing sumps, and changing the location of the new ones did not remove the danger of contaminating the river. Accordingly, in Oak Ridge, starting in 1964, instead of discarding liquid wastes of moderate activity into the ground, it has been decided to decontaminate them by evaporation on specially built equipment. The example given serves as a clear confirmation of the fact that discarding liquid wastes into the ground is not permissible unless there are favorable hydrogeological and sanitary conditions. Attention should be given to the experimental studies made at Oak Ridge on high-pressure injection of liquid wastes of moderate specific activity into geological structures, as well as the experience from burying them in worked-out salt mines (282, 783, 869).

Greatest interest centers on ways of solving the problem of removal and decontamination of liquid wastes of low specific activity ( $10^{-5}$ - $10^{-9}$  curie/liter), which are most often the cause of contamination of open bodies of water.

These problems are solved in different ways in different countries, which is due, in particular, to the natural and geographical conditions, the density of the population, etc., and to a considerable extent depends on whether we are dealing with conditions obtaining at operating installations, or with factories and atomic power stations that are being built and designed. It has been shown (282, 287, 869) in the USA that in operating industrial reactors and factories for reworking spent fuel, the low specific activity waste water gets down, as before, through a system of ponds, swamps, etc., into rivers having enormous flows (thousands of cubic meters per second). As a result of measures that have been taken in the last 3-5 years to reduce the amount of wastes rejected, the amount of radioactive material in the water of such rivers (287) has not, at the present time, exceeded the maximum permissible concentrations (MPC).

In recent years, in the USA, in removing liquid radioactive wastes at new factories for reworking nuclear fuel, and atomic power stations that are operating or being designed, in addition to reducing the volume of the wastes, a condition is achieved such that the concentration of radioactive materials in the waste water does not exceed the MPC. Further, use has been made of subsequent dilution in a body of water in such a way that the concentration of the radioactive materials in the water at the place where the wastes are dropped is 4-5 orders of magnitude less than the MPC (281).

In countries like Great Britain and India, where the installations are located close to the sea, and the hydrological conditions are favorable, it is possible to discard liquid wastes of low specific activity into the sea at quite a large distance from the shore, which makes sure that there is a large amount of dilution and, from the data of the authors of the paper (788), meets the requirements for radiation safety.

The problem of decontaminating solid wastes of any specific activity is solved in the majority of countries by burying the wastes in the ground (278, 379, 774, 813, 869, 870). The reliability and cheapness of this procedure has, in particular, put an end to disposal of solid radioactive wastes in the sea, which was formerly widely used in the USA and France (287, 869).

The decisive role in achieving radiation safety when solid wastes are buried in the ground is played by the principle of using favorable natural hydrogeological conditions. In many cases, this makes possible a considerable reduction in the requirements on the design of the burial site, up to the point where, under favorable conditions, the wastes may simply be buried in the ground (silty clay, etc.).

To decrease the transportation costs, and reduce the size of the burial sites, the greatest possible reduction is made in the amount of solid wastes that have to be buried. The greatest amount of attention is devoted to pressing. A large amount of interest attaches to the methods used in the USA for dry deactivation by shot-blasting cleaning (869), which are important economically for the subsequent utilization of contaminated metal structures. There is no doubt that if appropriate equipment is produced, these methods will be useful for deactivation of small metal parts.

In the papers presented at the Conference, there was insufficient discussion of problems of the removal of gaseous wastes. There was extremely little information on emission by reactors of radioactive noble gases, particularly Ar41, and the importance they have for health (582). Also, a very modest presentation was made of data on the

radioactive aerosols removed from atomic power stations and installations for reworking spent fuel. At the same time there is good reason for giving serious attention to the importance of  $I^{131}$ , which constitutes one of the most serious factors in radiation danger (186, 281, 869). This is due to the need to protect the bodies of children from overexposure, since they are the ones that are most sensitive to the effect of ionizing radiation (281). Rigid limitations on the amount of  $I^{131}$  in the atmospheric air in regions where sources of contamination are located are maintained in the USA by the use of special filters, which take out 99.5% of this isotope. Along with this, the problem is posed of the need for increasing the time spent fuel elements are held to 150 days (281).

In addition to measures directed toward providing radiation safety for the population during normal operation of the various factories and atomic reactors, there were some papers dealing with prevention of contamination of the surroundings by radioactive materials in case of reactor accidents (276, 282). These problems are solved in two ways, by preventing the accident and by localizing the contamination to the confines of the installation. In addition to purely engineering questions, related to improving means for preventing "leakage" of radioactive materials from the various systems, serious attention is given to confining the materials to the place where the reactor is located. One of the principal methods used for this purpose is to build a metal or reinforced concrete protective shell over the reactor. Such structures have found approval abroad, and have been rather widely used in practical reactor construction (276).

In spite of the achievements that have been made in limiting the amount and deactivating radioactive wastes, providing means of protection during accidents, etc., it is impossible to disregard the fact that factories for reworking spent fuel, reactors, and atomic power stations are potential sources of contamination of the surroundings, and this makes it necessary to locate these installations in sparsely settled regions. It was shown in the paper (281) that this rule is being followed in the USA in the construction of new factories for reworking spent fuel. Within a radius of about 40 km from such a factory, there are no inhabited points with more than 10,000 population, while the nearest inhabited point is at a distance of about 7 km. The reason for getting so far from habitation follows from the data given in the same paper, according to which the maximum concentrations of radioactive gases for normal operation of the factory and mean meteorological conditions are produced at a distance of 1500 m from the stack, while in inversions they occur at a distance of 4000-10,000 m from the stack.

Hence, it may be concluded that the fundamental aspect of the problem of leaving a space (health protection zone) between inhabited regions and industrial installations is solved in the USA in the same way as in the USSR. The only differences are in the actual distances used, and in the legal side of how they are set up.

In the USSR, as we know, for atomic power stations and other potential sources of contamination of the locality by radioactive materials, as is done by law for installations in other branches of industry, concrete dimensions for the health protection zones are set up depending on the type of danger, and appropriate sanitary precautions are taken within the limits of the zone.

It follows from paper (281) that the USA has no concrete definite dimensions for the protective zone. Nor does this paper give the nature and extent of the prophylactic measures taken in the zones. The concept of "controlled zones" used in the USA and some other countries has by now, from our point of view, lost its importance and meaning, since, in recent years, because of global fallout, a check on radiation conditions has been made everywhere.

The Canadian and American specialists showed a great deal of interest in the problems involved in fixing the sizes of the health protection zones in the Soviet Union.

Particular attention should be given to the problems of checking the activity of the wastes removed, and the radiation conditions that they produce in the surroundings (186, 278, 282, 287, 379, 794, 849, 870). Our attention is drawn to the appreciable progress that has been made in this field, consisting of the use of the most improved apparatus and methods, which make it possible, in a more functional way and with much less expenditure of energy, to carry out the amount of investigation required. The various radiochemical methods are being replaced wherever possible by  $\gamma$ -spectrometric methods, the system of periodic removal of samples is being replaced in some cases by continuous automatic measurements, etc. Since the measures used for sanitary protection of the surroundings from contamination by radioactive materials are not an end in themselves, but only a means for achieving radiation safety of the population, it is obvious that one of the basic aspects of the work is to determine the doses received by the various groups of the population. Accordingly, great importance attaches to methods of determining, under living conditions, what concentration of artificial radioactive substances is present in the organism, and identifying the doses produced by these isotopes. The existing methods of calculation in such cases can only give preliminary values. The



most accurate results are obtained by direct measurements. Confirmation of this is provided by the data of the paper (287) on the concentration of artificial radioactive substances in the human body, as measured by means of special spectrometers. There is no doubt that this method, which at the present time is being most widely used in the USA, completely justifies its use. It should be noted in this connection that, judging from the text of the paper (287), the USA is not yet making use of some of the methods for determining  $\text{Sr}^{90}$  under conditions of life that are used in the Soviet Union (by measuring the radiation from the teeth). The practical importance and the reliability of the methods of measurement under conditions of life give them greater promise for purposes of checking radiation conditions.

It should be emphasized in conclusion, that, in finding a correct solution to the problem of protecting the surroundings from contamination by the radioactive wastes from factories reworking spent nuclear fuel and atomic power stations, a very important role is played by the completeness of the program and the quality of the studies preceding the design of these installations. From this standpoint, definite interest is presented by the paper (281), which gives the approach made to these problems in the USA. It follows from the data of the paper that carefully conducted studies, as well as a detailed analysis of the results obtained, make it immediately possible to design a reliable and relatively cheap system for checking the radiation conditions. An analysis of the probable radiation conditions occurring in the vicinity of the factory during normal operation and under various accident conditions also makes it possible to provide for the necessary protective measures in the design.

The important advances made in providing for the radiation safety of the population in the regions where atomic power plants and other sources of radioactive wastes are located, as well as the practical nature of the studies made in this field, permit one to assume that this problem will be completely solved in the not too distant future.

DETERMINATION OF THE TOTAL ENERGY LOST BY A BEAM  
OF ELECTRONS AS A RESULT OF ITS INTERACTION WITH A PLASMA

(UDC 533.9)

A. K. Berezin, Ya. B. Fainberg, L. I. Bolotin, and G. P. Berezina

Translated from *Atomnaya Énergiya*, Vol. 18, No. 3,  
pp. 271-273, March, 1965  
Original article submitted June 4, 1964

Experiments have been described in previous reports [1,2] in which, by means of an electrostatic analyzer with a retarding field, the spectra were determined of the longitudinal energy component of a pulsed beam of electrons with a current of 5 and 8.5 A and energy 15 keV (pulse duration 3.6  $\mu$ sec) at the entrance into and at the exit from a region of interaction with a plasma in a longitudinal magnetic field of intensity 400-1320 Oe. In these experiments, however, only part of the beam was analyzed, amounting to 1-3% of the total current passing through the plasma.

In order to supplement these experiments, the relative total energy losses ( $\Delta W = \Delta W_{\perp} + \Delta W_{\parallel}$ ) were measured with a higher degree of accuracy by means of a sensitive calorimeter for an electron beam with the above-mentioned parameters as a result of its interaction with the plasma. In these experiments, and in contrast with the previous ones, the entire electron beam was analyzed. However, it was not possible with the calorimeter to obtain the energy spectra of the transmitted electrons, as was done previously. Thus, these two methods supplement and refine each other.

An open type circulating calorimeter was used for the measurements. The block diagram of the equipment together with the calorimeter is shown in Fig. 1. The equipment is described in detail in [1,2].

The tank was filled continuously from the water pipe. The inflow of water to the tank was so regulated that a constant pressure was maintained in the water circulation system. The water then passed along a copper tube, where the water temperature was raised to room temperature and entered a glass cone with the inlet and outlet located near its base. Gas bubbles were removed from the water in the cone. The valve, located in the upper part of the cone, enabled gas which had accumulated there to be removed periodically. The water flow through the calorimeter was controlled by a special valve.

From the cone the water entered the thermopile block, the heating element for the calibrator, the water load, again into the thermopile block, and then into the outlet tube. The temperature of the water stream at the inlet to and at the exit from the calorimeter was measured additionally by thermometers with a 0-50°C scale to an accuracy of  $\pm 0.1^{\circ}\text{C}$ . The temperature difference was measured by a thermopile, constructed in the following manner. Two parallel channels were drilled in a block of plastic, ensuring good electrical and thermal insulation. The water was conducted to the load through one of the channels and was led away from it through the second one. A copper-constantan thermopile of 16 elements was mounted in the block, such that the junctions were positioned approximately along the axial lines of the channels. The diameter of the wire from which the thermopile was made was 0.1 mm. The resistance of the thermopile  $R_C$  was  $\approx 20 \Omega$ .

A millivoltmeter, type M198/2, grade 1.0, with a 2.3-mV scale and resistance  $R_m \approx 230 \Omega$  was used as the measuring device.

TABLE 1. Relative Total Energy Losses of the Electron Beam as a Result of Its Interaction with the Plasma, %

Air pressure, mm Hg	Beam current, A	
	5	8.5
$2 \cdot 10^{-5}$	9	14
$2 \cdot 10^{-4}$	12	18
$4 \cdot 10^{-4}$	18	22
$6 \cdot 10^{-4}$	18	22
$2 \cdot 10^{-3}$	17	20

Note: The results presented are independent of magnetic field as a result of varying the latter within the limits 400 to 1320 Oe for a current of 5 A and 720-1320 Oe for a current of 8.5 A.

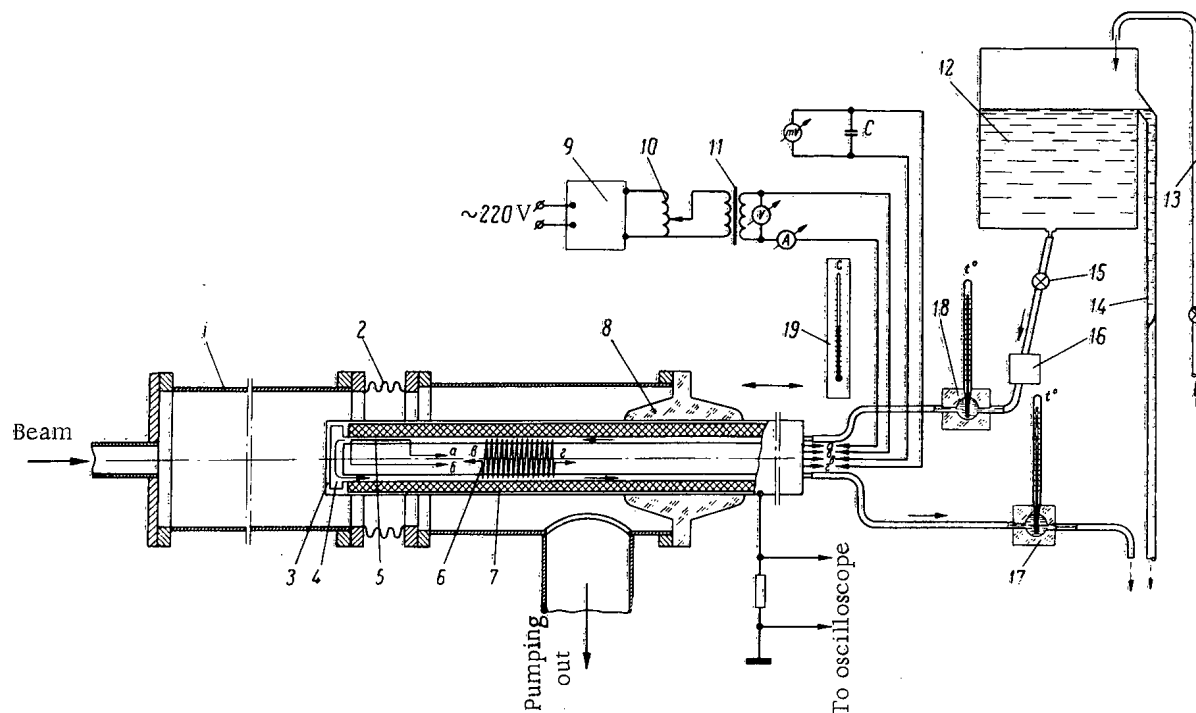


Fig. 1. Layout of equipment for measuring the total beam energy by means of a calorimeter. 1) Chamber; 2) bellows; 3) calorimeter; 4) water-cooled calorimeter chamber; 5) calibration element; 6) thermopile; 7) thermal insulator; 8) plastic insulator; 9) electronic stabilizer; 10) RNO-250-2 variac; 11) 220/20 V transformer; 12) water tank; 13) water pipe; 14) overflow tube; 15) valve for regulating water flow; 16) device for removing air bubbles from water stream; 17) thermometer for measuring temperature of water stream issuing from calorimeter; 18) thermometer for measuring temperature of water entering calorimeter; 19) thermometer for measuring temperature of surrounding medium.

TABLE 2. Values of  $\Delta W_{\parallel}$  for a Current of 5 A, %

Gas pressure, mm Hg	Longitudinal magnetic field intensity, Oe			
	1320	720	360	240
$2 \cdot 10^{-5}$	16	15	12	—
$9 \cdot 10^{-5}$	17	16	16	—
$(4-6) \cdot 10^{-4}$	22	22	18	23
$2 \cdot 10^{-3}$	25	26	26	—

TABLE 3. Values of  $\Delta W_{\parallel}$  for a Current of 8.5 A, %

Gas pressure, mm Hg	Longitudinal magnetic field intensity, Oe			
	1320	960	720	480
$2 \cdot 10^{-5}$	10	14	17	15
$9 \cdot 10^{-5}$	10	13	17	17
$(4-6) \cdot 10^{-4}$	15	15	17	19
$2 \cdot 10^{-3}$	27	—	26	23

For  $R_C \ll R_M$ , the instrument calibration in units of power was more linear than in the case when  $R_C \gg R_M$  [3,4]. In order to eliminate the effect on the millivoltmeter of high-frequency induced currents, the latter was shunted by a small capacitor ( $C = 0.05 \mu\text{F}$ ).

For a measured power of 12-22 W and a water flow through the calorimeter of about  $2 \text{ cm}^3/\text{sec}$ , the millivoltmeter ensured a reading within the limits of 40-75 scale divisions (100 divisions correspond to 2.3 mV). The thermal time-constant of the calorimeter at this flow rate was about 1.5 min. The heating element for calibration consisted of a length of high-resistance nichrome wire (diameter approximately 0.15 mm) stretched along the axis of the tube and fed by a stabilized 220-V supply from ac mains through a variac and a step-down transformer. Voltage stabilization was accomplished by an electronic stabilizer to an accuracy of better than  $\pm 0.5\%$ ; the resistance of the element at room temperature was about  $10 \Omega$ . The power running in the heating element was regulated by the variac and was measured by means of a voltmeter and ammeter, grade 0.5.

The entire calorimeter was mounted in a long tube which was vacuum-sealed so that during the experiment the calorimeter could be inserted initially into the chamber (for measuring the energy of the beam entering the

the chamber) and removed from it at the end (for measuring the energy of the beam after interaction with the plasma) without changing the vacuum in the chamber. The forward end of the calorimeter, on which the electron beam fell, in order to reduce secondary emission was covered by a thin layer of Aquadag. The measurement accuracy by means of the calorimeter described amounted to about  $\pm(1-1.5)\%$ .

Using this calorimeter, the average power was measured of the electron beam at the inlet to the chamber ( $W_1$ ) and at the exit from it ( $W_2$ ), depending on the beam current (5 and 8.5 A), the pressure of the air in the chamber (plasma density), the intensity of the longitudinal magnetic field within the limits 400-1320 Oe for a current of 5 A and 720-1320 for a current of 8.5 A. In order to verify the calorimetric method, the average power of the electron beam, measured by the method of substitution, was compared with the average power necessary for heating up a given flow of water passing through the calorimeter. For this, the water temperatures at the inlet to and exit from the calorimeter, and the average water flow rate, were measured. In all the measurements the temperature difference did not exceed  $3^\circ\text{C}$  and it was measured to an accuracy of  $\pm(6-7)\%$ . The flow rate was measured to an accuracy of  $5\%$ . The values of the average powers measured by the above-mentioned methods agreed to an accuracy of  $10\%$  which, probably, is explained by the measurement errors given above of the temperature difference and of the water flow rate.

The average power of the electron beam, as determined by means of the calorimeter, was also compared with the average power which could be obtained knowing the current, the energy of the beam, the pulse duration, and the transmission frequency. These data agreed within the limits of  $10-15\%$ . This is explained, probably, by the errors arising in measuring the beam parameters by means of a cathode ray oscillograph. The relative total energy losses of the electron beam as a result of its interaction with the plasma are determined from the relationship

$$\Delta W = 1 - \frac{W_2}{W_1} \quad (1)$$

and are given in Table 1. The measurement accuracy was  $\pm(2-3)\%$ .

For comparison, from the graphs given in Figs. 2 and 3 of [1], the relative average energy losses were determined of the longitudinal motion of the electron beam as a result of its interaction with the plasma.

It is well known that the average energy transferred by an electron beam whose electron energy spectrum is described by the function  $F(W)$  is equal to

$$W_{\text{av}} = \frac{\int_0^{\infty} W F(W) dW}{\int_0^{\infty} F(W) dW}, \quad (2)$$

where  $W$  is the energy. Hence, from the energy spectrum of the longitudinal motion of the electron beam at the inlet to the calorimeter [ $F_1(W)$ ] and at the exit from it [ $F_2(W)$ ], it is easy to find the relative average energy losses  $\Delta W_{\parallel}$  of the longitudinal motion of the electron beam as a result of interaction with the plasma. The values of

$\int_0^{\infty} F_1(W) dW$  and  $\int_0^{\infty} F_2(W) dW$  were determined by planimeter from graphs similar to those given in Figs. 2 and 3 of [1], but drawn on a larger scale. In order to determine  $\int_0^{\infty} W F_1(W) dW$  and  $\int_0^{\infty} W F_2(W) dW$  curves of

$W F_1(W)$  and  $W F_2(W)$  were constructed and the values of the above-mentioned integrals were found by means of a planimeter. The areas were measured with a mean-square error of  $\pm 1.5\%$ . The total measurement error was  $\pm 6\%$ .

The values of  $\Delta W_{\parallel}$  were calculated for currents of 5 and 8.5 A for different values of the longitudinal magnetic field intensity and of the working gas pressure in the plasma chamber (Tables 2 and 3). The mean square measurement error was  $\pm 6\%$ .

Comparison of the results given in Tables 2 and 3 with those of Table 1 shows that they agree with one another within the limits of the measurement errors.

LITERATURE CITED

1. A. K. Berezin et al., *Atomnaya energiya*, 14, 249 (1963).
2. A. K. Berezin et al., Collection: Plasma Physics and Problems of Controlled Thermonuclear Reactions [in Russian] (Izd. AN UkrSSR, Kiev, 1963), No. 3, p. 125.
3. Collection: Measurement Technology for Centimeter Waves, No. 2 [in Russian] (Sovetskoe radio, Moscow, 1949), p. 133.
4. E. A. Hinston, Centimetric Wave Measurements [Russian translation] (IL, Moscow, 1960), pp. 246, 247.

## THE OPERATION OF THE CYLINDERIZER IN THE STELLARATOR

(UDC 533.9)

B. I. Gavrilov, F. V. Karmanov, and G. P. Maksimov

Translated from *Atomnaya Énergiya*, Vol. 18, No. 3,  
pp. 273-275, March, 1965  
Original article submitted May 14, 1964

In investigating plasma physics and controlled thermonuclear reactions, use is made of magnetic fields having a complicated configuration. In particular, it is of interest to make a study of the magnetic field with helical symmetry which is used, for example in the stellarator [1], and is produced by superposition of a uniform longitudinal field and the field formed by  $n$  pairs of spiral conductors, with the current alternating in direction. A field of this type is interesting for the reason that, in closed systems, it has closed magnetic surfaces. The cross section of these surfaces, formed by a three-path helical winding ( $n = 3$ ) is in the form of figures having nearly the same shape as an equilateral triangle.

In working with mirrors using these fields, it is sometimes desirable to have parts where the magnetic field is axially symmetric. In these regions, the triangular magnetic surfaces must be converted to cylindrical surfaces and, so as not to disturb the closed magnetic surfaces, it is necessary to think about good "fitting" as they pass from the spiral region to the region with axial symmetry. This process is called "cylinderizing" of the magnetic surfaces, and the regions of the spiral conductors where the cylinderizing occurs have been given the name of cylinderizers. From the standpoint of construction, they may be made in the form of short sections of the spiral winding, which differ from the rest of the winding in either the magnitude of the current or the spacing.

Approximate designs of cylinderizers are given in [2]. The present paper gives the results of an experimental check of the operation of one type of cylinderizer.

Cylinderizing of the helical magnetic surfaces formed by a three-path helical winding was investigated by the electron beam scanning method. The electron source, which gave 19 electron beams, was placed in the axially symmetric magnetic field. The electron beams rotated in circles, and as they passed through the region of the spiral magnetic field under study along the magnetic lines of force, they were observed on a fluorescent screen.

The vacuum chamber of the equipment was made of 1Kh18N9T nonmagnetic stainless steel. The inside diameter was 10 cm and the distance from the electron source to the fluorescent screen was 2.3 m. The operating vacuum

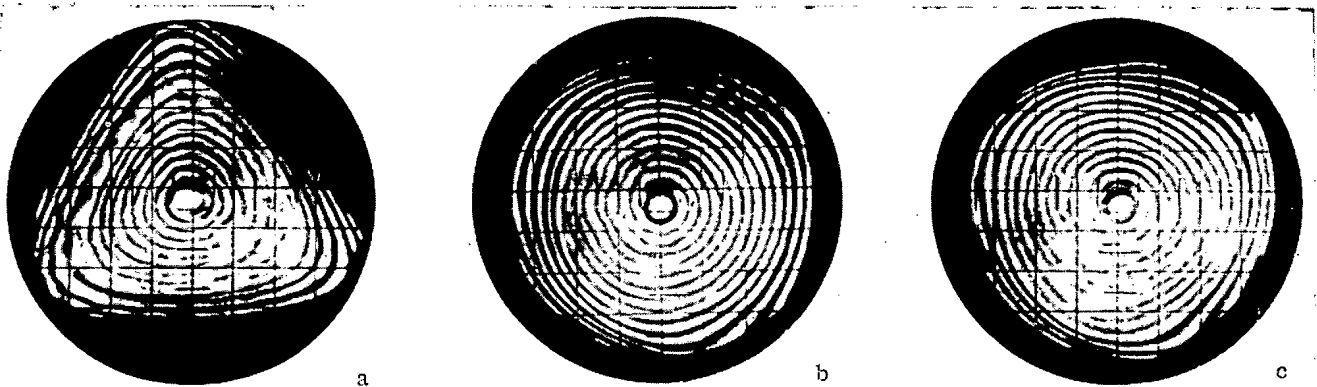


Fig. 1. Form of the magnetic surfaces in cylinderizing. Location of screen: a) in middle of spiral winding; b) at end of cylinderizer; c) in axially symmetric field at a distance of 30 cm from the cylinderizer.

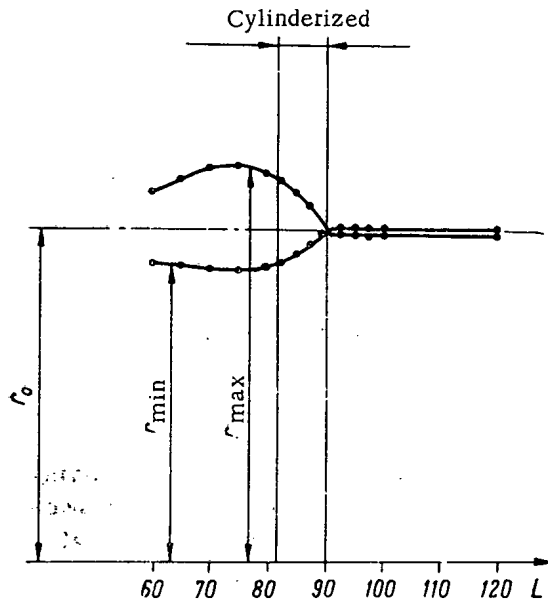


Fig. 2. Variation of  $r_{\min}$  and  $r_{\max}$  of the triangular form of the magnetic surface at different cross sections of the helical surface.

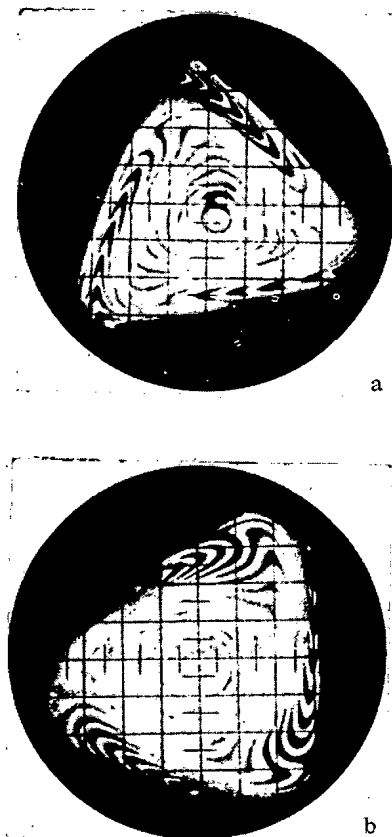


Fig. 3. Distortion of the magnetic surface in the absence of cylinderizers. Location of the screen: a) in the middle of the helical winding; b) outside the helical winding.

in the equipment was held in the range  $2 \cdot 10^{-5} - 8 \cdot 10^{-6}$  mm Hg.

The constant longitudinal magnetic field was produced by a system of windings separated from one another by two thirds of the mean radius of the windings ( $r_m = 15$  cm). The maximum field intensity was 500 Oe. The magnetic system was 4.4 m long.

The three-path helical winding ( $n = 3$ ) was 0.73 m long, with a turn spacing of  $L_0 = 1$  m ( $\alpha = 2\pi/L_0 = 6.28$  radians/m). The winding could be moved inside the main field coils along the vacuum chamber in such a way that the position of the electron beams at any part of the spiral field could be observed on the fluorescent screen. At the ends of the spiral winding were the cylinderizers. They consisted of short sections of a three-path spiral winding. The parameters of the cylinderizers were found from the formulas of [2]:

$$b\alpha_c = \frac{\pi}{3}, \quad \frac{I}{a} = \frac{2I_c}{a_c}.$$

Here,  $b$  is the length of the cylinderizer,  $\alpha_c = 2/L_c$ , where  $L_c$  is the spacing of the spiral winding of the cylinderizer, and  $I_c$  is the current in the conductors of the spiral winding of the cylinderizer. In our case, for  $I_c = 1$ ,  $\alpha_c = 12.56$  rad/m, and  $b = 8.3$  cm.

The experiments showed that cylinderizers with these parameters exerted too strong an effect on the magnetic surfaces. Cylinderizing of the magnetic surfaces occurs at distances smaller than the dimension of the cylinderizer and, after that, the magnetic surfaces again take on a triangular shape.

To reduce the effect of the cylinderizer, the current in it was reduced. Good cylinderizing was achieved by reducing the current 10% below the calculated value. It may be seen from the photographs of Fig. 1 that for a radius of up to 2.5 cm, cylinderizing was achieved with an accuracy of 1%. Figure 2 shows a graph of the variation of  $r_{\min}$  and  $r_{\max}$  of the triangular form of the magnetic surface at different cross sections of the spiral winding.

A second form of good cylinderizing was obtained by making a 10% reduction in the length of the cylinders.

The experiments led to the conclusion that the magnetic surfaces in the spiral region may be "fitted" with the axially symmetric region by satisfying the conditions:

$$b\alpha_c = \frac{\pi}{n}, \quad \frac{I}{a} = k \frac{I_c}{a_c}.$$

for a three-path spiral winding, in our case,  $k = 2.2$ .

Figure 3 gives photographs showing how the magnetic surfaces are distorted in the absence of cylinderizers.

LITERATURE CITED

1. A. I. Morozov, L. S. Solov'ev, Problems in Plasma Theory, No. 2 [in Russian] (Gosatomizdat, Moscow, 1963), p. 38.
2. E. Friman et al., The Proposed Model C Stellarator Facility Project Matterhorn. Ch. IV. NYO-7899, p. 78.



EXPERIMENTAL VERIFICATION OF THE POSSIBILITY  
OF USING STUB RETARDING SYSTEMS IN ACCELERATOR TECHNOLOGY

(UDC 621.384.612)

P. I. Gos'kov

Translated from *Atomnaya Energiya*, Vol. 18, No. 3,  
pp. 275-276, March, 1965  
Original article submitted July 6, 1964

In the 10-MeV waveguide electron synchrotron started up in 1963 at the Tomsk Polytechnic Institute [1], a closed bent diaphragmed waveguide is used as the accelerating system. However, it was shown in [2] that stub-retarding systems are more promising than diaphragmed waveguides for the accelerating systems of large electron synchrotrons. In order to get a final answer to the question of the advisability of using various structures in electron accelerators, it is necessary to find the shunt impedance of the stub systems, which determines the value of using retarding systems in accelerators.

Since it is very difficult to make an exact calculation of the shunt impedance of stub systems, the impedance must be found experimentally. Figure 1 shows the stub-retarding systems, the shunt impedance of which was found by using small perturbing bodies in the center of the space between the rows of stubs (in two-row stub systems), and in the space above the stubs (in single-row stub systems). A rocking frequency generator was used, synchronized with the oscillograph, the screen of which showed the resonance curves of the retarding systems. The measurements were made in the 10-cm range.

It was shown by the experimental studies that  $r_s$  as a function of the phase angle  $\psi$ , i.e., as a function of the operating conditions in the system (Fig. 2) exhibits a clearly defined maximum, the position of which is only slightly dependent on the dimensions of the stub systems.

Figure 2 also shows an experimentally determined curve of  $\theta = r_s(\gamma = 1)/r_{s \max}$  as a function of the period

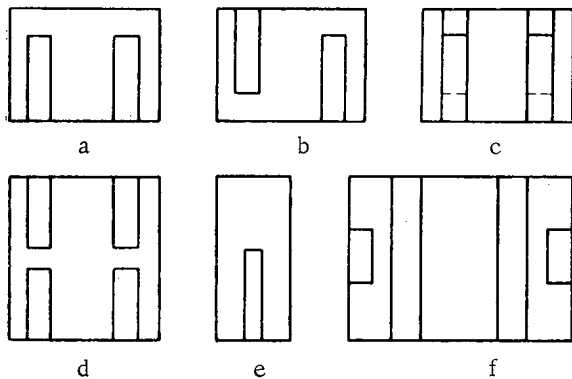


Fig. 1. Stub retarding systems: a) two-row arrangement; b) opposing rows of stubs; c) two-row opposing stub system; d) double two-row arrangement; e) single-row arrangement; f) two-row ladder with projections.

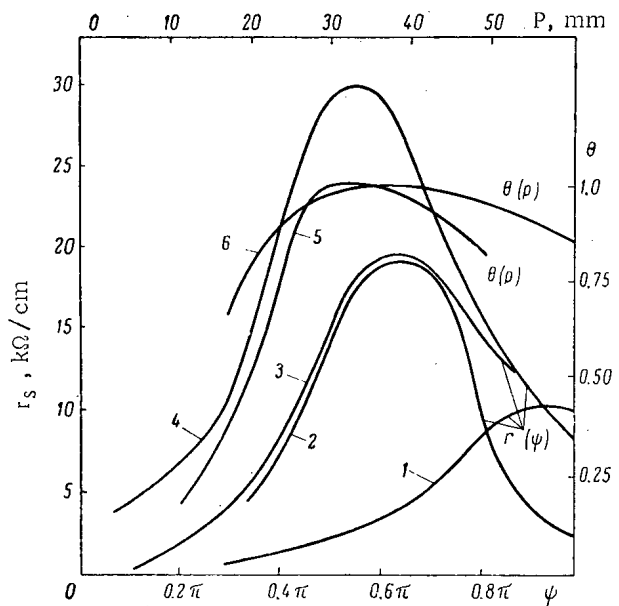


Fig. 2.  $r_s$  as a function of  $\psi$  and  $\theta$  as a function of  $P$ .  $r_s$  as a function of  $\psi$ : 1) two-row arrangement; 2) opposing rows of stubs; 3) single-row arrangement; 4) ladder with projections.  $\theta$  as a function of  $P$ : 5) ladder with projections; 6) two-row arrangement.

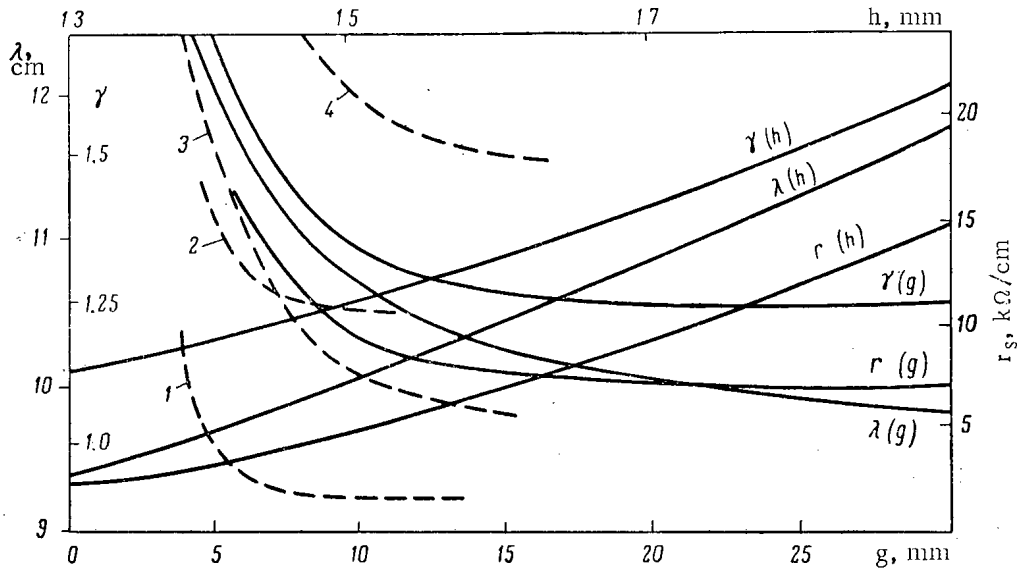


Fig. 3.  $r_s$ ,  $\lambda_{\psi=\pi}$ , and  $\gamma_{\psi=\pi}$  as a function of  $h$  and  $g$  for a two-row arrangement and  $\lambda_{\psi=\pi}$  as a function of  $g$ . 1) Single-row arrangement; 2) opposing rows of stubs; 3) two-row arrangement; 4) two-row opposing stub system.

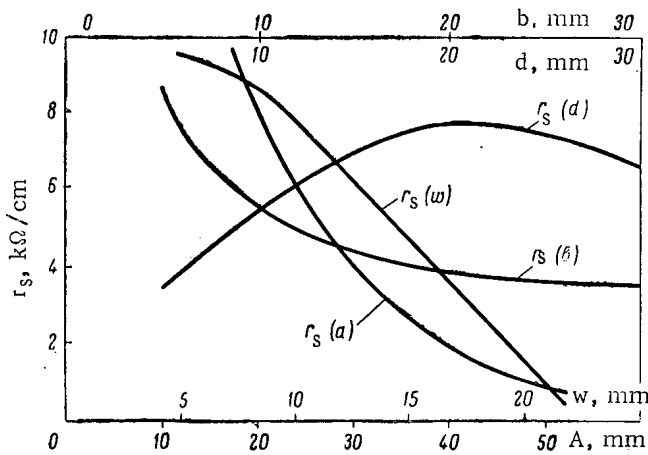


Fig. 4.  $r_s$  of a two-row arrangement as a function of width  $b$  and length  $d$  of the stub, and of the distance  $a$  between the rows and the distance  $w$  between the side wall and the stubs.

of the retarding system P, which shows that for the retardation  $\gamma = 1$  it is possible to get the maximum shunt impedance. By choosing the corresponding period of the system, it is possible to shift  $r_s$  max toward the range of small retardations.

Figures 3 and 4 give experimental curves of  $\lambda_{\psi=\pi}$  and  $\gamma_{\psi=\pi}$  as a function of the height  $h$  of the stub and of the space  $g$  above the stubs, as well as the curve of the shunt impedance as a function of the dimensions of the stub systems.

The results of the experimental studies confirm the fact that in the range of small retardations, stub retarding systems are highly effective, and may be used in accelerator technology.

LITERATURE CITED

1. A. A. Vorob'ev et al., Atomnaya énergiya (in press).
2. A. A. Vorob'ev and A. N. Didenko, Atomnaya énergiya, 12, 242 (1962).

TOTAL INTERACTION CROSS SECTION OF NEUTRONS  
WITH BENZENE, TOLUENE, AND SODIUM ACETATE  
IN THE ENERGY RANGE 0.03-0.5 eV

(UDC 539.125.5:539.121.7)

I. S. Anisimov, V. I. Nikitin, A. I. Saukov,  
and A. A. Ugodenko

Translated from *Atomnaya Énergiya*, Vol. 18, No. 3,  
pp. 277-278, March, 1965  
Original article submitted February 12, 1964

In calculating the moderation of neutrons, with energy below 1 eV, by hydrogen-containing media, it is necessary to allow for the bonds between the hydrogen atoms and the molecules. In [1-3], studies were made of the effect of chemical bonds to the hydrogen atoms on the moderation of neutrons by  $H_2O$ ,  $ZrH_{1.2-2}$ , and  $MgH_2$ . It is of interest to study this effect in organic compounds such as benzene and toluene.

We used the transmission method to measure the total interaction cross sections of neutrons with benzene, toluene, and sodium acetate in the range 0.03-0.5 eV. The neutron source was the reaction  $T(d,n)He^4$ , taking place in the tritium target of a pulsed accelerator tube. The target was surrounded by a paraffin layer 12-cm thick. The neutron detector was powdered LiF enriched with  $Li^6$  (30%) and ZnS (70%). The powder layer, of thickness 90 mg per  $cm^2$ , was enclosed in a thin-walled Plexiglas container and placed on the photocathode of an FÉU-43. The detector was placed in the collimated neutron beam, 3.3 m from the target. Using the time-of-flight method, we measured the neutron spectra before and after passage through the specimen. From the experimental transmission coefficients, we plotted the ratio of the cross sections for bound and free neutrons ( $\sigma$  and  $\sigma_0$ , respectively) against the neutron energy. The results are given in Fig. 1. The differences between the  $\sigma/\sigma_0$  values for  $C_6H_6$ ,  $C_6H_5CH_3$ , and  $CH_3COONa$  are seen to lie within the experimental error ( $\pm 5\%$ ). To approximately the same accuracy, the observed  $\sigma/\sigma_0$  values can be represented in this energy range by the empirical formula

$$f(E) = 1 + \frac{0.073}{E} - \frac{0.00076}{E^2},$$

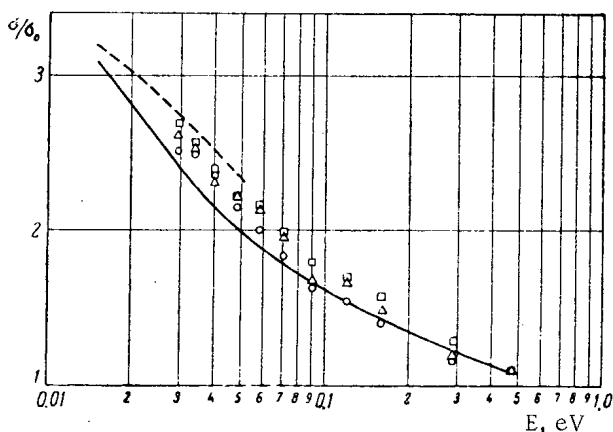


Fig. 1. Ratio of cross sections for bound and free hydrogen, plotted versus initial neutron energy.  $\circ$  - Benzene;  $\triangle$  - toluol;  $\square$  - sodium acetate. Solid line, water [4]; dashed line, benzene [5].

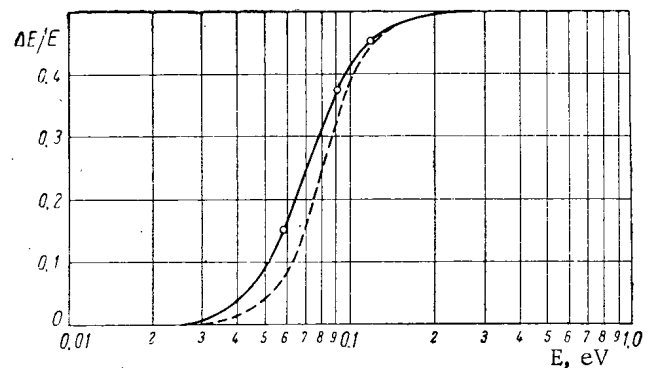


Fig. 2. Mean relative energy loss of neutron per collision with a molecule of water or test substance, plotted versus initial neutron energy. Solid line, water [2]; dashed line, benzene, toluene, sodium acetate.

where  $E$  is the neutron energy in electron volts. For comparison, Fig. 1 also gives  $\sigma / \sigma_0$  for water [4] and calculated values for  $C_6H_6$  [5]. The calculated values are about 10% larger than the experimental ones; this is evidently due to the presence of additional energy states of the  $C_6H_6$  molecule in the range 0.005-0.05 eV, which were not allowed for in the theory [6]; in particular, deformation vibrations of the benzene molecule are possible [7].

The present work did not include measurements of the neutrons' energy loss per single collision, which is also required in calculating the moderation. However, theoretical calculations based on moderation models involving the effective mass [3, 8] show that there is a relation between the cross section and the energy loss. These can be used to calculate the energy losses in the substances studied. As the cross section pertaining to one hydrogen atom is almost the same for the substances studied and for water, we can assume that the relation between energy losses and cross section is the same for them both.

It can be shown that  $\Delta E$ , the mean energy loss on scattering, will correspond with that for a scattering angle close to  $90^\circ$ . Using experimental data from [2] on the energy loss in water at  $\theta = 90^\circ$  and  $E = 0.059, 0.009, \text{ and } 0.117$  eV, and assuming that  $\Delta E/E \rightarrow 0.5$  when  $E \rightarrow 1$  eV,  $\Delta E/E \rightarrow 0$  when  $E \rightarrow 0.025$  eV, we calculated the mean relative energy loss of a neutron for one collision with benzene, toluene, and sodium acetate (Fig. 2).

#### LITERATURE CITED

1. M. Nelkin and E. Cowen, Proceedings of the Second International Conference on the Peaceful Uses of Atomic Energy, Geneva, 1958. Reports of Soviet Scientists [in Russian] (Atomizdat, Moscow, 1959), Vol. 2, p. 634.
2. A. MacReynolds et al., *Ibid.*, p. 648.
3. S. I. Drozdov et al., Proceedings of the Second International Conference on the Peaceful Uses of Atomic Energy, Geneva, 1958. Reports of Soviet Scientists [in Russian] (Atomizdat, Moscow, 1959), Vol. 1, p. 486.
4. D. Yuz, Atlas of Neutron Cross Sections [in Russian] (Atomizdat, Moscow, 1959), Vol. 2.
5. M. A. Kovner and G. I. Kolerov, Symposium: Neutron Physics. Edited by P. A. Drupchitskii [in Russian] (Gosatomizdat, Moscow, 1961), p. 100.
6. A. Mession, *Phys. Rev.*, 84, 204 (1951).
7. N. Sheppard, *Progress in Spectroscopy*. Edited by G. U. Thompson [Russian translation] (IL, Moscow, 1963), p. 354.
8. R. Sachs and E. Teller, *Phys. Rev.*, 60, 18 (1941).

RESONANCE STRUCTURE OF THE CROSS SECTIONS  
AND ITS INFLUENCE ON THE SCATTERING ANISOTROPY  
FOR FAST NEUTRONS AND THEIR TRANSMISSION IN IRON

(UDC 539.125.5:539.121.72)

A. P. Suvorov, A. G. Guseinov, and M. N. Nikolaev

Translated from *Atomnaya Énergiya*, Vol. 18, No. 3,

pp. 278-282, March, 1965

Original article submitted June 15, 1964

The influence of the resonance structure of the cross sections on the propagation and moderation of neutrons in various media is discussed in [1]. This paper also presents detailed studies of the changes in the neutron spectrum's "microstructure," which must be known in order to determine the mean cross sections. When the neutron flux  $F_0(r, E)$  changes relatively little over a distance of the order of the mean free path, i.e., when it obeys the condition  $\left| \frac{D\nabla^2 F}{F} \right| \ll \Sigma_a + \frac{\xi \Sigma_s}{\Lambda u}$ , the energy dependence of the neutron flux moments,  $F_l(r, E)$ , satisfies (for sufficiently sharp resonances), the approximate relation

$$F_l(r, E) \approx \Phi_l(r, E) \sum_{n=0}^l \frac{a_{l-n}}{\Sigma^{n+1}(E)}. \quad (1)$$

Here,  $\Phi_l(r, E)$  is a function weakly dependent on  $E$ , and the coefficients  $a_{l-n}$  are determined (with error  $\leq a_0$ ) by the recurrence formula

$$a_l = \frac{1}{1 - \left\langle \frac{\Sigma_s f_l}{\Sigma} \right\rangle} \sum_{n=0}^{l-1} \left\langle \frac{\Sigma_s f_l}{\Sigma^{n+2}} \right\rangle a_{l-n-1}, \quad (2)$$

where the brackets indicate averaging over the chosen energy range, and the  $f_l$  are the moments of the scattering indicatrix  $f(\mu, E)$ ,

$$f_l(E) = 2\pi \int_{-1}^{+1} d\mu P_l(\mu) f(\mu, E). \quad (3)$$

So, to determine the space and energy distributions of the neutrons, we must know the mean cross-sectional characteristics  $\left\langle \frac{1}{\Sigma^k} \right\rangle$  and  $\left\langle \frac{\Sigma_s f_l}{\Sigma^k} \right\rangle$ , where  $k = 1, 2, \dots, l, l+1$ .

The present paper studies the influence of the resonance structure of the cross sections on the passage of fast neutrons through iron. This element was chosen because it has a marked cross-sectional resonance structure up to energies of the order of several MeV [2], while its elastic scattering is strongly anisotropic in this energy region. Furthermore, iron is widely used in the construction and shielding of nuclear reactors, for which more exact values are required of the scattering anisotropy.

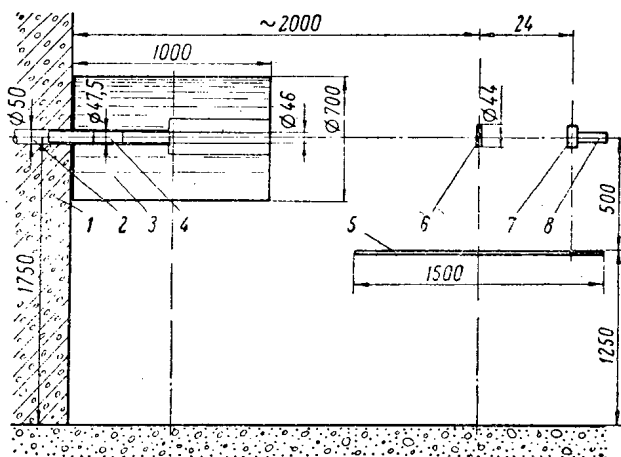


Fig. 1. Schematic diagram of experiment. 1) Shielding; 2) B-3 collimation channel; 3) collimator; 4) blocking specimen; 5) turntable; 6) diffuser; 7) detector; 8) preamplifier.

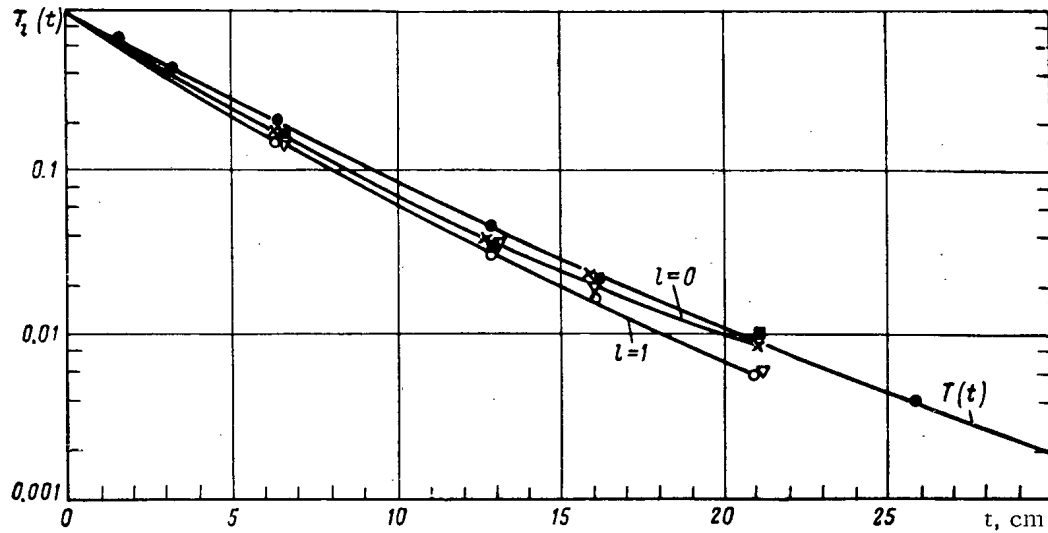


Fig. 2. Angular momenta  $T_l(t)$  and transmission  $T(t)$  and their approximations by two exponentials: ● -  $T(t)$ ; × -  $l = 0$ ; ○ -  $l = 1$ ; □ -  $l = 2$ ; ▽ -  $l = 3$ .

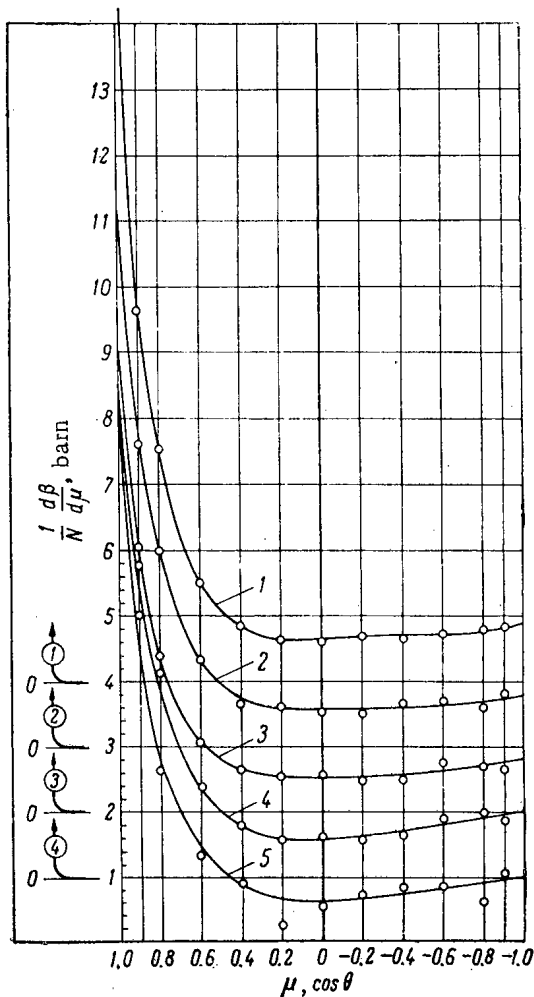


Fig. 3. Differential scattering cross sections  $\partial\sigma(t, \mu)/\partial\mu$  for various filter thicknesses. 1) Free beam; 2) 6.45 cm; 3) 12.85 cm; 4) 16.05 cm; 5) 20.94 cm.

Data on the angular distribution of fission neutrons, with  $E \geq 1.5$  MeV, scattered by thin specimens, are given in [3]. The apparatus for investigating resonance self-shielding of the partial cross sections is shown in Fig. 1. Fast neutrons leave the active zone of the BP-5 reactor [4], pass through an Armco iron filter in a 50-cm diameter hole in the paraffin collimator, and fall on the scatterer. The scattered neutrons are recorded by means of a multilayer ionization fission chamber containing  $\text{Th}^{232}$  (effective sensitivity threshold about 1.5 MeV). The chamber was placed 24 cm from the scatterer, and the distance pieces enabled the detector to be placed at any angle to the beam axis. The angular resolution was  $\Delta\theta \leq \pm 9^\circ$ . The scatterer was an iron disk of diameter 50 and thickness 8 mm, placed at  $45^\circ$  to the beam axis. Measurements were made of  $N(t)$  and  $N(t, \mu)$ , where  $N(t)$  is the count rate with a filter of thickness  $t$ ; and  $N(t, \mu)$  is the count rate for neutrons traversing a filter of thickness  $t$  and scattered at an angle arc  $\cos \mu$ .

We are interested in the group of neutrons able to cause fission in  $\text{Th}^{232}$ , associated with values measured from the following relation:

$$\left\langle \frac{1}{\Sigma^k} \right\rangle = \frac{1}{(k-1)! N(0)} \int_0^\infty dt t^{k-1} N(t),$$

TABLE 1. Total Cross-Section Characteristics (barn) of Iron for Neutrons with  $E > 1.5$  MeV

Characteristics	Exptl.	Calc.
	1	2
$\langle \sigma \rangle$	3.20	3.44
$\langle \sigma^{-1} \rangle^{-1}$	2.84	3.22
$\langle \sigma^{-2} \rangle^{-1/2}$	2.70	3.07
$\langle \sigma^{-3} \rangle^{-1/3}$	2.59	2.94
$\langle \sigma^{-4} \rangle^{-1/4}$	2.53	—

TABLE 2. Experimental and Theoretical Cross-Section Characteristics (barn) of Iron for Neutrons with E > 1.5 MeV

l	Experimental					Calculated			
	1	2	3	4	5	6	7	8	9
	$\langle \sigma_s f_l \rangle$	$\left\langle \frac{\sigma_s f_l}{\sigma^{l+1}} \right\rangle$	$\left\langle \frac{\sigma_s}{\sigma^{l+1}} \right\rangle$	$\langle \sigma_s f_l \rangle \left\langle \frac{\sigma_s}{\sigma^{l+1}} \right\rangle$	$\frac{\langle \sigma_s f_l F_l \rangle}{\langle F_l \rangle}$	$\sigma_s f_l$	$\overline{\sigma_s f_l}$	$\left\langle \frac{\sigma_s f_l}{\sigma^{l+1}} \right\rangle$	$\left\langle \frac{\sigma_s f_l}{\sigma^l} \right\rangle$
		$\left\langle \frac{1}{\sigma^{l+1}} \right\rangle$	$\left\langle \frac{1}{\sigma^{l+1}} \right\rangle$	$\langle \sigma_s \rangle \left\langle \frac{1}{\sigma^{l+1}} \right\rangle$				$\left\langle \frac{1}{\sigma^{l+1}} \right\rangle$	$\langle \sigma \rangle \left\langle \frac{1}{\sigma^{l+1}} \right\rangle$
0	2.56 ± 0.09	2.32 ± 0.13	2.32 ± 0.13	2.32 ± 0.13	2.32 ± 0.13	2.53	2.46	2.46	2.39
1	1.08 ± 0.054	0.75 ± 0.06	2.16 ± 0.14	0.915 ± 0.075	0.88	1.02	1.032	0.930	0.856
2	0.79 ± 0.07	0.61 ± 0.08	2.06 ± 0.18	0.636 ± 0.072	0.70	0.90	0.826	0.738	0.600
3	0.525 ± 0.032	0.34 ± 0.09	2.00 ± 0.24	0.41 ± 0.08	0.44	0.514	0.448	0.391	0.368
4	0.051 ± 0.038	—	—	—	—	0.248	0.155	0.139	0.115
5	0.062 ± 0.016	—	—	—	—	0.088	0.074	0.040	0.036

$$\left\langle \frac{\Sigma_s f_l}{\Sigma^h} \right\rangle = \eta \frac{1}{(h-1)! N(0)} \int_0^\infty dt t^{h-1} \int_{-1}^{+1} d\mu P_l(\mu) N(t, \mu), \tag{4}$$

where η is a constant coefficient depending on the geometry and detector efficiency.

The experimental results are shown in Fig. 2, where the values of the ratio  $T_l(t) = \frac{\int_{-1}^{+1} d\mu P_l(\mu) N(t, \mu)}{\int_{-1}^{+1} d\mu P_l(\mu) N(0, \mu)}$  for various values of t are compared with the transmission  $T(t) = N(t)/N(0)$ . In Fig. 3, the corresponding differential cross section  $\partial\beta(t, \mu)/\partial\mu$  is plotted versus μ, where  $\beta(t, \mu) = [N(t, \mu)]/N(t)$  for various values of t. Different angular distributions are found for different values of t. Column 1 in Table 1 and column 2 in Table 2 give the values of  $\left\langle \frac{1}{\sigma^{l+1}} \right\rangle$  and  $\left\langle \frac{\sigma_s f_l}{\sigma^{l+1}} \right\rangle / \left\langle \frac{1}{\sigma^{l+1}} \right\rangle$ , derived from the experimental data. For comparison, we also give the un-screened total cross section  $\langle \sigma \rangle$ , corresponding to the slope of the initial part of the transmission curve. In addition, Table 2 gives values of

$$\frac{\langle \sigma_s / \sigma^{l+1} \rangle}{\langle 1 / \sigma^{l+1} \rangle} = \eta \frac{\int_0^\infty dt t^l \int_{-1}^{+1} d\mu N(t, \mu)}{\int_0^\infty dt t^l N(t)}, \tag{5}$$

where ρ is the number of nuclei per cm<sup>3</sup>. It must be noted that the "screening" effect for these quantities can be divided into effects of the resonance structures of both the total and differential cross sections.

To separate the latter component of the effect, it is of interest to compare  $\langle \sigma_s f_l \rangle$ , measured with "zero-thickness" filter (see column 1, Table 2), with the values of  $\langle f_l \rangle \left\langle \frac{\sigma_s}{\sigma^{l+1}} \right\rangle \left\langle \frac{1}{\sigma^{l+1}} \right\rangle^{-1}$ , characterizing the effect of the cross-sectional resonance structure Σ and Σ<sub>s</sub> (see column 4, Table 2).

By comparing columns 1, 2, and 4 in Table 2, it is seen that, although most of the observed effect is due to blocking of the total cross section  $\Sigma$  and the integral cross section  $\Sigma_s$ , the shape of the angular curve is evidently also blocked: this is shown by the difference between the data in columns 2 and 4. Quantitative analysis is made difficult by the effect of changes in the neutron spectrum on transmission through the medium, caused not only by resonance structure of the cross sections, but also by the smooth change of the cross section with the energy.

To clarify the natures of the observed effects, an attempt was made to analyze the experimental results on the basis of present ideas of the structure of the iron cross section in the energy range in question [1,5], together with data on the angular distribution of scattered neutrons for monoenergetic sources [6,7]. For heavy enough elements, inelastic scattering can be considered isotropic. So, neglecting energy changes due to elastic retardation, and separating elastic and inelastic scattering, we can write

$$\Sigma_s f_l(E' \rightarrow E) = \Sigma_{el}(E') f_l(E') + \delta_{l,0} \Sigma_{in}(E' \rightarrow E). \quad (6)$$

The values of the scattering indicatrix moments were obtained by a specially developed method [8] of determining the coefficients of the interpolation polynomial:

$$f(\mu, E') = \sum_{n=0}^{10} \frac{2l+1}{4\pi} f_l(E') P_l(\mu). \quad (7)$$

For  $E' < 4$  MeV, we used data from [9] on the excitation functions of the individual nuclear levels of iron, allowing for inelastic scattering; for  $E' > 4$  MeV, we used the statistical theory (the "temperature" excitation of the iron nucleus was taken as 0.8 MeV [10]).

Column 6 in Table 2 gives calculated values of  $\langle \sigma_s f_l \rangle$ , which agree with the experimental results. To separate out that part of the effect which is due to changes in the neutron spectrum resulting from smooth energy-dependence of the cross section, we calculated  $\overline{\sigma_s f_l}$  by the usual formula for the mean, not allowing for the resonance structure of the cross section (see column 7, Table 2). Since the results diverge from the experimental values (see column 2) and are nearly the same as the data in column 6 (see Table 2), most of the effect must be due to the resonance structure.

Owing to the present absence of data on the fine structure of the differential cross sections, it is impossible at present to calculate  $\langle \frac{\Sigma_s f_l}{\Sigma^k} \rangle$ .

For the total cross sections we used the results of an analysis of the transmission curves for neutrons in fairly narrow energy intervals. Reference [2] gives mean values of  $\langle \Sigma^{-1} \rangle_j$ ,  $\langle \Sigma^{-2} \rangle_j$ ,  $\langle \Sigma^{-3} \rangle_j$ ,  $\langle \Sigma \rangle_j$ , and  $\langle \Sigma^2 \rangle_j$  in ranges  $\Delta E_j \approx 0.3$  MeV in the region 0.3-3 MeV. Column 2 of Table 1 gives the calculated moments of total cross section  $\langle \sigma^{-k} \rangle$  for this group of neutrons, taking account of these data. Table 1 shows that the group moments of the total cross sections agree with the data for narrow energy ranges [2].

Let us attempt to estimate the influence of the resonance structure of the cross sections, assuming that screening is absent in the angular distributions. Let us first assume that there is also no resonance structure of the cross sections for elastic scattering, and that within each sufficiently narrow energy interval the cross section can be written as

$$\Sigma_s(E, \mu) \approx \Sigma_{el}(\mu) + \Sigma_{in}(E). \quad (8)$$

Calculated results for this approximation are given in column 8, Table 2. Comparison with the experimental data shows that assumption (8) explains some of the effect, and is its lower limiting case.

Column 9, Table 2 gives results calculated on the assumption that the resonance structure of the cross sections is caused by the behavior of elastic scattering, but that there is no screening of the angular distributions, and that within each interval  $\Delta E_j$  it is true that  $f_l \Sigma_{el}(E) \propto \Sigma(E)$ . This is the upper limiting case for the experimental data in column 4, Table 2.

From Table 2 we can thus conclude that resonance screening of the angular distributions reduces by about 25% the anisotropy of the scattering of fast neutrons by iron nuclei. These results were, on the whole, based on analysis of the readings of a thorium detector, but they are very accurate for the group of neutrons with  $E \geq 1.5$  MeV, which confirms the results of averaging the cross section without allowing for the energy dependence of the detector.



TABLE 3. Characteristics of Iron Fission Subgroups for Neutrons with  $E \geq 1.6$  MeV (barn)

$i$	$B^i$	$\langle \sigma \rangle^i$	$\langle \sigma_s \rangle^i$	$\frac{\langle \sigma_s f_1 \rangle^i}{\langle \sigma_s \rangle^i}$	$\frac{\langle \sigma_s f_2 \rangle^i}{\langle \sigma_s \rangle^i}$	$\frac{\langle \sigma_s f_3 \rangle^i}{\langle \sigma_s \rangle^i}$
1	0.59	2.24	1.95	0.30	0.29	0.17
2	0.41	4.60	3.44	0.53	0.33	0.24

Column 5, Table 2 gives the effective one-group cross sections for neutrons with  $E \geq 1.5$  MeV, obtained by averaging by (1) and (2).

The results of the present work can be analyzed by the subgroup method [1, 11], in which each group of neutrons with a resonance structure of the cross sections is divided into several subgroups, in each of which the cross section is taken as constant.

For separation into subgroups, the curves in Fig. 3 must be put in the form

$$T_l(t) = \sum_i A_l^i \exp(-\Sigma^i t), \quad \sum_i A_l^i = 1, \quad T(t) = \sum_i B^i \exp(-\Sigma^i t), \quad \sum_i B^i = 1, \quad (9)$$

where  $B^i$  refers to the contribution made by the  $i$ -th subgroup,  $\frac{A_l^i}{B^i} = \langle \sigma_s f_l \rangle^i$  is the  $l$ -th moment of the indicatrix of scattering of neutrons of the  $i$ -th subgroup, and  $\langle \sigma_s f_l \rangle$  is the moment of the indicatrix measured with a zero-thickness filter (see column 1, Table 2).

In this case, as the screening effects are small, the functions  $T_l(i)$  can be written as the sum of two exponentials. By simultaneous analysis of the  $T(t)$  and  $T_l(t)$  curves, the group of neutrons able to cause fission in  $\text{Th}^{232}$  was separated into two subgroups with characteristics given in Table 3.

Using these data, we can employ the above method to illustrate how the accuracy of calculation of resonance self-screening affects the problem of neutron transmission through a thick layer. Assuming that the cross section of a transition from one subgroup to another is proportional to the width of the subgroup in which the transition takes place, and assuming that the transition is isotropic, the asymptotic relaxation length  $\lambda$  of the neutron flux from a plane fission source in an extended iron shield, calculated in the  $P_4$  approximation [12], is 8.4 cm. If we use a one-group constant, calculated by (1) and (2) from the data in Tables 1 and 2, this length comes to 8.0 cm. Note that this value is obtained by using one-group constants which were averaged by assuming the truth of the relation

$F_l(r, E) \approx \frac{\Phi_l(r, E)}{\Sigma^{l+1}(E)}$ , obtained by neglecting the scattering anisotropy. For comparison, we give the value of this quantity which is obtained by using the grouped constants, not allowing for the resonance structure of the cross sections. In this case,  $\lambda = 6.6$  cm.

The following conclusions may be drawn from the above:

1. The resonance structure of the cross sections has a marked effect on the transmission of neutrons in media containing middle-weight nuclei. A large effect is expected in the region of low energies (0.5-2 MeV).
2. In calculating the effect of the resonance structure of the cross sections, one cannot neglect the screening of the angular distribution.
3. For accurate calculation of the resonance structure, it is necessary to use the subgroup method.

The authors wish to thank V. V. Orlov, A. A. Luk'yanov, and the late I. I. Bondarenko for their interest in this work and valuable comments.

#### LITERATURE CITED

1. L. P. Abagyan et al., Report No. 357, Presented by the USSR to the Third International Conference on the Peaceful Uses of Atomic Energy (Geneva, 1964).
2. M. I. Nikolaev, V. V. Filippov, and I. I. Bondarenko, Physics of Fast and Intermediate Reactors, IAEA, Vienna (1962), p. 85.
3. A. G. Guseinov and M. N. Nikolaev, Symposium: Handbook of Nuclear Physics Constants for Calculations on Reactors [in Russian] (Gosatomizdat, Moscow, 1963), Appendix 9.
4. A. I. Leipunskii et al., Atomnaya Energiya, 11, 498 (1961).

5. D. Hughes and J. Harvey, Neutron Cross Sections, 2nd Edition, BNL-325 (1958).
6. A. Langsdorf, R. Lane, and J. Monahan, Phys. Rev., 107, 1077 (1957); Neutron Angular Distributions, ANL-5567 (1956).
7. M. Goldberg, V. May, and J. Stehn, Angular Distribution in Neutron-Induced Reactions, 2nd Edition, V. II, BNL-400 (1962).
8. S. Snowdon, L. Eisenbud, and J. E. Marshall, J. Appl. Phys., 29, 950 (1958).
9. D. L. Broder et al., Symposium: Theory and Methods of Mathematical Analysis of Nuclear Reactors [in Russian] (Gosatomizdat, Moscow, 1962), p. 254.
10. D. Thomson, Phys. Rev., 129, 1649 (1963).
11. M. N. Nikolaev and V. V. Filippov, Atomnaya énergiya, 15, 493 (1963).
12. D. L. Broder et al., Collection: Proceedings of the Second International Conference on the Peaceful Uses of Atomic Energy. Reports of Soviet Scientists, Geneva, 1958.[in Russian] (Atomizdat, Moscow, 1959), Vol. 2, p. 674.

MEASURING THE MODERATION LENGTH OF NEUTRONS  
FROM A Po - Be SOURCE IN GRAPHITE - WATER LATTICES

(UDC 589.125.523.5/621.039.51:14)

Yu. M. Shalashov

Translated from *Atomnaya Énergiya*, Vol. 18, No. 3,

pp. 282-284, March, 1965

Original article submitted March 23, 1964; revised June 3, 1964

The authors measured the moderation length of neutrons from a Po-Be source up to the resonance energy of indium (1.46 eV) in graphite-water heterogeneous systems (graphite cylinders<sup>1</sup> of height 900 and diameter 60 mm in a triangular lattice, the steps between the cylinder axes being 62, 67, or 77 mm in normal water). Measurements were made both parallel ( $\tau_{\parallel}$ ) and perpendicular ( $\tau_{\perp}$ ) to the cylinder axes, both with the graphite lattice and in plain water.

The lattice and water were contained in a steel tank 1000 × 1000 × 1500 mm in size. The Po-Be source had diameter 19 and height 40 mm and the intensity used was about  $(2-3) \cdot 10^7$  neutrons/sec. The source was placed at the geometrical center of the moderator. The maximum corrections for source and indicator extension were about 5% for the points nearest the source in the experiments with H<sub>2</sub>O, and not more than 2% in the remaining experiments. As these points make only a small contribution to  $\tau$ , no corrections were made.

The estimate in [1] of self-screening in the source shows that in this case the correction is negligible. The relative spatial distribution of moderated neutrons was measured with indium indicators in the form of disks of thickness 0.1 mm (0.090 g/cm<sup>2</sup>) and diameter 10 or 39.5 mm.

The activities of the indium foils were measured by a method which avoided calculations associated with corrections for radioactive decay. This method was suggested by A. I. Mogil'ner. The indicator activities were determined by cyclic interchange under counters. For example, for two indicators (one the monitor M), after two measurement cycles we obtained

$$\frac{a'_I}{a'_M} = \sqrt{\frac{a_I \varepsilon_A \theta_1 a_I \varepsilon_B \theta_2}{a_M \varepsilon_B \theta_1 a_M \varepsilon_A \theta_2}}$$

where  $a_I$  and  $a_M$  are the indicator activities at time  $t_0$ ;  $\varepsilon_A$  and  $\varepsilon_B$  are the counting efficiency of counters A and B, and  $\theta_1$  and  $\theta_2$  are factors representing radioactive decay in time  $t_0$  before and during the measurements. The method is valid for any number of indicators.

The square of the moderation length was calculated by the formula

$$\bar{r}^2 = \frac{1}{6} \bar{r}^2 = \frac{1}{6} \cdot \frac{\int_0^{\infty} Ar^4 dr}{\int_0^{\infty} Ar^2 dr} = \frac{1}{6} \cdot \frac{\int_0^R Ar^4 dr + \int_R^{\infty} kr^2 e^{-r/\lambda} dr}{\int_0^R Ar^2 dr + \int_R^{\infty} ke^{-r/\lambda} dr},$$

where  $A$  is the indicator activity,  $r$  is the distance from the source center to the indicator,  $R$  is the distance from the source to the farthest measurement point,  $k$  is a coefficient of proportionality, and  $\lambda$  is the relaxation length of neutrons from the source.

<sup>1</sup>Graphite density = 1.33 g/cm<sup>3</sup>.

TABLE 1. Measured and Calculated Values of Square of Neutron Moderation Length

Moderator	Lattice repeat distance, mm	$\rho C/\rho_{H_2O}$	Volume proportion of water in unit cell	Square of moderation length, cm <sup>2</sup>		$\bar{\tau} = \frac{2}{3}\tau_{\perp} + \frac{1}{3}\tau_{\parallel}$	$\tau$ (calc), cm <sup>2</sup>
				$\tau_{\perp}$	$\tau_{\parallel}$		
Graphite-water lattice . . . . .	77	2.44	0.45	131±2	148±6	137±2	126
	67	5.67	0.26	167±3	236±15	190±5	185
	62	11.30	0.15	208±4	287±30	234±10	255
H <sub>2</sub> O . . . . .	—	—	1.00	56.6±4.5	—	—	66.9
C . . . . .	—	—	0	—	—	—	614

The integrals  $\int_0^R Ar^4 dr$  and  $\int_0^R Ar^2 dr$  were determined by numerical integration. At great distances from

the source, where the cadmium ratio  $R_{Cd} \approx \text{const}$ , the distribution of moderated neutrons has the same form as the distribution of neutrons from the source which have made one collision in the medium. In this region,  $A = k \exp(-r/\lambda)/r^2$ . In all the lattices investigated, the measurements were made at great enough distances for the determination of  $\lambda$  and  $k$  ( $R = 60$  cm for  $\tau_{\parallel}$  and  $R = 77$  cm for  $\tau_{\perp}$ ). The constants  $\lambda$  and  $k$  in the extrapolation integrals were calculated by drawing the graph of  $\ln Ar^2 = f(r)$ . In the region where  $R_{Cd} \approx \text{const}$ , this relation is linear. From six or seven experimental points in this region, the method of least squares was used to determine the parameters of the line  $y = a + br$ , where  $a = \ln k$  and  $b = -1/\lambda$ . The results of the measurements and calculations are given in the table. The moderation length of the neutrons in pure water was also determined, to test the method of measurement. The observed square of the moderation length agrees with the results in [1,2]. The moderation length of the neutrons in the graphite-water lattice was measured in a system of finite dimensions. The dimensions of the system in the direction of measurement must exceed the region of the steady neutron spectrum, where the distribution of moderated neutrons follows the law  $A = [k \exp(-r/\lambda)]/r^2$ . This condition was satisfied for all the lattices measured.

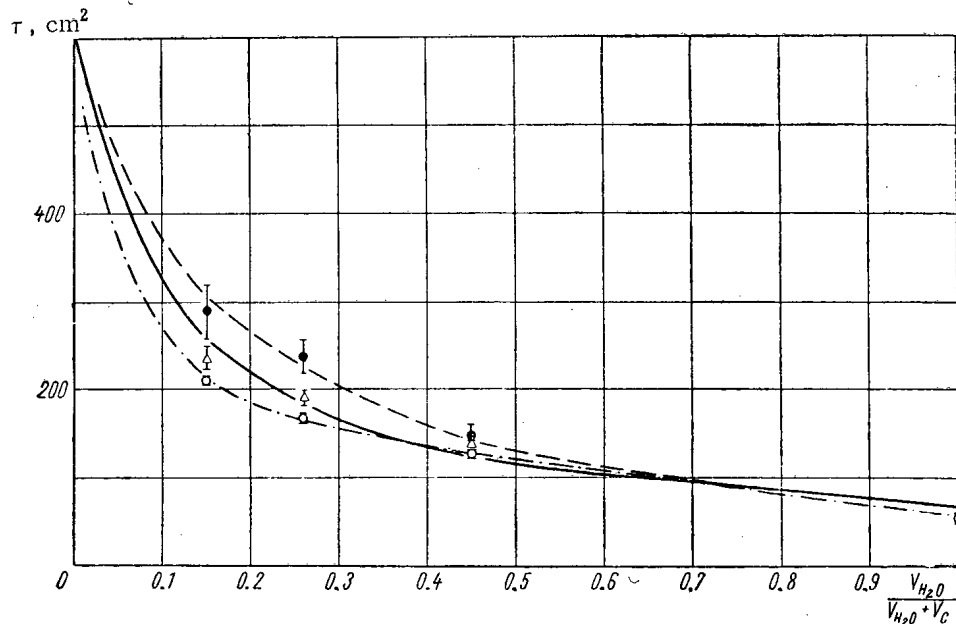


Fig. 1. Experimental and theoretical values of  $\tau$ , plotted versus volume proportion of water,  $V_{H_2O}/(V_{H_2O} + V_C)$ , where  $V_{H_2O}$  and  $V_C$  are the volumes of water and graphite in the unit cell. ● —  $\tau_{\parallel}$ , ○ —  $\tau_{\perp}$ , Δ —  $\bar{\tau} = \frac{2}{3}\tau_{\perp} + \frac{1}{3}\tau_{\parallel}$ , — — calc.

The effect of the closeness of the lattice boundaries to the source and indicator were estimated by experiment. For this purpose, experiments were made on the activation of the indium indicators when the thickness of the medium behind the source and indicator was varied. Determinations were made of the minimum distance to the boundaries of the medium at which source and indicator could be placed for measurements nearest and farthest from the neutron source. For distances of 120-150 mm, the boundary effect leads to additional errors of 2.5%. The greatest error in determining the moderation length was introduced by the extrapolation additions  $\left( \int_R^{\infty} ke^{-r/\lambda} r^2 dr \text{ and } \int_R^{\infty} ke^{-r/\lambda} dr \right)$ .

The errors in determining the extrapolation integrals for all lattices were within 10-20% in both directions. The errors in determining  $\int_0^R Ar^4 dr$  and  $\int_0^R Ar^2 dr$  were 0.2-0.7% (for all lattices in both directions). The moderation lengths were calculated in the age approximation, for homogeneous mixtures of water and graphite with the same nuclear concentration ratios as the lattices, and also for the pure moderators. The method was that of [3].

Comparison of the experimental and theoretical data shows that the value of  $\tau$  observed for pure water (56.6 cm<sup>2</sup>) is about 18% less than the corresponding theoretical value (66.9 cm<sup>2</sup>), but agrees, within the experimental error, with the value calculated in [2] (58.5 ± 1.5 cm<sup>2</sup>).

Possible reasons for this discrepancy include the following:

1. Inaccuracy in the source spectrum. The neutron spectrum of the Po-Be source was taken from [4]. This agrees with that measured in [5]. The mean neutron energy is 4.38-4.62 MeV. The spectrum in [4] was used in [6] for a number of calculations.
2. The use of formulas [3], based on certain assumptions.
3. Inelastic scattering by oxygen was allowed for in the calculations, but not the resultant decrease in neutron energy. The neglect of this effect, which is particularly important in the region of neutron energies greater than 4 MeV, would lead to a high calculated value of  $\tau$ .

The diagram plots the experimental and theoretical values of  $\tau$  versus the volume of water in the graphite-water lattice. The obvious difference between the  $\tau_{\parallel}$  and  $\tau_{\perp}$  curves can be explained by the anisotropy of the system, causing the  $\tau_{\parallel}$  curve to be above the  $\tau_{\perp}$  curve. As shown by experiments on the way in which the boundaries of the graphite system affected the distribution of moderated neutrons,  $\tau$  cannot be significantly reduced by neutron leakage, as this effect does not exceed the experimental error.

The diagram also gives calculated value of  $\tau$  for a homogeneous graphite-water mixture, and the "mean" experimental values, determined by the formula  $\tau = \frac{2}{3}\tau_{\perp} + \frac{1}{3}\tau_{\parallel}$ , derived by analogy with that for the neutron migration area [7]. The mean experimental values  $\bar{\tau}$ , differ from the theoretical values by only 10%; however, this is greater than the experimental error.

The reasons for this discrepancy are possibly the same as for pure water. However, the calculations were made for a homogeneous C-H<sub>2</sub>O mixture, while the experimental values refer to a heterogeneous lattice.

The measurements allow  $\tau$  to be plotted versus the nuclear proportions of water and graphite over a fairly wide range.

In conclusion, the authors wish to thank G. Ya. Artyukhov for valuable advice and instructions.

#### LITERATURE CITED

1. H. Goldstein, P. Zweifel, and D. Foster, Proceedings of the Second International Conference on the Peaceful Uses of Atomic Energy. Selected Reports of Foreign Scientists [in Russian] (Atomizdat, Moscow, 1959), Vol. 2, p. 688.
2. G. Joanou, A. Goodjohn, and N. Wikner, Nucl. Sci. and Engng., **13**, 171 (1962).
3. V. P. Kochergin and V. V. Orlov, Atomnaya énergiya, **6**, 34 (1959).
4. B. Whitmore and W. Baker, Phys. Rev., **78**, 799 (1950).
5. A. G. Khabakhpashev, PTÉ, No. 1, 25 (1960).
6. M. Reier, F. Obenshain, and R. Hellens, Nucl. Sci. and Engng., **4**, 1 (1958).
7. E. V. Wigner and A. V. Weinberg, Physical Theory of Nuclear Reactors [Russian translation] (IL, 1961), p. 682.

METHOD OF INVESTIGATING  $\gamma$ -RADIATION  
FROM THE  $(n, \gamma)$  REACTION ON SEPARATED ISOTOPES

(UDC 539.172.4)

É. A. Rudak and E. I. Firsov

Translated from *Atomnaya Énergiya*, Vol. 18, No. 3,  
pp. 285-287, March, 1965

Original article submitted April 20, 1964

Many experimental investigations of spectra of  $\gamma$ -radiation from the  $(n, \gamma)$  reaction on thermal neutrons have been carried out. The most complete analysis of the methods used in these investigations is given in [1]. As a rule, the main difficulty encountered by experimenters is a poor effect-to-background ratio, especially in those cases where specimens containing small amounts of matter must be used in investigations. For instance, it is virtually impossible to investigate  $\gamma$ -radiation produced by the  $(n, \gamma)$  reaction on separated isotopes by means of magnetic spectrometers, since the quantities of matter that can be used in these cases amount to a few grams, while specimens weighing approximately 1 kg are necessary for ensuring an acceptable effect-to-background ratio [2]. However, investigations on separated isotopes make it possible to obtain the most complete and accurate picture of the processes occurring in the radiative capture of neutrons; these investigations are also of great interest.

One of the possible ways of improving the effect-to-background ratio is to reduce the background by changing the design of the standard channels in reactors since, in the final analysis, the intensity of the background determines the minimum amount of matter in the specimen. In radial channels, i.e., channels which are oriented along the radius toward the center of the reactor core, it is difficult to eliminate the background of  $\gamma$  rays issuing from the core. A bismuth or a lead block placed between the core and the specimen for the purpose of filtering out the  $\gamma$ -radiation from the core reduced the thermal neutron flux at the specimen's location while not eliminating the background of  $\gamma$  rays which reach the channel beyond the block as a result of scattering.

It is somewhat less complicated to reduce the background in tangential channels, which are oriented along the tangent to the reactor core. Two  $\gamma$ -background sources exist in a tangential channel. The first of these sources are the  $\gamma$  rays from the core which are scattered by the specimen, the  $\gamma$ -beam collimators, and the channel walls. The second  $\gamma$ -background source is the radiative capture of thermal neutrons by the walls and the bottom of the channel, since standard tangential channels end immediately beyond the core. The  $\gamma$  rays from the core can be attenuated by means of a lead shield placed between the core and the tangential channel. The  $\gamma$  radiation produced by the radiative capture of thermal neutrons by the channel walls can be eliminated by means of a system of lead collimators [1].

However, in the existing tangential channel designs, it is impossible to eliminate completely the background produced by the capture of neutrons in the channel bottom, which is located in the immediate vicinity of the core. In this case, perhaps the best method for reducing the background in the channel consists in lengthening the

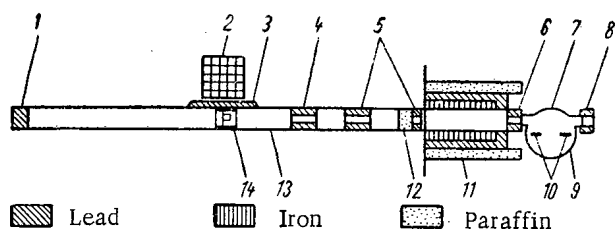


Fig. 1. Schematic diagram of experimental setup. 1) Lead block screening the channel bottom; 2) reactor core; 3) lead shield; 4) shaping collimator; 5) collimators for protection from scattered  $\gamma$  rays; 6) collimator shaping the  $\gamma$  beam with respect to the radiator dimensions; 7) spectrometer radiator; 8)  $\gamma$ -beam collimator at the exit from the spectrometer chamber; 9) spectrometer chamber; 10) Geiger counters; 11) radiation shield outside the channel; 12) thermal neutron filter; 13) tangential channel; 14) graphite container with specimen.

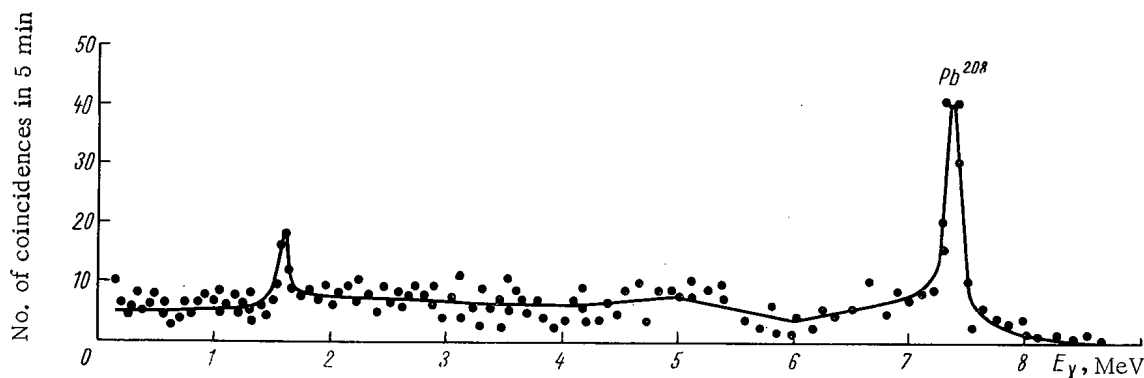


Fig. 2.  $\gamma$ -Radiation background in the channel.

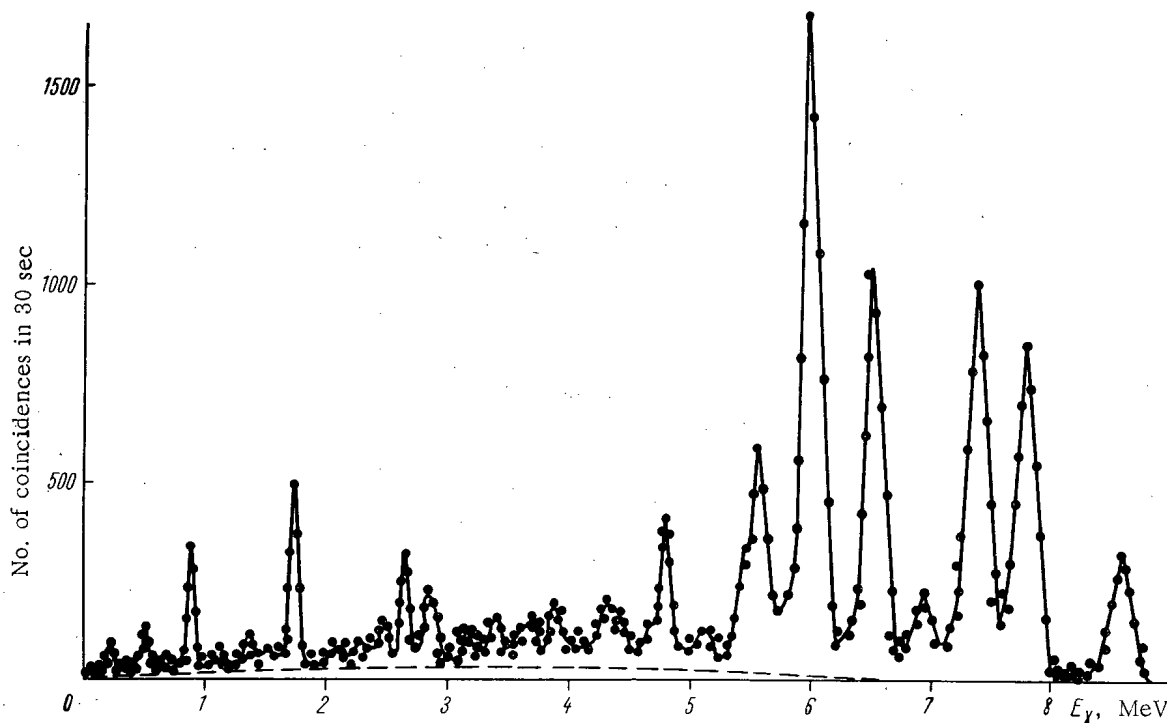


Fig. 3. Spectrum of  $\gamma$  radiation due to the  $\text{Cl}^{35}(\text{n}, \gamma)\text{Cl}^{36}$  reaction.

channel, since its bottom will then be brought out of the neutron flux and will not serve as a background source. This experiment was performed in the tangential channel of the IRT AN Belorus, SSR reactor. A Compton spectrometer with a 2% resolution and 0.3 MeV as the lower limit of the measurement range, was installed in the channel[3]. The schematic diagram of the experimental setup is shown in Fig. 1.

The specimen, enclosed in a graphite container, was placed to face the center of the reactor's core, where the thermal neutron flux was approximately equal to  $3 \cdot 10^{12}$  neutrons/( $\text{cm}^2 \cdot \text{sec}$ ). The  $\gamma$ -beam from the specimen was collimated by means of a system of lead collimators and extracted from the reactor channel and brought to the radiator of the Compton spectrometer. The distance between the specimen and the spectrometer radiator was equal to 4.5 m. The recoil electrons knocked out of the radiator within an angle of  $1^\circ$  from the direction of the incident beam are forced into orbit by the magnetic field and are analyzed with respect to pulses.

The specific feature of this setup and of similar ones where the method of irradiating the specimen with neutrons in the reactor channel is used is the large distance between the specimen and the spectrometer radiator. However, due to the large distance, the loss in the intensity of the  $\gamma$ -radiation flux is compensated by the large value of the neutron flux at the specimen's location and the very good collimation of the  $\gamma$  beam.

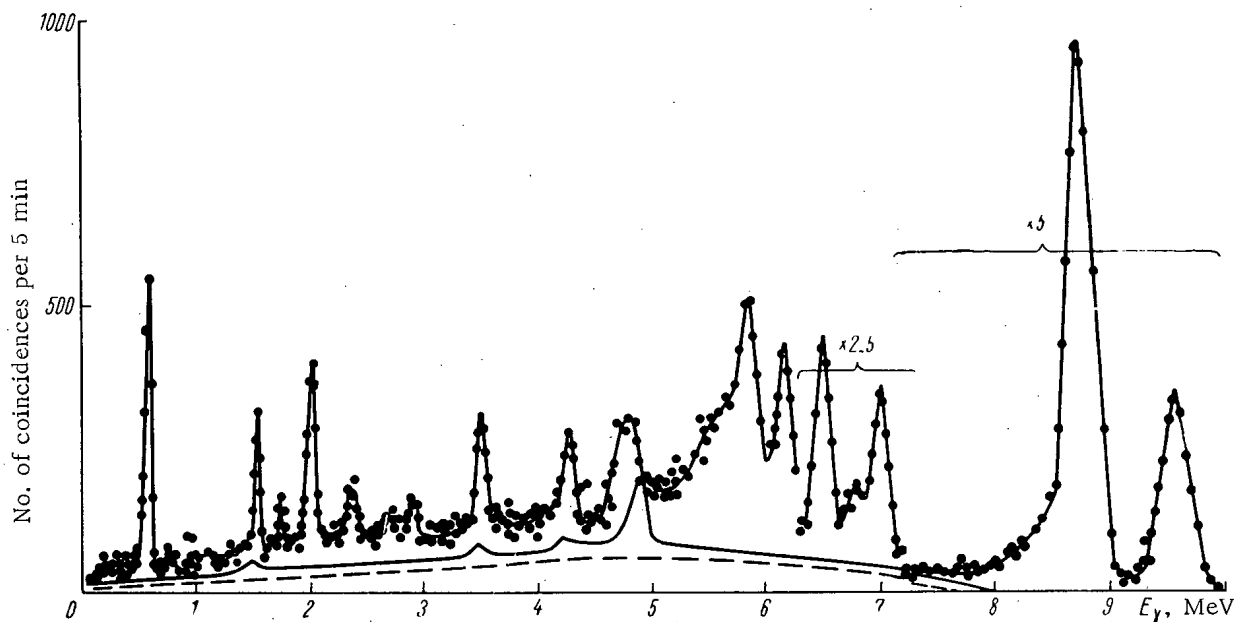


Fig. 4. Spectrum of  $\gamma$  radiation due to the  $\text{Cr}^{53}(n, \gamma)\text{Cr}^{54}$  reaction.

In our experiment, the most important features were the extended tangential channel and the system for collimating the  $\gamma$  beam. As is shown by background measurements, the background of the channel walls that arises as a result of the  $\text{Al}^{27}(n, \gamma)\text{Al}^{28}$  reaction can be reduced to an insignificant level if the  $\gamma$  beam is well collimated. The most important role in eliminating this background is played by the first lead collimator that forms the  $\gamma$  beam. The diameter of the opening in this collimator is equal to 30 mm; it is located in the first section of the slide block from the core. The collimator is shielded from the core radiation by a water layer with a thickness of about 0.5 m and by other structural parts of the reactor. Figure 2 shows the  $\gamma$ -radiation background in the channel corresponding to the geometry shown in Fig. 1, but without the specimen and the graphite container. In this spectrum, only the 7.38-MeV line from the  $\text{Pb}^{207}(n, \gamma)\text{Pb}^{208}$  reaction could be reliably separated. A small peak at 1.76 MeV, whose origin is not known, is also observed. The 7.73-MeV line from the  $\text{Al}^{27}(n, \gamma)\text{Al}^{28}$  reaction could not be detected, which indicated that the spectrometer was reliably shielded from the background  $\gamma$ -radiation of the channel walls. If the shaping collimator is placed closer to the core, the background conditions in the channel sharply deteriorate due to the scattering of  $\gamma$  rays from the core on this collimator. The other two lead collimators serve for shielding the spectrometer from the  $\gamma$  rays scattered in the channel. A thermal-neutron filter consisting of a mixture of paraffin and boron carbide (4:1) was also placed in the outside section of the slide block. The filter thickness was equal to 70 mm.

In order to check the operation of the device and obtain a rough estimate of its possibilities, we plotted the spectrum of  $\gamma$  rays produced by the  $\text{Cl}^{35}(n, \gamma)\text{Cl}^{36}$  reaction (Fig. 3). A hexachlorobenzene tablet, weighing 30 g, was used as the specimen. The spectrum obtained was similar to the  $\gamma$ -ray spectrum produced by the same reaction, which was given in [2]. The only line that was not detected was the 1.72-MeV line, which agreed with the data given in [4]. We also plotted the spectrum of the background of electrons produced in the generation of electron-positron pairs in the spectrometer radiator (see Fig. 3, dashed curve). Moreover, we investigated the spectrum of the background of  $\gamma$  rays from the core that were scattered on the specimen, the collimator, and the channel walls. It proved to be much lower than the background of electron pairs, so that it could be neglected in  $\text{Cl}^{35}$  measurements.

In the case of  $\text{Cl}^{35}$ , the effect-to-background ratio was not less than 10 in any region of the spectrum. In principle, this ratio cannot be improved, since the background is almost completely determined by the spectrum of the specimen's  $\gamma$ -radiation. For other isotopes, the background of scattered  $\gamma$  rays from the core should be more intensive. The point is the  $\text{Cl}^{35}$  has a rather large cross section of the thermal neutron  $(n, \gamma)$  reaction (31b), so that a reduction in the cross section of this reaction would result in a relative increase in the  $\gamma$ -radiation background produced by the core. The spectrum of  $\gamma$  rays from the  $\text{Cl}^{35}(n, \gamma)\text{Cl}^{36}$  reaction was obtained over a period of 10 h of continuous operation of the spectrometer, which was possible due to the short time necessary for obtaining data for



a single point (0.5 min). Consequently, if a maximum exposure of 10 min is used for a point, this device makes it possible to obtain spectra of  $\gamma$  rays produced by the  $(n, \gamma)$  reaction on specimens where the product between the mass and the cross section  $\sigma(n, \gamma)$  is of the order of 20-30 g · barns. However, the quality of the statistical data will be slightly worse than in the case of  $\text{Cl}^{35}$ .

As an example, Fig. 4 shows the spectrum of  $\gamma$  radiation due to the  $\text{Cr}^{53}(n, \gamma)\text{Cr}^{54}$  reaction. It was obtained by means of a specimen containing 7.26 g chromic oxide. The dashed line represents the electron background due to pair generation in the radiator, while the solid line indicates the total background of the core  $\gamma$ -radiation scattered on the specimen, the collimators, and the channel walls, and also the background of electron pairs. The background due to scattered  $\gamma$ -radiation from the core is less intensive than the background of electron pairs. The lines in the background spectrum are due to the reaction of radiative capture of neutrons in the  $\text{C}^{12}$ ,  $\text{Al}^{27}$ , and  $\text{Pb}^{207}$  isotopes contained in the materials of which the specimen container, the thermal neutron filter, and the  $\gamma$ -beam collimators are made. These lines can be eliminated by using beryllium in constructing the specimen container and by improving the design of the first collimator.

In conclusion, the authors hereby acknowledge their indebtedness to L. V. Groshev and A. M. Demidov for their useful advice and direct assistance in constructing the device.

#### LITERATURE CITED

1. A. M. Demidov, Methods of Investigating Nuclear Radiation in Radiative Neutron Capture [in Russian] (Gosatomizdat, Moscow, 1963).
2. L. V. Groshev et al., Atlas of Spectra of  $\gamma$ -Rays Produced in Radiative Capture of Thermal Neutrons [in Russian] (Atomizdat, Moscow, 1958).
3. L. V. Groshev, B. P. Ad'yasevich, and A. M. Demidov, Collection: Physical Investigations. Transactions of the International Conference on the Peaceful Uses of Atomic Energy, Geneva, 1955. Reports by Soviet Scientists [in Russian] (Izd. AN SSSR, Moscow, 1955), p. 255.
4. L. V. Groshev, A. M. Demidov, and V. N. Lutsenko, *Izv. AN SSSR, Ser. Fiz.*, 24, 833 (1960).

DEPENDENCE OF THE COUNTING EFFICIENCY IN RECORDING  
FAST NEUTRONS ON THE GEOMETRY OF PLASTIC SCINTILLATORS

(UDC 539.107.483)

V. G. Zolotukhin and G. G. Doroshenko

Translated from *Atomnaya Énergiya*, Vol. 18, No. 3,  
pp. 287-290, March, 1965

Original article submitted June 8, 1964

Information on the counting efficiency in recording fast neutrons is necessary in studying fluxes and spectra of these neutrons [1]. Several articles devoted to this problem have been published [2-5], but the data given there are incomplete and contradictory. The present article provides the results obtained in calculating the recording efficiency by means of the Monte Carlo method for four different geometries of a cylindrical stilbene crystal (see Fig. 1). For each of the geometries, the calculations were performed for 55 initial neutron energies in the 0.5- to 18-MeV range. These energies were chosen by taking into account the resonance structure of the cross section of interaction between neutrons and carbon nuclei. The calculation method was described in [6]. The statistical accuracy of calculations was equal to 0.2-0.8%.

The effect of the resonance structure of the carbon cross section is manifested in all cases of the stilbene crystal geometries under consideration; with an increase in the scintillator dimensions, this effect is intensified. The character of the resonance structure of efficiency and the relationship between the exactly calculated efficiency and the efficiency calculated in the approximation of single (n-p)-scattering can be explained by considering, besides the single scattering on hydrogen and carbon nuclei, also the contribution of multiple interaction processes to the efficiency.

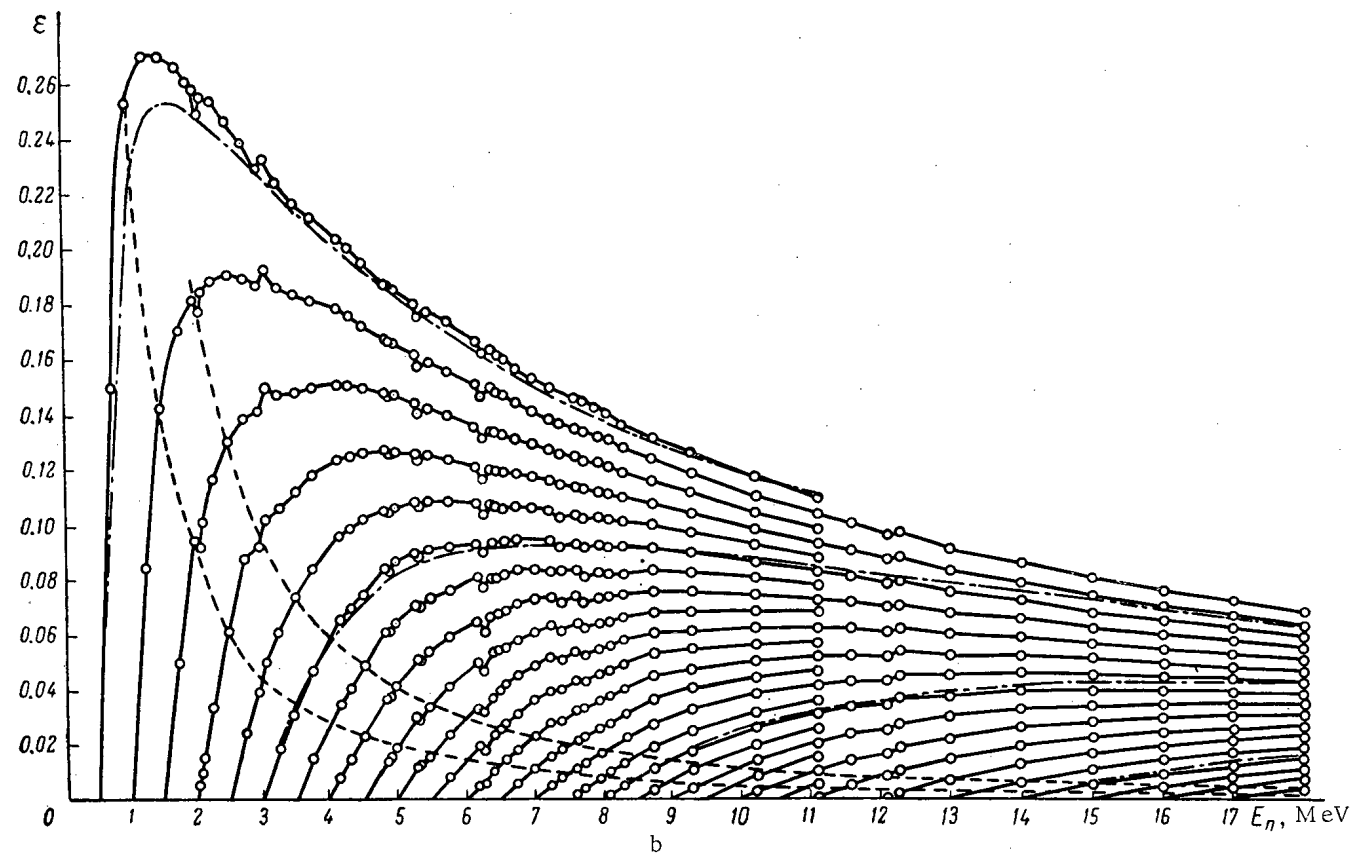
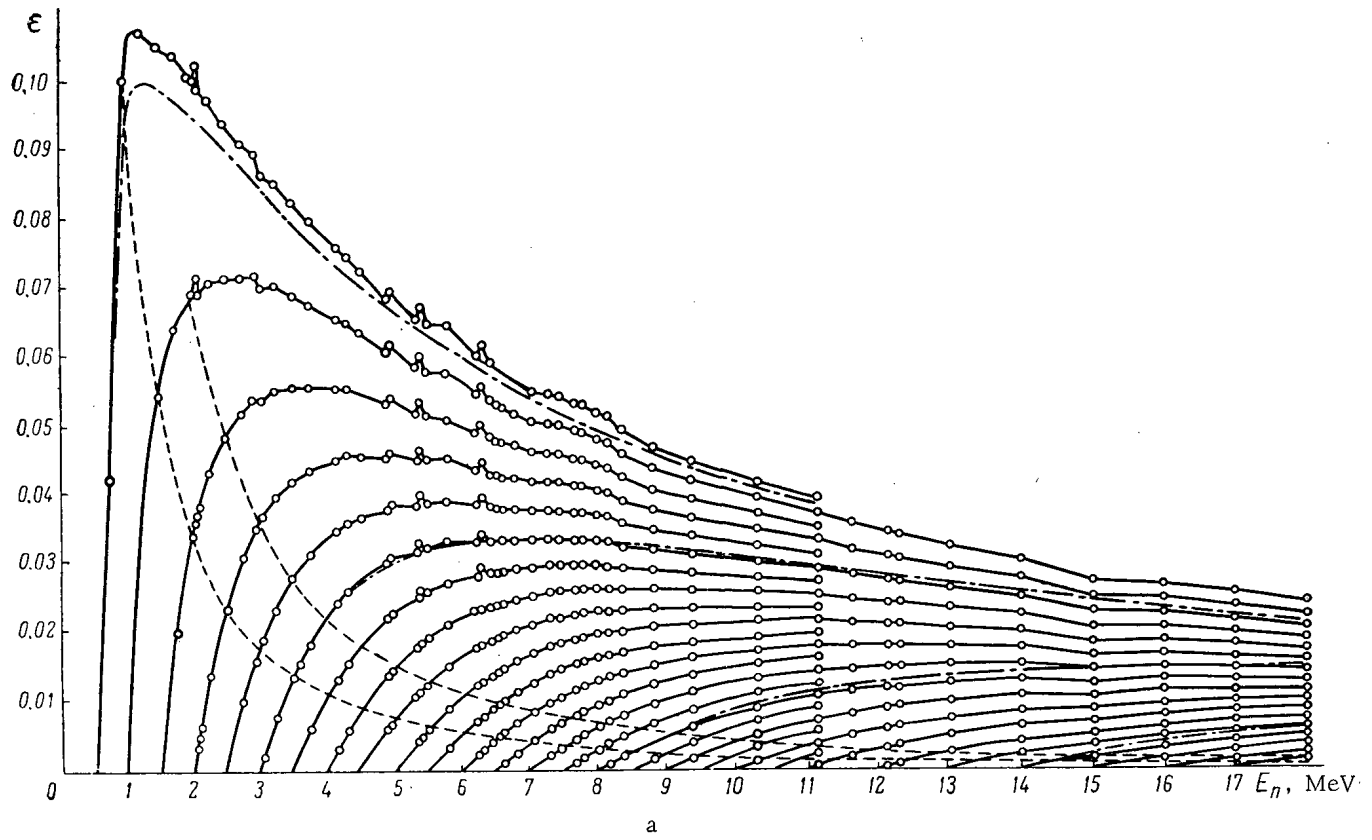
For a qualitative estimate, we shall consider double interaction processes. As was shown in [6], the contribution of double (n-p)-scattering processes to the efficiency is significant only for  $E \approx B$ , while the contribution of processes where the first scattering occurs on carbon nuclei and the second on protons is significant throughout the entire energy range. In this, the above contribution actually compensates the reduction in efficiency caused by the first scattering on carbon with an accuracy to terms of the order of  $H^2$  [6]. This explains the fact that the single (n-p)-scattering approximation yields results that are in good agreement with the actual efficiency in the range of up to 10 MeV. At higher energies this compensation is only partially effective due to processes where neutron absorption takes place [reactions (n, $\alpha$ ) and (n,3 $\alpha$ )].

The above compensation depends on the sign of the following quantity [6]:

$$q\Sigma_{C,s} - \frac{1}{2}(\Sigma_t - \Sigma_H) \quad (1)$$

Here,  $\Sigma_{C,s}$ ,  $\Sigma_t$ , and  $\Sigma_H$  are the macroscopic cross sections of scattering on carbon, the total cross section of interaction between neutrons and the scintillator material, and the (n-p)-scattering cross section, respectively;  $q = \langle L \rangle / H$ , where  $\langle L \rangle$  is the mean path traversed by a neutron after scattering on a carbon nucleus;  $H$  is the scintillator thickness. For  $\Sigma_t = \Sigma_{C,s} + \Sigma_H$  (no absorption), the value of (1) is proportional to  $(q - \frac{1}{2})$ . In the case where  $q < \frac{1}{2}$ , the resonances in the carbon cross section produce peaks on the efficiency curves while for  $q > \frac{1}{2}$ , these resonances produce dips (see Fig. 1a,b).

The results obtained in our experiments show that the expression for efficiency in the single (n-p)-scattering approximation can be successfully applied in the energy range of up to 10 MeV by using relatively small scintillators in cases where a high accuracy is not required. For more accurate calculations, all the necessary data for crystals with dimensions different from those considered here can be obtained by interpolating the graphs given in the present article.



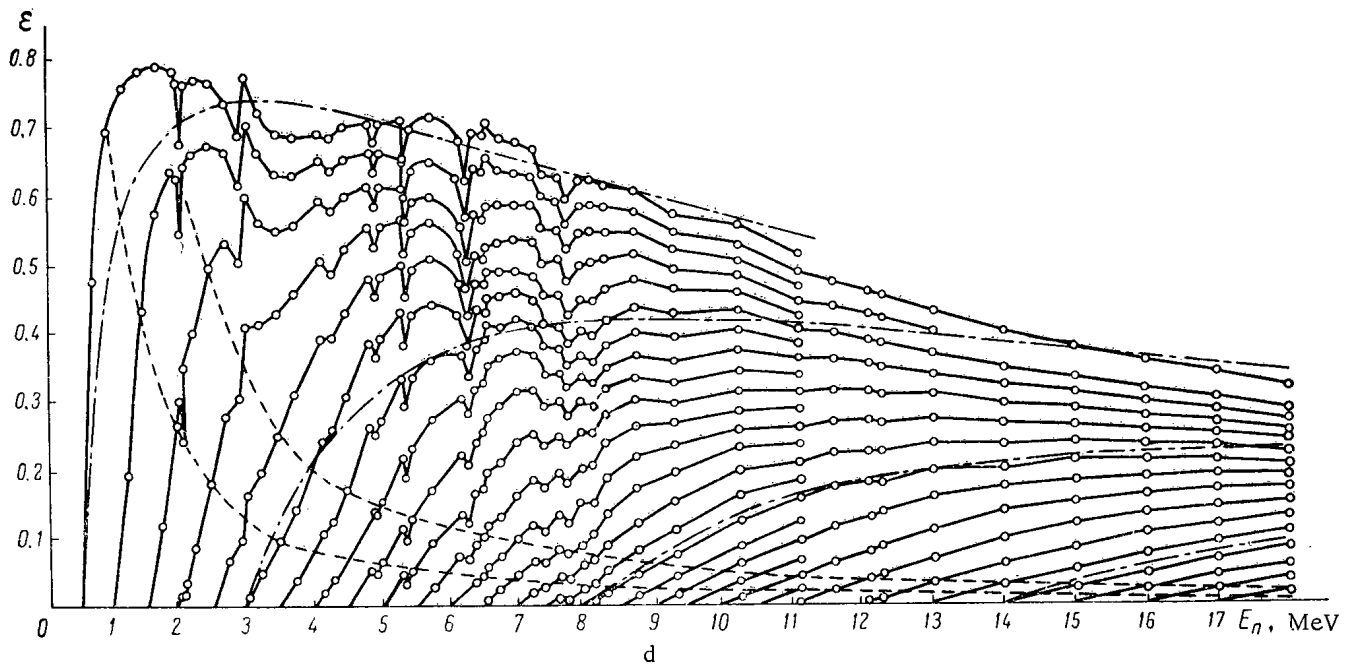
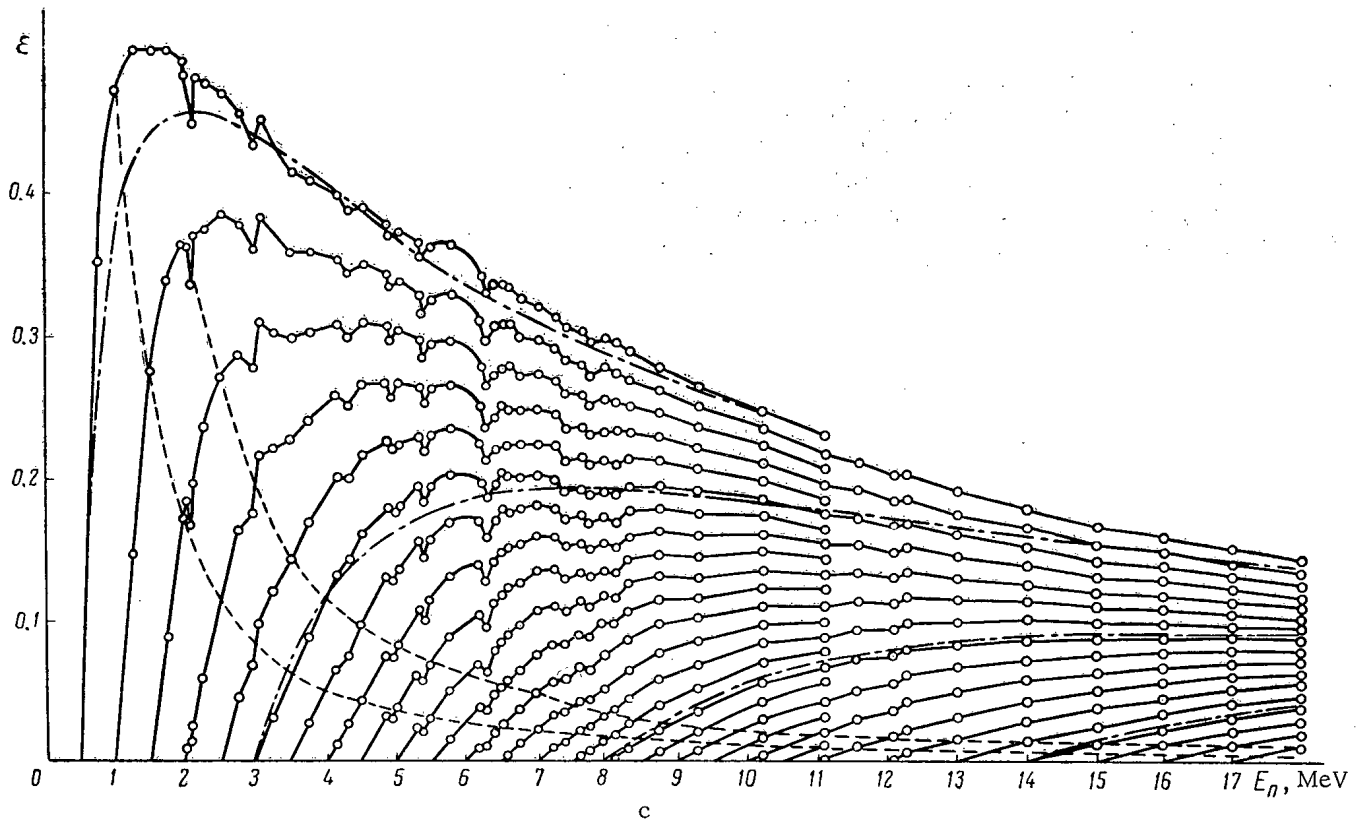


Fig. 1. Dependences of the counting efficiency in recording fast neutrons on the incident neutron energy for different recording thresholds for stilbene crystals with the following dimensions (mm): a)  $h = 10, d = 30$ ; b)  $h = 30, d = 30$ ; c)  $h = 70, d = 70$ ; d)  $h = 200, d = 200$ . Solid line, results obtained by means of the Monte Carlo method; dashed line, efficiency calculation in the approximation of single (n-p)-scattering.

LITERATURE CITED

1. G. G. Doroshenko et al., *Izv. AN SSSR, Ser. Fiz.*, 27, 1308 (1963).
2. T. Hardy, *Rev. Scient. Instrum.*, 29, 705 (1958).
3. H. Grassler and K. Tesch, *Nucl. Instrum. and Methods*, 10, 353 (1961).
4. R. Batchelor et al., *Nucl. Instrum. and Methods*, 13, 70 (1961).
5. C. Wiegand et al., *Rev. Scient. Instrum.*, 33, 526 (1962).
6. V. G. Zolotukhin, G. G. Doroshenko, and B. A. Efimenko, *Atomnaya Énergiya*, 15, 194 (1963).

CALCULATION OF THE EFFECTIVE RESONANCE INTEGRAL  
FOR A LUMP CONSISTING OF A MIXTURE OF NUCLEI  
OF A RESONANCE ABSORBER AND A CONTINUOUS  
CROSS-SECTION ABSORBER

(UDC 621.039.512.26)

Yu. G. Pashkin and V. V. Chekunov

Translated from *Atomnaya Énergiya*, Vol. 18, No. 3,  
pp. 290-292, March, 1965

Original article submitted April 4, 1964; revision submitted July 31, 1964

In calculating the effective resonance integral for a lump consisting of a mixture of nuclei of a resonance absorber and an absorber with a continuous cross section (for instance, an absorbing rod consisting of borides of rare-earth elements, etc.), it is necessary to take into account the mutual blocking of these nuclei.

The blocking of nuclei with a continuous absorption cross section by nuclei with resonance absorption can be taken into account by using, for instance, the results given in [1].

We shall present here a method for calculating the effective resonance integral for nuclei with a resonance absorption cross section by taking into account the screening effect of nuclei with a continuous absorption cross section.

The resonance integral in which we are interested can be written thus:

$$J_{\text{eff}} = \int_{-\infty}^{\infty} \frac{\sigma_r(u)}{\Sigma_t(u)} \psi(u) du, \quad (1)$$

where  $\psi(u)$  is the mean collision density of neutrons with the lethargy  $u$  in a lump placed in a medium with an isotropic flux  $n v = 1$ ,  $\sigma_c(u)$  is the absorption cross section at resonance, and  $\Sigma_t(u) = \Sigma_r(u) + \Sigma_c^{\text{con}}(u) + \Sigma_p(u)$  is the total cross section of the lump, which is equal to the sum of the total cross section at resonance  $\Sigma_r(u)$ , the continuous cross section  $\Sigma_c^{\text{con}}$ , and the cross section  $\Sigma_p(u)$  of potential scattering of the material in the lump.

In the general case,  $\psi(u)$  can be determined from the following equation, which was given in [2]:

$$\psi(u) = \frac{S}{4V} W(u) + [1 - P(u)] \int_{u-r}^u \psi(u') \frac{\Sigma_p(u')}{\Sigma_t(u')} f(u-u') du', \quad (2)$$

where  $S/4$  is the total flux of neutrons with the lethargy  $u$  from the medium surrounding the lump which passes through the lump's surface area  $S$  per unit interval of lethargy,  $f$  is the scattering function,  $V$  is the lump volume,  $W(u)$  is the probability of neutron collision in the lump, and  $P(u)$  is the probability of the emergence of neutrons moderated in the lump where, according to [3], the following expression holds for an isotropic flux in the lump:

$$P(u) du = \frac{S}{4V} \cdot \frac{W(u)}{\Sigma_t(u)} du. \quad (3)$$

If the resonance is narrow, i.e., if its width is much smaller than the mean energy loss in collision, the flux of neutrons with the lethargy  $u$  [ $\psi(u')/\Sigma_t(u')$ ] can be replaced by a flux of neutrons with the same lethargy in the absence of resonance  $\psi^0(u')/\Sigma_t^0(u')$  under the integral sign in Eq. (2).

The solution for  $\psi^0(u)$  can be found from Eq. (2) under the assumption that, in the  $\Delta u = r$  interval,  $\Sigma_c^{\text{con}}$  and  $\Sigma_p$  do not depend on the lethargy and are equal to their values at the resonance energy  $E_0$ . In this case, considering the normalization of the scattering function  $\int_{u-r}^u f(u-u') du' = 1$  and relationship (3), we can write Eq. (2) for  $\psi^0(u)$  in the following form:

$$\psi^0 = (1 - P^0) \frac{\Sigma_p}{\Sigma_t^0} \psi^0 + P^0 \Sigma_t^0$$

and, consequently,

$$\psi^0 = \frac{P^0 \Sigma_t^0}{1 - (1 - P^0) \frac{\Sigma_p}{\Sigma_t^0}} \quad (4)$$

With a consideration of (3) and (4), the solution of (2) will now have the following form:

$$\psi(u) = \frac{P^0 \Sigma_p}{1 - (1 - P^0) \frac{\Sigma_p}{\Sigma_t^0}} + P(u) \left[ \Sigma_t(u) - \frac{P^0 \Sigma_p}{1 - (1 - P^0) \frac{\Sigma_p}{\Sigma_t^0}} \right]$$

or

$$\psi(u) = \Sigma_p^* + P(u) [\Sigma_t(u) - \Sigma_p^*], \quad (5)$$

where

$$\left. \begin{aligned} \Sigma_p^* &= \Sigma_p \frac{P^0}{1 - (1 - P^0) \frac{\Sigma_p}{\Sigma_t^0}}, \\ \Sigma_t^0 &= \Sigma_c^{\text{con}} + \Sigma_p. \end{aligned} \right\} \quad (6)$$

By substituting expression (5) for  $\psi(u)$  in (1), we obtain the expression for the effective resonance integral

$$J_{\text{eff}} = \int_{-\infty}^{\infty} du \left\{ \sigma_c(u) \frac{\Sigma_p^*}{\Sigma_t(u)} + \sigma_c(u) \frac{\Sigma_t(u) - \Sigma_p^*}{\Sigma_t(u)} P(u) \right\}, \quad (7)$$

i.e., the usual expression for  $J_{\text{eff}}$  (see, for instance [4]), the numerator of which contains, instead of  $\Sigma_p$ ,  $\Sigma_p^*$ , which is determined by expression (6).

The probability that moderated neutrons will emerge from the lump without collisions is determined by the expression [3]

$$P(u) = \frac{\langle 1 - \exp[-l \Sigma_t(u)] \rangle}{\Sigma_t(u) \langle l \rangle}, \quad (8)$$

where the symbol  $\langle \rangle$  denotes averaging with respect to all possible orientations in the lump ( $\langle l \rangle = 4v/S = \bar{l}$ ).

If the resonance has the Breit-Wigner form, we obtain the following after integrating (7) and taking into account the Doppler effect:

$$J_{\text{eff}} = J_\gamma \frac{1}{(1 + \alpha) [1 + h]} \cdot \frac{\Sigma_p^*}{\Sigma_p} \left\{ \eta_1 + \left[ \frac{h}{1 + h} \eta_2 + 2 \left[ (1 + \alpha) \frac{\Sigma_p}{\Sigma_p^*} - 1 \right] \eta_1 \right] \frac{\langle F(\beta, h, \alpha) \rangle}{2 \langle \beta \rangle} \right\}. \quad (9)$$

Here,  $J_\gamma$  is the actual resonance integral;

$$h = \frac{\Sigma_r^0}{\Sigma_p + \Sigma_c^{\text{con}}}, \quad \alpha = \frac{\Sigma_c^{\text{con}}}{\Sigma_p}, \quad \beta = l(\Sigma_c^{\text{con}} + \Sigma_p),$$

the functions  $\eta_1(\xi, h)$  and  $\eta_2(\xi, h)$  were tabulated in [5]:

$$\langle F(\beta, h, \alpha) \rangle = \frac{\left\langle \int \frac{\Sigma_c (\Sigma_r - \Sigma_p^*)}{\Sigma_t^2} (1 - e^{-l\Sigma_t}) du \right\rangle}{\left\langle \int \frac{\Sigma_c (\Sigma_r - \Sigma_p^*)}{\Sigma_t^2} du \right\rangle}, \quad (10)$$

where  $\langle F(\beta, h, \alpha) \rangle$ , which, for  $\alpha = 0$ , coincides with  $F(\beta, h)$  from [5], requires numerical integration.

The magnitude of the effect under consideration can be estimated with a sufficient accuracy by writing the effective integral to be determined in the following form:

$$J_{\text{eff}} = J_{\text{eff}}^0 K,$$

where  $J_{\text{eff}}^0$  is the effective resonance integral, determined according to the method given in [4] without taking into account the screening effect of nuclei with a continuous cross section;

$$K = \frac{J_{\text{eff}}}{J_{\text{eff}}^0}.$$

In calculating  $K$ , the Wigner approximation can be used for the probability that a neutron will pass through the lump without collision [6]:

$$P^0 = \frac{1}{1 + l\Sigma_0^0} \text{ and } P(u) = \frac{1}{1 + l\Sigma_t(u)}.$$

In this case,

$$\begin{aligned} \Sigma_p^* &= \Sigma_p \frac{1}{1 + l\Sigma_c^{\text{con}}} \\ J_{\text{eff}} &= J_\nu \frac{1}{1 + l\Sigma_c^{\text{con}}} \frac{1}{\sqrt{1 + h'}} \eta_1(\xi, h'), \\ J_{\text{eff}}^0 &= J_\nu \frac{1}{\sqrt{1 + h_0'}} \eta_1(\xi, h_0'), \\ h' &= \frac{\Sigma_{r0}}{\Sigma_c^{\text{con}} + \Sigma_p'}, \quad h_0' = \frac{\Sigma_{r0}}{\Sigma_p'}, \quad \Sigma_p' = \Sigma_p + \frac{1}{l} \end{aligned}$$

and, consequently,

$$K = \frac{1}{1 + l\Sigma_c^{\text{con}}} \sqrt{\frac{1 + h_0'}{1 + h'}} \quad (11)$$

We give below the  $K$  value calculated by means of Eq. (11) for two  $\text{Hf}^{177}$  resonances in a cylindrical lump consisting of hafnium diboride  $\text{HfB}_2$  with a diameter of 10 mm (density  $11.2 \text{ g/cm}^3$ ):

$E_0, \text{ eV}$	1.095	2.38
$\sigma_{r0}, \text{ b}$	$3.01 \cdot 10^4$	$6.8 \cdot 10^4$
$K$	0.284	0.338

In conclusion, the authors extend their thanks to A. A. Luk'yanov for the useful discussion and valuable remarks.

#### LITERATURE CITED

1. T. V. Golashvili, *Atomnaya Énergiya*, 12, 155 (1962).
2. A. A. Luk'yanov and V. V. Orlov, Collection: *Theory of Nuclear Reactors and Methods for their Calculation* [in Russian] (Gosatomizdat, Moscow, 1962), p. 179.
3. B. Spinrad, Z. Cernik, and I. Korngold, *Transactions of the Second International Conference on the Peaceful Uses of Atomic Energy*, Geneva, 1958. Selected Reports by Foreign Scientists [Russian translation] (Atomizdat, Moscow, 1960), Vol. 2, p. 539.



4. V. V. Orlov, T. V. Golashvili, and A. I. Vaskin, Collection: Neutron Physics [in Russian] (Gosatomizdat, Moscow, 1961), p. 116.
5. G. I. Marchuk, Methods for Calculating Nuclear Reactors [in Russian] (Gosatomizdat, Moscow, 1961), p. 418.
6. L. Dresner, Resonance Absorption in Nuclear Reactors [Russian translation] (Gosatomizdat, Moscow, 1962).

PRESENTATION OF THE REACTOR DYNAMICS EQUATIONS  
IN TERMS OF THE RECIPROCAL PERIOD

(UDC 621.039.512)

N. G. Chelintsev

Translated from Atomnaya Énergiya, Vol. 18, No. 3,

pp. 292-294, March, 1965

Original article submitted April 2, 1964

As is known [1], the dynamic behavior of a reactor in operation at a low power level can be represented by the equations

$$\frac{dn}{dt} = \frac{\rho - \beta}{l} n + \sum_{i=1}^6 \lambda_i C_i + S, \quad (1)$$

$$\frac{dC_i}{dt} = \frac{\beta_i}{l} n - \lambda_i C_i. \quad (2)$$

Let us differentiate Eq. (1) after replacing the quantity  $dC_i/dt$  by its value from Eq. (2) and divide both equations by  $n$ . Then,

$$\frac{1}{n} \cdot \frac{d^2 n}{dt^2} = \frac{1}{l} \cdot \frac{d\rho}{dt} + \frac{\rho - \beta}{l} \cdot \frac{1}{n} \cdot \frac{dn}{dt} + \frac{1}{l} \sum_{i=1}^6 \lambda_i \beta_i - \sum_{i=1}^6 \lambda_i^2 \frac{C_i}{n},$$

$$\frac{1}{n} \cdot \frac{dC_i}{dt} = \frac{\beta_i}{l} - \lambda_i \frac{C_i}{n}.$$

It should be noted that

$$\frac{d}{dt} \left( \frac{1}{n} \cdot \frac{dn}{dt} \right) = \frac{1}{n} \cdot \frac{d^2 n}{dt^2} - \left( \frac{1}{n} \cdot \frac{dn}{dt} \right)^2,$$

$$\frac{d}{dt} \left( \frac{C_i}{n} \right) = \frac{1}{n} \cdot \frac{dC_i}{dt} - \frac{C_i}{n} \cdot \frac{1}{n} \cdot \frac{dn}{dt},$$

where the  $dn/ndt$  value is the reciprocal of the reactor period. By denoting  $dn/ndt = a$ , we finally obtain

$$\frac{da}{dt} + a^2 = \frac{1}{l} \cdot \frac{d\rho}{dt} + \frac{\rho - \beta}{l} a + \frac{1}{l} \sum_{i=1}^6 \lambda_i \beta_i - \sum_{i=1}^6 \lambda_i^2 \frac{C_i}{n}, \quad (3)$$

$$\frac{d}{dt} \left( \frac{C_i}{n} \right) + \frac{C_i}{n} (a + \lambda_i) = \frac{\beta_i}{l}. \quad (4)$$

In the absence of a source ( $S = 0$ ), Eq. (1) can be represented directly in terms of the reciprocal period after division by  $n$ :

$$a = \frac{\rho - \beta}{l} + \sum_{i=1}^6 \lambda_i \frac{C_i}{n}. \quad (5)$$

In certain cases, the use of Eqs. (3)-(5) instead of Eqs. (1) and (2) for the determination of  $a$  (or  $T = 1/a$ ) makes it possible to simplify the solution. We shall give two simple examples.

whence

$$W(j\omega) = \frac{\delta U_{\text{dif}}(j\omega)}{\delta a(j\omega)} = \frac{kT_{\text{dif}}}{T_{\text{dif}} j\omega + 1}$$

In deriving the transfer function of a period meter whose input receives a signal proportional to  $\delta n/n$ , it is necessary to impose the limitation  $\delta n \ll n$  [3]. In our case, it is not necessary to impose any limitation on the input quantity.

#### LITERATURE CITED

1. M. Schultz, Control of Nuclear Power Reactors [Russian translation] (IL, Moscow, 1957).
2. J. Franz and N. Simcic, Trans. IRE, Nucl. Sci., 4, No. 1, 11-14 (1957).
3. A. R. Mirzoyan and I. N. Briker, Atomnaya énergiya, 15, 74 (1963).

EFFECT OF PRESSURE ON THE HEAT TRANSFER  
IN NUCLEATE BOILING OF LIQUID METALS

(UDC 621.039.533.3)

V. M. Borishanskii and K. A. Zhokhov

Translated from *Atomnaya Énergiya*, Vol. 18, No. 3,  
pp. 294-296, March, 1965  
Original article submitted June 30, 1964

Many experiments [1-7] have been performed with the aim of investigating the heat transfer in the boiling of liquid-metal coolants. It was found in these experiments that the heat transfer coefficient in the boiling of liquid metals, as well as nonmetallic liquids, depends on the physical properties of coolants at the saturation curve, the specific thermal load, and the saturation pressure (or temperature). Considering that the physical properties at the saturation curve constitute a well-defined function of pressure, we can write

$$\alpha = Aq^n f(p). \quad (1)$$

Here,  $\alpha$  is the heat transfer coefficient,  $A$  is a constant factor for a certain combination of the heating surface and the coolant,  $q$  is the specific thermal load,  $p$  is the saturation pressure, and  $n$  is the exponent.

On the basis of the published experimental data on the nucleate boiling of liquid metals in the absence of additional thermal resistances at the heating surface (for instance, scale) and the boiling of nonmetallic liquids, it can be assumed that  $n = 0.7$  in the first approximation. It is more difficult to determine the effect of pressure on heat transfer. The comparatively small number and the considerable scatter of experimental points do not make it possible to establish a dependence of the heat transfer coefficient on pressure directly from the experimental data obtained by various authors in the investigated narrow ranges of operating parameters. Therefore, in order to be able to establish a more general dependence, we shall give below a generalization of the experiments performed by various authors, using the law of corresponding states.

The fundamentals of the application of the law of corresponding states in heat transfer were given in [8, 9]. In [9], one of the authors of the article provided a generalization of the physical properties of various substances (nonmetals) at the saturation curve in terms of thermodynamic similarity criteria and also a generalization of the experimental data on heat transfer and critical loads in the boiling of large-volume nonmetallic liquids. The possibility of generalizing the physical properties of liquid metals on the basis of the thermodynamic similarity of physical properties of coolants was demonstrated in [1]. Hence, we conclude that it is advisable to generalize the experimental data on heat transfer in the boiling of liquid-metal coolants on the basis of adding to the system of equations describing the boiling phenomenon the equations of the law of corresponding states of physical properties.

According to [9], the generalization is carried out by using the following coordinates:

$$\frac{\alpha_p^*}{\alpha_{p_*}^*} = f(p/p_{cr}), \quad (2)$$

where  $\alpha_p^* = \alpha/q^n$  is the value of the characteristic for the pressure  $p$  under consideration,  $\alpha_{p_*}^*$  is the value of the characteristic for the reference pressure  $p_* = 0.003p_{cr}$ , and  $p_{cr}$  is the critical pressure.

With such processing, data on the heat transfer in the nucleate boiling of metallic and nonmetallic liquids can be compared.

The experimental data on the heat transfer in the boiling of mercury [5], mercury-magnesium amalgams [3, 5], and sodium [4], given in the coordinate system defined by (2), are compared in the figure. Data on the heat transfer to boiling water [10-14] are also given here for the sake of comparison. The basic parameters used in the generalization of the experimental data are given in the table.

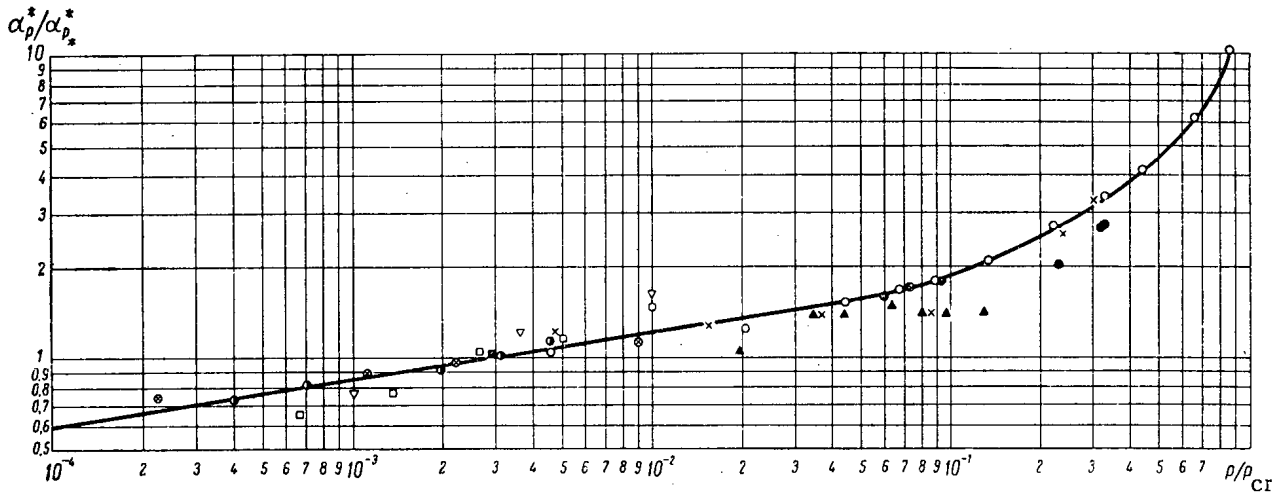


Fig. 1. Comparison of the experimental data on the heat transfer in boiling given in terms of thermodynamic similarity criteria. The points correspond to the numbers given in the table.  $\blacktriangle$  - 1;  $\square$  - 2;  $\nabla$  - 3;  $\square$  - 4;  $\circ$  - 5;  $\bullet$  - 6;  $\circ$  - 7;  $\circ$  - 8;  $\times$  - 9.

TABLE 1. Basic Characteristics of the Experimental Data Used for Generalization ( $p_*/p_{Cr} = 0.003$ )

No.	Working substance	Pressure, kg/cm <sup>2</sup>	Ref. pressure, $p_*$ , kg/cm <sup>2</sup>	Ref. relative heat transfer $\alpha_{p*}$	Critical pressure $p_{Cr}$ , kg/cm <sup>2</sup>	Literature
1	Mercury-magnesium amalgam	2-14	0.321	4.1	107	[2, 3, 6]
2	Mercury	0.068-3.1	0.321	1.1	107	[5]
3	Mercury-magnesium amalgam	0.113-1.08	0.321	2.5	107	[6]
4	Sodium	1.033	1.07	7	357	[4]
5	Water	1.033-200	0.677	3.1	225, 65	[10, 11]
6	»	1.033-74	0.677	3.1	225, 65	[11]
7	»	0.05-2.02	0.677	3.1	225, 65	[12]
8	»	0.09-1.082	0.677	3.1	225, 65	[13]
9	»	1.033-71.4	0.677	3.1	225, 65	[14]

Remark. In dependences (1) and (4), the exponent  $n$  was assumed to be equal to 0.7 for the thermal load  $q$  for all liquids.

The value of the scale characteristic  $\alpha_{p*}^*$  of heat transfer is determined from the experimental curve  $\alpha = f(q)$  for the reference pressure  $p_*$ .

In contrast to the generalization made in [9], the value  $p_*/p_{Cr} = 0.003$  was used for the pressure scale. This was connected with the fact that the experimental data on the boiling of liquid metals were obtained mainly for low saturation pressures.

It is seen from the graph that the experimental data for water and metallic liquids agree throughout the entire range of relative pressures  $p/p_{Cr}$ . In the range of relative pressures covered in experiments on the boiling of liquid metals ( $0.0001 \leq p/p_{Cr} \leq 0.1$ ), the experimental points were close to a straight line (in a logarithmic plot) whose slope was 0.15. The scatter of experimental points did not exceed  $\pm 30\%$ . Thus, it can be assumed that the exponent in the dependent of the heat transfer on pressure is close to 0.15 for the above range of relative pressures  $p/p_{Cr}$ . In this case, Eq. (2) becomes

$$\frac{\alpha_p^*}{\alpha_{p*}^*} = A_1 (p/p_{Cr})^{0.15}. \tag{3}$$

Here, the coefficient  $A_1$  takes into account the scale of the graph (see figure):

$$A_1 = (p_*/p_{Cr})^{-0.15} = 2.39.$$

Thus, in the above range of relative pressures, the following dependence can be used for the heat transfer coefficient:

$$\alpha = A_1 \alpha_{p_*}^* q^n (p/p_{Cr})^{0.15}, \quad (4)$$

where the reference value of the relative heat transfer  $\alpha_{p_*}^*$  generally constitutes a function of a complex of the liquid's physical properties. As a rule, the value of  $\alpha_{p_*}^*$  corresponding to the pressure  $p_*$ , which is constant for a certain given liquid (for the assigned  $p^*/p_{Cr} = \text{idem}$  value) is determined experimentally. The table provides the values of  $\alpha_{p_*}^*$  and  $p_{Cr}$  for some of the liquids considered in the present article. If the  $\alpha_{p_*}^*$  value is not known, but the experimental value of the relative heat transfer coefficient  $\alpha_{p_0}^*$  is known for any pressure  $p_0$  (in the range  $0.001 \leq p_0/p_{Cr} \leq 0.1$  of relative pressures), the reference value  $\alpha_{p_*}^*$  can be determined by using the expression

$$\alpha_{p_*}^* = \frac{\alpha_{p_0}^*}{A_1} (p/p_{Cr})^{-0.15}. \quad (5)$$

A comparison of the data on heat transfer in boiling apparently indicates a certain generality of the mechanism of nucleate boiling of metallic and nonmetallic liquids if the heating surface is wetted by the liquid. This fact provides a regular basis for generalizing the experimental data on the boiling of liquid metals in the systems proposed for the generalization of data on heat transfer in ordinary liquids, which agrees with the statement of the problem given in [1].

#### LITERATURE CITED

1. S. S. Kutateladze et al., Liquid-Metal Coolants. Supplement No. 2 to Atomnaya énergiya for 1958 [in Russian] (Atomizdat, Moscow, 1958).
2. M. I. Korneev, Teploénergetika, No. 4, 44 (1955).
3. M. I. Korneev, Teploénergetika, No. 7, 25 (1955).
4. R. Lyon, A. Foust, and D. Katz, Chem. Engng. Progr. Sympos. Series, No. 17, 51 (1955).
5. C. Bonilla et al., Ibid., 53, 51 (1957).
6. Collection: Liquid Metals. Edited by V. M. Borishanskii et al. [in Russian] (Gosatomizdat, Moscow, 1963).
7. P. A. Andreev, A. A. Kanaev, and E. D. Fedorovich, Liquid-Metal Coolants for Nuclear Reactors [in Russian] (Sudpromgiz, Leningrad, 1959).
8. I. I. Novikov, Collection: Problems of the Heat Transfer and Hydraulics of Two-Phase Media [in Russian] (Gosénergoizdat, Moscow, 1961), p. 7.
9. V. M. Borishanskii, Collection: Problems of the Heat Transfer and Hydraulics of Two-Phase Media [in Russian] (Gosénergoizdat, Moscow, 1961), p. 75.
10. V. M. Borishanskii, G. I. Bobrovich, and F. P. Minchenko, Collection: Problems of the Heat Transfer and Hydraulics of Two-Phase Media [in Russian] (Gosénergoizdat, Moscow, 1961), p. 75.
11. V. M. Borishanskii, Éngomashinostroenie, No. 7, 5 (1958); ZhTF, No. 2 (1956); Kotloturbostroenie, No. 4, 22 (1952).
12. F. P. Minchenko and É. V. Firsova, Collection: Problems of the Heat Transfer and Hydraulics of Two-Phase Media [in Russian] (Gosénergoizdat, Moscow, 1961), p. 117.
13. W. McAdams, Heat Transmission (McGraw-Hill Book Co., Inc., New York, 1954).
14. M. Cichelley and C. Bonilla, Trans. Am. Inst. Chem. Engng., No. 6, 41, 755 (1945).

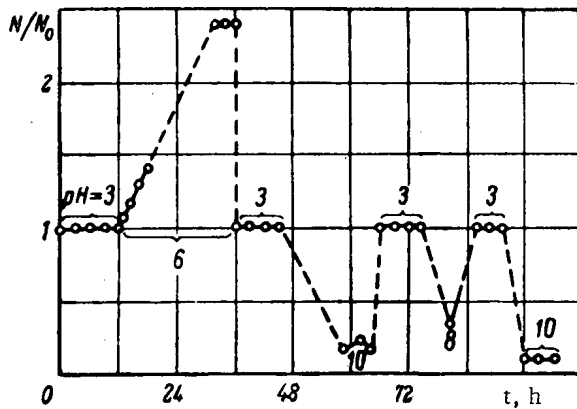


Fig. 1. Variation in time of the surface radioactivity of solutions of  $\text{Ce}^{144}$  salts with different acidities.

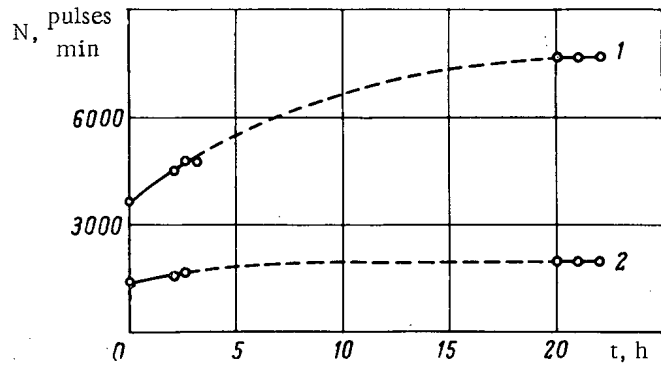


Fig. 2. Increase in the surface radioactivity of  $\text{Ce}^{144}$  solutions for  $\text{pH} = 6$  in time. 1) Without absorber; 2) with absorber.

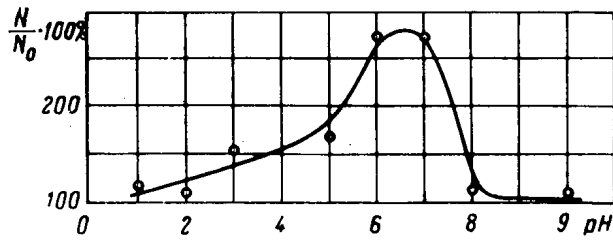


Fig. 3. Dependence of the surface  $\alpha$ -activity of an aqueous solution of  $\text{Po}^{210}$  nitrate on  $\text{pH}$ , reduced to the solution's activity for  $1.5 \text{ N HNO}_3$  ( $N/N_0$ ).

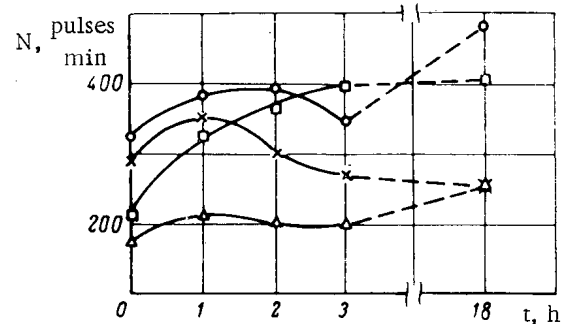


Fig. 4. Variation in time of the radioactivity measured at the surface of a  $\text{Pu}^{239}$  solution in  $1 \text{ N HNO}_3$ .

$= 6-7$ , the surface radioactivity increases by a factor of about 3 in comparison with a polonium solution in  $1.5 \text{ N HNO}_3$ . The rise of the surface activity of  $\text{Po}^{210}$  in time was also observed in an acid medium ( $1.5 \text{ N HNO}_3$ ), but to a much lesser extent.

It was calculated that, for a solution with  $\text{pH} = 6-7$ , the  $\text{Po}^{210}$  concentration in the surface layer exceeds the volume concentration by a factor of  $10^5-10^6$ . In this case, the monomolecular surface layer had not yet been saturated with  $\text{Po}^{210}$  atoms. With an increase in the concentration of polonium in the solution, its sorption increased. In this, the increase in the surface radioactivity was not proportional to the volume concentration of polonium. The increase in the measured radioactivity of  $\text{Po}^{210}$  solutions with  $\text{pH} = 6-7$  is due to the sorption of the products of polonium hydrolysis at the air-water interface, which continued until the solubility product was established in the solution's volume.

The intensity of polonium sorption sharply increased in the presence of certain surface-active substances. Thus, for instance, with the addition of heptadecyldimethylamine to the polonium solution, ( $\text{pH} = 9$ ), the activity measured at the surface increased by a factor of 30-50. The addition of an electrolyte (sodium sulfate) also resulted in an increase in the sorption of  $\text{Po}^{210}$ . However, certain organic substances (for instance, sulfonaphthenic acids) produced an opposite effect - the surface layer became impoverished in  $\text{Po}^{210}$  atoms.

$\text{Pu}^{239}$ . In measuring the  $\text{Pu}^{239}$  activity at the surface of aqueous solutions, considerable discrepancies between parallel samples were observed not only for alkaline and weakly acid solutions, but also for acid solutions ( $0.5$  and  $1.0 \text{ N HNO}_3$ ). The measured activity of these samples also varied in time. Even for a  $1 \text{ N}$  solution of  $\text{HNO}_3$ , these changes were most irregular (Fig. 4). The activity sometimes varied as the sample was poured. These phenomena could be explained by the sorption of  $\text{Pu}^{239}$  on minute amounts of extraneous impurities on the solution's surface.

INVESTIGATION OF SORPTION OF RADIOIODINE ON ACTIVATED CHARCOAL,  
AND STUDY OF FORMS OF GASEOUS IODINE IN AIR

(UDC 621.039.72)

T. I. Smolkina and A. A. Chubakov

Translated from *Atomnaya Énergiya*, Vol. 18, No. 3,  
pp. 298-299, March, 1965

Original article submitted August 14, 1963

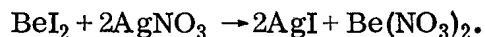
Radioactive iodine is capable of existing in air in two phases: an aerosol phase and a vapor phase. Useful tools for determining the concentration of radioiodine in air and for removing it from the air are, therefore, not only aerosol particulate filters but also filters or sorbing agents capable of trapping gaseous iodine [1-4]. The authors made a study of the sorption of iodine vapor emerging in a stream of air from a spent fuel element heated to 900-1000°C on activated BAU grade charcoal at an air flow speed of 20 cm/sec. The fuel elements were fabricated of beryllium oxide and enriched uranium dioxide with no fragment-proof cladding. The radioiodine concentration was  $10^{-9}$  to  $10^{-11}$  Ci/liter. The iodine vapor distribution curves over the length of the BAU charcoal bed are plotted in Fig. 1. The radioiodine concentration in air was found to be reduced by a factor of about 500 by using a BAU charcoal bed 10 cm long.

On the basis of the data plotted in Fig. 1, a proposition was advanced, and confirmed experimentally, to the effect that iodine is found in two or more forms in the vapor phase: in the form of elemental iodine and in the form of iodine compounds. When iodine sorption on potash and on FPP-15 filters treated with a 10% solution of caustic potash in alcohol ("alkali" filters) was investigated, the same pattern came into focus: the principal iodine activity was detected on the first filter; the activity on the subsequent filters differed imperceptibly. This is accounted for by the fact that potash lye traps elemental iodine in the reaction



but fails to trap compounds formed by iodine with uranium and beryllium. The efficiency of the alkali filters depended on the temperature of the fuel element: it was slight (7-10%) at low temperatures, and rose to a figure of 90% at temperatures elevated to 800-900°C (Fig. 2). The reason for this is that iodine passes into the air at low temperatures primarily in the form of compounds impervious to trapping by lye. As the temperature of the fuel element is increased, the iodine compounds begin to decompose and give off elemental iodine, whereupon the efficiency of the filters improves.

When the alkali filters were replaced by FPA or FPP filters treated with  $AgNO_3$  solution, a "burst" of activity was observed on the latter filters, as a consequence of the fact that the iodides become trapped by the silver:



In studying the filters which are efficient trappers of iodides,<sup>1</sup> we successfully established that iodine compounds are present in three forms in the vapor phase: elemental iodine, iodides, iodates, and possibly even a mixture of several compounds. It was found that as the temperature of the furnace in which the fuel elements are heated was increased, the percentage of iodides in the iodine vapor mixture gradually diminished, the percentage of the third form of iodine vapor showed a sudden steep decline at first, but leveled off later at a constant figure of  $\approx 0.5-1\%$  (Fig. 3). The largest amount of iodides in the iodine vapor mixture was observed experimentally at temperatures 100-200°C (75%), while the content of the third form was 25% in this instance. In order to obtain confirmation of the presence of the

<sup>1</sup>These filters were made available to us through the kindness of M. S. Misin and E. T. Surovaya.



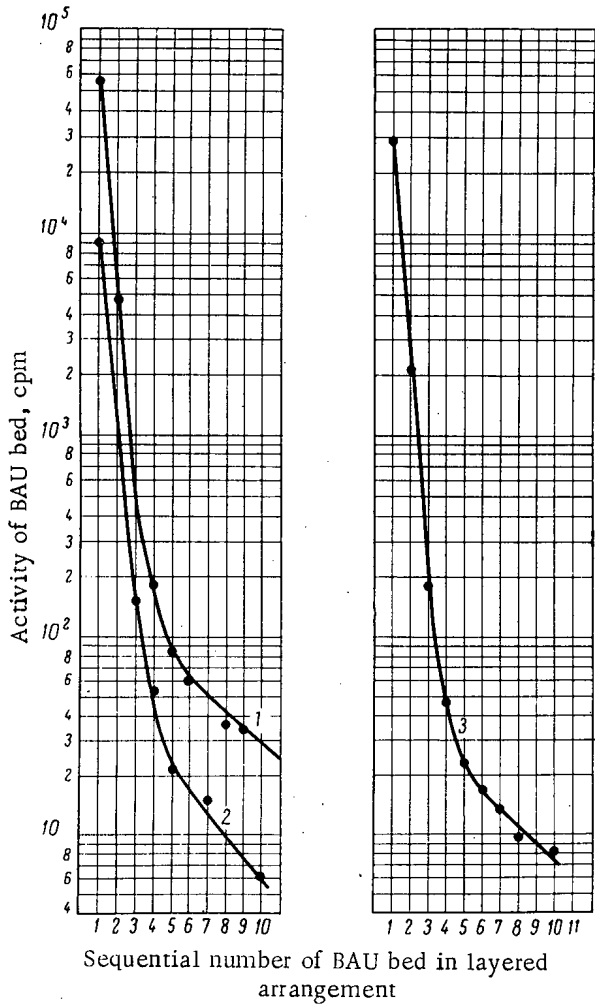


Fig. 1. Distribution curves of iodine vapor activity over BAU activated charcoal beds; length of each bed is 1.1 cm. 1) Experiment No. 19; 2) experiment No. 14; 3) experiment No. 21.

third form of iodine vapor in the gaseous phase, air samples were taken on bubbler devices containing carbon tetrachloride and water with carriers in the form of  $I_2$ , KI, and  $NaIO_3$ , with the temperature of the furnace containing the fuel elements varied in 200°C steps. FPP-15 filters were placed ahead of the bubblers to trap out aerosols.

The activity of the iodine isolated with the carrier  $NaIO_3$  [6] at first declined precipitously as the fuel elements were heated to higher temperatures, and then leveled off at an almost constant figure. Graphs of the percentage composition of iodine isolated with  $NaIO_3$  carrier as a function of the fuel-element temperature showed the same shape as the curve in Fig. 3.<sup>1</sup> This confirms the assertion that the iodine vapor exists in three forms under the stated experimental conditions: in the form of elemental iodine, in the form of iodides (beryllium and uranium iodides, to be sure), and in the form of iodates of the same elements; and possibly also in the form of a mixture of several iodine compounds in which iodine exhibits positive valence.

As  $I^{131}$  sublimates from the irradiated tellurium metal in the vapor phase, no less than two forms of iodine were recorded, the reader will also note. In this case, the forms could be elemental iodine, iodine compounds formed with tellurium  $TeI_2$ ,  $TeI_4$  (melting point 259°C), and possibly even tellurium iodates [7, 8].

<sup>1</sup>The content of the third form in the iodine vapor mixture was assigned the value unity over the 20-200°C temperature range.

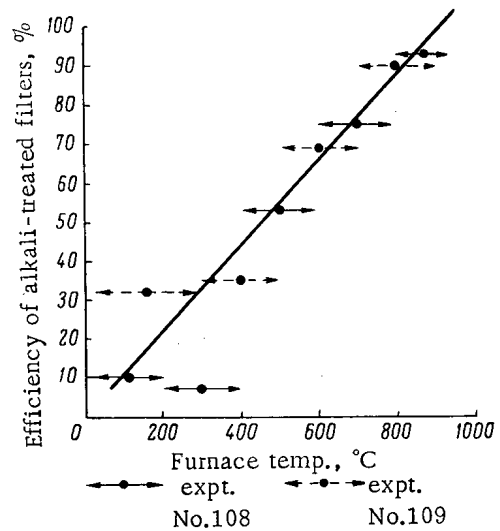


Fig. 2. Graph of trapping efficiency of "alkali" filters, with respect to iodine vapor, as a function of temperature to which fuel elements were heated.

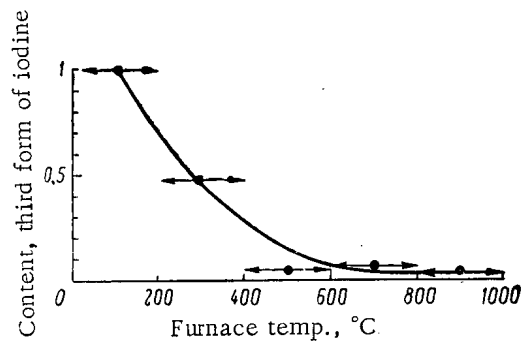


Fig. 3. Graph of content of third form of iodine vapor as a function of temperature to which fuel elements were heated.

LITERATURE CITED

1. Handbook of Radiochemical and Dosimetric Procedures. Edited by N. G. Gusev et al. [in Russian] (Medical Press, Moscow, 1959).
2. C. Sill and T. Flygare, *Health Physics*, 2, 261 (1960).
3. T. Smith and R. Crawley, *Nucl. Engng.*, 6, 428 (1961).
4. A. Blasewitz and W. Schmidt, Conference on the Peaceful Uses of Atomic Energy, Geneva, 1958. P/397.
5. V. I. Ksenzenko and A. S. Stasinevich, Bromine and Iodine Technology [in Russian] (State Chemical Press, Moscow, 1960).
6. Helge Bergh. Conference on the Peaceful Uses of Atomic Energy, Geneva, 1958. P/586; R. Constant, *Ibid.*, P/1675.
7. D. R. Stell, Tables of Vapor Pressures of Individual Substances. Edited by Prof. S. V. Gorbachev and V. V. Mikhailov [Russian translation] (IL, Moscow, 1949).
8. Handbook of Chemistry and Physics. Edited by D. Charles and M. Hodgman. 33rd Edition (Cleveland, 1951-1952).

RADIOACTIVE FALLOUT ON THE FAR-EASTERN SHORELINE  
OF THE PACIFIC OCEAN IN 1962-1963

(UDC 551.577.7)

E. I. Markichev, A. D. Shramchenko, A. S. Lapardina,  
V. V. Peretti, E. I. Vasil'kov, and V. V. Skornyakov

Translated from *Atomnaya Énergiya*, Vol. 18, No. 3,  
pp. 300-301, March, 1965

Original article submitted March 19, 1964

Observations of radioactive fallout were carried out in 1962-1963 at four points on the far-eastern shoreline. Samples were taken daily of dry fallout of radioactive products at each of them and the  $\beta$ -activity was measured; atmospheric rainfall samples were collected, their specific  $\beta$ -activity and the total activity were measured for a month; determinations were made of the radioactive contamination of the surface layer of soil.

The methods used for collection, processing, and determination of the  $\beta$ -activity of the dry fallout and of the atmospheric rainfall are described in [1]. The atmospheric rainfall samples for one month were collected by means of a precipitation gage with a collecting surface of 200 cm<sup>2</sup>. Determinations were made daily of the radioactive contamination of the soil layer by means of an appropriately calibrated field type  $\gamma$ -radiation meter.

The results obtained at all the points were averaged in order to obtain the characteristics of the radioactive fallout products on the shoreline as a whole. The monthly fallout, calculated by the measurement results from fission products on the earth's surface are shown in Fig. 1 (the total of the dry fallout and the fallout from atmospheric rainfall for each month). It can be seen from these data that the fallout of radioactive products on the earth's surface

was nonuniform in time. The increase of fallout intensity in the summer period (from June to September) has a seasonal nature and is due to the fact that in the Far East the greater portion of the annual rainfall occurs during this period [2]. The significant increase of the summer maximum of fallout in 1962 above the maximum for the same period of 1963, for almost identical quantities of rainfall (513.6 and 488.0 mm, respectively), was caused by the series of nuclear explosions carried out at Christmas Island and Johnston Island in the Pacific Ocean from April 25 to November 4, 1962.

The average specific activity of rainwater from June to September was 2 nCi/liter in 1962 and 1 nCi/liter in 1963. The reduction in the specific activity is due to dilution of the fission products in the stratosphere and also to the radioactive decay and fallout of fission products

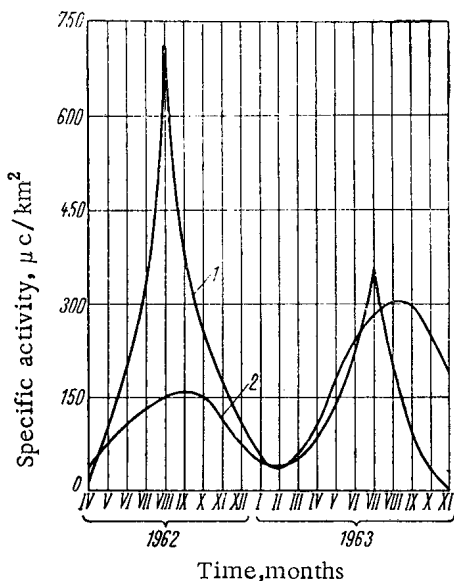


Fig. 1. Monthly fallout of fission products (1) and radioactive contamination on a surface layer of soil (2) on the far-eastern coastline of the Pacific Ocean in 1962-1963.

TABLE 1. Energy Composition of the  $\beta$ -Radiation from Radioactive Fallout on Far-Eastern Shoreline of Pacific Ocean, %

Period of sample collection	Maximum energy of $\beta$ -radiation, MeV			
	$\leq 0.6$	1.5	2.3	$\geq 3.0$
October, 1962	65.0	25.0	10.0	—
August, 1963	55.0	—	40.0	5.0

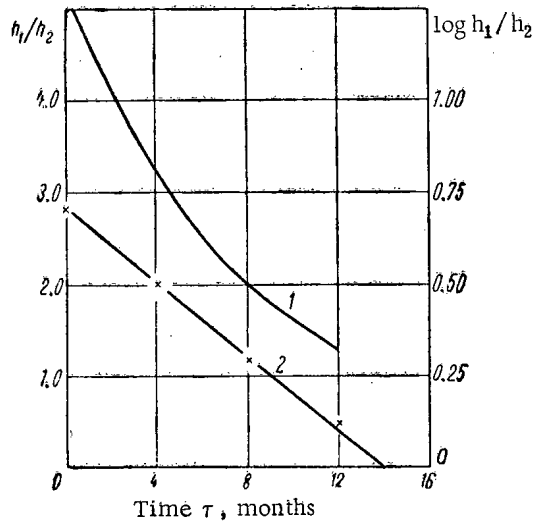


Fig. 2. Variation with time of the ratio of intensities  $h$  of fallout at two sampling points ( $h_1$  and  $h_2$ ) after cessation of the arrival of fission products in the stratosphere: 1)  $h_1/h_2 = \varphi(\tau)$ ; 2)  $\log(h_1/h_2) = f(\tau)$ .

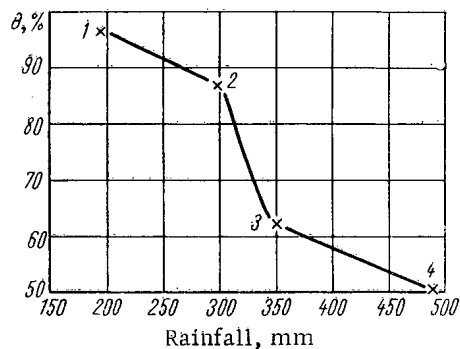


Fig. 3. Relationship between the degree of retention  $\theta$  of fission products in a surface layer of soil and their growth and quantity of atmospheric rainfall. 1) October 1962; 2) November 1962; 3) July 1963; 4) August 1963.

on the earth's surface during the year. The maximum specific activity of rainwater (64 nCi/liter) was noted on August 23, 1962.

Over the period of the nuclear tests, the excess of fallout intensity in the southern regions of the coastline compared with northern regions was considerable but subsequently decreased with time (Fig. 2). It can be seen from Fig. 2 that the fission products in the stratosphere in the meridional direction are propagated according to an exponential law, which confirms the diffusion nature of this process [1]. Extrapolation of the function  $\log(h_1/h_2) = f(\tau)$  to zero value indicates that for a given mutual geographical position of the sample collection points and regions of nuclear tests, balancing of the activity concentration in the stratosphere begins 14 months after cessation of the accumulation of fission products in the stratosphere.

The radioactive contamination of a surface layer of soil (see Fig. 1) varied analogously with the variation in intensity of fission product fallout. However, the level of soil contamination in the period of the summer maximum in 1963 was higher than in 1962 as a result of the inverse ratio of the fallout intensity. This was due to a reduction in the contribution of short-lived isotopes in the total activity of the fission products during the year and a correspondingly higher accumulation of radioactive products in the soil in 1963. The experimentally determined average half-lives of the radioactive fallout in the summers of 1962 and 1963 amounted to 13 and 147 days, respectively.

The calculated values of the cumulative fission product activity in the surface of soil, taking account of their growth and decay, are greater than the measured values of its contamination, which is explained by the partial penetration of the fission products into the depths of the soil. The degree of retention of fission products in the surface layer of soil amounts to 50-95% and depends on the quantity of atmospheric rainfall and the growth of the fission products (Fig. 3). Deviation from a linear relationship to the side of sharper reduction of the degree of retention in July-August 1963 compared with the autumn period of 1962, is associated, obviously, with the reduction in the contribution of the well-absorbed  $\text{Sr}^{89}$ ,  $\text{Zr}^{95}$ - $\text{Nb}^{95}$ ,  $\text{Ba}^{140}$ , and  $\text{Ce}^{141}$  [1] to the total activity of the fission products as a consequence of the considerable growth of these isotopes.

In certain samples of dry fallout and rainwater, the energy of the  $\beta$ -radiation was measured by the method of  $\beta$ -particle absorption curves in aluminum. The average results of the measurements are given in the table.

The absence of  $\beta$ -radiation with a maximum energy of 1.5 MeV in August 1963 is due to the disappearance of the isotope  $\text{La}^{140}$  from the fission product mixture and the significant decay of the isotopes  $\text{Sr}^{89}$  and  $\text{Y}^{91}$  after a ten-month period. The hard component ( $E_{\beta \text{ max}} \geq 3.0$  MeV) belongs to the isotopes  $\text{Pr}^{144}$  and  $\text{Rh}^{106}$ , the contribution of which in the  $\beta$ -radiation from the fission product mixture of the specified growth is close to maximum [3].

The calculated values of the average maximum  $\beta$ -emission energy of the fallout in October 1962 and August 1963 are respectively 1.0 and 1.4 MeV, which is in agreement with data from the literature [4].

LITERATURE CITED

1. Collection: Radioactive Contamination of an External Medium. Edited by V. P. Shvedov and S. I. Shirokov [in Russian] (Gosatomizdat, Moscow, 1962).
2. L. P. Sharapova, Scientific Annals of the Far Eastern University [in Russian], No. 6, 79 (1963).
3. A. G. Bykov, P. V. Zimakov, and V. V. Kulichenko, Atomnaya énergiya, 10, 362 (1961).
4. Atomnaya tekhnika za rubezhom, No. 11, 31 (1963).

PHYSICAL STARTUP OF THE VK-50 BOILING WATER REACTOR  
AT THE UL'YANOVSK NUCLEAR POWER STATION

A. Kubrochenko and V. Parfir'ev

Translated from Atomnaya Énergiya, Vol. 18, No. 3,  
p. 302, March, 1965

The physical startup of the nuclear reactor at the Ul'yanovsk nuclear power station was completed in December 1964 at the Atomic Reactor Research Institute (Melekes, Ul'yanovsk district) of the State Committee on Uses of Atomic Energy of the USSR. The results of studies of the physical characteristics of the reactor core confirmed the correctness of the physical calculations.

The Ul'yanovsk power station is an experimental atomic power facility with a water-boiling thermal reactor of 70 MW electric power rating and 250 MW thermal power rating.

The heat from the reactor core is carried off by natural coolant circulation. The water-steam mixture formed in the core is separated at the exit from the core, and the saturated steam is directed to a turbine after being dried first in steam separators.

The coolant circulation through the reactor is intensified and the steam capacity of the reactor facility is enhanced by the use of three circulation loops designed to generate secondary steam in steam generator units. The reactor is built to operate in the pressure range from 35 to 100 atm.

The reactor core stands 2 meters high and 2.7 meters in diameter, and is housed in a pressure vessel of special heat-resistant steel plated with stainless steel. The pressure vessel is a cylindrical container measuring 3.8 meters in outer diameter and standing 11 meters high.

The core loading amounts to 26 tons of uranium in 1.5% enrichment. Rod-type fuel elements 10.2 meters in diameter with uranium dioxide meat and zirconium alloy cladding are used in 187 assemblies.

Investigations within the framework of this program are currently under way to study the behavior of the experimental facility.

NUCLEAR INSTRUMENTATION DISCUSSED AT COMECON

N. A. Shekhovtsov

Translated from Atomnaya Énergiya, Vol. 18, No. 3,  
pp. 302-303, March, 1965

The need to develop a large variety of scientific instruments, equipment, and facilities, and to produce them on industrial scales, is dictated by the broad and intensive scope of theoretical and experimental nuclear physics research and the vigorous advances achieved in nucleonics.

Equipment intended for recording and measuring flux and for spectrometry of nuclear radiation energies has already passed beyond the physics laboratory stage and is now being used on a broad scale in the most contrasting fields of science and industry. Nuclear radiation instruments feature enormously sensitive response; they can be employed to detect microscopic quantities of radioactive isotopes; they are capable of observing phenomena associated with nuclear transformations, of studying interactions of elementary particles, of performing process monitoring functions, protection and control functions in nuclear power installations, and ultimate activation analysis of matter; they are capable of fulfilling the functions of highly sensitive relays, sensors for radioactive radiations, etc.

The capabilities inherent in nuclear instrumentation are nowhere near being exhausted. Their range of application is being steadily broadened. It suffices to point out that nucleonic instruments are valuable not only for the functions for which they were directly designed, but are now successfully branching out into chemistry, physics, biology, medicine, geological prospecting, in outer-space research, and in any number of fields in the national economy, primarily in the area of process analysis, monitoring and control, and in the elaboration of new substances and new materials. Even now, it is safe to state that it is difficult to find any area into which radiometric, dosimetric, electron physics, or radioisotope instruments have not penetrated.

The development and production of scientific and technical instruments in the nuclear physics line is at present a definitively established branch of nuclear instrument design.

A Permanent Commission on the Peaceful Uses of Atomic Energy has been set up under the auspices of the Council of Mutual Economic Aid (COMECON). The working organs of the Commission are teams of specialists from the member nations of COMECON. Team No. 1 has the task of developing and preparing recommendations on scientific and technical cooperation in nuclear instrument design and production.

The team is directed in its activities by the decisions of the Permanent Commission and by the decisions of the COMECON executive committee on the development of economic and scientific-technical collaboration between member nations of COMECON, on the acceleration of scientific and technical progress based on joint scientific research and design projects, on improving coordination in scientific research plans, on the development and promotion of standardization and specialization in production, on the scheduling of scientific-technical conferences and congresses of specialists, and on the exchange of results of scientific research and development projects between member nations of COMECON.

Peculiar difficulties and complications related to the stormy and impetuous development of this branch of industry, to the absence of set standards and absence of uniformity in approach to problems, to the striking contrasts in the levels achieved, to the different standards arrived at in the several member nations of COMECON, and other such factors, stand in the way of solving the involved problems in nuclear instrument design and production on an international scope. Working team No. 1 has already taken some steps in the development of scientific-technical collaboration between the socialist countries: a catalog classifying nuclear instrumentation has been compiled and published. Proposals on unified design and dimensioning of stands, subassembly housing, and electron physics components have been brought into some order of agreement on the basis of a 20-mm module arrangement. In using the recommendations put forth, designers in the German Democratic Republic, the Czechoslovak Socialist Republic, and the USSR have come up with blueprints and first-stage plans for the design of a unified modular system of nucleonic instruments. Matched proposals on unification of input and output parameters of functional circuits and components in electron physics instruments have been agreed upon, including voltage ratings for power supplies and sensor units.

Recommendations on the specialization of 25 instruments and their major components were adopted in 1963. For example, Hungary will be specializing in the production of multichannel time analyzers and pulse height analyzers, and in recorders to serve them in operation, as well as medical circulographic instruments, while the Czechoslovak Socialist Republic and the Hungarian Peoples Republic will share the load in specializing in scintillator production. The development and production of electrometric amplifiers with electrodynamic capacitors is the task of the German Democratic Republic and the Rumanian Peoples Republic, electromechanical counters will be produced by the Peoples Republic of Bulgaria and by the Czechoslovak Socialist Republic, and gas-filled counters will be produced by the German Democratic Republic and the Polish Peoples Republic. The German Democratic Republic and the Czechoslovak Socialist Republic are specializing in instruments designed to determine the concentration of radioactive aerosols in air, and the Czechoslovak Socialist Republic is specializing in instruments for determining radioactive substances in liquids and for measuring soft  $\beta$ -emissions (tritium,  $C^{14}$ ), and in betatron production. Instruments for estimating the levels of radioactive contaminants on the surface of work areas, on personnel protective clothing, on hands and bodies of workers in exposure areas, will be the specialty of the Hungarian Peoples Republic and the Polish Peoples Republic, and the Polish Peoples Republic will specialize in high-precision time measurements.

Duties relating to the coordination of scientific research and experimental design work on itemization of available nuclear physics instruments were distributed among the various member nations of COMECON to facilitate a preliminary working out of proposals and recommendations on specialization of instrument production, and also in order to assure a high scientific and technical level in new research and development work. For example, the German Democratic Republic will shoulder the responsibility for dosimeters, Czechoslovakia will be responsible for radiometers and spectrometers, Poland for radioisotope instrumentation, Hungary for electronic components and devices for nuclear physics work, and for medical instruments employed in the measurement of ionizing radiations.

A unified procedure for testing radioisotope relay devices has been developed, and a program has been outlined for work in the standardization, modularization, and unification of instrument designs in this line. The possibility of using these advances in a universal automatic monitoring and control system is under study.

At the eighth session of working team No. 1, held in Sofia in October 1964, the specialists from member nations of COMECON agreed upon a list of standardized Geiger-Müller counters fabricated in East Germany and Poland. Basic operating parameters, testing methods, and conditions were also drawn up and agreed upon for multichannel pulse height analyzers. The Hungarian Peoples Republic proposed to the regular session of the team that it accept the responsibility of developing similar engineering data and specifications for multichannel time and multidimensional analyzers.

A summary of scientific research on standardization and development of interchangeable modules for scintillation sensors, including phototube multipliers and scintillators, and semiconductor detectors, was drawn up. This led to the adoption of recommendations on a system of dimensions for phototube multipliers (diameters of effective photocathode area, tube envelopes, sockets and bases, screens), scintillation crystals, and other components. Terminology and standards, definitions and nomenclature, measuring conditions and methods for testing the operational parameters of photomultipliers, scintillators, and scintillation counters were also agreed upon. This work provided a sound basis for specialization in the production of these instruments in the several member nations and for promoting a more widespread use of these instruments throughout the socialist countries.

In addition, the eighth session of team No. 1 agreed upon a sequential order in the development of a prospective plan of scientific and technical collaboration, adopted a plan on standardization, and also a plan for scheduling scientific and technical conferences and meetings of specialists on nuclear instrument design and standardization.

The first steps taken in the direction of scientific and technical collaboration by member nations of COMECON in the field of nuclear instrument design have now laid down a firm basis for further expansion of collaboration in unification, standardization, and international specialization and cooperation in this area of production.

Specialists laid repeated stress on what they consider the prime economical factor in the development and probing of these outlooks and problems, not only on the rational distribution of production and labor tasks between the several nations, but on the use of the most advanced nucleonic instrumentation in scientific research, in the analysis of the composition of matter, in automation, in process monitoring and control, and in similar vital functions.

The widespread use of nuclear instrumentation raises the level of scientific and technical progress in each nation and thereby opens up new opportunities for increasing labor productivity.



## SYMPOSIUM ON THE RADIATION CHEMISTRY OF POLYMERS

M. Kaplunov

Translated from *Atomnaya Énergiya*, Vol. 18, No. 3,  
pp. 304-305, March, 1965

An All-Union Symposium on Polymer Radiation Chemistry at which papers discussing the last 3-4 years' work in this area were widely discussed was held in Moscow in November 1964 under the joint auspices of the Academy of Sciences of the USSR and other organizations.

Participating in the work of the symposium were representatives of 93 scientific and industrial institutions throughout the country; over 90 papers and communications presented by 35 research organizations were read and discussed. The transactions of the symposium took place in two sessions.

The first session provided opportunity for discussion of work done in the field of radiation-induced polymerization, studies of polymerization kinetics and mechanisms in the solid phase, radiation-induced polymerization of fluoro-olefins, new information on the kinetics and underlying mechanisms in copolymerization processes, advances in the radiation synthesis of grafted polymers by vapor-phase techniques, and other topics.

The participants of the symposium displayed intense interest in those reports dealing with studies of the solid-phase radiation polymerization of certain monomers (8 papers discussed this topic), in reports presented by the Institute of Chemical Physics of the Academy of Sciences of the USSR, the L. Ya. Karpov Physical Chemistry Institute, the Leningrad State University, the Plastics Scientific Research Institute, and other organizations.

The special features of the kinetics of radiation solid-phase polymerization and post-polymerization were discussed; it was shown that the polymeric yield increases in proportion to the exposure dosage up to high degrees of transformation; a mechanism was proposed to take into account special aspects of solid-phase polymerization of hexamethyl cyclotrisiloxane and trioxane (V. I. Gol'danskii and N. S. Yenikolopyan, "Some aspects of solid-phase radiation-induced polymerization"; I. M. Barkalov et al., "Radiation-induced polymerization of hexamethyl cyclotrisiloxane in the solid phase"; G. M. Timofeeva et al., "Kinetics of trioxane post-polymerization", etc.).

M. A. Bruk, A. D. Abkhin, and P. M. Khomikovskii studied the process of solid-phase polymerization of tetrafluoroethylene and copolymerization of tetrafluoroethylene and trifluorochloroethylene, and suggested an ion mechanism to account for the reactions investigated.

Yu. G. Chikishev et al. demonstrated that the process of solid-phase radiation-initiated polymerization of diphenylvinylphosphine oxide is characterized by certain new regularities which have not been observed earlier in a single one of the cases of polymerization of solid monomers which have undergone study hitherto. The principal peculiarity of this process is singled out by the investigating author to be the formation of solid solutions of polymer and monomer which do not break down up to the point where the monomer transformation has gone to completion.

The problem of how to synthesize higher carboxylic acids from ethylene and carbonic acid by catalytic reactions aided by radiation was the subject of a paper by Yu. A. Kolbanovskii, L. S. Polak, et al. These authors developed suitable conditions for carrying out the synthesis reactions and obtaining higher order carboxylic acids which are uniform in composition. The resulting carboxylic acids were demonstrated to possess powerful adhesive properties with respect to a variety of materials, and to be capable of forming stable emulsions.

Radiation-initiated three-dimensional polymerization of oligomers obtained by condensation of methacrylic acid, butanediol, and phthalic acid was discussed in a report presented by V. I. Gol'danskii et al. Here it was shown that, in contrast to chemical initiation, 100% conversion to polymer may be achieved even at room temperature in radiation initiation. The resulting polymers evince higher thermostability than their chemically initiated counterparts.

One of the sessions in this group was devoted to a discussion of radiation-initiated polymerization of fluorinated olefins (6 papers). In studies performed by E. V. Volkova and associates, findings showed fluorinated olefins to be

radiation-polymerized with a higher rate of formation of high-molecular weight products, and the proclivity to polymerize falls off as the quantity of fluorine atoms available to one monomer molecule is diminished.

X-ray studies of fluoropolymers revealed the crystal lattice and chain configuration (e.g., in Teflon) to be independent of the way in which the polymer was obtained. In polymers produced by radiation-initiated polymerization, greater order is observed in the chains within the crystals.

The papers presented by the Institute of Heteroorganic Compounds of the Academy of Sciences of the USSR, the Institute of Physical Chemistry of the Academy of Sciences of the USSR, the A. V. Topchiev Institute of Petrochemical Synthesis of the Academy of Sciences of the USSR, and the Artificial Fibers All-Union Research Institute were received with close attention; these papers (8 in all) were devoted to radiation synthesis of grafted polymers by the vapor-phase technique. As mentioned in the papers, the technique of vapor-phase radiation-initiated graft polymerization opens up broad opportunities for modifying the widest range of disparate materials, such as both polymeric (fibers, films, fabrics) and mineral (metal oxides, sorbents, etc.), conferring upon them the properties of ion-exchange materials, semiconducting, and other properties. Some of the resulting materials exhibit enhanced radiation-chemical stability, a feature of major importance in practical applications.

Kh. U. Usmanov and associates demonstrated, in their report, "Radiation technique of graft polymerization of vinyl monomers on cullol cellulose from the vapor phase," that grafting adds refractory qualities to cellulose and pulp materials, enhances thermostability and resistance to degradation, and improves the abilities of the materials to take acid dyes.

The effect of methanol vapors in vapor-phase graft polymerization on polyamide and polyester fibers was discussed in a paper submitted by E. F. Mertvyachenko, A. A. Kachan et al., in which the participation of methanol in the grafting process on polyamides was revealed and its role in polymerization processes involving those monomers which fail to interact with fiber material under ordinary conditions was demonstrated; some points on the mechanism underlying the effect of methanol in the grafting copolymerization process were taken up.

The second session dealt with techniques for modifying and vulcanizing by radiation, investigations into structural changes in rubbers and plastics, the development of techniques for speeding radiation-induced crosslinking processes in polyolefins, and methods for vulcanizing rubbers based on various crude rubbers, the study of thermoradiative vulcanization of rubber stocks, radiation stability of polymers, of ion exchange materials, of fibers, and ways of enhancing radiation stability, etc.

A. D. Grishinoi, N. A. Bakh et al. have come up with some interesting data on structural changes in polyethylene and on its reactivity at ultrahigh dosages (>10 rad). The appearance of a highly developed system of polyconjugations in a polymer was shown to indicate semiconducting properties. The type of polyene structure found in a polymer was demonstrated by the authors to be a function of the exposure dose.

Papers by N. A. Slovokhotova, V. A. Kargin, and others dealt with research on structural changes in natural rubber, polyisoprene and divinyl synthetic rubbers, and in polyvinyl chloride, employing infrared spectroscopy techniques. Irradiation by fast electrons in vacuum was shown to be accompanied by cis-trans isomerization, in addition to the phenomenon of double bonds becoming used up in the formation of crosslinkages. Moreover, irradiation was shown to result in the appearance of cyclohexene structures in the rubbers. As the authors reported, the double bonds appearing in response to irradiation of polyvinyl chloride function as centers for the subsequent dehydrochlorination of the polymer.

The effect of technological additives and sensitizers for the radiation-initiated crosslinking process on the properties of several polymers was discussed in four papers submitted by V. L. Karpov, M. N. Shteding, E. E. Finkel', S. S. Leshchenko, and associates. These authors showed that the introduction of such additives substantially modifies the effective irradiation dose level, as well as certain characteristics of the irradiated polymeric material. Some of the polyfunctional monomers investigated are effective sensitizers for the radiative crosslinking of polyolefins. The sensitizing effect of  $N_2O$  is ascribed by the authors to the inhibition of polymer degradation.

Six papers took up the topic of research on radiation-promoted vulcanization of synthetic rubbers and rubber mixtures.

A. S. Kuz'minskii et al. presented some research findings on radiative vulcanization of rubbers with an ethylene-propylene base; they established the superiority of radiation-produced vulcanizates over peroxide vulcanizates; this

advantage is expressed in the higher resistance of the radiation-cured rubbers to heat aging both in air and in vacuum.

I. Ya. Poddubnyi and S. A. Aver'yanov turned their attention to the fact that radiation curing is one of the most promising trends in techniques for modifying the properties of silicone rubbers. They took note of the effect of low-molecular-weight additives on the enhanced thermostability of radiation-cured silicone rubbers in air up to 420°C. The possible production of thermostable self-sealing rubbers exhibiting improved physical and mechanical properties was firmly established.

G. A. Blokh and associates probed into techniques for producing leather-like rubbers through continuous radiation vulcanization.

Data on a process for thermoradiative vulcanization of rubbers by accelerated electrons were communicated by M. Ya. Kaplunov, Z. N. Tarasova et al. The change in the effectiveness of the structuration and nonuniformity in the physicochemical and chemical properties of rubber in depth was shown to be due to the depth distribution of the dose field. The formation of a vulcanization network, in response to bombardment by accelerated electrons, went unaccompanied by degradation or oxidation of the rubber hydrocarbons.

The problem of radiation stability of rubbers, polyamides, ion exchange materials, and miscellaneous polymers was taken up in seven papers. A. S. Kuz'minskii and M. A. Zakirova developed new ways for enhancing the stability to radiation of rubbers functioning under static stress loads by studying the effect of the nature of the crude rubber, fillers, and curing agents on radiation aging of the rubbers in stress-free and stressed states.

In studying the stability to radiation of various plastics, N. S. Tikhomirova and associates demonstrated the possibility of improving upon the physicomachanical properties of some elastomer sealants; the polymer exhibiting the best stability to radiation is polyamide-IG irradiated in a vacuum.

A report by K. V. Chmutov et al. was devoted to an investigation of the radiation behavior and protection of ion exchange resins. A proposal aimed at successfully producing radiation-stable ion exchange resins was to introduce compounds containing highly conjugated condensed benzene rings (acenaphthalene, naphthalene, anthracene, etc.) into the structure of the resins. The concentration of the ring structures introduced must be taken into account, however, if precipitous deterioration of the kinetical properties of the ion exchange resin is to be avoided.

In the concluding plenary session of the symposium, delegates listened with close interest to a report by V. L. Tal'roze on the role of ion and ion-molecular reactions in condensed systems. The author surveyed the research undertaken at the Institute of Chemical Physics of the Academy of Sciences of the USSR, and expressed some views on the trends evident in research in the future.

Special emphasis was laid on the development of research geared to practical needs at this symposium.

The proceedings of the symposium will be published in 1965 by "Nauka" press.

PLASMA PHYSICS SEMINAR AT TRIESTE

Translated from Atomnaya Énergiya, Vol. 18, No. 3,  
pp. 305-306, March, 1965

The recently formed IAEA International Theoretical Physics Center at Trieste, set up for the purpose of contributing to further advances in theoretical physics in research and training of cadres, was host to the first seminar on plasma physics, held October 5-31, 1964, in Trieste.

Young scientists from a variety of countries came to the seminar to be brought up to data on the present status of plasma theory.

The seminar attracted 60 scientists, mostly from European countries (France, Italy, West Germany, Czechoslovakia). Also in attendance were representatives of India, Japan, and several other nations. Over a score of leading scientists in the field of plasma physics were invited to give lectures during the seminar.

An introductory course of lectures geared to the level of the less specialized part of the audience was given during the first two-week period. The second half of the seminar period was devoted to the present status of plasma physics in lectures geared to listeners of more advanced background. These lectures were valuable not only to the listening audience, but also to the lecturers themselves, in that the latter were afforded an opportunity to acquaint themselves with the results of recent plasma theory investigations carried out in a wide range of countries.

The Soviet delegation, which took part in the second half of the seminar and consisted of Corresponding Members of the Academy of Sciences of the USSR R. Z. Sagdeev and B. B. Kadomtsev, and Candidate in Phys. Math. Sci. M. S. Ioffe, delivered 12 lectures on plasma turbulence, turbulent heating of plasma, and magnetic mirror traps.

American, British, French, and West German scientists threw new light, in their lectures, on plasma confinement, plasma instabilities, astrophysical plasma research, turbulence, and other topics.

Useful discussions were held at the seminar on the most important and interesting topics in plasma theory, particularly on the theory of nonlinear processes. The seminar provided the opportunity for a detailed familiarization of those in attendance with the over-all status and latest findings in plasma theory.

## FRENCH RESEARCH REACTORS AND POWER REACTORS

V. A. Tsykanov

Translated from Atomnaya Énergiya, Vol. 18, No. 3,  
pp. 306-309, March, 1965

A Soviet delegation headed by N. A. Dollezhal', in acceptance of an invitation kindly tendered by the Commissariat de l'Énergie Atomique, visited several research reactors and critical assemblies at research centers in France during September 1964, at Saclay, Fontaine-aux-Roses, and Cadarache, and also visited the nuclear electric power stations, now operating or under construction, of the state firm Électricité de France.

Critical assemblies and low-power research reactors. There are five critical assemblies at Saclay, France's largest scientific research center. Of these, two are homogeneous reactors (Roserpine and Alecta) and were not included in the program. But a brochure on the Saclay facilities indicates that the first consists of a set of vessels of different diameter which can be surrounded by a water reflector in case of need; they serve the function of research on critical masses in homogeneous slurries containing uranium-235 or plutonium. Critical conditions in slurry vessels containing plutonium are studied in the second assembly.

The remaining three facilities, all housed in a common hall at the center, are heterogeneous critical assemblies. The heavy-water critical assembly Aquilon II burning uranium oxide rod elements is employed in experiments on the design of heavy-water power reactors, with particular emphasis on the EL-4 project.

Highly enriched uranium in U-Al alloy is used in Alice II, a light-water assembly. The fuel elements are plates of the alloy mentioned, with aluminum cladding. The plates are assembled in cartridges at arbitrary pitch, with plates of steel, zirconium, and other materials inserted when required, to simulate a variety of structural materials that might form part of the core in the reactors being studied. This makes for remarkable flexibility, allowing cores of greatly varied composition in their several constituents to be studied with ease. Close attention is being given to experiments on the use of boron control via dissolution of boron in water.

A third assembly, Rubéole, is used in the study of uranium-beryllium lattices. The outstanding feature of this assembly is the way criticality is achieved by removing a bundle of absorbing tubes encompassing each fuel element individually from the core. This device makes it possible to obtain the critical height of the assembly at any specified diameter.

These three critical assemblies are soon to be disassembled and taken off to Cadarache, the research center of the Commissariat, where basic research on reactor physics and technology is concentrated.

The pool-type reactor Minerva (at Fontaine-aux-Roses), 100 W maximum power rating, is used in the study of the physics of light-water and heavy-water reactors. The core is assembled from plate-type fuel elements with high-enrichment of uranium. Heavy-water lattices are studied in subcritical inserts placed in the core. Slugs appropriately dimensioned may be arranged around the core for the study of various reflectors. Since the size and geometry of the core depend on the nature of the experiment, control rods may be placed at any point, and their drives are mounted on movable arms to facilitate this purpose. The central channel of the assembly is used under a pile oscillator which may yield stepwise (off 0.5 sec, on 10 sec) and sinusoidal (period from 5 to 15 sec) fluctuations in reactivity. The pile oscillator has the function of measuring the neutron cross sections of structural materials, and of fresh and spent fuel.

The set of reactors Triton I and Triton II at Fontaine-aux-Roses is noteworthy with respect to the components. These reactors are in a common pool divided into three compartments: a center compartment and two end compartments. The central one, which is the largest, and one of the end compartments, are concrete-shielded and filled with water, while the other end compartment is left dry.

Triton I is suspended from a moving bridge and may be displaced from the end compartment of the pool to the center compartment, and vice versa. In the end compartment, the reactor is capable of operation at power levels to

TABLE 1. Basic Characteristics of French Research Reactors

Characteristics	Pegase	Siloe-15	Siloe-30 (project)	Osiris
Power, MW . . . . .	30	15	30	50
Amount of U <sup>235</sup> , kg . . . . .	8	5.5	7.1	10.4
Neutron flux, neutrons/(cm <sup>2</sup> · sec):				
thermal. . . . .	1.5 · 10 <sup>14</sup>	6.3 · 10 <sup>13</sup> (reflector)	—	—
flat (E ≥ 1 MeV). . . . .	—	1.2 · 10 <sup>14</sup>	—	2.5 · 10 <sup>14</sup>
Heat loading, kW/liter:				
average. . . . .	165	134	268	303
peak. . . . .	—	373	579	710
Core volume, liters . . . . .	182	112	112	165

TABLE 2. Basic Characteristics of French Power Reactors

Characteristics	EDF-1	EDF-2	EDF-3	EDF-4
Effective electric power, MW . . . . .	70	200	480	500
Thermal power, MW . . . . .	300	848	1560	1650
Number of turbogenerators, power in MW . . . . .	1 × 83	2 × 115	2 × 250	2 × 250
Number of steam generators. . . . .	1	4	4 pairs	4
Steam pressure, atm. . . . .	21.3	32.6	52.5	—
Number of gas blowers . . . . .	1	4	4	4
Fuel loading, tons . . . . .	140	240	400	400
Startup date . . . . .	Feb. 1964 (on full power)	1965	1966	1968

2 MW [maximum thermal flux  $2.5 \cdot 10^{13}$  neutrons/(cm<sup>2</sup> · sec)]. Its purpose is to irradiate materials, produce isotopes, and aid in the execution of various experiments, for which radial and tangential neutron beams are made available. Reactor power may not exceed 1 MW in the center compartment of the pool. In that compartment, all arrangements are made to study shielding consisting of a combination of various shielding materials and water.

The reactor Triton II has 100 MW power rating [maximum thermal flux  $1.5 \cdot 10^{12}$  neutrons/(cm<sup>2</sup> · sec)]. It stands on a fixed base in the center compartment of the pool against the wall separating this section from the dry end of the pool. The reactor is used for the study of shielding which contains no water. Shielding blocks are assembled in the dry compartment, pile neutrons are led there through a 2 × 2 m aluminum window.

The reactor physics division of the Cadarache research center gives close attention to the study of safety problems in bringing prompt-neutron reactors up to criticality, and to studies of the effect of hydraulic and thermal effects accompanying rapid reactor power rises on reactor stability, as well as the behavior of fuel elements in power surges. The pulsed pool reactor Cobrie, with plate-type fuel elements, is employed for these purposes. Excess reactivities of  $2\beta_{\text{eff}}$  can be achieved in this reactor, the pulse duration is  $10^{-4}$  sec, and the pulse power is 800 MW. The control panels are situated 300 m apart from the reactor. Reactor controls and processing of results are done by electronic computer; closed-circuit TV is installed for visual monitoring of the reactor processes.

High-flux research reactors. The first French high-flux reactor is a heavy-water reactor. This is the EL-3 at Saclay, which went critical in April 1958. It develops 18-MW power, and the maximum thermal flux is  $10^{14}$  neutrons/(cm<sup>2</sup> · sec). Rod-type fuel elements containing uranium (1.6% enrichment) were used until mid-1964. The reactor had been redesigned by the time the delegation got to visit it, with the innovation of the "snow crystal" type fuel assemblies (containing seven tubular fuel elements). Uranium enrichment is now 4%. Burnable poison in the form of a B<sup>10</sup> compound with aluminum will be used to compensate reactivity. After the reactor has been completely rebuilt, a lower thermal power will be required to achieve the same high neutron flux.

The further development of high-flux research reactors goes hand in hand with improvements in pool-type reactors. Thanks to the intensified cooling of the core by means of a high water flowrate, such progress has been achieved in raising the power of pool-type reactors that these reactors are now comparable in their physical characteristics to the well-known high-flux research reactors already in operation elsewhere. The heat loading of the cores attained in these reactors ranges from 500 to 700 kW/liter, which assures high fast and thermal flux densities. At the present time, two of these reactors are in operation in France: the 30-MW Pegase reactor at Cadarache and the 15-MW Siloe reactor at Grenoble. A plan is underfoot to step up the power of the latter to 30 MW. Construction of the 50-MW Osiris reactor is in progress at Saclay; this project envisages six loop channel simultaneously in the core.

The great advantage of the pool-type reactor, compared to similar pressure-vessel and channel-type reactors, is that it renders the reactor best adaptable to experimental design and its operation involves no complicated technological operations. The only deficiency of the pool-type reactor, felt with particular sharpness when the power is stepped up, is facing of the core on the pool surface. But French specialists have hit upon effective measures to cope with this problem. The Pegase reactor core is so designed that the pool volume is separated off from the reactor by a lightweight aluminum vessel and the water in the primary loop cannot mix with the pool water.

The Siloe reactor has no pressure vessel; to prevent water carrying oxygen activity from reaching the pool surface, a heated layer is set up at a slight depth below by feeding in water from a special heating unit.

The Osiris reactor now being built has no pressure vessel either, and the problem of water radioactivity will be solved by organizing a specially designed hydraulic setup: the water coolant leaving at the top of the core will be collected in tubes lying deep below the surface in the pool, while clean water from the surface will also be partially admitted into these tubes to provide counterflow (100 m<sup>3</sup>/h from the pool at a water flowrate of 3600 m<sup>3</sup>/h in the coolant loop).

The basic characteristics of these reactors are listed in Table 1.

The advantages of the pool-type reactor for performing experiments is illustrated in clearcut manner by the Pegase reactor. The loop channels along with all the coolant loop equipment are mounted on a special structure built to move along the pool bottom. An overhead crane extending above the reactor enables the entire loop to be raised from the pool to the upper water level and to be displaced through a sluice gate from the reactor pool into a technological process pool where the work on experimental preparation of the loop is carried out. Channel refueling and other "hot" operations are carried out with the loop under water, placed underneath a hot cave equipped with a set of power-actuated electrical and manual manipulators. Eight loop facilities with channels that can be moved right up to the core vessel are accommodated simultaneously in the reactor pool. More efficient utilization of the reactor is achieved when all preparatory operations are carried out in the process pool where standby loop accessories are available.

The Électricité de France nuclear electric power stations. Two types of thermal power reactors are being developed in France: a heavy-water moderated and gas-cooled type, and a graphite-moderated gas-cooled type. Carbon dioxide gas is the coolant in both instances.

A nuclear electric power station with a heavy-water reactor rated at 80 MW(e), including 5 MW for its own power needs, is now being built at the town of Brenelisse (in northwestern Brittany). The power station is scheduled to go on the line in 1966. The volume of heavy water in the loop is 100 m<sup>3</sup>, with 75 m<sup>3</sup> present in the reactor pressure vessel. Circulation through heat exchangers is provided for in order to cool the heavy water; another loop is built for recombination of the detonating gas, in which the latter, removed from the water by helium, is catalytically recombined. This is one complication due to the presence of heavy water. The gas temperature at the reactor exit is 475°C (and can be increased to 500°C), allowing for steam generation at 70 atm pressure and 455°C temperature (with the possibility of increasing the pressure to 85 atm and temperature to 490°C). The channels are arranged horizontally in the reactor. There are nine fuel assemblies, each 500 mm in length in each channel. There are two auxiliary machines: a fuel loading machine on one side of the core and an unloading machine on the other. Cadmium salt is dissolved to compensate for the heavy-water reactivity, and this salt is then removed from the loop with the aid of ion exchange columns.

Graphite gas-cooled reactors have been built at Chinon (EDF-1, EDG-2, and EDF-3), and are being built in the town of St. Laurent located about 80 km northeast of Chinon (EDF-4 and EDF-5). The development of graphite-

gas reactors is pursued in the direction of increasing the power in one unit and increasing the fuel burnup (Table 2). Natural uranium metal with 0.5% molybdenum is the fuel in EDF-1, and the same with 1% molybdenum is used in the remaining EDF line reactors. The fuel is clad in extended-surface magnesium. Starting with the EDF-2 reactor, the fuel elements have been encased in graphite jackets to provide greater convenience in reloading.

The EDF-1 reactor is a prototype designed for testing out all the components and subassemblies of future reactors in its line. It differs from the other reactors in that fuel reloading is done from below. Loading of fuel elements from above was resorted to in the later reactors, and the operations on the EDF-2 reactor were carried out sequentially by two loading machines, one of which carried out the preliminary operations to refueling; a single refueling machine is employed at the EDF-3 and EDF-4 reactors. Refueling is done with the reactor on power (except in the case of the EDF-1 prototype), and the refueling machines are operated automatically with the aid of a programming system.

The EDF-1 and EDF-2 pressure vessels are of stainless steel, and the other piles are enclosed in prestressed concrete vessels. The turbogenerators are located outside the reactor building in all the cases. A pressure-tight spherical containment shell was built around the EDF-1 reactor; this was eliminated in the later designs.

The volume of operations entrusted to electronic computers is gradually being expanded in order to simplify the control of the power station and to reduce the number of personnel required. Only data on the pressure-tightness of the fuel elements is being analyzed on the computer serving the EDF-1 facility; the computer serving the EDF-2 also analyzes all signals arriving from a battery of monitoring and measuring instruments, i.e., this computer actually performs automatic control of the power station. The EDF-3 computer will control refueling operations at the same time as it performs the other functions.

Fast power reactor research and development. Fast power reactor projects are being handled by the Commissariat in collaboration with Euratom. The fast reactor "Rhapsodie" is currently being built at Cadarache in France, and is designed as a prototype to aid in the development of fast power reactor technology and equipment. The reactor is scheduled to go into operation in late 1966. The "Rhapsodie" reactor is rated at 20 MW(th), with peak fast flux of  $2.2 \cdot 10^{15}$  neutrons/(cm<sup>2</sup> · sec), core volume of 40 liters, sodium coolant temperature of 450°C at the pile entrance and 540°C at the exit. The fuel elements are rod-type elements with a ceramic core of uranium oxide and 25% plutonium oxide, and stainless steel cladding. A project now under study envisages building a similar fast power reactor of 1500 MW(th) rating with a core volume of 5500 liters.



AMERICAN WATER DESALINIZATION SPECIALISTS

VIEW SOVIET WORK

Translated from Atomnaya Énergiya, Vol. 18, No. 3,  
p. 309, March, 1965

A delegation of American specialists in desalinization of water visited the Soviet Union in November 1964. They made stopovers in Moscow, Obninsk, Sverdlovsk, Alma-Ata, Baku, Shevchenko (on the eastern shore of the Caspian Sea), visited and inspected pilot plants and experimental facilities for water desalting, and engaged in talks with Soviet colleagues.

The USA specialists manifested interest in the work done by Soviet scientists on desalinization, showing particular interest in the seeding technique. At Shevchenko, the methods in use for distillation of the Caspian Sea salt waters call for the use of natural chalk as "initiator" to precipitate out of this brine the magnesium salts responsible for scale on steam boiler walls or on other heat-transfer surfaces. This technique attracted the attention of the American visitors for the particular reason that there are no desalinization plants operating on that principle in the USA.

The visitors manifested particularly keen interest in the work done by Soviet scientists on desalinization nuclear reactors. In their visit to the Power Physics Institute, they became familiar with the research on fast reactors designed for desalinization. They were informed of the BN-350 reactor to be built at Shevchenko; the American scientists visited the laboratories of the Institute and inspected the BR-5 fast reactor and other facilities.

The possible use of heavy-water organic-cooled reactors for water salinization is under study in the USA. The USA water desalinization program looks ahead to the construction of large-scale reactor facilities by 1975 for combined electric power generation and water desalinization. Experience in operation of the Piqua reactor and studies carried out on test loops will be exploited in bringing this program to fruition.

The American specialists were acquainted with the many directions now being pursued by Soviet scientists in tackling the problem of desalting water, with special emphasis on the design of small-scale desalting facilities which can be used successfully in arid regions by geological teams, etc. Work on electro dialysis desalinization facilities of low capacity is also being pursued in the USSR.

At a concluding talk held with the USSR State Committee on the Uses of Atomic Energy, members of the American delegation expressed their gratitude for the interesting program worked out for their visit, and for the useful discussions they had with their Soviet colleagues. The head of the delegation, J. Calhoun, reported that the members of the American delegation saw many interesting things, and were particularly impressed by research for which no counterpart currently exists in the USA. He stated that the American specialists were highly pleased by the water desalinization plant built to supply the city of Shevchenko with potable water. The statement by the American specialists mentioned work in progress in the USA on improving currently known desalinization techniques: distillation, freezing-out of impurities, filtration, and treatment with ion-exchange resins. Efforts to seek out new ways of desalting water are also being pursued.

The joint efforts of Soviet and American scientists and engineers will unquestionably lead to the successful solution of the problem of desalinizing sea water.

The outcome of the visit by the American desalinization experts to the Soviet Union was an excellent first step taken in the realization of the agreement recently signed by the USSR and the USA on collaborative efforts in this area.

BRITISH SCIENTISTS VISIT THE USSR

Translated from Atomnaya Énergiya, Vol. 18, No. 3,  
pp. 309-310, March, 1965

A delegation of British specialists on isotope production and applications visited the Soviet Union from November 23 to December 4, 1964, as part of the agreement on collaboration in the peaceful exploitation of atomic energy drawn up by the USSR State Committee on the Uses of Atomic Energy and the United Kingdom Atomic Energy Authority. Six members of the delegation were staff members of the Wantage research center, where research deals mainly with isotope applications in industry, and two others were staff members of the Amersham radiochemical research center, which is primarily engaged in the production and marketing of isotopes and labeled compounds.

During their stay, the British delegation was afforded the opportunity of visiting the Department of Applied Atomic Physics and Radiochemistry of the K. A. Timiryazev Agricultural Academy, where they were brought up to date on the scientific and educational activities of the department and the equipment in use. The visitors were greatly pleased by their visit to the Shcherbakov Combine, where they were shown the use of isotopes in textiles production to eliminate static electricity. The British scientists mentioned the simplicity, reliability, and high efficiency of the instrument used in their talk with the management of the textiles combine.

At the V. G. Khlopin Radium Institute in Leningrad, the delegation learned about the techniques of radiometric analysis and the radiometric equipment employed by Soviet scientists in their work.

After visiting the All-Union "Izotop" Organization and inspecting the demonstration and lecture halls, the British scientists held a talk with the directors on the problems and functions of "Izotop," in the course of which the British specialists took note of the close attention given to advertising and to the adoption of isotope instruments in industry.

In their visit to the Institute of Nuclear Physics of the Academy of Sciences of the Uzbek SSR, the delegation members showed intense interest in the work of Uzbeki scientists on pre-sowing exposures of cotton seeds to increase crop yield.

At the Ferrous Metallurgy Research Institute, the British specialists were brought up to date on applications of isotopes and nuclear radiations in studies of diffusion and distribution of the elements in metals, as well as on applications of isotopes in blast furnace and steelmaking processes.

## RADIOISOTOPE ADVANCES IN THE LITHUANIAN SSR

S. Geciauskas and K. Valacka

Translated from *Atomnaya Énergiya*, Vol. 18, No. 3,  
pp. 310-311, March, 1965

The development of industry and scientific research in the Lithuanian SSR has had, as a by-product, an extensive use of radioisotope techniques, and instruments, and radiation sources.

The Isotopes Laboratory of the Central Agricultural Design Bureau, organized in late 1962, shoulders the main responsibility for the implementation of radioisotopes techniques in industry.

Radioisotope counters for counting the number of parts passing a point on the line or the filling of containers are being used at the Salcininkaj and Panavezis alcohol plants, the Klaipeda confectionary plant ("Geguzes Pirmoj"), and elsewhere. At the Kaunas radio equipment plant and the Vilnius television parts plant, object counters have been developed and put into production through the sole efforts of the plant staff. About 50 PT-1 and PT-2 isotope-operated temperature controllers are on stream in the plastics department of the Kaunas radio equipment plant. They are employed to maintain temperature levels in the molds of hydraulic presses installed in the plastics department.

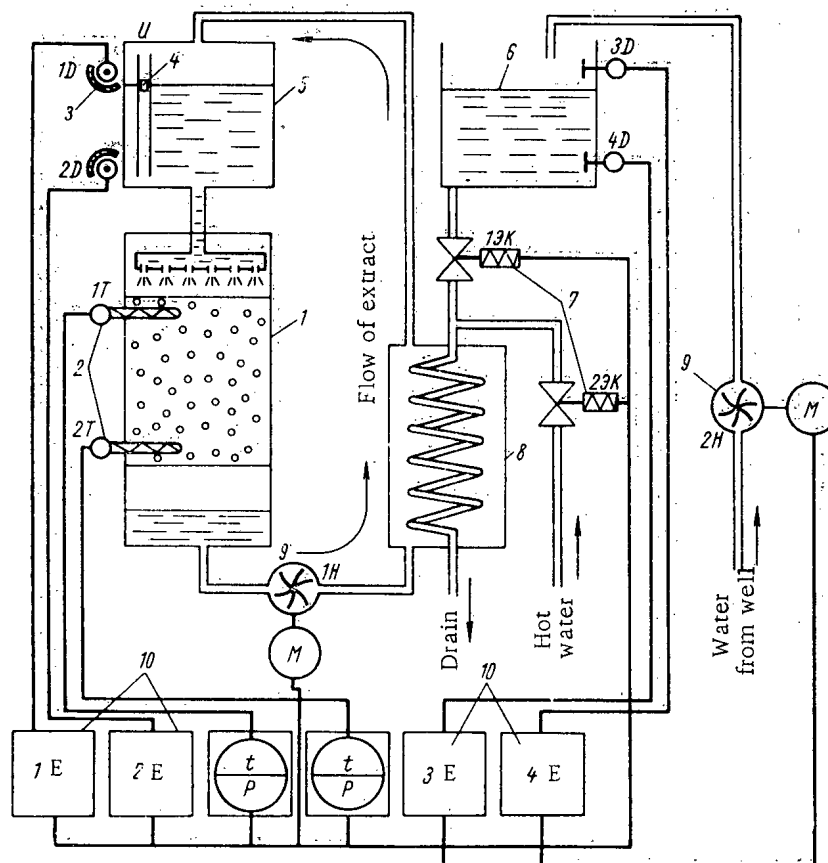


Fig. 1. Simplified automation layout of oxidizer. 1) Oxidizer; 2) thermometers; 3) level gage (sensor); 4) level gage radiation source; 5) intervening vessel; 6) vat; 7) electromagnetic valves; 8) oxidizer-heat exchanger; 9) pumps; 10) electronic circuits.

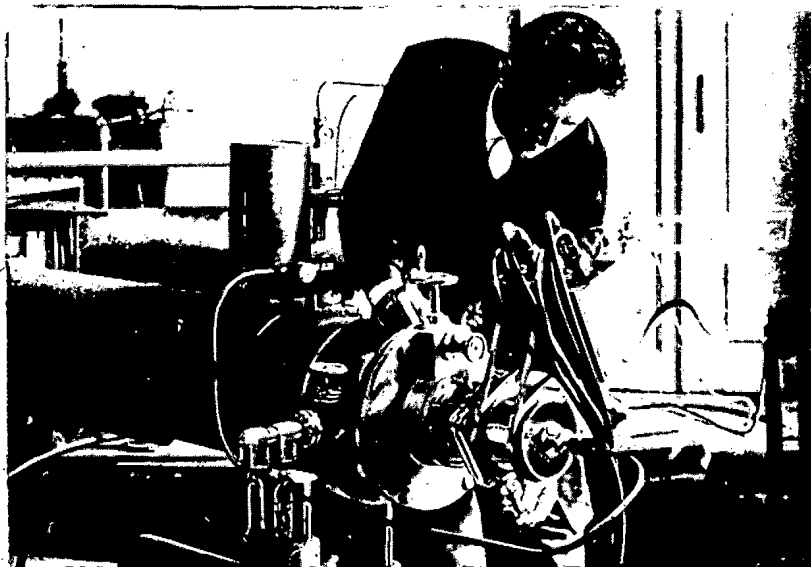


Fig. 2. Adjusting the UMB-1 spectrometer.

Figure 1 shows a simplified layout for the automation of the vinegar fabrication process. The layouts are built around four oxidizers. When this control system was put on a production footing at the Salcininkaj plant, the annual savings were 4.5 thousand rubles as against expenditures of 7.5 thousand rubles.

A similar controls system has been introduced into the production of glutamic acid and vitamin B-12 at the Panevezis plant. Automation of the plant processes by means of radioactive isotopes now means about 9 thousand rubles a year in savings.

A plan for automating the operation of rubber blenders at the Vilnius chemical plant has been drawn up and put into effect. The over-all control system incorporates monitoring of the fill levels of crumb rubber in cyclones by means of gamma-ray level gages, remote charging of blenders, automatic maintenance of temperature conditions in blenders, and programming of the production cycle time. Termination of distinct production periods is annunciated on lighted panels. Some of the vulcanizing presses in the same plant were converted to semi-automatic operation in 1964.

The experimental part of the work on applications of radioisotope thickness gages for monitoring the thickness of rubber sheet in calendering of pure rubber and textiles has been carried out. Isotope thickness gages are now being installed on five calenders of the "Inkaras" rubber goods combine in Kaunas. The data obtained in this work will provide a basis for attempts to achieve automatic control of the thickness of the rubber sheet produced.

Certain advances were achieved in engineering new applications of radioisotopes and radiation sources in medicine. Radiological laboratories are operative in six large medical institutions in the republic, with radioactive isotopes and sources of radioactive radiations being used for the diagnosis and therapy of a variety of ailments. Radioactive isotopes are also being used to treat patients in the Vilnius Oncological Research Institute and in several other medical research institutions.

A heavy research program is in progress at the isotopes laboratory of the Lithuanian Animal Husbandry Research Institute. In recent years, studies have been made at the laboratory of the activity of the thyroid gland in breeder bulls, with the aid of the radioisotope  $I^{131}$ . Similar studies have been carried out on calves of large cattle. The  $F^{31}$  isotope is a useful tool in investigations of the effect of the level and type of feeding on the age of puberty in calves, on the duration of spermatogenesis, and on the quality of sperm in breeding bulls.

Work on the study of wear on rubbing parts in low-power internal-combustion engines and compressors manufactured by the industry of the republic is being carried out in the isotopes laboratory of the Kaunas Polytechnic Institute, under the Department of Automotive Engineering. The laboratory is quite well equipped with modern research apparatus.

Radioactive isotopes are being employed in research aimed at using the method of angular correlations of gamma rays to study internal fields in semiconductor crystals, at the Institute of Physics and Mathematics of the Academy of Sciences of the Lithuanian SSR. The spectra of internal-conversion electrons and the effect of the physical-chemical structure of semiconducting materials into which radioactive isotopes have been introduced on conversion electrons are being studied on the large UMB-1 magnetic beta-ray spectrometer (Fig. 2).

At the Institute of Botany of the Academy of Sciences of the Lithuanian SSR, a study is being made of the distribution of radioactive aerosols in the lower layers of the atmosphere, and of self-decontamination of the air with the elimination of natural and artificial contamination by radioactive aerosols.

Radioisotope dilution methods and techniques for determining trace impurities in high-purity materials, including semiconductor materials under study in various research organizations throughout the republic, are being developed at the isotopes laboratory of the chemistry department of the V. Kapsukas Vilnius State University. The photoelectrical properties of high-resistivity semiconductors are being studied over a broad range of wavelengths extending far into the gamma-ray region, in the semiconductor physics department of that university.

Radioisotope techniques are also being explored on a broad scale in geological work. Gamma-ray logging is a familiar tool in work carried out by the Geology and Mineral Resources Conservation Board.

Construction work has begun on the radiological laboratory of the Academy of Sciences of the Lithuanian SSR, with rooms and equipment set aside for physicists, biologists, biochemists, and medical technicians. The laboratory will be ready for service in 1966, and will become the scientific center of the republic in matters of radioisotope techniques applications.

## Soviet Journals Available in Cover-to-Cover Translation

ABBREVIATION	RUSSIAN TITLE	TITLE OF TRANSLATION	PUBLISHER	TRANSLATION Vol.	Issue	BEGAN Year
AÉ	Atomnaya énergiya	Soviet Journal of Atomic Energy	Consultants Bureau	1	1	1956
Akust. zh.	Akusticheskii zhurnal	Soviet Physics - Acoustics	American Institute of Physics	1	1	1956
Astron. zh(urn).	Astronomicheskii zhurnal	Soviet Astronomy - AJ	American Institute of Physics	34	1	1957
Avto(mat). svarka	Avtomatskaya svarka	Automatic Welding	Br. Welding Research Assn. (London)	12	1	1959
	Avtomatika i Telemekhanika	Automation and Remote Control	Instrument Society of America	27	1	1956
	Biofizika	Biophysics	National Institutes of Health*	6	1	1961
	Biokhimiya	Biochemistry	Consultants Bureau	21	1	1956
Byull. éksp(erim). biol. (i med.)	Byulleten' éksp(erim)tal'noi biologii i meditsiny	Bulletin of Experimental Biology and Medicine	Consultants Bureau	41	1	1959
		Doklady Biological Sciences Sections (includes: Anatomy, biochemistry, biophysics, cytology, ecology, embryology, endocrinology, evolutionary morphology, genetics, histology, hydrobiology, microbiology, morphology, parasitology, physiology, zoology)	National Science Foundation*	112	1	1957
		Doklady Botanical Sciences Sections (includes: Botany, phytopathology, plant anatomy, plant ecology, plant embryology, plant physiology, plant morphology)	National Science Foundation*	112	1	1957
		Proceedings of the Academy of Sciences of the USSR, Section: Chemical Technology	Consultants Bureau	106	1	1956
		Proceedings of the Academy of Sciences of the USSR, Section: Chemistry	Consultants Bureau	106	1	1956
		Proceedings of the Academy of Sciences of the USSR, Section: Physical Chemistry	Consultants Bureau	112	1	1957
		Doklady Earth Sciences Sections (includes: Geochemistry, geology, geophysics, hydrogeology, lithology, mineralogy, oceanology, paleontology, paleontology, petrography)	American Geological Institute	124	1	1959
		Proceedings of the Academy of Sciences of the USSR, Section: Geochemistry	Consultants Bureau	106-	1	1956-
		Proceedings of the Academy of Sciences of the USSR, Section: Geology	Consultants Bureau	112-	6	1957-
		Proceedings of the Academy of Sciences of the USSR, Section: Geology	Consultants Bureau	123	6	1958
		Soviet Mathematics - Doklady	American Mathematical Society	130	1	1960
		Soviet Physics - Doklady (includes: Aerodynamics, astronomy, crystallography, cybernetics and control theory, electrical engineering, energetics, fluid mechanics, heat engineering, hydraulics, mathematical physics, mechanics, physics, technical physics, theory of elasticity sections)	American Institute of Physics	106	1	1956
		Telecommunications	Consultants Bureau	106-	1	1956-
		Entomological Review	Consultants Bureau	123	6	1958
		Physics of Metals and Metallurgy	Consultants Bureau	112-	1	1957-
		Soviet Physics - Solid State	Consultants Bureau	123	6	1958
		Sechenov Physiological Journal USSR	Consultants Bureau	130	1	1960
		Plant Physiology	American Institute of Physics	106	1	1956
		Geodesy and Aerophotography	National Institutes of Health**	47	1	1961
		Geochemistry	National Science Foundation*	4	1	1957
		Petroleum Geology	American Geophysical Union	4	1	1962
		Geomagnetism and Aeronomy	The Geochemical Society	1	1	1956
		Artificial Earth Satellites	Petroleum Geology	2	1	1958
		Measurement Techniques	Geomagnetism and Aeronomy	1	1	1961
			Consultants Bureau	1	1	1958
			Instrument Society of America	7	1	1958
			Am. Inst. of Electrical Engineers	1	1	1957
			National Science Foundation**	37	1	1958
			Acta Metallurgica	5	1	1957
			American Institute of Physics.	1	1	1959
			National Institutes of Health**	47	1	1961
			National Science Foundation*	4	1	1957
			American Geophysical Union	4	1	1962
			The Geochemical Society	1	1	1956
			Petroleum Geology	2	1	1958
			Geomagnetism and Aeronomy	1	1	1961
			Consultants Bureau	1	1	1958
			Instrument Society of America	7	1	1958

The translation of this journal  
is published in sections

Elektrosvyaz'  
Entomologicheskoe obozrenie  
Fizika metallov i metallovedenie  
Fizika tverdogo tela  
Fiziologicheskii zhurnal imeni  
I.M. Sechenov  
Fiziologiya rastenii  
Geodeziya i aerofotogramka  
Geokhimiya  
Geologiya nefli i gaza  
Geomagnitizm i aeronomiya  
Iskustvennye sputniki zemli  
Izmeritel'naya tekhnika

DAN (SSSR)  
Doklady Akademii  
Nauk SSSR

ABBREVIATION

RUSSIAN TITLE

Atomnaya énergiya  
Akusticheskii zhurnal  
Astronomicheskii zhurnal  
Avtomatskaya svarka  
Avtomatika i Telemekhanika  
Biofizika  
Biokhimiya  
Byulleten' éksp(erim)tal'noi  
biologii i meditsiny

TITLE OF TRANSLATION

Soviet Journal of Atomic Energy  
Soviet Physics - Acoustics  
Soviet Astronomy - AJ  
Automatic Welding  
Automation and Remote Control  
Biophysics  
Biochemistry  
Bulletin of Experimental  
Biology and Medicine  
Doklady Biological Sciences Sections  
(includes: Anatomy, biochemistry, biophysics,  
cytology, ecology, embryology,  
endocrinology, evolutionary morphology,  
genetics, histology, hydrobiology,  
microbiology, morphology, parasitology,  
physiology, zoology)

PUBLISHER

Consultants Bureau  
American Institute of Physics  
American Institute of Physics  
Br. Welding Research Assn. (London)  
Instrument Society of America  
National Institutes of Health\*  
Consultants Bureau  
Consultants Bureau

TRANSLATION

Vol.

Issue

BEGAN  
Year

1  
1  
34  
12  
27  
6  
21  
41  
112

1  
1  
1  
1  
1  
1  
1  
1  
1

1956  
1956  
1957  
1959  
1956  
1961  
1956  
1959  
1957

Life  
Sciences

Chemical  
Sciences

Earth  
Sciences

Mathematics

Physics

Table with columns: Izv. AN SSSR (Russian), O(td), Kh(im), N(auk) (Latin), O(td), T(ekhn), N(auk); (see Met. i top) (English), Izvestiya Akademii Nauk SSSR: Otdeleniye khimicheskikh nauk (Russian), Bulletin of the Academy of Sciences of the USSR: Division of Chemical Science (English), 1952-1961 (Dates), 16-11 (Counts), Consultants Bureau (Organizations), 1952-1961 (Dates), 16-11 (Counts), Consultants Bureau (Organizations), 1952-1961 (Dates), 16-11 (Counts), Consultants Bureau (Organizations).

\*Sponsoring organization. Translation published by Consultants Bureau. \*\*Sponsoring organization. Translation published by Scripta Technica.

**RUSSIAN TO ENGLISH**

# scientist-translators wanted



You can keep abreast of the latest Soviet research in your field while supplementing your **income** by translating **in your own home** on a part-time basis. In the expanding Consultants Bureau publishing program, we **guarantee a continuous flow of translation** in your specialty. If you have a native command of English, a good knowledge of Russian, and experience and academic training in a scientific discipline, you may be qualified for our program. Immediate openings are available in the following fields: physics, chemistry, engineering, biology, geology, and instrumentation. Call or write now for additional information: TRANSLATIONS EDITOR



**CONSULTANTS BUREAU**

227 West 17 Street, New York, N. Y. 10011 • (Area Code: 212) AL-5-0713



**NEW FROM**  
 **CONSULTANTS BUREAU**  
 **PLENUM PRESS**

**SPACE SCIENCES AND ASTROPHYSICS**

**STELLAR EVOLUTION**

Edited by A. G. W. Cameron and R. F. Stein. This comprehensive collection of 41 authoritative papers on stellar structure and evolution treats such topics as stellar energy balances, radiative absorption, turbulent convection, neutrino generation, pre-main sequence evolution, the dependence of evolution on stellar mass, white dwarfs, novae and supernovae, and composition differences between the galaxy and the Magellanic Clouds. A Plenum Press book.

472 pages 1965 \$19.50

**SOLAR SYSTEM  
RADIO ASTRONOMY**

Edited by Jules Aarons. Contains review papers on all aspects of the radio and radar exploration of the sun, moon, and planets, including topics such as interferometric measurements of the centers of solar activity and flares, the density of the interplanetary medium, the nature of the lunar surface as indicated by radar reflections and apparent temperature at different wavelengths, and planetary radio emissions. A Plenum Press book.

430 pages 1965 \$17.50

**SPACE PHYSICS WITH  
ARTIFICIAL SATELLITES**

By Ya. L. Al'pert, A. V. Gurevich, and L. P. Pitaevskii. The first study of its kind, this monograph is devoted to a theoretical investigation of phenomena attending the movement of a space satellite through a highly rarefied plasma. Two cases are considered: a body with velocity greater than the thermal motion of neutral particles and ions and dimension larger than the Debye radius; and a body with dimension comparable to or smaller than the Debye radius and velocity comparable to that of the particles. Translated from Russian and published by Consultants Bureau.

250 pages 1965 \$25.00

**TWILIGHT**

By G. V. Rozenberg. This is the only book in the world scientific literature devoted to the discussion of twilight as an optical phenomenon and as a means for investigation of the atmosphere — especially its high layers. It gives a general outline of the present status of the problem and presents in full for the first time concepts developed by the author over a period of some years. Includes data resulting from experimental investigations of the twilight sky. A Plenum Press book translated from Russian.

Approx. 380 pages 1965 \$20.00

**PEACEFUL USES OF AUTOMATION  
IN OUTER SPACE**

Edited by John A. Aseltine. These papers, presented at Oslo this fall at the first international meeting on this subject, present the newest concepts, designs and ideas on injection into space, attitude stabilization, remote control in space vehicles, manned systems, ground systems, advanced components, digital and analog computers, and future problems. All papers are in English. A Plenum Press book.

475 pages 1965 \$17.50

**NATURAL ELECTROMAGNETIC  
PHENOMENA BELOW 30 kc/s**

Edited by D. F. Bleil. Contains sixteen lectures by prominent scientists on the static and dynamic electromagnetic phenomena in the space environment of the Earth. Papers of special interest include a presentation of the hydromagnetic theory of the magnetosphere, which indicates that it is of limited extent and shows the predicted distortion of this field due to the solar wind; a description of an interesting and useful technique of spectral, cross-spectral, and bispectral analysis of low-frequency electromagnetic data; and a theoretical treatment of magnetic storms. A Plenum Press book.

482 pages 1964 \$17.50

 **CONSULTANTS BUREAU /  PLENUM PRESS**  
 227 West 17th Street, New York, New York 10011